

SYNTHESIS AND CHARACTERIZATION OF ISOMERS OF FUNCTIONALIZED
DOUBLE-DECKER-SHAPED SILSESQUIOXANES

By

Aditya N Patil

A DISSERTATION

Submitted to
Michigan State University
in partial fulfillment of the requirements
for the degree of

Chemical Engineering – Doctor of Philosophy

2023

ABSTRACT

Functionalizing the incompletely condensed octaphenyl double-decker silsesquioxane tetrasilanol, $\text{Ph}_8\text{-DDSQ}(\text{OH})_4$, with reactive dichlorosilanes forms condensed, hybrid molecules with reactive organic groups on the opposite edge of the inorganic $\text{SiO}_{1.5}$ core, surrounded by phenyl moiety. This unique phenyl moiety surrounded SQ core provides additional thermo-oxidative stability for high temperatures, organic thermoplastics, and thermosetting polymers. Unlike corner-capped functional POSS, condensing DDSQ with dichlorosilane enables different chemical moieties on the opposite side of the SQ core, allowing SQ to act as the "bridging" chemical needed for bonding two different classes of materials. In addition, another benefit that is unique when condensing DDSQ-tetrol is the formation of isomers. $\text{Ph}_8\text{DDSQ}(\text{OH})_4$, when fully condensed with $\text{R}_1\text{R}_2\text{SiCl}_2$, is the formation of conformational isomers or regioisomers. (Isomers about the SQ core) The conformational isomer mixture often exhibited lower liquidus temperature than pure isomers, which benefits when mixed with organic resins at lower temperatures. Structural isomerism is the most radical type wherein the two compounds have the same number of atoms, but their chemical and physical properties are entirely different since they have logically distinct bonds.

This work examines an asymmetrically capped DDSQ system synthesized as a coupling agent between graphene oxide (GO) nanofiller and styrene vinyl ester (VE) resin. The DDSQ-modified GO is dispersed into VE resin with only a simple mechanical stirring at room temperature. This work studies the different isomers of the DDSQ system. Firstly, *meta* and *para* isomeric moieties of phenyl ethynyl phenyl (PEP) dichlorosilane were obtained via the Sonogashira reaction and by subsequent reaction with trichlorosilane. The synthesized dichlorosilanes were reacted with $\text{DDPh}_8\text{T}_8(\text{OH})_4$, and the relevant reaction conditions and yield were presented. The reaction led to the formation of *cis* and *trans* isomers. These isomers form a eutectic mixture with a sharp melting point upon varying the ratio of *cis* and *trans* products. Upon using a mixture of *meta* and *para*

dichlorosilanes as capping reagents, the reaction yielded a 6-isomer mixture of compounds. This isomeric mixture did not exhibit sharp melting characteristics as the individual isolated compounds exhibited. The sharpness of the solid-liquid transition character can also be dampened when long-chain chlorosilanes are used as capping agents for tetrol.

This work also investigated the effect of constitutional isomerism in cage-like silsesquioxanes. Precisely, edge-open octaphenyl silsesquioxane diol condensed with tetramethyl dichlorosiloxane and double-decker-shaped silsesquioxane tetraol condensed with dimethyl dichlorosilanes form structural isomers. The interactions between the organic group bonded to the D-Si and the adjacent phenyl group connected to the T-Si of DDSQ molecules have a defining effect on the internal configuration of the DDSQ cage. This change affects phase transformation between liquid and solid states, forming a glassy state in a pure isolated compound.

Copyright by
ADITYA N PATIL
2023

TO MY FAMILY

ACKNOWLEDGMENTS

Sitting down to write the last section of my Ph.D. thesis, I cannot believe that my days in the state of Michigan are numbered. This transformative graduate school experience at Michigan State University has affected my core principles and helped me to revise and refine my fundamentals. My method to approach a problem, to access, read, think, and process knowledge, to write and analyze scientific reports, to view the world as a research scientist, to interconnect with colleagues, behave myself in a professional environment, and manage resources and time, have all been strengthened over the last six years. This remodel occurred because of the people surrounding me and my workplace. I will eternally be grateful to them. It is nearly not probable to name every person that contributed to helping me in graduate school, as well as the individuals with whom I spent a fantastic time in Michigan.

To start with, I need to eternally thank my family. To my parents, Narendra and Aruna, and my sister Chinmayee: your constant belief in me made all the difference. Next, I want to acknowledge the professors on my research committee. Firstly, I would like to highlight the guidance and patience of my advisor Dr. Andre Lee. He accepted me as his student in the Fall of 2017, and every day, he challenged me to change my method of thinking, how to work experimentally to achieve targets, to optimize the efforts to become a better researcher, and formulate questions to find solutions to any scientific problem. His contribution was beyond his duty, and he helped me to become a better scientist. Secondly, I would like to highlight Dr. Robert Maleczka for his guidance through the organic chemistry problems and his disposition to answer my questions every time his door was open. His contributions to this project were invaluable. Next, I would like to highlight Dr. Shiwang Cheng for his dedication to quality science, and I have always admired his passion for the students. Lastly, I would like to highlight Dr. Ramanini Narayan for his support. I recognize he plays many roles, but I have never met a PI that better encompasses the term mentor. Beyond

the committee members, I would like to express my gratitude to my friends in chemistry. To my lab mates, Jonathan Dannett, Fangyi Shen, Badru-Deen Barry, Pepe Montero, Emmanuel Maloba, Thomas Oleskey, Arzoo Chhabra, Anshu Yadav, David Vogelsang, and Tyler Johnson: Working with you guys has been an honor, and I dearly hope to keep in close contact over the years. To my close friends:- Kalyani Jangam – The ‘USA exploration’ experience and amazing cuisines we have sampled cannot be put into words. Apoorva Kulkarni – From fighting over home-works to fun cookouts we had, Affan Malik – From playing board games, to real life games and sports, Gouree Kumbhar – From trying Pumpkin Spice Lattes to trying out new cafes, Shalin Patil – My flatmate, COD teammate and in being together in all crazy scenarios, Ishita Chandra – From the Neehes trips and unlimited gossips, Vishal Asnani – From playing FIFA to going places for a simple cup of coffee, Nikita Sharma – Eating good food together, Nidhi Kalani: From trying bougie places to home cooked Paneer dishes I have learned so much from you both in and outside the realm of science. I could never ask for a better group of friends. I want to mention to the CHEMS department staff that all of them did a great job with paperwork, orders, solving visa issues, and much more. Also, in the CHEMS department faculties, from whom I learn several new ideas and concepts through seminars, conferences, and classes. I want to thank Michigan State University through the CHEMS department for the unconditional financial support.

TABLE OF CONTENTS

LIST OF ABBREVIATIONS	x
1 INTRODUCTION	1
1.1 Background	2
1.2 Silsesquioxanes	7
1.3 Capped DDSQ systems	11
1.4 Isomers of capped DDSQ compounds	11
1.5 Motivation	14
REFERENCES	16
2 APPLICATION OF ASYMMETRICALLY CAPPED DDSQ AS A BRIDGING AGENT	19
2.1 Introduction	20
2.2 Formulation of modified Derakene™ resins	23
2.3 Characterization of cured Derakene™ resin samples	26
2.4 Experimental Details	30
REFERENCES	35
APPENDIX	39
3 PHENYL ETHYNYL PHENYL DDSQ SYSTEMS.....	45
3.1 Introduction	46
3.2 Reagent synthesis	47
3.3 Synthesis of dichlorosilanes	52
3.4 Capping of DDPPh ₈ T ₈ (OH) ₄	60
3.5 Separation of DDPPh ₈ T ₈ isomers	60
3.6 Experimental details	62
REFERENCES	68
APPENDIX	69
4 EFFECTS OF USING BULKY CAPPING GROUPS	80
4.1 Introduction	81
4.2 Synthesis of isomers of capped DDSQ structures	82
4.3 Thermal Analysis using DSC	86
4.4 Experimental details	91
REFERENCES	95
APPENDIX	97
5 SOLVENT EFFECT FOR CAPPING OF DDPPh₈T₈(OH)₄	111
5.1 Introduction	112
5.2 DDSQ tetrol capping reaction using a good solvent	113
5.3 DDSQ tetrol capping reaction using a poor solvent	117
5.4 Experimental Details	120
REFERENCES	125
APPENDIX	127

6	INCOMPLETELY CONDENSED CAGE-LIKE SILSESQUIOXANES.....	138
6.1	Introduction.....	139
6.2	Synthesis of Incompletely Condensed Cage diol.....	140
6.3	Thermal properties of model compounds	144
6.4	Synthesis and Characterization of constitutional isomers	146
6.5	Thermal and Rheological Property of isomers: TGA, DSC, and Viscosity	152
6.6	Rheological data.....	155
6.7	Experimental Details.....	157
	REFERENCES	169
	APPENDIX.....	172
7	SIGNIFICANCE AND PERSPECTIVE	229
7.1	Significance.....	230
7.2	Perspectives.....	231

LIST OF ABBREVIATIONS

AB	Asymmetric double-decker-shaped silsesquioxane
BCl ₃	Boron Trichloride
BMI	bismaleimides
BODA	bis- <i>o</i> -diynyl arene
CDCl ₃	Deuterated chloroform
CuI	Cuprous iodide
CuCl ₂	Cupric Chloride
DABPA	O, O'-diallyl bisphenol A
DCM	Dichloromethane
DDSQ	Double-decker shaped silsesquioxane
DDPh ₈ T ₈ (OH) ₄	Tetra-silanol double-decker-shaped silsesquioxane
DDPh ₈ T ₈ (2(R ₁ R ₂))	Difunctional capped Double-decker-shaped silsesquioxane
DSC	Differential scanning calorimetry
Et ₃ N	Triethylamine
GC- MS	Gas chromatography – Mass spectroscopy
GO	Graphene Oxide
LiAlH ₄	Lithium Aluminium hydride
LiBr	Lithium Bromide
Me	Methyl
MeSiCl ₃	Methyl trichlorosilane
Mg	Magnesium
NMR	Nuclear magnetic resonance

$\text{PdCl}_2(\text{PPh}_3)_2$	Bis(triphenylphosphine)palladium (II) dichloride
PEB	Phenyl ethynyl benzene
PEP	Phenyl ethynyl phenyl
PEPI	Phenyl ethynyl phenyl imide
PETIs	Polyetherimide
POSS	Polyhedral oligomeric silsesquioxane
PMR	Polymerization of Monomer Reactants
R.T.	Room temperature
RTM	Resin transfer molding
$\text{R}_1\text{R}_2\text{SiCl}_2$	Difunctional dichlorosilane
, SOPh_8T_8	Side open di-silanol silsesquioxane
t-BuLi	tertiary butyl lithium
TCCA	Trichloroisocyanuric acid
TGA	Thermogravimetric Analysis
THF	Tetrahydrofuran
VARTM	Vacuum-assisted Resin transfer molding

1 INTRODUCTION

1.1 Background

High-performance thermosets are three-dimensional cured network structures. High-temperature polymeric materials exhibit high glass transition temperature ($>300\text{ }^{\circ}\text{C}$) and excellent mechanical properties along with high decomposition temperature ($>450\text{ }^{\circ}\text{C}$). These polymeric materials must be thermally and oxidatively stable without affecting the mechanical properties. Such materials often had an extensive aromatic backbone as the sp^2 hybridized carbon atoms have higher bond dissociation energy than the sp^3 hybridized carbon atoms.¹

Although various thermosets could withstand high-temperature ranges ($300\text{ }^{\circ}\text{C}$ - $400\text{ }^{\circ}\text{C}$), processing these thermosets was a tenuous task due to the inherent rigidity of the aromatic backbone of these thermosets. Polyimides have shown remarkable potential as thermally stable materials suitable as advanced structural resins for a wide range of applications.^{2,3} Polyimides contain a repeating imide structural unit and can be generally synthesized using condensation polymerization of dianhydride and diamine monomers. Avimid NTM is a commercially used condensation polyimide. It has a glass transition temperature of $360\text{ }^{\circ}\text{C}$. The polyimides synthesized using condensation usually produce intermediate isoimide structures, leading to incomplete polymerization. It affects the mechanical strength of the polymer due to the poor mechanical strength of lower molecular-weight polymer chains. Also, the fabrication process must be carefully designed considering the high pressure required for molding and dissipating the volatile byproducts formed. To find a solution to the issues mentioned above, a new approach, PMR (*in-situ* Polymerization of Monomer Reactants), was used by NASA⁴. This technique was highly successful because of the ease of processability of the reactant monomer and the ensuing oligomers. Also, the polymerization proceeds via an addition type reaction rather than a condensation type, thus avoiding the formation of volatile byproducts. The mechanical properties

of the cured network can be tailor-made by simple variation of the chemical structure of aromatic diamines or the diester acids used or by changing the stoichiometry of monomers used in the reaction. Along with this approach, many reactive groups have been used to end cap the thermoset resins. The mechanical properties of the cured network depend on the chemistry of cross-linking, cure rate, and the number of end groups. The end groups remain dormant during the fabrication process. After the fabrication step, temperature increases to induce homo-polymerization of the end groups, the final cured network cannot be reprocessed by melting, but it has enhanced thermochemical properties.

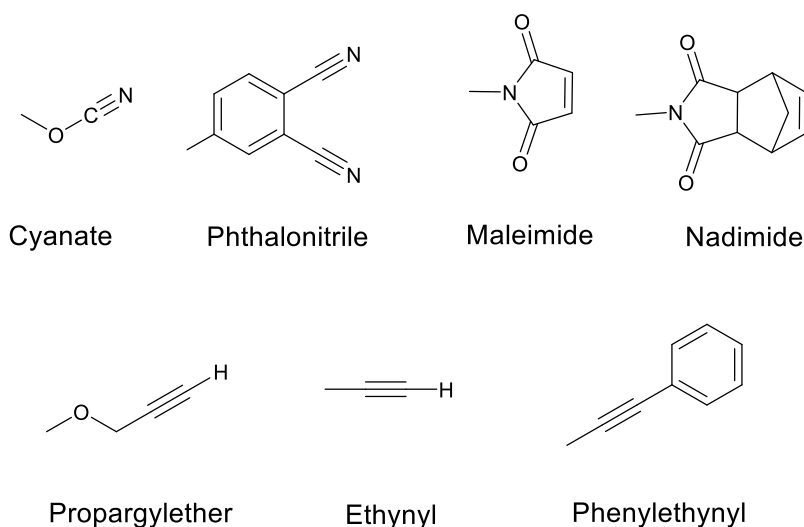


Figure 1-1 : Functional groups used as end-capping reagents.

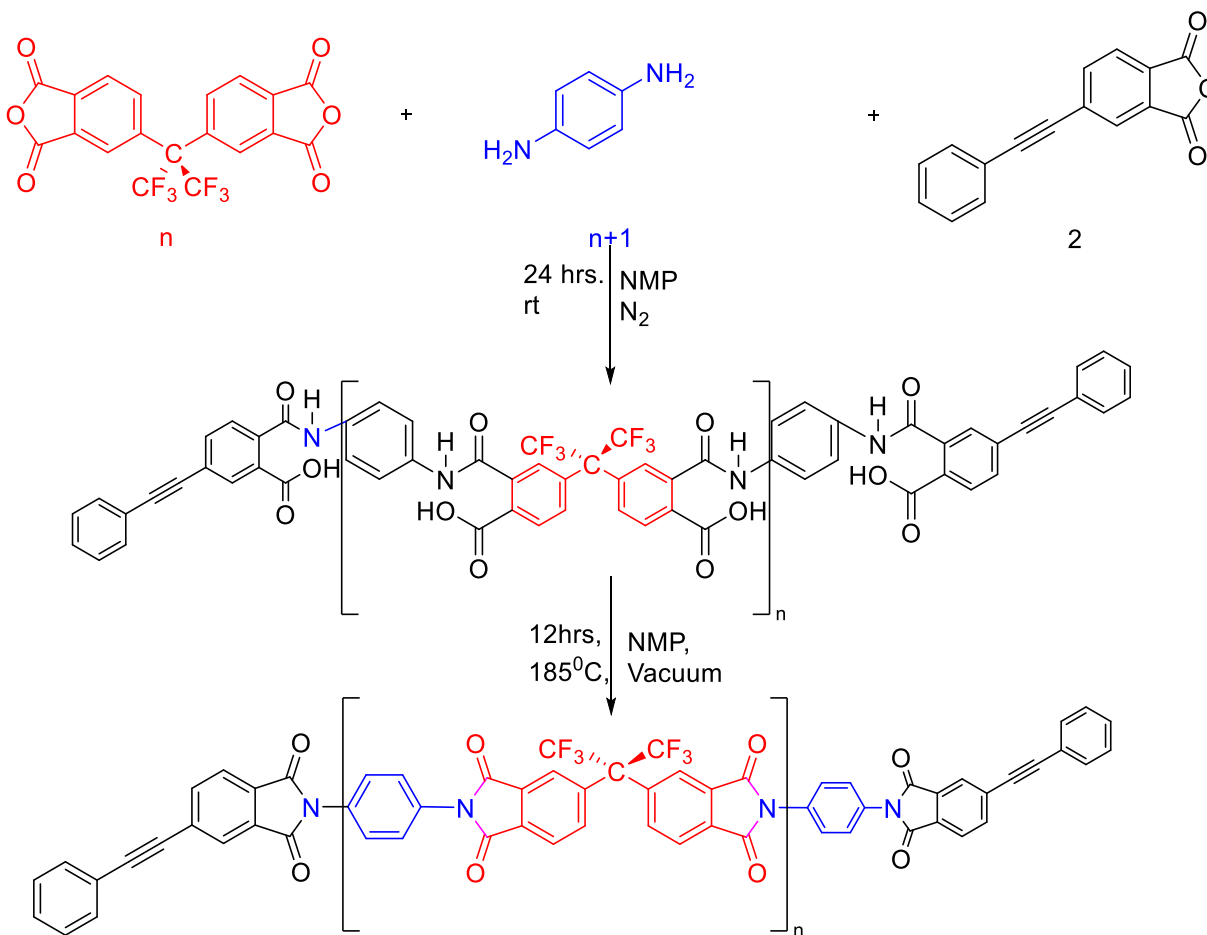
Cyanate-terminated polyamide thermosets can be used as flame retardant agents. These thermosets can be used in the microelectronics industry, as they have low dielectric constant and high dielectric breakdown strength.⁵ Maleimide terminated thermosets are widely used as high-performance thermosets in oil-field operations. These thermosets can effectively perform in got/wet fluid conditions with pressure up to 70MPa and temperatures in the 200 °C.³ Nadimide-terminated thermosets can be used as high-temperature adhesives to bond metals.⁶ LARC-13 is a commercialized nadimide end-capped thermoset with a low softening temperature of 266-316 °C.

Hence, it can be used for specialized bonding applications. Despite the ease of processability of maleimide-terminated oligomers via melt-based processing, the after-cure products are brittle with low toughness and may contain voids because of the out-gassing of volatiles. PMR-15 is an alternative norbornene end capped addition type cured thermoset used for various aircraft engine applications. It has post-cure T_g of 365 °C and can withstand temperatures up to 230 °C for longer than 10,000 h. The drawback of PMR-15 lies in using methylene di-aniline monomer, a carcinogenic material. Also, the cost of processing was still very high for commercial usage of PMR-15. These issues led to exploring new end-group chemistries that could circumvent the existing issues. Acetylene functionalized moieties have been shown to be promising alternatives as reactive end-groups. They can undergo thermally induced addition reactions yielding a complex cross-linked network.⁷ The acetylene group formed an aromatic ring through cyclo-trimerization for low molecular weight compounds, but for the high molecular weight oligomers, the procedure involved forming *ene-yne* type structures. These structures are then further homopolymerized to give the cross-linked structure. The final cross-linked structure consists of polycyclic aromatic structures, bridged structures, backbone addition structures, and cyclotrimerized aromatic structures. Thermid 600®, developed by Gulf Chemicals, was the most widely used acetylene-terminated oligomer for polyimides. Thermid 600® has a glass transition temperature of 370 °C, a tensile strength of 96.5MPa, and a modulus of 3.79 GPa. It was found to be an excellent adhesive for titanium. The shortcoming of these end groups was the homopolymerization temperature around 200 °C. It led to a limited processing window for oligomers, and hence high melting, all aromatic backbone oligomers could not be processed. These limitations were overcome by replacing the terminal proton of the acetylene end group with a phenyl ring.⁸ This feature helped to postpone the cross-linking temperature beyond 300 °C, providing a larger window for

processing of the oligomers. NASA demonstrated the promising nature of these end groups in the High-Speed Civil Transport Program, where a series of phenyl-ethynyl terminated polyetherimides (PETIs) were synthesized and characterized.^{8,9} PETI-5 has a molecular weight of 5000 g/mol and has a glass transition temperature of 270 °C after curing it at 371 °C for one hour. It also shows 32% elongation at break with a modulus 3.0GPa and 130MPa tensile strength.

To make further improvements to the thermal and oxidative stability of the polymer as well as to improve the ease of processing the oligomer melt and the AFR-PE-*n* class of thermosets was introduced in 1994.¹⁰ The oligomers for the synthesis of AFR-PE- *n* thermosets were synthesized by cyclodehydration reaction between hexafluoro dianhydride and phenyldiamine. Phenylethynyl phthalic anhydride was used as an end-capping reagent. These oligomers are then thermally cured to obtain the final cross-linked network. The length of the repeating units in the oligomer was represented by '*n*.' The value of '*n*' varied from 1,2,4, and 8. This value determined all the mechanical and thermal properties and the ease of processability of the oligomer. Oligomer characterization using chromatography and mass spectrometry revealed a broad molecular weight distribution for *n* =1,2,8. The distribution was narrow in the *n* =4 system, with an average of 4. AFR-PE- *n* systems exhibit a glass transition temperature of around 450 °C, significantly improving the mechanical properties of the previously studied polyimides.¹¹ The rheological properties and thermal stability of the systems were studied. The AFR-PE-2 system exhibited minimum complex viscosity of 10 Poise at a cure temperature of 371 °C, whereas the minimum complex viscosity for AFR-PE-8 systems was 540 Poise. By interpolating, it can be assumed that the minimum complex viscosity for AFR-PE-4 systems lies in this range. The study of thermal decomposition temperatures showed that the cured networks were stable up to a range of 489 °C - 548 °C based on the heating rates used irrespective of the value of '*n*'. Despite the promising

properties polyamides synthesized from AFR-PE-4 oligomers, the moisture absorption rate was considerably high making them unsuitable for marine applications.



Scheme 1-1 : Synthesis of AFR-PE-*n* imide oligomers¹¹

Also, the value and temperature of the minimum melt viscosity of the oligomeric system, along with the solid-liquid phase transition temperature, needed to be lowered to facilitate the increase to increase the processing window. Additionally, the molecular weight for the oligomeric systems was not constant since the value of *n* varies, and therefore the properties vary with the molecular weight of the oligomeric systems.¹²

1.2 Silsesquioxanes

1.2.1 Condensed Polyhedral Oligomeric Silsesquioxanes.

Organo-functionalized silsesquioxanes have emerged as a fascinating novel field for modern technology.^{13–16} Polyhedral oligomeric silsesquioxanes (POSS) are unique hybrid organic-inorganic materials with a general chemical composition of $(\text{RSiO}_{1.5})_n$, where each silicon atom is connected to three oxygen atoms. The R group can be a hydrogen atom, or it can be any alkyl, alkylene, aryl, arylene, or organo-functional derivatives of alkyl, alkylene, aryl, or arylene groups¹⁷, and the shape of the structure varies between partial cages, closed cages

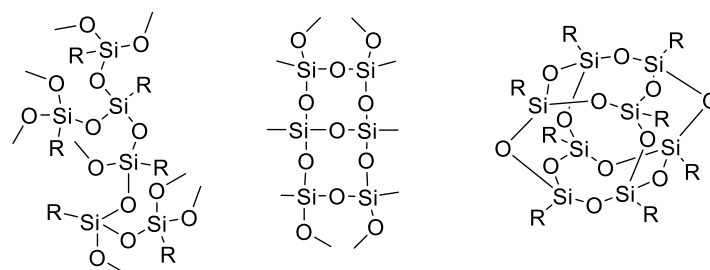
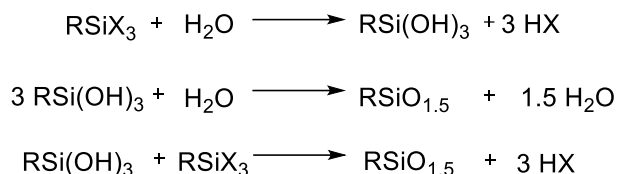


Figure 1-2 : Random, ladder and cage-like structures of silsesquioxanes

or random cages as shown in Figure 1-2. The term oligo- denotes the presence of several silsesquioxane units in the compound. The term silsesquioxane can be divided as *sil-* silicon; *sesqui-* each Si atom is bound to an average of one and a half oxygens; *ane-* each Si atom is attached to one hydrocarbon group; the silicon-oxygen cluster forms a polyhedron (cage) and not a cube as the bond angles between Si-O-Si and O-Si-O is not equal to 90 °C. Among these POSS materials, octa-silsesquioxanes ($\text{R}_8\text{Si}_8\text{O}_{12}$, T_8) have been primarily investigated; they consist of a rigid, cubic inorganic silica core with eight organic corner groups.

Silsesquioxane was first synthesized in 1946 from the thermal analysis of the polymeric products of the hydrolysis of methyl trichlorosilane reaction by Scott.¹⁸ The two-step synthetic process involves the hydrolysis of methyl trichlorosilane to form the trisilanol derivative, followed by condensation to form thermally- stable organofunctional silsesquioxanes. Sprung and Guenther¹⁹

later initiated the development of this area by modifying and optimizing the method done by Scott. The most used reaction for synthesizing POSS is via hydrolytic condensation of trifunctional monomers where 'X' can be a reactive group such as halogen or alkoxy, or acetoxy group and 'R'



Scheme 1-2 : Synthesis of POSS molecule via hydrolytic condensation of monomers

is a thermally stable group such as alkyl or phenyl.²⁰ The yield of the reaction depends on various processing factors such as the type of the functional group used, the concentration of the reactants and the intermediates in the reaction, the nature of the solvent used for the reaction, the type of catalyst used, the temperature at which the reaction is carried out and finally upon the rate and quantity of water addition in the reaction. After numerous optimization trials, the silsesquioxanes can now be obtained in the 88-89 % yield range. These POSS molecules have some definite advantages over the other nanosized fillers. To begin with, most of the other nanoscale inorganic agents have a size distribution, which leads to non-uniform dispersion in the matrices of the thermosets. The POSS moieties have a well-defined shape and can be well dispersed in polymer matrices with proper functionalization. Also, the number of active functional groups on other nanoscale agents is poorly defined. This various number of active functional groups led to variations in the properties of the final product with variations in synthesis batches. POSS has an exact number of organic groups on the corners. These groups can be altered to be reactive or non-reactive to suit the application's needs.

One of the most synthesized POSS cages around the year 1980s was Hydrido-octasilsesquioxane, ($\text{H}_8\text{Si}_8\text{O}_{12}$) and Octakis-(Hydridodimethylsiloxy)Octasilsesquioxane, ($\text{H}(\text{CH}_3)_2\text{SiO}_8\text{Si}_8\text{O}_{12}$). The POSS cages were further modified via hydrosilylation reaction using polymerizable groups to form

octa-functional macromers to modify various polymers. POSS can be introduced into polymer matrices to produce novel composite materials with various advantageous properties.^{21–24}

1.2.2 Incompletely Condensed Polyhedral Oligomeric Silsesquioxanes

Incompletely condensed polyhedral oligomeric silsesquioxanes $[R_7Si_7O_9(OH)_3]$ contain Si-OH groups, which can be found in silica or silicate surfaces, thus providing a pathway for a suitable model compound for investigating and the study of silica surfaces and their interactions with polymeric surfaces. The incompletely condensed contain freely available hydroxyl groups, which can be readily reacted with alkoxysilanes or chlorosilanes to form functional end groups. Despite synthesizing and characterizing various incompletely condensed silsesquioxanes, the commonly synthesized incompletely condensed silsesquioxane is the trisilanol POSS $[R_7T_4D_3(OH)_4]$, which is readily available on a multi-kilogram scale. The most pioneering work performed on these trisilanol cages is done by the Fajer group.^{25–29} The group synthesized incompletely condensed silsesquioxanes via acid/base mediated hydrolytic cleavage of condensed POSS cages. The reaction can be carried out using triflic acid or methanesulfonic acid, which can cause cleavage of the Si - O framework, leading to the rearrangement of the cages to form incompletely condensed silsesquioxanes. A base such as NEt_3OH can also be used to rearrange the cages and, upon further hydrolysis, form trisilanol cages.

Kawakami *et.al*^{30,31} developed incompletely condensed octa-phenyl double-decker-shaped silsesquioxane tetra-silanol ($DDPh_8T_8(OH)_4$) by cleavage and rearrangement of POSS cages. These $DDPh_8T_8(OH)_4$ moieties can be mono-, di- or tetra-functionalized using chlorosilanes. Functionalization usually occurs via side capping of the silanol groups in the presence of a weak base. Numerous functional groups can be side capped onto the $DDPh_8T_8(OH)_4$, forming a stable

DDSQ cage that can be further used as a monomer to form thermally stable thermosets, as a filler in a polymer matrix, or as a nanosized coupling agent between polymer matrix and carbon filler.

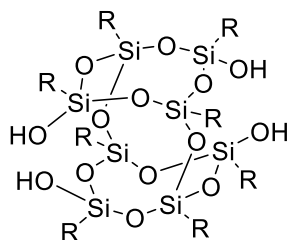


Figure 1-3 : Partially condensed Octa phenyl double-decker shaped silsesquioxane tetra-silanol
Barry et al. have established a novel synthetic route to obtain the symmetrical partially condensed Octa phenyl double-decker-shaped silsesquioxane tetra-silanol using dodecaphenylT₁₂ (Ph₁₂T₁₂) as a starting material. Ph₁₂T₁₂ was treated with four equivalents of aqueous NaOH in isobutanol at 90 °C for 24 h. It was found that reacting completely condensed Ph₁₂T₁₂ with NaOH affected the selective fissure of Si-O-Si bonds.

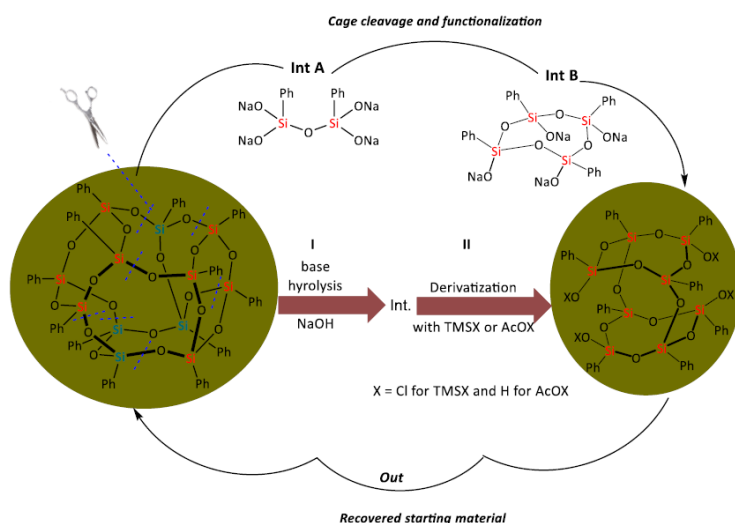


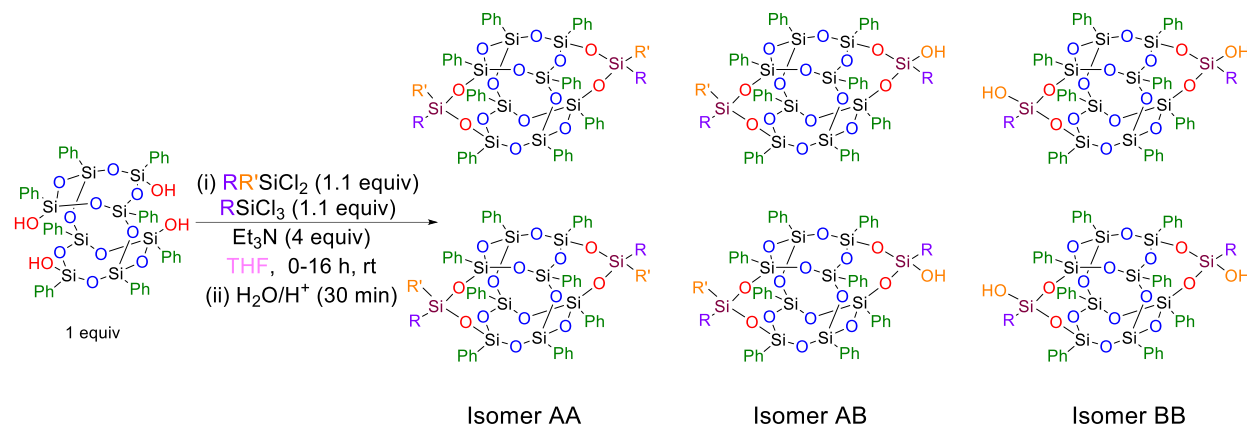
Figure 1-4 : Graphical abstract for Base-Promoted Hydrolysis of Dodecaphenyl Silsesquioxane into partially condensed octaphenyl silsesquioxane

The crude product was silylated with TMSCl in order to aid in the identification of the reaction products; upon studying the mass spectral data from a time-resolved point to early formation of a tetracyclo siloxane as a critical intermediate for the formation of the ‘double-decker’ shaped silsesquioxane.

1.3 Capped DDSQ systems

The DDSQ tetrol can be capped using dichlorosilanes, leading to the unavoidable production of isomers. The capping reaction and the ratio of the isomers depend on the type of dichlorosilane used.

The work on the isolation of these isomers has been minimal. The primary method of separating these isomers is based on solubility differences and hence via fractional recrystallization. The isomers have vastly different properties when isolated compared to the isomeric mixture. Properties such as melting temperature and rheology of the isolated compounds are vastly different from the isomeric mixture and vary with the compounds' ratio in the isomeric mixture.



Scheme 1-3 : Capping of DDSQ tetrol using dichlorosilanes.

1.4 Isomers of capped DDSQ compounds

In 2013, low-viscosity DDSQ-based polyamides were reported by Schoen³³. *meta* and *para* methyl-amino phenyl dichlorosilanes were used together to condense $\text{Ph}_8\text{DDSQ}(\text{OH})_4$. This capping scheme created a mixture containing regio- (*meta* and *para*) and stereo- (*cis* and *trans*) isomers in the final condensed product. Once the products had been synthesized, phenyl ethynyl phthalic anhydride was used to form fully imidized oligomers (DDSQ-PEPI) (Figure 1-5). Compound 3a is a symmetrical *meta-meta* structure, 3c is a symmetrical *para-para* structure, and 3b is an asymmetrical *meta-para* structure.

All the systems have *cis* and *trans* isomers concerning the DDP₈T₈ cage about the D-Silicon. Based on the assumption of a rate-independent reaction between dichlorosilane and silanol, the isomer mixture as prepared (in Figure 1-5) should contain 25% of isomer AA, 25% of isomer BB, and 50% isomer AB. The thermal stability of all these five samples in air and nitrogen was evaluated using thermogravimetric Analysis (TGA). The steady-state shear results suggest that the mixture's viscosity can be altered by orders-of-magnitude by altering the ratios of isomers. The *trans* para-DDSQ-PEPI showed a more substantial effect on the viscosity alteration than the *cis* para-DDSQ-PEPI. No significant differences were found. The mixtures also exhibited eutectic-like characteristics. Due to the organic content of the imide group, the amount of crystallinity is lowered, but the *trans-cis* mixture retains its crystallinity. Thus, the inorganic core provides the durability needed at elevated temperatures and relatively low-moisture uptake, while organic moiety enables processing to composite structures. This class of low-viscosity oligoimide thermosetting materials can provide needed control in viscosity which is expected to reduce the processing hurdles of reinforced composites by controlling the ratio of isomers in resin while retaining oxidative thermal stability over the current organic oligoimide resins.

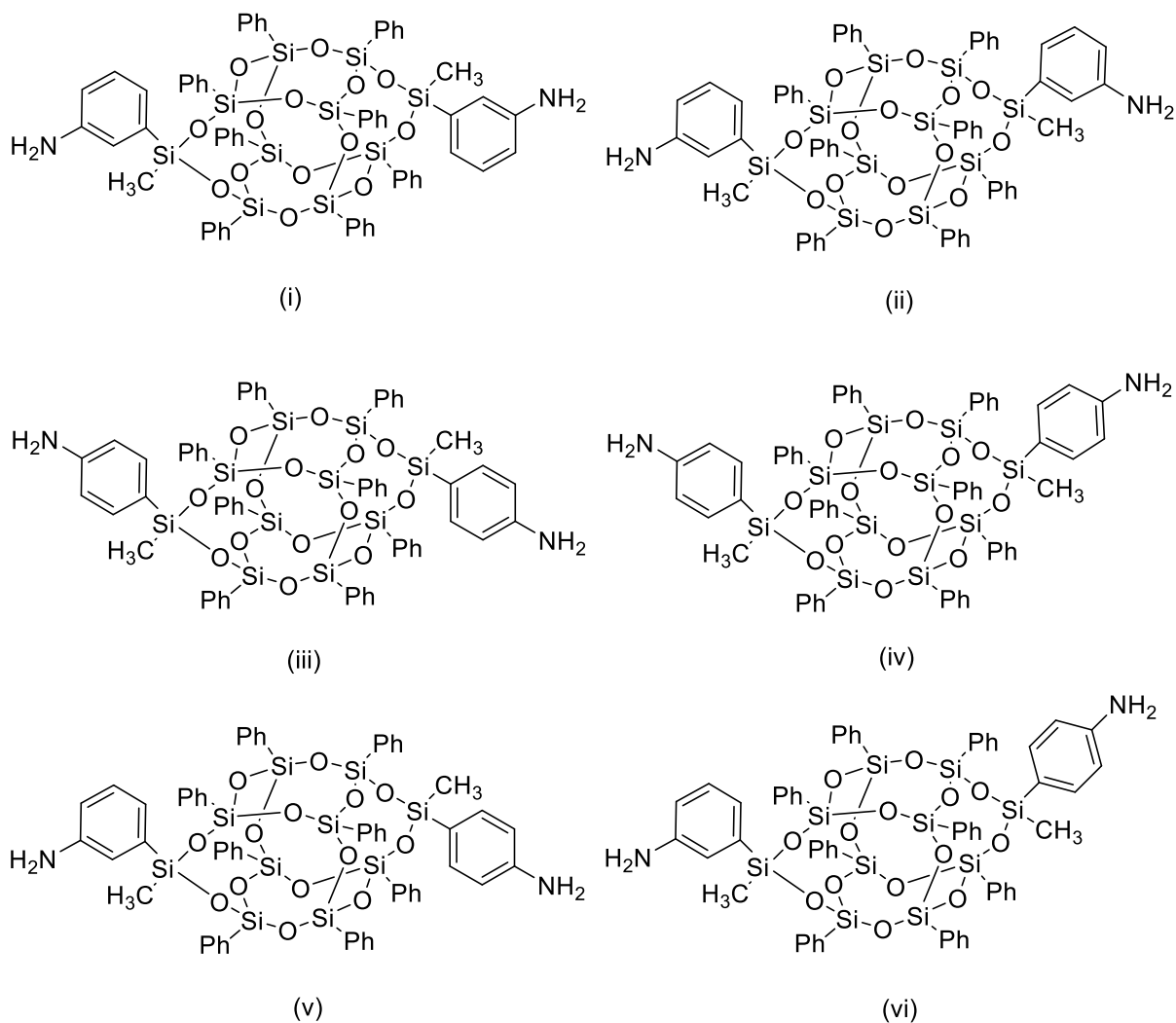


Figure 1-5 : Different isomers of octaphenyl double-decker shaped silsesquioxane tetrasilanol - (i) trans-Ph₈DDSQ (meta-aminophenyl)₂(Me)₂ (ii) cis Ph₈DDSQ (meta-aminophenyl)₂(Me)₂ (iii) trans-Ph₈DDSQ (para-aminophenyl)₂(Me)₂ (iv) cis Ph₈DDSQ (meta-aminophenyl)₂(Me)₂ (v) trans-Ph₈DDSQ (meta-aminophenyl)(para-aminophenyl)(Me)₂ (vi) cis Ph₈DDSQ (meta-aminophenyl)(para-aminophenyl)(Me)₂

The attempted synthesis of DDPH₈T₈-PEPI possessed several disadvantages, such as diminished yields and being time intensive. Even though the moisture uptake has been reduced compared to AFR-PE-4 material, it may be possible to further reduce the uptake by eliminating the imide group and directly capping the DDPH₈T₈(OH)₄ cage with phenylethynyl end-capped chlorosilanes.

Vogelsang D.³⁴ also successfully separated the *cis* and *trans* isomers of capped DDSQ compounds using HPLC. He discovered that a polar group's presence could significantly help separate the isomers from obtaining nearly pure *cis* and near pure *trans* compounds. It was observed that with the addition of two different chlorosilanes for capping sites on DDP₈T₈(OH)₄, symmetrically and

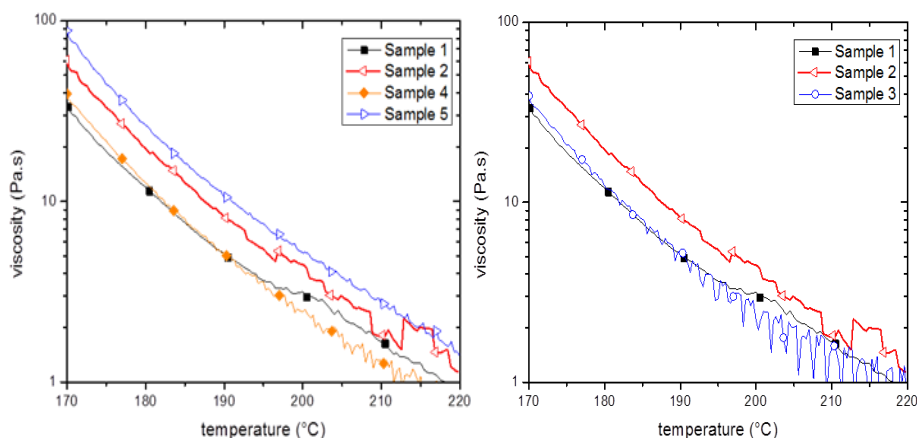


Figure 1-6 : Viscosity measurements for PEP amide based isomeric system

asymmetrically capped DDP₈T₈ mixtures are produced. Separating these products was possible because various hydroxyl groups are present in each molecule. By changing the ratios of the chlorosilanes, an attempt can be made to achieve the statistical ratio of isomers. The deviations from the statistical ratio of isomers are due to the difference in the rate of side-capping being significantly affected by steric hindrance from the side-capping agent.

1.5 Motivation

The AFR PE-n system of organic polyamides provides high thermal stability and good mechanical properties for high-temperature applications. The system can be tuned to meet the application's specific requirements using a blend of AFR PE-n systems. This fine-tuning might lead to a lowering of T_g . Also, water is formed during the synthesis step, which might get trapped in the final structure leading to weakening mechanical properties. DDSQ PEPI systems have a robust hybrid core that helps achieve high T_g values. These capped DDSQ structures can be easily

synthesized using dichlorosilanes, and based on the polarity difference in the isomers, nearly pure forms of the isomers can be obtained by column chromatography techniques. By adjusting the ratio of cis and trans isomers, it is possible to adjust the final properties of the network structure. Also, it may be possible to alter the crystallinity and viscosity of the system by having different isomeric configurations of a capped functional group on either side of the cage, thereby helping to improve the cure kinetics. To this effect, a clean, optimized route must be developed to synthesize the chlorosilanes required to side-cap the cage structures. The structure's mechanical, thermal, and rheological properties must be studied. The aims of this report include the following:

1. To explore material applications based on the possible capped cage structures to be synthesized from this work.
2. To explore an alternative methodology for capping DDSQ tetrol to study the effect of non-solvent on the ratio of isomeric products.
3. Design and carefully analyze the synthesis routes to obtain clean chlorosilanes and synthesize an isomeric mixture of phenylethynyl end-capped DDP₈T₈ cages.
4. Synthesis of a novel partially capped Ph₈T₈ diol and further capping with chlorosilanes to synthesize capped basket-like asymmetrical DDSQ compounds.
5. Study of thermal and structural characteristics for capped DDP₈T₈ cages.

REFERENCES

- (1) Luo, Y.-R. Bond Dissociation Energies. *CRC Handbook of Chemistry and Physics* 2012, 89, 89.
- (2) Kreuz, J. A. Copolyimide-Iosimide Polymers. 3413267, November 26, 1968. <https://pdfpiw.uspto.gov/67/132/034/1.pdf> (accessed 2020-03-22).
- (3) Broome, J. T.; Voll, B. A.; Corbett, G.; GB; Goodson, J.; Yuan, Y.; Peterson, E. R. United States Patent: 6305468 - Downhole Screen and Method of Manufacture. 6305468, October 23, 2001. <http://patft.uspto.gov/netacgi/nph-Parser?Sect1=PTO1&Sect2=HITOFF&d=PALL&p=1&u=%2Fnetacgi%2FPTO%2Fsrchnum.htm&r=1&f=G&l=50&s1=6305468.PN.&OS=PN/6305468&RS=PN/6305468> (accessed 2020-03-22).
- (4) Vannucci, R. D. PMR Polyimide Compositions for Improved Performance. *32nd International SAMPE Symposium and Exhibition* 1987, 13.
- (5) Srinivasan, S. A.; McGrath, J. E. Amorphous Phenolphthalein-Based poly(Arylene Ether) Modified Cyanate Ester Networks: 1. Effect of Molecular Weight and Backbone Chemistry on Morphology and Toughenability. *Polymer* 1998, 39 (12), 2415–2427. [https://doi.org/10.1016/S0032-3861\(97\)00598-3](https://doi.org/10.1016/S0032-3861(97)00598-3).
- (6) Clair, A. K. S.; Clair, T. L. S. Structure-Property Relationships of Isomeric Addition Polyimides Containing Nadimide End Groups. *Polymer Engineering & Science* 1976, 16 (5), 314–317. <https://doi.org/10.1002/pen.760160507>.
- (7) Swanson, S. A.; Fleming, W. W.; Hofer, D. C. Acetylene-Terminated Polyimide Cure Studies Using Carbon-13 Magic-Angle Spinning NMR on Isotopically Labeled Samples. *Macromolecules* 1992, 25 (2), 582–588. <https://doi.org/10.1021/ma00028a015>.
- (8) Harris, F. W.; Pamidimukkala, A.; Gupta, R.; Das, S.; Wu, T.; Mock, G. Synthesis and Characterization of Reactive End-Capped Polyimide Oligomers. *Journal of Macromolecular Science: Part A - Chemistry* 1984, 21 (8–9), 1117–1135. <https://doi.org/10.1080/00222338408056595>.
- (9) Connell, J. W.; Smith, J. G.; Hergenrother, P. M.; Rommel, M. L. Neat Resin, Adhesive and Composite Properties of Reactive Additive/PETI-5 Blends. *High-Performance Polymers* 2000, 12 (2), 323–333. <https://doi.org/10.1088/0954-0083/12/2/307>.
- (10) Johnston, J. A.; Li, F. M.; Harris, F. W.; Takekoshi, T. Synthesis and Characterization of Imide Oligomers End-Capped with 4-(Phenylethynyl)Phthalic Anhydrides. *Polymer* 1994, 35 (22), 4865–4873. [https://doi.org/10.1016/0032-3861\(94\)90745-5](https://doi.org/10.1016/0032-3861(94)90745-5).
- (11) Lincoln, J. Structure-Property Processing Relationships and the Effects of Physical Structure on the Hygro-Thermal Durability and Mechanical Response of Polyimides, Michigan State University, 2001.

- (12) Simone, C. D.; Scola, D. A. Phenylethynyl End-Capped Polyimides Derived from 4,4'-(2,2,2-Trifluoro-1-Phenylethylidene)Diphthalic Anhydride, 4,4'-(Hexafluoroisopropylidene)Diphthalic Anhydride, and 3,3',4,4'-Biphenylene Dianhydride: Structure–Viscosity Relationship. *Macromolecules* 2003, 36 (18), 6780–6790. <https://doi.org/10.1021/ma0300701>.
- (13) Constable, G. S.; Lesser, A. J.; Coughlin, E. B. Morphological and Mechanical Evaluation of Hybrid Organic–Inorganic Thermoset Copolymers of Dicyclopentadiene and Mono- or Tris(Norbornenyl)-Substituted Polyhedral Oligomeric Silsesquioxanes. *Macromolecules* 2004, 37 (4), 1276–1282. <https://doi.org/10.1021/ma034989w>.
- (14) Xu, H.; Kuo, S.-W.; Lee, J.-S.; Chang, F.-C. Preparations, Thermal Properties, and T_g Increase Mechanism of Inorganic/Organic Hybrid Polymers Based on Polyhedral Oligomeric Silsesquioxanes. *Macromolecules* 2002, 35 (23), 8788–8793. <https://doi.org/10.1021/ma0202843>.
- (15) Harrison, P. G. Silicate Cages: Precursors to New Materials. *Journal of Organometallic Chemistry* 1997, 542 (2), 141–183. [https://doi.org/10.1016/S0022-328X\(96\)06821-0](https://doi.org/10.1016/S0022-328X(96)06821-0).
- (16) Fu, B. X.; Lee, A.; Haddad, T. S. Styrene–Butadiene–Styrene Triblock Copolymers Modified with Polyhedral Oligomeric Silsesquioxanes. *Macromolecules* 2004, 37 (14), 5211–5218. <https://doi.org/10.1021/ma049753m>.
- (17) Baney, R. H.; Itoh, M.; Sakakibara, A.; Suzuki, T. Silsesquioxanes. *Chem. Rev.* 1995, 95 (5), 22. <https://doi.org/10.1021/cr00037a012>.
- (18) Scott, D. W. Thermal Rearrangement of Branched-Chain Methylpolysiloxanes ¹. *J. Am. Chem. Soc.* 1946, 68 (3), 356–358. <https://doi.org/10.1021/ja01207a003>.
- (19) Sprung, M. M.; Guenther, F. O. The Partial Hydrolysis of Ethyltriethoxysilane. *J. Am. Chem. Soc.* 1955, 77 (15), 3996–4002. <https://doi.org/10.1021/ja01620a014>.
- (20) Voronkov, M. G.; Lavrent'yev, V. I. Polyhedral Oligosilsesquioxanes and Their Homo Derivatives.
- (21) Gnanasekaran, D.; Madhavan, K.; Reddy, B. S. R. Developments of Polyhedral Oligomeric Silsesquioxanes (PaSS), Pass Nanocomposites and Their Applications: A Review. 28.
- (22) Han, D.; Wen, T.; Han, G.; Deng, Y.; Deng, Y.; Zhang, Q.; Fu, Q. Synthesis of Janus POSS Star Polymer and Exploring Its Compatibilization Behavior for PLLA/PCL Polymer Blends. *Polymer* 2018, 136, 84–91. <https://doi.org/10.1016/j.polymer.2017.12.050>.
- (23) Han, D.; Zhang, Q.; Chen, F.; Fu, Q. Using POSS–C₆₀ Giant Molecules as a Novel Compatibilizer for PS/PMMA Polymer Blends. *RSC Adv.* 2016, 6 (23), 18924–18928. <https://doi.org/10.1039/C6RA00218H>.
- (24) Fina, A.; Monticelli, O.; Camino, G. POSS-Based Hybrids by Melt/Reactive Blending. *J. Mater. Chem.* 2010, 20 (42), 9297. <https://doi.org/10.1039/c0jm00480d>.

- (25) Feher, F. J.; Newman, D. A.; Walzer, J. F. Silsesquioxanes as Models for Silica Surfaces. *J. Am. Chem. Soc.* 1989, *111* (5), 1741–1748. <https://doi.org/10.1021/ja00187a028>.
- (26) Lichtenhan, J. D.; Vu, N. Q.; Carter, J. A.; Gilman, J. W.; Feher, F. J. Silsesquioxane-Siloxane Copolymers from Polyhedral Silsesquioxanes. *Macromolecules* 1993, *26* (8), 2141–2142. <https://doi.org/10.1021/ma00060a053>.
- (27) Jones, W. D.; Feher, F. J. Comparative Reactivities of Hydrocarbon Carbon-Hydrogen Bonds with a Transition-Metal Complex. *Acc. Chem. Res.* 1989, *22* (3), 91–100. <https://doi.org/10.1021/ar00159a002>.
- (28) Feher, F. J.; Budzichowski, T. A.; Blanski, R. L.; Weller, K. J.; Ziller, J. W. Facile Syntheses of New Incompletely Condensed Polyhedral Oligosilsesquioxanes: [(C-C5H9)7Si7O9(OH)3], [(c-C7H13)7Si7O9(OH)3], and [(c-C7H13)6Si6O7(OH)4]. *Organometallics* 1991, *10* (7), 2526–2528. <https://doi.org/10.1021/om00053a070>.
- (29) Feher, F. J.; Budzichowski, T. A.; Rahimian, K.; Ziller, J. W. Reactions of Incompletely-Condensed Silsesquioxanes with Pentamethylantimony: A New Synthesis of Metallasilsesquioxanes with Important Implications for the Chemistry of Silica Surfaces. *J. Am. Chem. Soc.* 1992, *114* (10), 3859–3866. <https://doi.org/10.1021/ja00036a038>.
- (30) Lee, D. W.; Kawakami, Y. Incompletely Condensed Silsesquioxanes: Formation and Reactivity. *Polym J* 2007, *39* (3), 230–238. <https://doi.org/10.1295/polymj.PJ2006169>.
- (31) Li, Z.; Kawakami, Y. Formation of Incompletely Condensed Oligosilsesquioxanes by Hydrolysis of Completely Condensed POSS via Reshuffling. *Chem. Lett.* 2008, *37* (7), 804–805. <https://doi.org/10.1246/cl.2008.804>.
- (32) Humphreys, J.; Pop, F.; Hume, P. A.; Murphy, A. S.; Lewis, W.; Davies, E. S.; Argent, S. P.; Amabilino, D. B. Solid State Structure, and Properties of Phenyl Diketopyrrolopyrrole Derivatives. *CrystEngComm* 2021, *23* (8), 1796–1814. <https://doi.org/10.1039/D1CE00039J>.
- (33) Schoen, B. Aminophenyl Double Decker Silsesquioxanes: Spectroscopic Elucidation, Physical and Thermal Characterization, and Their Applications, Michigan State University.
- (34) Vogelsang, D. F.; Dannatt, J. E.; Maleczka, R. E.; Lee, A. Separation of Asymmetrically Capped Double-Decker Silsesquioxanes Mixtures. *Polyhedron* 2018, *155*, 189–193. <https://doi.org/10.1016/j.poly.2018.08.016>.

2 APPLICATION OF ASYMMETRICALLY CAPPED DDSQ AS A BRIDGING AGENT

2.1 Introduction

Vinyl ester resins belong to the thermoset polymeric materials widely used in the composites industry.^{1,2} Vinyl ester resin is synthesized by esterifying epoxy resins with unsaturated monocarboxylic acids. Vinyl ester resins have numerous applications requiring high chemical and corrosion resistance. They are also used in applications where properties such as enhanced water barrier and low moisture uptake, low shrinkage, and good dimensional stability are required. Generally, these resins are used in marine, pipeline, automotive, and electronics industries.³⁻⁹ A graphene sheet is a single atomic layer of carbon atoms (sp^2 hybridized) in a two-dimensional array. Since the discovery of graphene in 2004,¹⁰ various graphene-filled composites have been synthesized and studied to achieve better mechanical, thermal, and electrical properties.^{3,11-14} The improved properties are due to the large surface area of graphene compared to other carbon-based nano-fillers. The graphene sheets help improve the material's fracture toughness, mitigating the crack propagation mechanism. The moisture uptake is reduced as the path of fluids becomes more tortuous through the polymer matrix. The graphene sheets must be well dispersed in the matrix and strongly bond with the matrix to enhance the graphene composites' properties.⁴ But they tend to agglomerate due to strong Van-der Waals forces between the sheets.¹⁵ The surface is almost inert with the presence of a small percentage of non-carbon functional groups leading to a poor bonding between the matrix and the filler.

There are several common approaches to the surface treatment of graphene, each serving a specific purpose and achieving distinct modifications¹⁶. Some prominent techniques include chemical functionalization, physical modifications, and deposition of thin films or coatings.¹⁶ Chemical functionalization involves introducing various chemical groups or molecules onto the graphene surface, altering its properties. Functionalization can enhance the dispersibility of graphene in

solvents, improve its compatibility with polymers or other materials, and introduce specific functionalities. Standard chemical functionalization methods include covalent functionalization and non-covalent functionalization^{17–19}. In covalent functionalization, reactive species, such as diazonium salts or organic molecules containing functional groups (e.g., -OH, -COOH), react with the carbon atoms on the graphene surface, forming covalent bonds. Covalent functionalization can alter graphene's electronic structure, surface energy, and chemical reactivity. The most used covalent functionalization technique is oxidation. Oxidation treatment involves exposing graphene to oxidizing agents such as oxygen, ozone, or nitric acid. This process introduces oxygen-containing functional groups, such as hydroxyl (-OH), carbonyl (C=O), or carboxyl (-COOH) groups, onto the graphene surface. Oxidation can render graphene more hydrophilic, increase its compatibility with other materials, and provide sites for further functionalization. In the non-covalent functionalization approach, the adsorption of molecules or nanoparticles onto the graphene surface through weak molecular interactions such as Van der Waals forces or π - π stacking. Non-covalent functionalization can improve the dispersion of graphene in solvents or matrices, and it is reversible, allowing for easy removal of the functionalizing agents.

Physical treatments can alter the graphene surface by mechanical, thermal, or plasma-based methods.^{20–23} These modifications can enhance graphene's structural integrity, wettability, and adhesion. The various types of physical treatment techniques are listed. In mechanical exfoliation, the controlled application of mechanical forces, such as rubbing or peeling, to detach graphene flakes from a graphite source is done. Mechanical exfoliation is the basis for obtaining high-quality graphene flakes, such as those used in research or device fabrication. The next type of physical treatment is annealing. Annealing refers to the controlled heating of graphene to modify its structure and properties. Thermal treatment can improve the crystallinity, remove defects, and

restore the sp^2 carbon network of graphene, leading to improved electrical conductivity and carrier mobility. Plasma treatment involves subjecting graphene to low-pressure plasma, which can introduce functional groups, etch the surface, or enhance its adhesion to other materials. Plasma treatment can also improve the hydrophilicity or hydrophobicity of graphene, depending on the specific plasma chemistry used.

Surface treatments can also involve depositing thin films or coatings onto the graphene surface to impart specific functionalities or enhance performance^{16,20,24–26}. These methods include chemical vapor deposition and atomic layer deposition. CVD is a widely used technique to grow thin films or layers of materials on graphene. By controlling the deposition parameters, various materials like metals, metal oxides, or polymers can be deposited onto graphene, imparting properties such as electrical conductivity, barrier properties, or mechanical strength. Atomic layer deposition (ALD) is a precise thin film deposition technique that enables the growth of conformal and uniform coatings on graphene. ALD can deposit thin layers of materials like metal oxides or organic polymers with controlled thickness and composition, offering precise tailoring of surface properties.

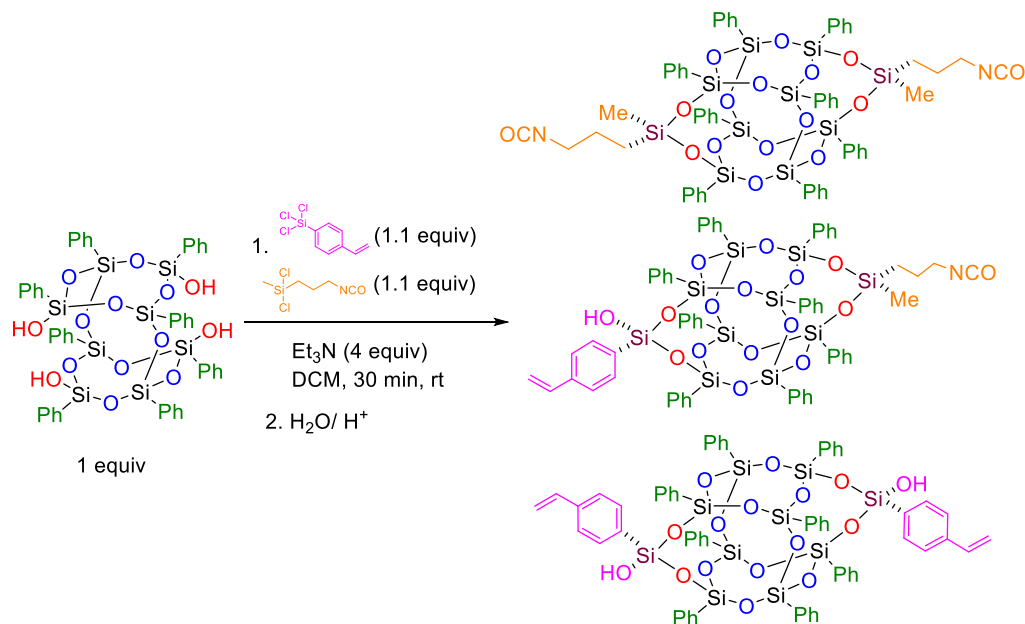
The oxidized graphene (GO) derivative increases the surface's quantity of non-carbon functional groups. GO sheet has epoxide and hydroxyl groups on the basal plane, whereas the edges have carboxyl and carbonyl functional groups. The functional groups make GO water dispersible and can be used to improve nanofiller dispersion in the matrix²⁷. GO is usually synthesized from Graphene nanoplatelets using the modified Hummer's process.^{28,29} To meet the ever-increasing demand for high-performance thermosets, efforts have been made to incorporate GO nanofillers into polymer matrices.^{4,5,14,29–32} The most common way to disperse these GO nanofillers is using sonicators. Sonicators use large amounts of energy and can be challenging to use commercially.

Also, SEM images show the agglomeration of GO nanofillers in the matrix. The bonding between the GO surfaces functional groups and the matrix was improved using various coupling agents. These coupling agents include small molecules such as silanes or organo-amines, but they can also include polymeric macromolecules such as epoxy or nylon, or polypropylene. The surface of GO was intercalated with organic moieties to ensure the separation of layers, but due to the absence of a rigid three-dimensional structure, the method proved to be ineffective.

2.2 Formulation of modified Derakene™ resins

POSS has been proved to be an effective dispersant in multiple cases. Based on this approach, an asymmetrically capped DDSQ system was developed as a coupling agent between the GO nanofiller and the polymer matrix. Derakene 411-350™ is a styrene-vinyl ester resin used as the polymer matrix. One end of the DDSQ system was capped with a cyanate group, while the other was capped with styrene moiety. The coupling between the nanofiller and the coupling agents can be done by simple mechanical stirring using a magnetic stirrer. Although using a molecule that has isocyanate and styrene at the opposite ends may enable GO to form a covalent bond to VE resin, the advantage of using the asymmetric DDSQ is the 3D nature of the SiO core and (maybe the phenyl group surrounding the SiO core). Using X-ray diffraction, we observed increases in the layer spacing of graphene nanoplate when GO is modified with isocyanate-DDSQ-styrene. Increases in the layer spacing of plate-like reinforcement such as GO can significantly improve mechanical performance and reduce moisture transport of polymer with the addition of plate-like reinforcement. The cyanate moiety on DDSQ is bounded covalently with the hydroxyl groups on GO, whereas the styrene moiety is incorporated along with the polymer matrix as seen from Scheme 2-2

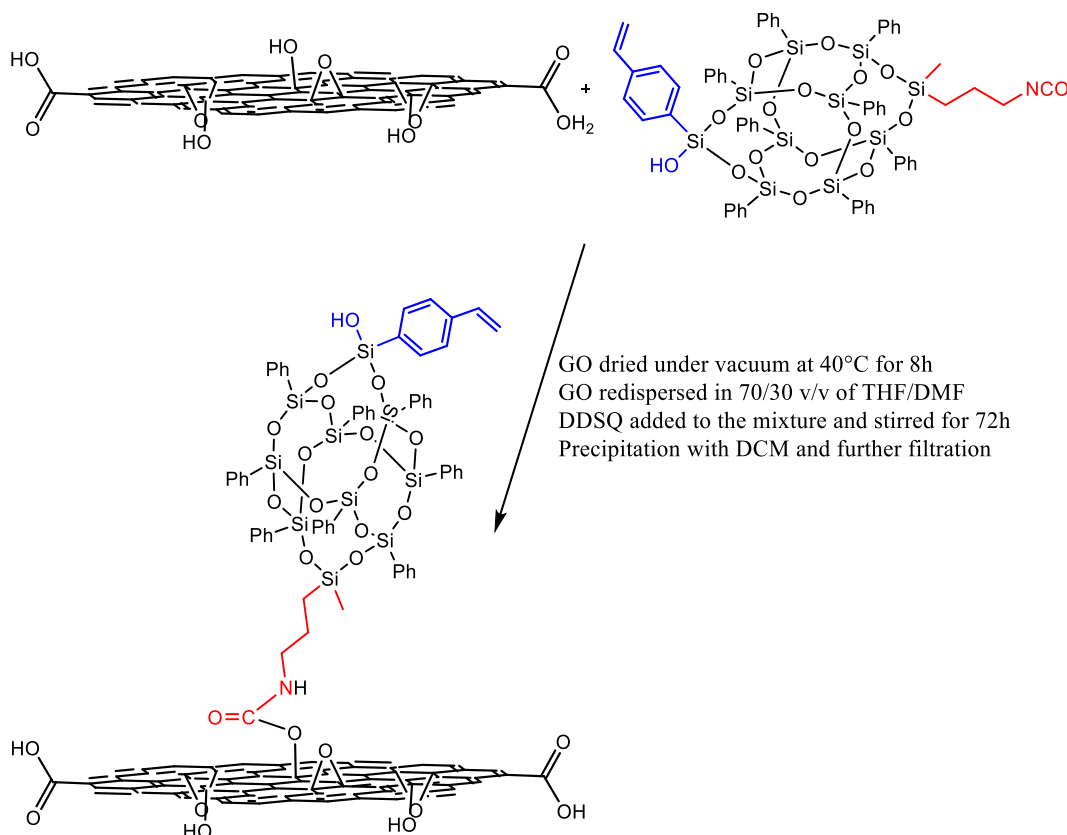
The asymmetrically capped DDSQ compound was synthesized by capping with methyl propyl isocyanate dichlorosilane and styrene trichlorosilane. These chlorosilanes were synthesized using starting from essential reagents. The detailed synthesis of these chlorosilanes has been shown in SI. Once the dichlorosilanes have been synthesized, the capping reaction onto the DDSQ tetrol has



Scheme 2-1 : Asymmetrically capped DDSQ coupling agent grafting with graphene oxide.

been done using DCM as a capping solvent, as shown in Scheme 2-1. The capping reaction produces three different isomeric products. These isomeric products can be separated based on the polarity of the products using flash column chromatography. The hydroxyl group on the capped isomers helps to impart polarity to the capped DDSQ structures. The isomer with two hydroxyl groups is the most polar and elutes last from the column, and the asymmetrical product elutes in between the three isomeric products, whereas the compound with no hydroxyl group elutes first from the column. After separation, the asymmetrically capped DDSQ compound is then grafted onto GO. No high-energy methods, such as sonicators, were used to perform the grafting. A simple grafting method, such as mechanical stirring using a magnetic stirrer, has been employed. The solvent used to disperse GO was a 70/30 v/v mixture of THF and DMF. The solution was stirred

for 5 minutes. Afterward, the asymmetrically capped DDSQ was added and stirred for 72 hours. The isocyanate group on asymmetrical DDSQ covalently bonds to the hydroxyl group on the GO surface, giving a firm connection between the GO and the bridging agent. The other end of the asymmetrical DDSQ compound has a styrene handle that can copolymerize with styrene groups in the Derakene™ resin. The grafted DDSQ-GO complex was then dispersed in Derakene resin with a magnetic stirrer for 24 hours. Methyl ethyl ketone peroxide was added to the resin mixture and stirred with a glass rod. The sample was then cast in silicon molds for room temperature curing for 24 hours, followed by curing at 120 °C for 2 hours.



Scheme 2-2 : Grafting of asymmetrically capped DDSQ onto GO surface

2.3 Characterization of cured Derakene™ resin samples

In order to confirm the bridging between GO, the hybrid organic-inorganic bridging material, IR analysis was done, as shown in Figure 2-1. The peaks of interest in this IR data are the peak representing the -OH group and the peak representing the -NH group. The -OH peak present on GO disappears from the grafted DDSQ-GO complex. The -NH group peak can be seen almost overlapping with the peak of the carbonyl group, but it can be distinguished between the peaks seen in GO versus those seen in the DDSQ-GO complex. Also, the -NCO peak in the asymmetrically capped DDSQ compound disappears from the grafted DDSQ-GO complex. This

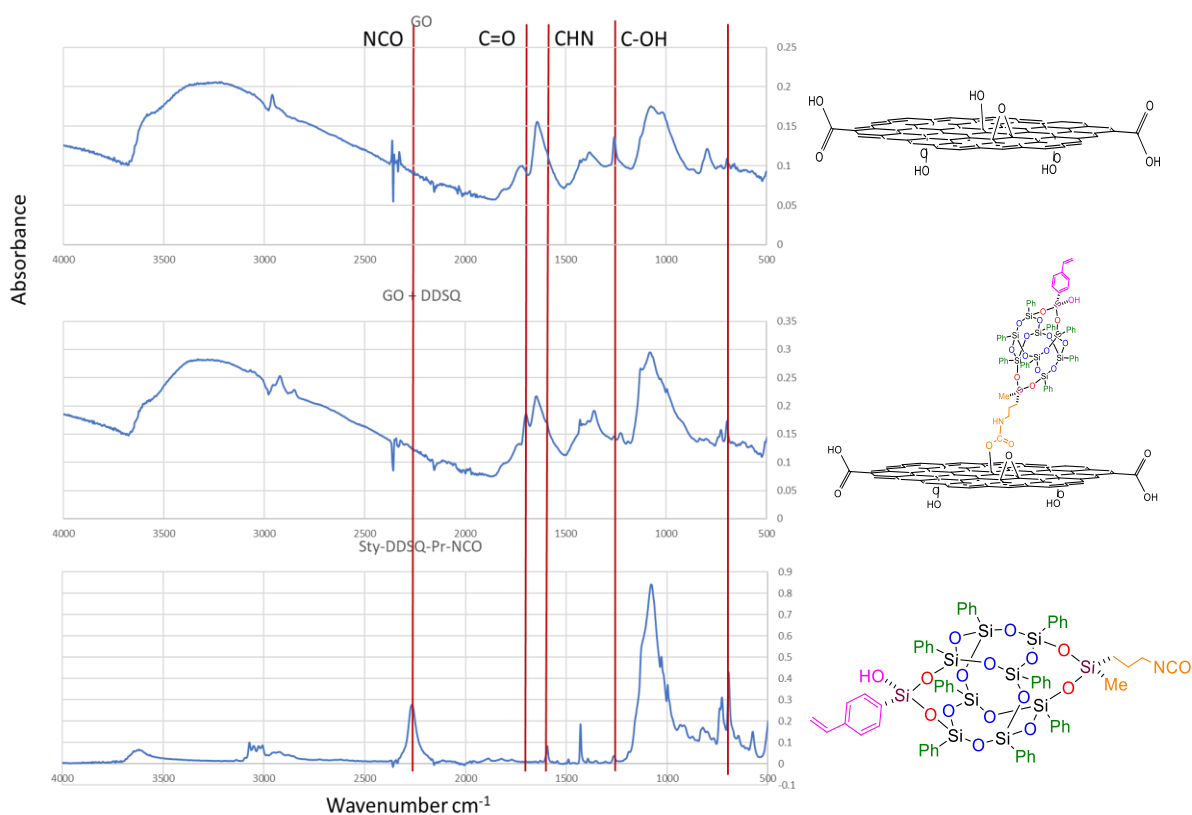


Figure 2-1 : IR analysis to verify grafting of GO with DDSQ compound.

peak demonstrates the strong covalent bonding between the DDSQ and GO. The dispersion of grafted DDSQ-GO complex was studied using optical imaging, as seen in Figure 2-2.

The optical analysis of post-cured resin showed the effectiveness of DDSQ as a coupling agent and a dispersant. As seen in Figure 2-2, the top image is the neat Derakene™ resin with no GO added to it. It is a clear transparent sample. The middle sample represents the Derakene™ sample

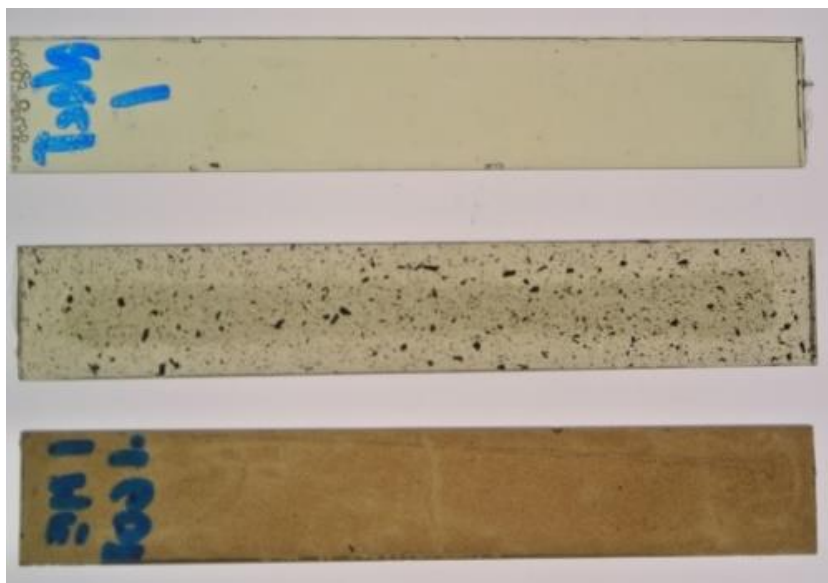


Figure 2-2 : Optical analysis of post cured Derakene resin

mixed with non-treated GO. The image shows that the GO is not well dispersed in the resin. The agglomerated GO spots are visible in the image. The third image shows Derakene™ resin mixed

Table 2-1 : Mechanical properties of modified Derakene™ samples

Sample	Strength (MPa)	Failure Strain (%)
Neat Resin	54.7 ± 19.3	1.6 ± 1.0
+ 0.1 wt% treated GO	51.7 ± 7.5	1.5 ± 0.7
+ 0.2 wt% treated GO	105.1 ± 12.8	3.5 ± 0.8
+ 0.4 wt% treated GO	108.1 ± 19.4	3.9 ± 1.0

with grafted DDSQ-GO complex. The image shows that GO has been well dispersed throughout the resin. Resin samples treated with 0.1, 0.2, and 0.4 wt % DDSQ-GO complex have been formulated, and mechanical testing has been carried out on these samples. The mechanical testing shows that the strength and strain to failure increase upon adding a modified DDSQ-GO complex

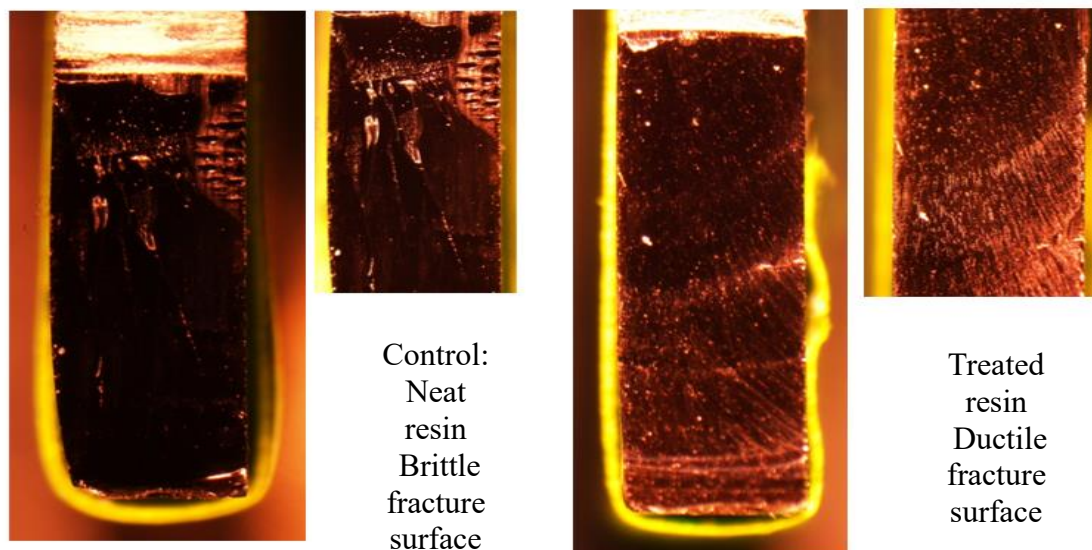


Figure 2-3 : Optical images post fracture surface testing of the samples

to the resin. As the table above shows, adding 0.2 wt % of modified DDSQ-GO complex doubles the strain to failure and the strength of resins. Continued addition above 0.2 wt % results in no change in the strain to failure and the strength of resins. The fracture surface of the resin samples was studied post-sample fracture, as seen in Figure 2-3. Due to GO sheets in the resin samples, the fracture surface and characteristics change from brittle to ductile fracture. This transition is evident from the clean and sharp surface cuts in the control resin, whereas the treated sample has the plastic deformation characteristics as seen in ductile fracture.

In conclusion, a simple, efficient way to disperse Graphene oxide into a polymeric matrix such as Derakene™ was developed. This methodology used simple magnetic stirring to disperse modified GO into polymeric resin compared to high-energy techniques such as sonicators. The bridging between the polymeric matrix and GO has been done using capped DDSQ. Asymmetrically capped

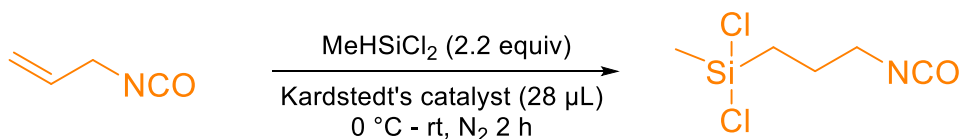
DDSQ formed an amide bridge between the isocyanate group on the DDSQ and the hydroxyl groups on the Graphene oxide surface; the styrene group on DDSQ was polymerized with the Derakene network structure. The nanocomposites of Derakene™ and graphene oxide exhibit a significant improvement in strength and ductility compared to the neat sample.

2.4 Experimental Details

2.4.1 General Information

All manipulations were done under a nitrogen atmosphere using standard Schlenk techniques except otherwise stated. All commercially available chemicals were used as received unless otherwise indicated. Methyl trichlorosilane (MeSiCl_3), Karstedt's catalyst, styrene trimethoxysilane, methyldichlorosilane, vinyl cyanate, boron trichloride (1.0M in hexanes), deuterated chloroform with 1 vol % tetramethylsilane (CDCl_3 -1%TMS), were purchased from Sigma-Aldrich. Graphene nanoplatelet was obtained from XG Sciences. $\text{DDPh}_8\text{T}_8(\text{OH})_4$ was obtained from Hybrid Plastics. Triethylamine (Et_3N) was purchased from Avantor and distilled over calcium hydride before use. Tetrahydrofuran (THF), dichloromethane (DCM), and methanol (MeOH) n-hexanes were purchased from Sigma-Aldrich. THF was distilled over benzophenone and sodium metal at 50 °C under nitrogen. Toluene was distilled over calcium hydride at a temperature of 120 °C. The other solvents were used as purchased without further purification, and the glassware was oven dried. All ^1H , ^{13}C , and ^{29}Si NMR were acquired on an Agilent DirectDrive2 500 MHz NMR spectrometer equipped with a OneProbe operating at 500 MHz for ^1H NMR, 126 MHz for ^{13}C NMR, and 99 MHz for ^{29}Si NMR using CDCl_3 and recorded at 25 °C. ^1H -NMR spectra were recorded with eight scans, a relaxation delay of 1s, and a pulse angle of 45° and referenced to the residual protonated solvent in CDCl_3 (7.24 ppm). ^{13}C -NMR spectra were collected with 254 scans, a relaxation delay of 0.1 s, and a pulse angle of 45°. ^{29}Si NMR spectra were recorded with either 256 scans, a relaxation delay of 25 s, and a pulse angle 45°. Column chromatography was performed on EMD Millipore silica gel 60 columns of 40– 63 Å silica, 230– 400 mesh. Thin-layer chromatography (TLC) was performed on plates of EMD 250- μm silica 60-F254.

2.4.2 Synthesis of methyl(3-propyl isocyanate)dichlorosilane



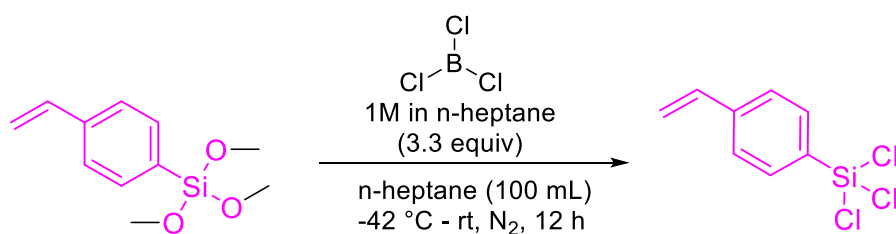
Scheme 2-3 : Reaction scheme for the synthesis of methyl(3-propyl isocyanate)dichlorosilane

To a 100 mL round bottom flask, vinyl isocyanate (1 g, 0.012 mol, one equiv) and a stir bar were added under the N₂ atmosphere. Kardstedt's catalyst (~ 2 % Pt in Xylene) (28 µL), methyl dichlorosilane (2.76 g, 0.024 mol, two equiv), and THF (20 mL) were charged to the flask. The reaction was stirred at room temperature for two h. The solvent and excess methyl dichlorosilane were evaporated at the end of the reaction time. The liquid obtained is then subjected to vacuum distillation (0.01 torr) at 90 °C to obtain the pure product as a liquid in the condensation flask, which was used as is for the next step. The yield of the reaction is 72%

¹H NMR (500 MHz, Chloroform-*d*) δ 3.37 (t, *J* = 6.6 Hz, 2H), 1.85 – 1.76 (m, 2H), 1.22 – 1.14 (m, 2H), 0.80 (d, *J* = 3.6 Hz, 3H). ¹³C NMR (126 MHz, Chloroform-*d*) δ 44.74, 24.44, 18.59, 5.11.

²⁹Si NMR (99 MHz, Chloroform-*d*) δ 32.19.

2.4.3 Synthesis of styryl trichlorosilane



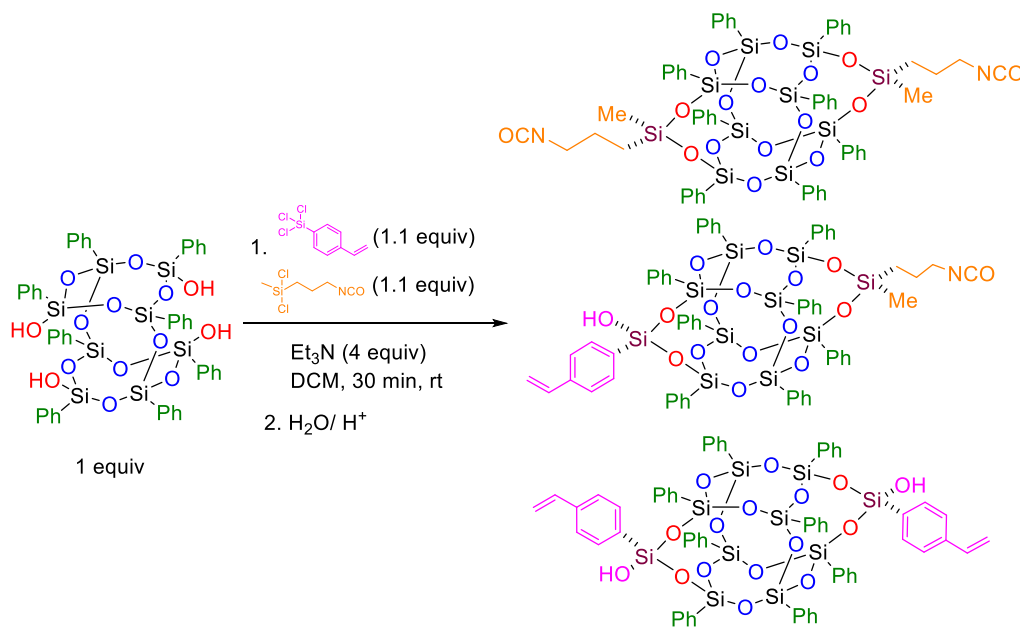
Scheme 2-4 : Reaction scheme for the synthesis of styryl trichlorosilane

To a 100 mL round bottom flask, styrene trimethoxysilane (5 g, 0.022 mol, one equiv) and a stir bar under the N₂ atmosphere were added. The reaction flask was placed in an acetonitrile/ dry ice cooling bath. Boron trichloride (1M in heptane) (78 mL, 0.078 mol, 3.5 equiv) and n-heptane (15

ml) was charged to the flask. The reaction flask was then placed in the ice bath for one h, followed by stirring at room temperature for 18 h. At the end of the reaction time, vacuum distillation was carried out at 0 °C to remove the volatiles and then at room temperature to obtain the product in a condensation flask as a pale-yellow liquid. The yield of the reaction was 89%

^1H NMR (500 MHz, Chloroform-*d*) δ 7.83 – 7.72 (m, 2H), 7.56 – 7.49 (m, 2H), 6.77 (dd, J = 17.6, 10.9 Hz, 1H), 5.95 – 5.86 (m, 1H), 5.46 – 5.36 (m, 1H). ^{29}Si NMR (99 MHz, Chloroform-*d*) δ -1.19.

2.4.4 Synthesis of (1R,3R,5S,7R,9s,11S,13S,15R,17S,19r)-19-(3-isocyanatopropyl)-19-methyl-1,3,5,7,11,13,15,17-octaphenyl-9-(4-vinylphenyl)-2,4,6,8,10,12,14,16,18,20,21,22,23,24-tetradeca-1,3,5,7,9,11,13,15,17,19-decasilapentacyclo[11.7.1.13,11.15,17.17,15]tetracosan-9-ol



Scheme 2-5 : Synthesis of asymmetrically capped DDSQ nanobridge

To a 250 mL round bottom flask was added DDPh₈T₈(OH)₄ (2.15 g, 0.002 mol, one equiv), styrene trichlorosilane (0.48 g, 0.002 mol, one equiv), methyl(propyl isocyanate)dichlorosilane (0.40 g, 0.002 mol, one equiv) and a stir bar. The flask was placed under an N₂ atmosphere, and freshly

distilled DCM (~50 mL) was added. Et₃N (0.815 g, 0.008 mol, 4 equiv) was added dropwise to this solution. Upon complete addition of the triethylamine, the white-colored reaction mixture turned colorless. The reaction mixture was stirred for 5 min, after which solvent was removed using a rotary evaporator, and then THF (~ 15 mL) was added to create a slurry. This slurry was filtered through a medium frit funnel to obtain the crude product.

It should be noted that this is a mixture of the three isomers - two symmetrically capped DDSQ systems and one asymmetrically capped DDSQ system. The products were isolated using silica column chromatography. A glass preparatory chromatography column, 60 cm long and 4 cm internal diameter, with a 500 mL round top reservoir, was packed with Si-gel, resulting in a packing height of about 75% of the total column height. DCM used as a mobile phase was flushed through the packed bed under pressure generated by a dry N₂ stream. The mobile phase was passed through the column multiple times until no air bubbles or dry space was observed. A concentrated solution of the product mixture with DCM was gently injected from the top of the wet Si-gel bed and pushed into the packed bed until no solution was observed above the packed bed. The column was then gently charged with 500 mL of DCM and flushed using the N₂ stream. Fractions of 20 mL were collected at the bottom of the column until the DCM reached the top of the bed. Each fraction was sealed on 5 cm TLC plates of Si-gel supported on aluminum. Fractions were eluted with DCM and then analyzed under a 245 nm UV-lamp. Similar fractions were combined and dried. The asymmetrically capped DDSQ compound is eluted out as the second batch of fractions from the column. The yield is 12 %.

2.4.5 Graphene oxide sample preparation

To a 100 mL round bottom flask, graphene oxide(GO) (0.12 g) and a stir bar were added under the N₂ atmosphere. A solvent mixture of 7:3 THF: DMF (~ 50 mL) was charged into the flask.

Asymmetrically capped DDSQ synthesized in the previous step (0.21 g) was added to the flask. The reaction mixture was stirred for 72 h. At the end of the reaction time, the solvent was removed using a rotary evaporator. The reaction mixture was washed with fresh DCM (~3x15 mL) to remove the excess asymmetrically capped DDSQ. The black-colored solid GO was filtered and dried.

2.4.6 Composite sample preparation

To a 20 mL flask, a stir bar and Derakene™ resin were added. 0.1wt% GO with asymmetrically capped DDSQ was added. The reaction mixture was stirred at room temperature for 24 h. At the end of the reaction time, 1% methyl ethyl ketone peroxide was the curing agent added to the mixture. Rectangular slabs were cast using silicone casts. The curing was done at room temperature for 24 h. post-curing was done at 120 °C for two hours.

REFERENCES

- (1) Jang, C.; Lacy, T. E.; Gwaltney, S. R.; Toghiani, H.; Pittman, C. U. Relative Reactivity Volume Criterion for Cross-Linking: Application to Vinyl Ester Resin Molecular Dynamics Simulations. *Macromolecules* 2012, 45 (11), 4876–4885. <https://doi.org/10.1021/ma202754d>.
- (2) Liao, S.-H.; Hsiao, M.-C.; Yen, C.-Y.; Ma, C.-C. M.; Lee, S.-J.; Su, A.; Tsai, M.-C.; Yen, M.-Y.; Liu, P.-L. Novel Functionalized Carbon Nanotubes as Cross-Links Reinforced Vinyl Ester/Nanocomposite Bipolar Plates for Polymer Electrolyte Membrane Fuel Cells. *Journal of Power Sources* 2010, 195 (23), 7808–7817. <https://doi.org/10.1016/j.jpowsour.2009.10.020>.
- (3) Zhang, H.-B.; Zheng, W.-G.; Yan, Q.; Yang, Y.; Wang, J.-W.; Lu, Z.-H.; Ji, G.-Y.; Yu, Z.-Z. Electrically Conductive Polyethylene Terephthalate/Graphene Nanocomposites Prepared by Melt Compounding. *Polymer* 2010, 51 (5), 1191–1196. <https://doi.org/10.1016/j.polymer.2010.01.027>.
- (4) Tang, L.-C.; Wan, Y.-J.; Yan, D.; Pei, Y.-B.; Zhao, L.; Li, Y.-B.; Wu, L.-B.; Jiang, J.-X.; Lai, G.-Q. The Effect of Graphene Dispersion on the Mechanical Properties of Graphene/Epoxy Composites. *Carbon* 2013, 60, 16–27. <https://doi.org/10.1016/j.carbon.2013.03.050>.
- (5) Wan, Y.-J.; Tang, L.-C.; Gong, L.-X.; Yan, D.; Li, Y.-B.; Wu, L.-B.; Jiang, J.-X.; Lai, G.-Q. Grafting of Epoxy Chains onto Graphene Oxide for Epoxy Composites with Improved Mechanical and Thermal Properties. *Carbon* 2014, 69, 467–480. <https://doi.org/10.1016/j.carbon.2013.12.050>.
- (6) Tang, L.-C.; Wan, Y.-J.; Peng, K.; Pei, Y.-B.; Wu, L.-B.; Chen, L.-M.; Shu, L.-J.; Jiang, J.-X.; Lai, G.-Q. Fracture Toughness and Electrical Conductivity of Epoxy Composites Filled with Carbon Nanotubes and Spherical Particles. *Composites Part A: Applied Science and Manufacturing* 2013, 45, 95–101. <https://doi.org/10.1016/j.compositesa.2012.09.012>.
- (7) Thostenson, E. T.; Chou, T.-W. Processing-Structure-Multi-Functional Property Relationship in Carbon Nanotube/Epoxy Composites. *Carbon* 2006, 44 (14), 3022–3029. <https://doi.org/10.1016/j.carbon.2006.05.014>.
- (8) Guo, Z.; Pereira, T.; Choi, O.; Wang, Y.; Hahn, H. T. Surface Functionalized Alumina Nanoparticle Filled Polymeric Nanocomposites with Enhanced Mechanical Properties. *J. Mater. Chem.* 2006, 16 (27), 2800. <https://doi.org/10.1039/b603020c>.
- (9) Rafiee, M. A.; Rafiee, J.; Wang, Z.; Song, H.; Yu, Z.-Z.; Koratkar, N. Enhanced Mechanical Properties of Nanocomposites at Low Graphene Content. *ACS Nano* 2009, 3 (12), 3884–3890. <https://doi.org/10.1021/nn9010472>.
- (10) Novoselov, K. S. Electric Field Effect in Atomically Thin Carbon Films. *Science* 2004, 306 (5696), 666–669. <https://doi.org/10.1126/science.1102896>.

- (11) Song, P.; Cao, Z.; Cai, Y.; Zhao, L.; Fang, Z.; Fu, S. Fabrication of Exfoliated Graphene-Based Polypropylene Nanocomposites with Enhanced Mechanical and Thermal Properties. *Polymer* 2011, 52 (18), 4001–4010. <https://doi.org/10.1016/j.polymer.2011.06.045>.
- (12) Rafiq, R.; Cai, D.; Jin, J.; Song, M. Increasing the Toughness of Nylon 12 by the Incorporation of Functionalized Graphene. *Carbon* 2010, 48 (15), 4309–4314. <https://doi.org/10.1016/j.carbon.2010.07.043>.
- (13) Yan, J.; Wei, T.; Shao, B.; Fan, Z.; Qian, W.; Zhang, M.; Wei, F. Preparation of a Graphene Nanosheet/Polyaniline Composite with High Specific Capacitance. *Carbon* 2010, 48 (2), 487–493. <https://doi.org/10.1016/j.carbon.2009.09.066>.
- (14) Liu, T.; Zhao, Z.; Tjiu, W. W.; Lv, J.; Wei, C. Preparation and Characterization of Epoxy Nanocomposites Containing Surface-Modified Graphene Oxide. *J. Appl. Polym. Sci.* 2014, 131 (9), n/a-n/a. <https://doi.org/10.1002/app.40236>.
- (15) Stankovich, S.; Dikin, D. A.; Piner, R. D.; Kohlhaas, K. A.; Kleinhammes, A.; Jia, Y.; Wu, Y.; Nguyen, S. T.; Ruoff, R. S. Synthesis of Graphene-Based Nanosheets via Chemical Reduction of Exfoliated Graphite Oxide. *Carbon* 2007, 45 (7), 1558–1565. <https://doi.org/10.1016/j.carbon.2007.02.034>.
- (16) Dey, A.; Chroneos, A.; Braithwaite, N. St. J.; Gandhiraman, R. P.; Krishnamurthy, S. Plasma Engineering of Graphene. *Applied Physics Reviews* 2016, 3 (2), 021301. <https://doi.org/10.1063/1.4947188>.
- (17) Liu, H.; Liu, Y.; Zhu, D. Chemical Doping of Graphene. *J. Mater. Chem.* 2011, 21 (10), 3335–3345. <https://doi.org/10.1039/C0JM02922J>.
- (18) Li, D.; Müller, M. B.; Gilje, S.; Kaner, R. B.; Wallace, G. G. Processable Aqueous Dispersions of Graphene Nanosheets. *Nature Nanotech* 2008, 3 (2), 101–105. <https://doi.org/10.1038/nnano.2007.451>.
- (19) Stankovich, S.; Dikin, D. A.; Piner, R. D.; Kohlhaas, K. A.; Kleinhammes, A.; Jia, Y.; Wu, Y.; Nguyen, S. T.; Ruoff, R. S. Synthesis of Graphene-Based Nanosheets via Chemical Reduction of Exfoliated Graphite Oxide. *Carbon* 2007, 45 (7), 1558–1565. <https://doi.org/10.1016/j.carbon.2007.02.034>.
- (20) Xu, Y.; Liu, Z.; Zhang, X.; Wang, Y.; Tian, J.; Huang, Y.; Ma, Y.; Zhang, X.; Chen, Y. A Graphene Hybrid Material Covalently Functionalized with Porphyrin: Synthesis and Optical Limiting Property. *Adv. Mater.* 2009, 21 (12), 1275–1279. <https://doi.org/10.1002/adma.200801617>.
- (21) Schedin, F.; Geim, A. K.; Morozov, S. V.; Hill, E. W.; Blake, P.; Katsnelson, M. I.; Novoselov, K. S. Detection of Individual Gas Molecules Adsorbed on Graphene. *Nature Mater* 2007, 6 (9), 652–655. <https://doi.org/10.1038/nmat1967>.

- (22) Kosynkin, D. V.; Higginbotham, A. L.; Sinitskii, A.; Lomeda, J. R.; Dimiev, A.; Price, B. K.; Tour, J. M. Longitudinal Unzipping of Carbon Nanotubes to Form Graphene Nanoribbons. *Nature* 2009, 458 (7240), 872–876. <https://doi.org/10.1038/nature07872>.
- (23) Jiang, D.; Sumpter, B. G.; Dai, S. Unique Chemical Reactivity of a Graphene Nanoribbon's Zigzag Edge. *The Journal of Chemical Physics* 2007, 126 (13), 134701. <https://doi.org/10.1063/1.2715558>.
- (24) Giovannetti, G.; Khomyakov, P. A.; Brocks, G.; Karpan, V. M.; van den Brink, J.; Kelly, P. J. Doping Graphene with Metal Contacts. *Phys. Rev. Lett.* 2008, 101 (2), 026803. <https://doi.org/10.1103/PhysRevLett.101.026803>.
- (25) Malec, C. E.; Davidović, D. Electronic Properties of Au-Graphene Contacts. *Phys. Rev. B* 2011, 84 (3), 033407. <https://doi.org/10.1103/PhysRevB.84.033407>.
- (26) Chen, W.; Chen, S.; Qi, D. C.; Gao, X. Y.; Wee, A. T. S. Surface Transfer P-Type Doping of Epitaxial Graphene. *J. Am. Chem. Soc.* 2007, 129 (34), 10418–10422. <https://doi.org/10.1021/ja071658g>.
- (27) Konios, D.; Stylianakis, M. M.; Stratakis, E.; Kymakis, E. Dispersion Behaviour of Graphene Oxide and Reduced Graphene Oxide. *Journal of Colloid and Interface Science* 2014, 430, 108–112. <https://doi.org/10.1016/j.jcis.2014.05.033>.
- (28) Marcano, D. C.; Kosynkin, D. V.; Berlin, J. M.; Sinitskii, A.; Sun, Z.; Slesarev, A.; Alemany, L. B.; Lu, W.; Tour, J. M. Improved Synthesis of Graphene Oxide. *ACS Nano* 2010, 4 (8), 4806–4814. <https://doi.org/10.1021/nn1006368>.
- (29) Yu, Z.; Drzal, L. T. Functionalized Graphene Oxide as Coupling Agent for Graphene Nanoplatelet/Epoxy Composites. *Polymer Composites* 2020, 41 (3), 920–929. <https://doi.org/10.1002/pc.25423>.
- (30) Lavoratti, A.; Zattera, A. J.; Amico, S. C. Mechanical and Dynamic-Mechanical Properties of Silanized Graphene Oxide/Epoxy Composites. *J Polym Res* 2019, 26 (6), 140. <https://doi.org/10.1007/s10965-019-1805-6>.
- (31) Mehrabi-Kooshki, M.; Jalali-Arani, A. Preparation of Binary and Hybrid Epoxy Nanocomposites Containing Graphene Oxide and Rubber Nanoparticles: Fracture Toughness and Mechanical Properties. *J Appl Polym Sci* 2019, 136 (4), 46988. <https://doi.org/10.1002/app.46988>.
- (32) He, S.; Qian, Y.; Liu, K.; Macosko, C. W.; Stein, A. Modified-Graphene-Oxide-Containing Styrene Masterbatches for Thermosets. *Ind. Eng. Chem. Res.* 2017, 56 (40), 11443–11450. <https://doi.org/10.1021/acs.iecr.7b02583>.
- (33) Fox, D. M.; Maupin, P. H.; Harris, R. H.; Gilman, J. W.; Eldred, D. V.; Katsoulis, D.; Trulove, P. C.; De Long, H. C. Use of a Polyhedral Oligomeric Silsesquioxane (POSS)-Imidazolium Cation as an Organic Modifier for Montmorillonite. *Langmuir* 2007, 23 (14), 7707–7714. <https://doi.org/10.1021/la0636863>.

- (34) Jerman, I.; Koželj, M.; Orel, B. The Effect of Polyhedral Oligomeric Silsesquioxane Dispersant and Low Surface Energy Additives on Spectrally Selective Paint Coatings with Self-Cleaning Properties. *Solar Energy Materials and Solar Cells* 2010, 94 (2), 232–245. <https://doi.org/10.1016/j.solmat.2009.09.008>.

APPENDIX

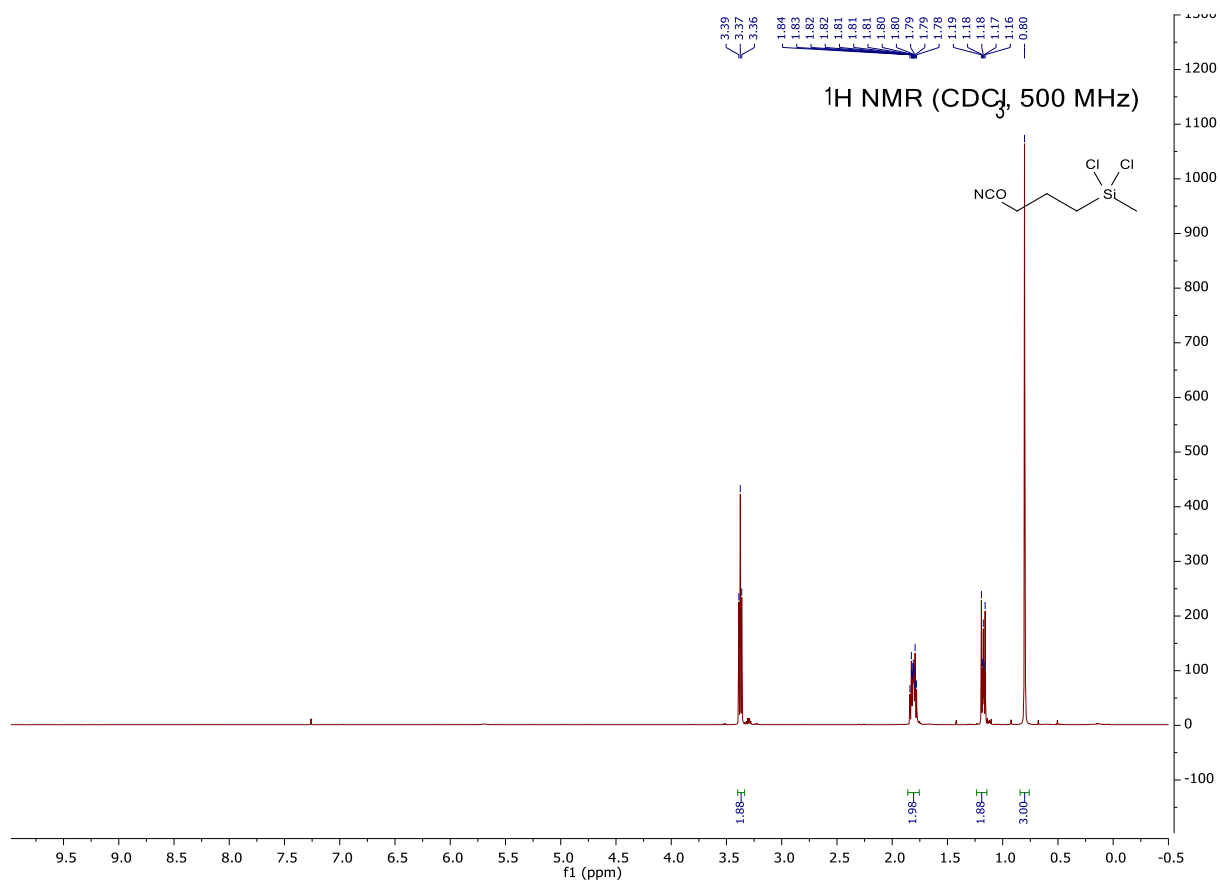


Figure 2-4 : ¹H NMR (CDCl₃, 99 MHz)

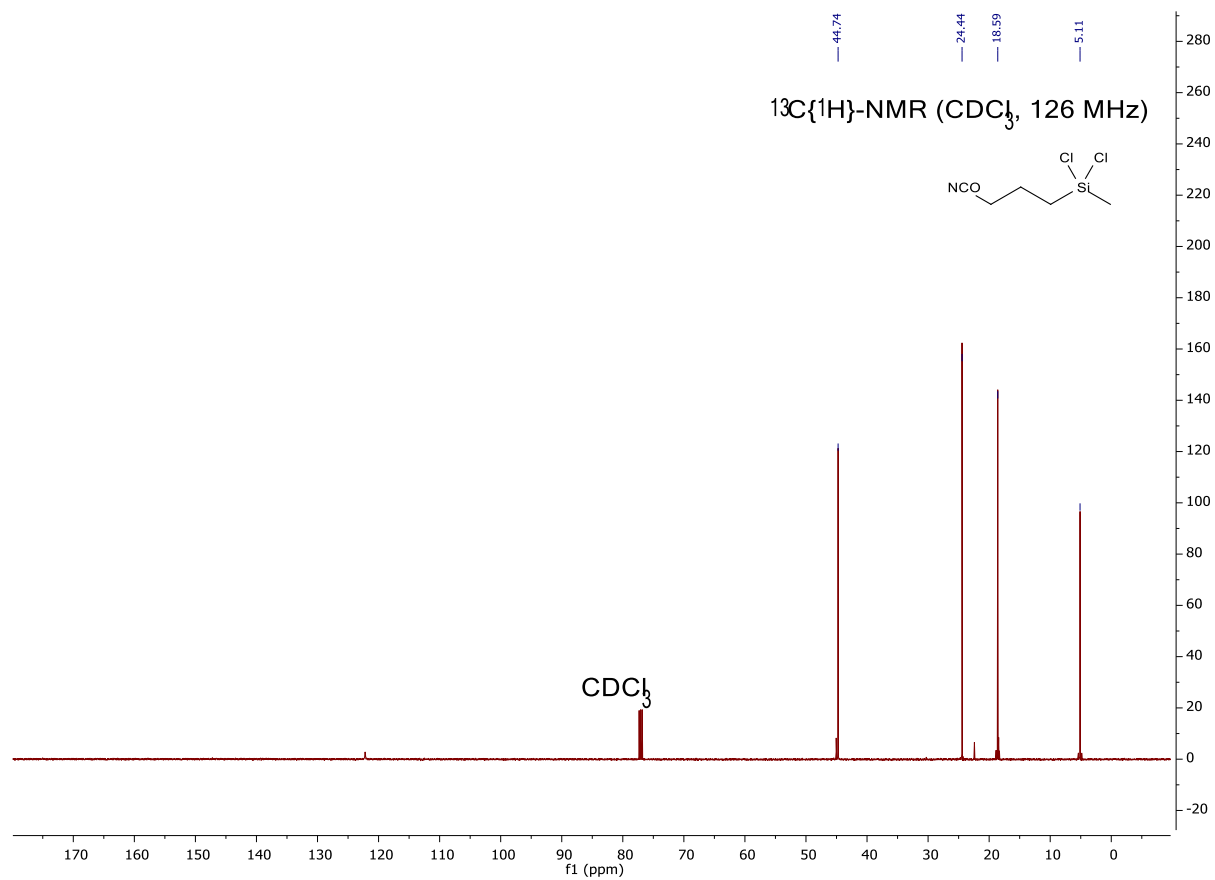


Figure 2-5 : ^{13}C -NMR (CDCl_3 , 126 MHz)

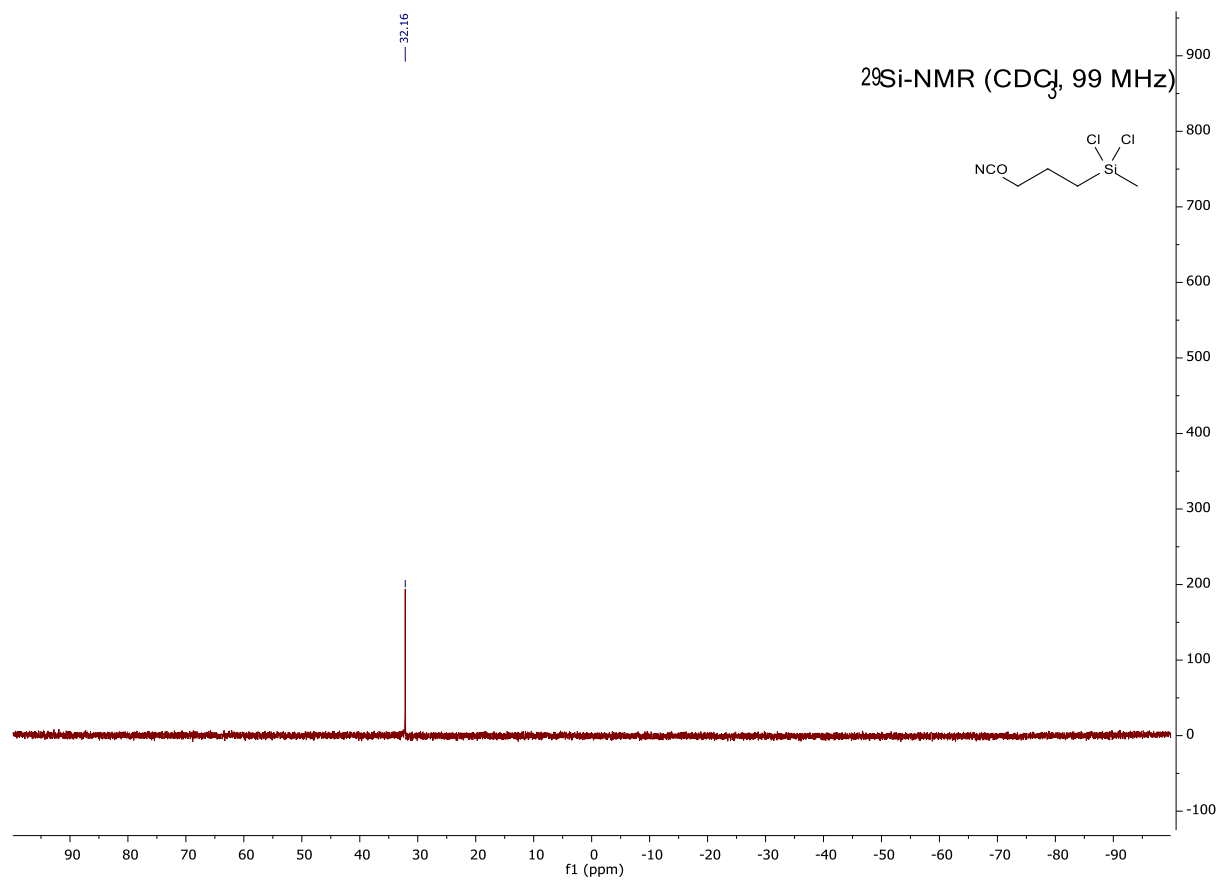
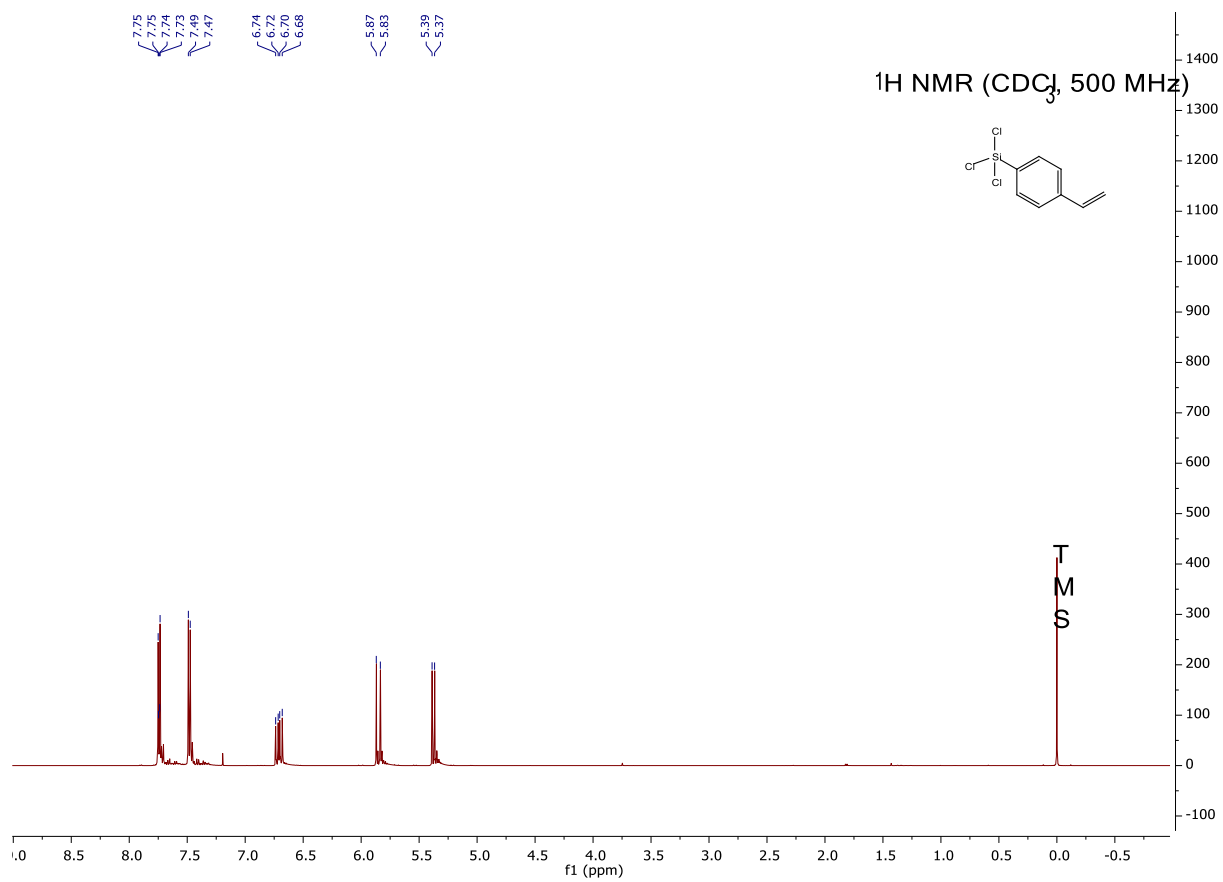
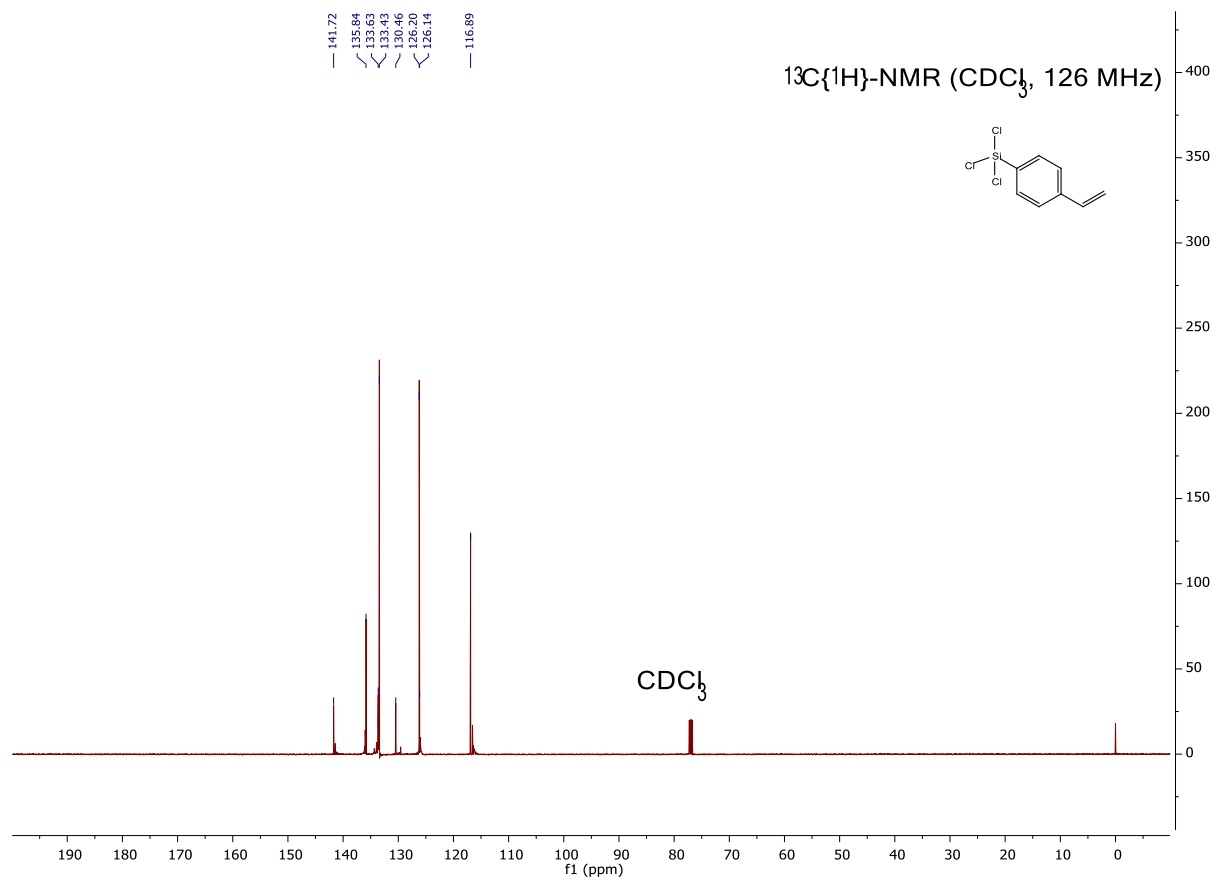


Figure 2-6 : $^{29}\text{Si}\{^1\text{H}\}$ -NMR (CDCl_3 , 99 MHz)





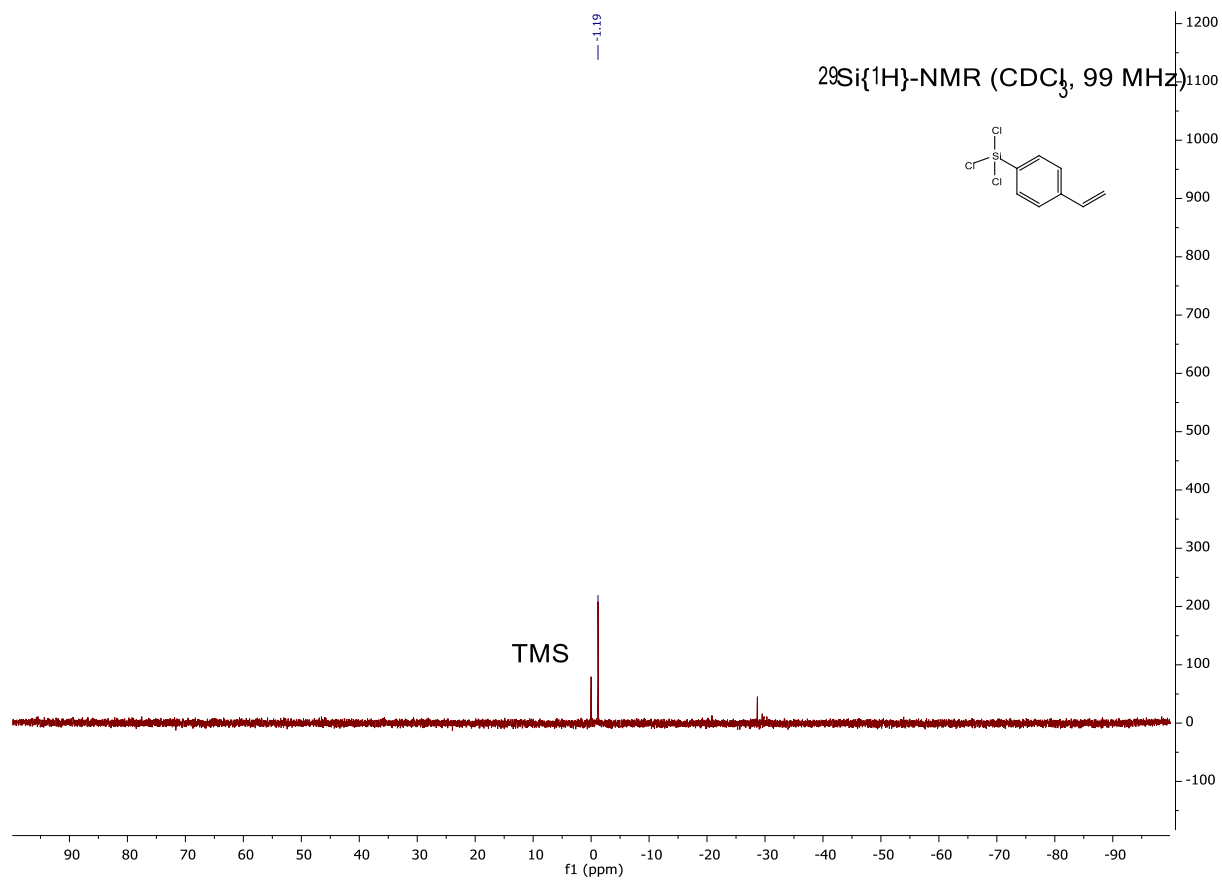


Figure 2-9 : $^{29}\text{Si}\{^1\text{H}\}$ -NMR (CDCl_3 , 99 MHz)

3 PHENYL ETHYNYL PHENYL DDSQ SYSTEMS

3.1 Introduction

Polyhedral oligomeric silsesquioxanes (POSS) are unique hybrid organic-inorganic materials with a general chemical composition of $(\text{RSiO}_{1.5})_n$. The R group can be a hydrogen atom or alkyl, alkylene, aryl, arylene, or organo-functional derivatives of alkyl, alkylene, aryl, or arylene groups.¹ The structures of silsesquioxanes can be cage structures, partial cage structures, ladder structures, or random structures. POSS can be introduced into polymer matrices to produce novel composite materials with various advantageous properties.²⁻⁵

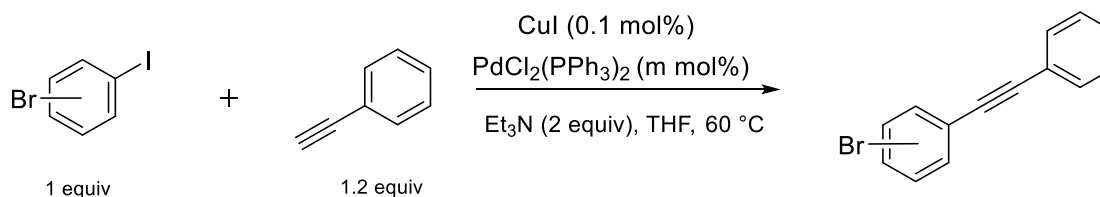
In 2013, low-viscosity DDSQ-based polyamides were reported by Schoen⁶. *meta* and *para* methyl-aminophenyl dichlorosilanes were used together to condense $\text{Ph}_8\text{DDSQ}(\text{OH})_4$. This capping scheme created a mixture containing regio- (*meta* and *para*) and stereo- (*cis* and *trans*) isomers in the final condensed product. The attempted synthesis of $\text{DDPh}_8\text{T}_8\text{-PEPI}$ possessed several disadvantages, such as diminished yields and being time intensive. Even though the moisture uptake has been reduced compared to AFR-PE-4 material, it may be possible to further reduce the uptake by eliminating the imide group and directly capping the $\text{DDPh}_8\text{T}_8(\text{OH})_4$ cage with phenylethynyl end-capped chlorosilanes.

The work presented in this report begins with the synthesis of *meta/para* phenylethynylphenylbromide – the precursor reagent for synthesizing dichlorosilanes. The amount of Palladium catalyst used in this reaction was optimized to obtain maximum yield with the least amount of Palladium catalyst. Grignard and lithiation routes were explored upon successfully synthesizing the precursors to obtain clean dichlorosilanes. The advantages and disadvantages of each route have been thoroughly explained, and an optimized reaction pathway to obtain clean dichlorosilanes has been demonstrated. These dichlorosilanes were then capped on to DDSQ to

obtain *cis/trans* isomeric mixtures. The conversion of dichlorosilanes to silanes has been explored to solve storage issues.

3.2 Reagent synthesis

A general class of dichlorosilane is used to get the various chlorosilanes for side-capping of $\text{DDPh}_8\text{T}_8(\text{OH})_4$. These dichlorosilanes are synthesized starting from brominated phenylethynyl benzene. Different isomers of the starting reagent can be obtained depending on the position of the bromine group to the triple bond. The reaction to obtain these reagents using the Sonogashira reaction was given by Dannatt⁷, as shown in Scheme 3-1. A study of the effects of reaction conditions on the kinetics of the reaction was studied. The catalyst concentration was varied, and the extent of reaction completion was obtained from GCMS by calculating the area under the peak for the product molecule. Similarly, the amount of base equivalence was optimized to get a higher product yield.



Scheme 3-1 : Reaction pathway for synthesis of bromo-phenyl ethynyl benzene

3.2.1 Reaction kinetics

The reaction rate depends on the temperature at which the reaction is carried out. As the general thumb rule, the rate of reaction doubles for every 10 °C rise in temperature of the reaction conditions. This observation is known as the Arrhenius equation and is supported by the collision theory of chemical reactions. According to the Arrhenius equation, the rate constant (k) of a reaction is directly proportional to the exponential factor of the activation energy (E_a) divided by the product of the gas constant (R) and the temperature (T) in Kelvin:

$$k = A * e^{\left(\frac{-E_a}{R*T}\right)}$$

Where:

k: Rate constant of the reaction

A: Pre-exponential factor (related to the frequency of collisions between reactant molecules)

E_a: Activation energy (the minimum energy required for a reaction to occur)

R: Gas constant (8.314 J/(mol*K))

T: Temperature in Kelvin

The equation shows that an increase in temperature (T) will lead to a higher value for the exponential factor, resulting in a higher rate constant and a faster reaction rate. This effect is because as the temperature rises, the kinetic energy of the reactant molecules also increases. Consequently, the molecules move faster, leading to more frequent and energetic collisions, which enhances the likelihood of a successful reaction.

The limiting factors in increasing the reaction mixture's temperature are either the reactants' stability concerning temperature or the boiling point of the solvent used in the reaction. In this case, the reactants bromiodine and phenylacetylene are stable up to their melting points. The solvent used in this case is THF which has a boiling point of 66 °C and hence is the limiting factor for the reaction temperature conditions. Thus, the temperature is set to reflux conditions to facilitate the increase in reaction rate. The reaction rate also depends on the two reactants used in the reaction. The effects of sterics and electronics of the reactants used in the reaction have been discussed below.

3.2.2 Catalyst Cycle

Various physical pathways suggest a plausible pathway for the reaction; based on identifying some of the transient species formed in the catalytic reactions, it is a challenging task to isolate

and characterize the organometallic intermediates to validate a mechanism beyond any doubt. The copper co-catalyzed Sonogashira reaction is predicted to be following the pathway shown in Figure

3-1

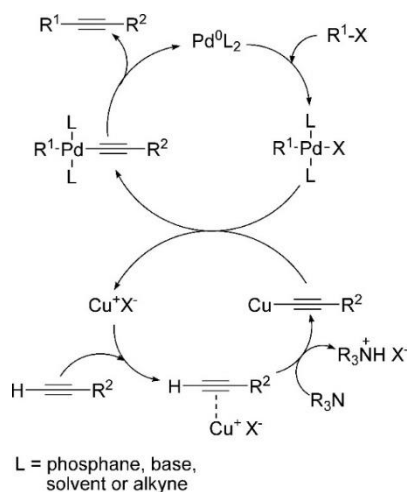


Figure 3-1 : Catalyst cycle for Sonogashira reaction⁸

The Pd (II) catalyst generates in-situ Pd (0) species, the actual catalytic moiety participating in the reaction. The palladium cycle proceeds via a fast-oxidative addition of aryl halide to the 14 electron $\text{Pd}(0)\text{L}_2$ intermediate. The kinetics of this step depends on how efficiently the electron density around the carbon-halide bond is lowered. The copper cycle proceeds via the activation of aryl alkyne by the base. Usually, the base is not strong enough to deprotonate the alkyne. Hence, using copper salts generate a π -alkyne-Cu complex, making the alkyne proton more acidic for more accessible abstraction by the weak base. This use of copper salts leads to the formation of copper acetylide, which undergoes transmetalation with the intermediate formed in the palladium cycle. Transmetalation is the rate-determining step in which the intermediate formed undergoes reductive elimination to give the final product and, thus, regenerate the catalyst.

3.2.3 1-bromo-3-(phenylethynyl)benzene

The palladium Cycle

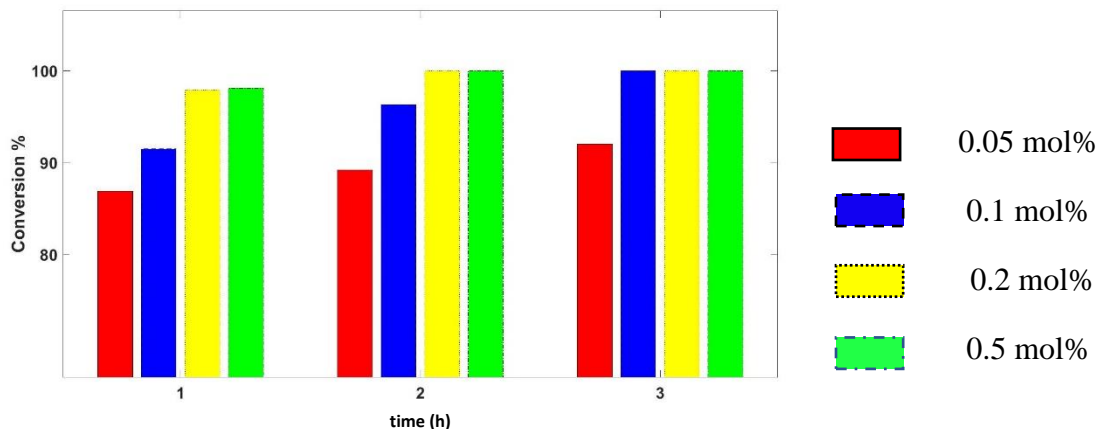


Figure 3-2 : Effect of varying Pd catalyst concentration on the extent of reaction. The bar graphs represent different amounts of catalyst loading used in the reaction.

In the first optimization scenario, following procedure from the literature⁷, the initial Pd (PPh₃)₂Cl₂ catalyst amount was set at 0.05 mol%, and the base used was one equivalent. After every hour, 0.1 mL of the reaction mixture was quenched with 1.5 mL methanol and then analyzed by GCMS. After analyzing the area under the peak for product molecules in the GCMS spectrum, it was found that 85 % of the reaction was completed in the first hour. In 2 h, 89 % of the reaction was completed, and the rate plateaued out after that, evident from the 90 % completion at the end of 3 h. On increasing the catalyst loading to 0.2 mol%, the initial rate of the reaction improved to 91% completion of the reaction in the first hour. Continued analysis at the 2 h and 3 h mark gave an extent of conversion of 96% and 100%, respectively. On increasing the catalyst amount to 0.3% and 0.5%, the extent of reaction at 1 h was around 97%, reaching completion within the 2 h mark.

The base equivalency

The base in the reaction is used to neutralize the byproduct hydrogen halide and activate the aryl acetylene. The reactions were carried out using optimized palladium catalyst conditions, varying

the base amount used in the order 1 equiv/2 equiv. After every hour, 0.1 mL of the reaction mixture was quenched with methanol and then analyzed by GCMS. After analyzing the area under the peak for product molecule by GCMS, it is evident from Figure 3-3 that the reaction reaches the experimental maximum value in 2 h.

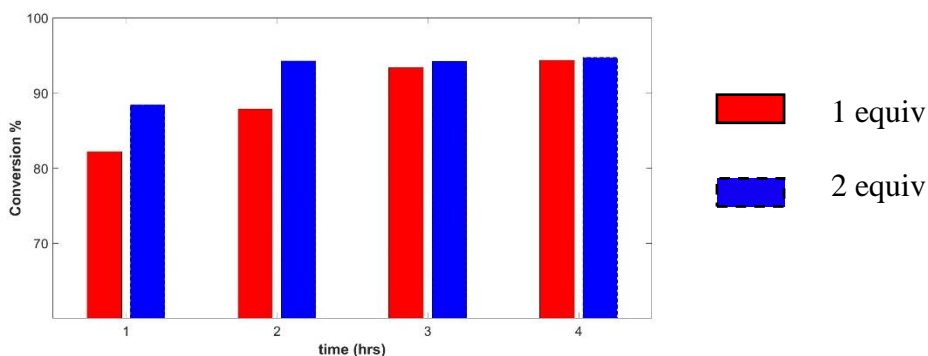


Figure 3-3 : Effect of varying the base equivalence on the extent of conversion of reaction

3.2.4 1-bromo-4- (phenyl ethynyl) benzene

Based on the optimization conditions for synthesizing 1-bromo-3-phenylethynyl benzene, optimum conditions for the efficient synthesis of 1-bromo-3-phenylethynyl benzene can be obtained. In order to achieve the optimized conditions, the amount of CuI and Et₃N were kept constant, and the amount of palladium catalyst was varied starting from 0.05 mol%. The rate of conversion increases as the amount of palladium catalyst increases. It can be observed from the reaction kinetics that the extent of the reaction for *para* systems is lower than the meta systems for given reaction conditions. Also, due to the even distribution of electron cloud density in 1-bromo-4-iodobenzene, the oxidative addition step is slower than that of 1-bromo-3-iodobenzene.

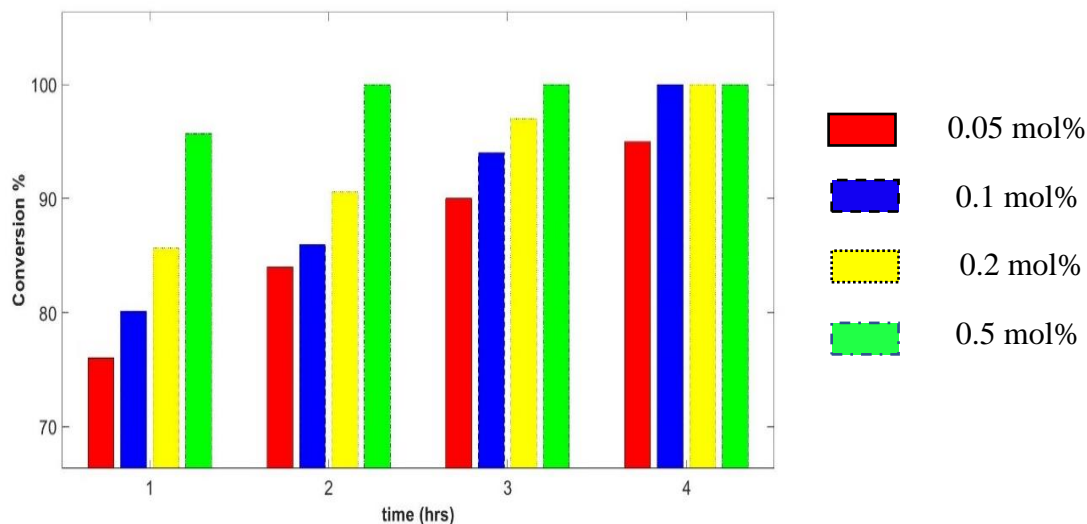


Figure 3-4 : Effect of varying Pd catalyst concentration on the extent of reaction. The bar graphs represent different amounts of catalyst loading used in the reaction.

3.2.5 Summary

An analysis of optimization conditions for the Sonogashira reaction was carried out for iodobromobenzene. Based on the catalyst cycle, the amount of CuI was kept constant, whereas the amount of palladium catalyst used was varied. It was found that 0.2mol% of the $\text{Pd}(\text{PPh}_3)\text{Cl}_2$ catalyst was the optimum condition for the synthesis of 1-bromo-4-(phenyl ethynyl)benzene. 2 equivalents of base are used in the reaction. This excess base amount helps extract the phenylacetylene's acidic hydrogen. Also, due to the even distribution of electron cloud density in 1-bromo-4-iodobenzene compared to 1-bromo-3-iodobenzene, the oxidative addition step is slower than that of 1-bromo-3-iodobenzene. Hence the reaction time is almost doubled from 2 h to 4 h.

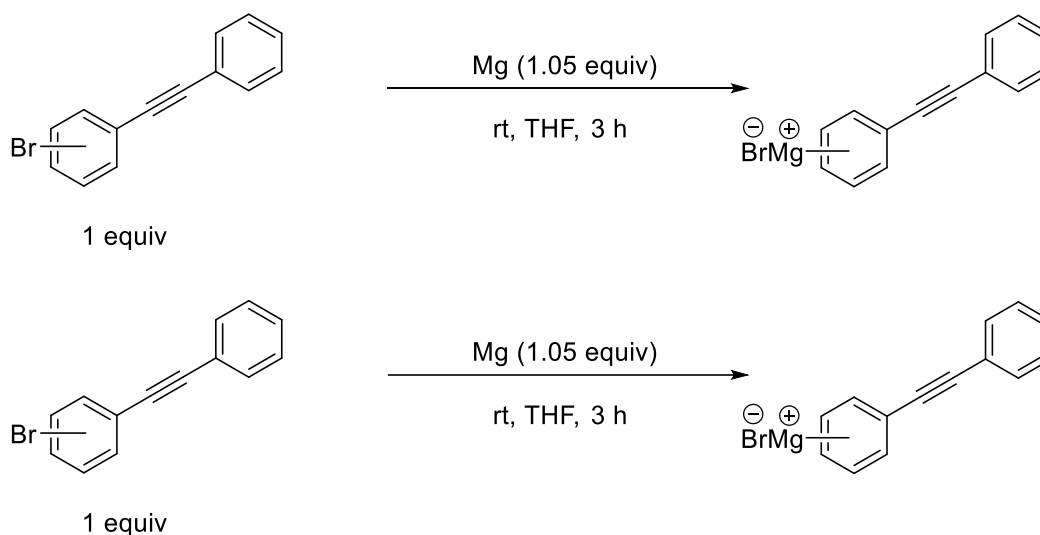
3.3 Synthesis of dichlorosilanes

Once the (*para/meta*) bromo-phenyl ethynylbenzene (Br-PEB) has been synthesized, the next step is converting them into suitable chlorosilanes to act as side-capping agents to $\text{DDPh}_8\text{T}_8(\text{OH})_4$. The dichlorosilanes are highly moisture sensitive and readily decompose into silanols on exposure to moisture. Conversion to dichlorosilanes begins with the metalation of the C-Br bond present in the

precursor. The use of magnesium or organo-lithium agents has been explored for this purpose. Once the metalation is complete, the next step involves using trichlorosilanes to convert the organometal compounds to dichlorosilanes.

3.3.1 Grignard reaction pathway

The use of Grignard reagents for forming new carbon-carbon bonds has been known for a century. Magnesium is used to generate the Grignard reagent. The reaction pathway for the generation of Grignard reagent from Br-PEB is shown in Scheme 3-2

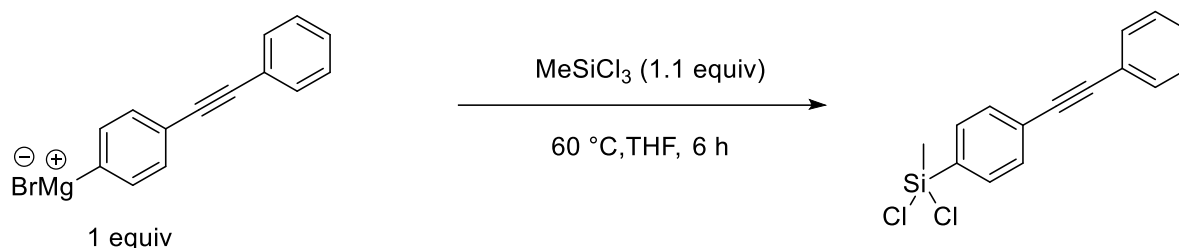


Scheme 3-2 : Reaction pathway for Grignard reagent synthesis

The outer layer of Mg is covered with magnesium oxide making it inert for the halo-organic compound to react. The reactant Mg must be activated using sonication or rapid stirring. Water or even air in ppm quantities can destroy the reagent by protonolysis. In order to analyze the progress during the reaction, a sample aliquot is quenched in methanol and tested using a GCMS. The Grignard species reacts with the proton from the alcohol to give diphenylacetylene which is detected by mass spectrometry.

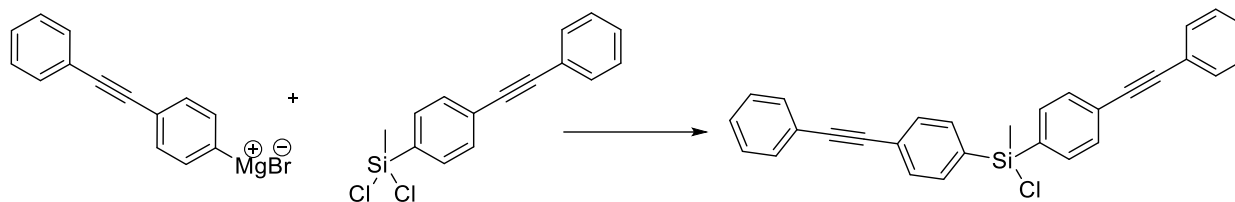
Synthesis of para-dichlorosilane

In order to synthesize the desired dichlorosilane, methyl trichlorosilane is reacted with the Grignard reagent formed in the previous step.



Scheme 3-3 : Reaction pathway for para-dichlorosilane synthesis

An excess of trichlorosilane is required to ensure the conversion to the desired dichlorosilane and to avoid the formation of undesired monochlorosilane in the process, as shown in Scheme 3-4.

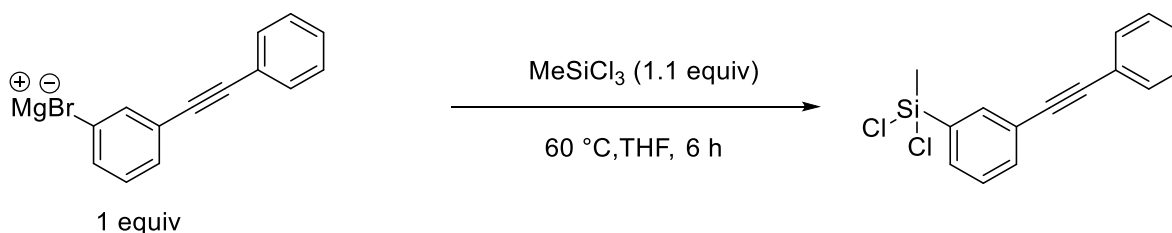


Scheme 3-4 : Undesired side reaction during the dichlorosilane synthesis step

The reaction leads to the formation of MgBrCl salt. If the crude reaction mixture is used directly in the DDPh₈T₈(OH)₄ capping, the salt causes significant issues leading to scrambled cage-like structures and hence needs to be filtered out from the reaction mixture. Thus, to isolate the clean dichlorosilane, distilling the chlorosilane was suggested. In practice, distillation causes charring of the product molecule. Sublimation proved to be adequate to isolate the dichlorosilane. A 53% yield was obtained.

Synthesis of meta-dichlorosilane

The *meta*-isomer of the dichlorosilane has been synthesized using the same approach as that of the *para* isomer, as shown in Scheme 3-5.

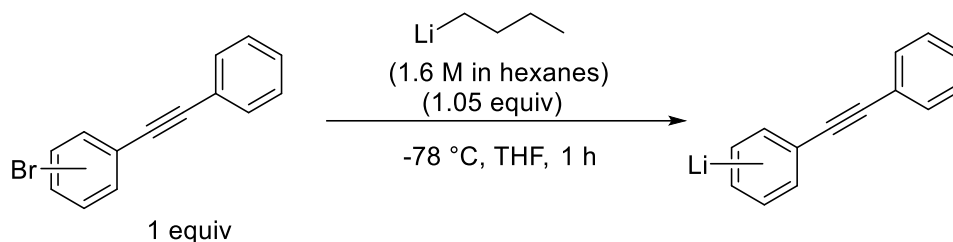


Scheme 3-5 : Reaction pathway for meta-dichlorosilane synthesis

GCMS proved to be an efficient way to monitor the real-time progress of the reaction. Upon completion of the reaction, the solvent was evaporated, and the mixture was washed with hexanes. The organic products dissolved in hexanes were separated from the salts via filtration. Sublimation under vacuum conditions was attempted to isolate pure *meta*-dichlorosilane. The temperature varied from room to 120 °C, and the vacuum was maintained at 0.01 torr. It was found that no solid product was obtained throughout the whole temperature range. As the temperature increased, the reaction mixture became a charred mass lump. Distillation was also not effective in isolating the final product. Column chromatography techniques cannot be used as chlorosilanes would react with the column material to form silanols. The chlorosilanes can also cause erosion of the columns, thus rendering the HPLC technique inappropriate. In the case of *para*-dichlorosilane, the mixture in the sublimator was analyzed after the completion of the sublimation step. It was found that there was still a finite amount of *para*-dichlorosilane left. This leftover product could not be distilled off despite increasing the sublimation temperature from 70 °C to 120 °C, beyond which complete charring was observed.

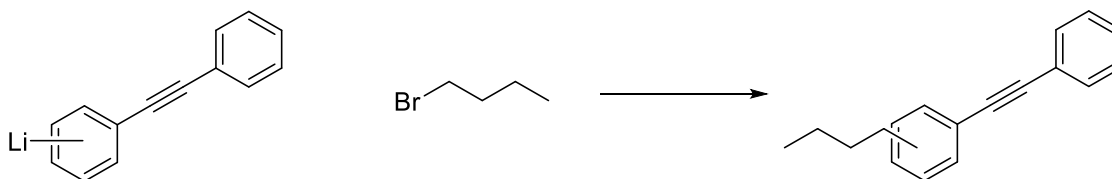
3.3.2 n-Butyl lithium reaction pathway

In order to convert the Br-PEB to dichlorosilanes, a metal-halogen exchange is required. In order to achieve this, n-butyl lithium is used as a lithiation agent, as shown in Scheme 3-6.



Scheme 3-6 : Reaction pathway for lithiation of Br-PEB

The reaction needs to be carried out in a moisture-free atmosphere. n-Butyl lithium is a highly active pyrophoric compound. Hence, all the glassware used is heat dried and flushed with nitrogen. The temperature needs to be maintained low because n-butyl lithium is a highly reactive species that can lead to the formation of undesired products, as shown in Scheme 3-7.



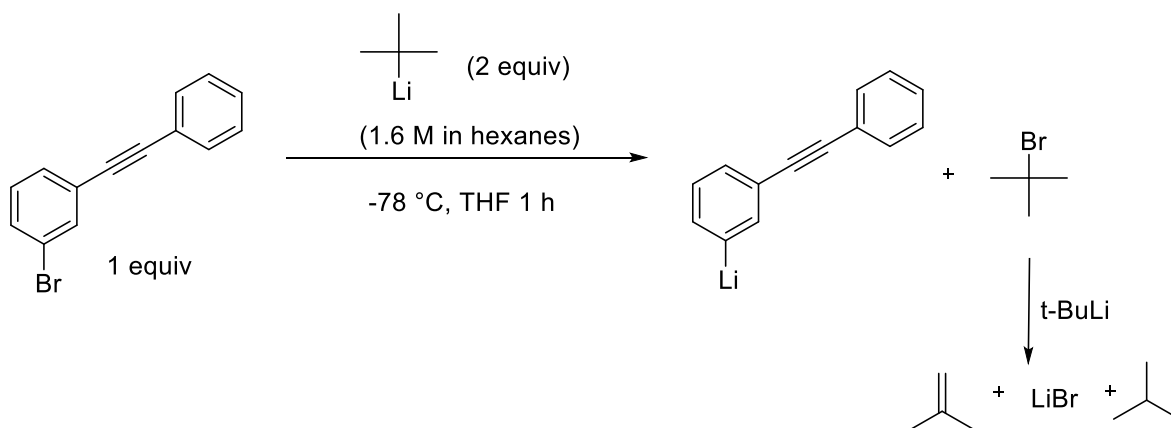
Scheme 3-7 : Reaction pathway for side reactions in lithiation reaction

A sample aliquot is quenched in methanol and analyzed by GCMS to analyze the reaction progress. The lithiated species reacts with the proton from the alcohol to give diphenylacetylene which is detected by mass spectrometry. Despite maintaining the temperature at $-78\text{ }^{\circ}\text{C}$, almost 30% of the reactant is wasted as the undesired side product. Due to the poor yields and difficulty in handling the reagents, this route does not seem to be a promising reaction pathway.

3.3.3 tert-butyllithium reaction pathway

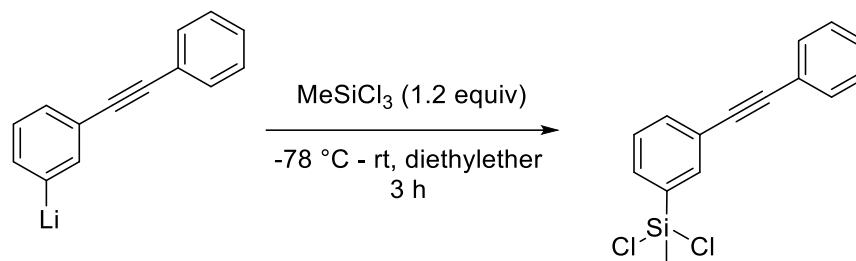
With multiple obstacles in obtaining the pure *meta*-PEP dichlorosilane, a better and more efficient route was taken to fulfill the objective. The reagent used for metalation was tertiary butyl lithium. t-Butyllithium is a pyrophoric organolithium compound that acts as a strong base and can deprotonate many carbon acids, including benzene. Ether solvents can also decompose; hence, low temperatures must be used to conduct the reactions. The metalation of *meta*-bromoPEB is shown in Scheme 3-8. The flask was thoroughly flushed with nitrogen to make sure the atmosphere within

the flask was air-free. Although the solvent was diethyl ether, the reaction temperature was kept at -78 °C using a dry ice-acetone bath. This low reaction temperature avoided the degradation of the organolithium compound via the solvent. Two equivalents of t-butyllithium reagent are required as the tertbutyl bromide product formed during the reaction further reacts with the organolithium compound to form LiBr, isobutylene, and isobutane and smaller hydrocarbons. In order to monitor the progress during the reaction, a sample aliquot is quenched in methanol and analyzed by GCMS. The reaction color was initially colorless and turned yellow upon adding the organolithium compound and finally to a reddish-brown color. The reaction is complete in 1 h with no undesired side products.



Scheme 3-8 : Reaction pathway for lithiation of Br-PEB

Upon completion of the lithiation reaction, the reaction mixture is cannula transferred into a flask containing methyl trichlorosilane. This flask is kept at -78 °C to avoid the degradation of the lithiated compound during the transfer. Upon completion of the transfer, the flask is taken out of the cold bath and allowed to warm up to room temperature. The reaction mixture turned bright red upon adding the lithiated compound; the color eventually turned light yellow.

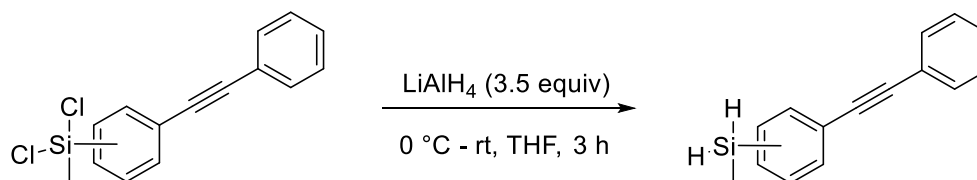


Scheme 3-9 : Reaction pathway for meta-dichlorosilane synthesis.

In order to monitor the progress during the reaction, a sample aliquot is quenched in methanol and analyzed by GCMS. The reaction was completed in 3 h. After completion, the salts were filtered off the reaction mixture using a cannula filter. The filtrate that contains the excess unreacted methyl trichlorosilane and other side products, along with the desired dichlorosilane, is subjected to vacuum distillation leaving behind the *meta*-PEPdichlorosilane along with diphenyl ethynyl. Although the formation of this compound leads to the loss of yield of dichlorosilane, it does not interfere with the capping of $\text{DDPh}_8\text{T}_8(\text{OH})_4$ and hence does not affect the project's overall goal.

3.3.4 Silanes as a long-term storage option

Dichlorosilanes are highly moisture sensitive and need special storage conditions. The purification of dichlorosilanes requires vacuum distillation, leading to poor yield of dichlorosilanes. Silanes are not water sensitive and can be isolated using column chromatography. Long-term storage is also not an issue, as the silanes are not air-sensitive. They can be stored in a sealed container for considerably more extended than chlorosilanes without considering the need to replenish the inert atmosphere in the container constantly. The chlorosilanes can be converted to corresponding silanes via reduction using lithium aluminum hydride, as shown in Scheme 3-10.



Scheme 3-10 : Reaction pathway for silane synthesis from dichlorosilane

The reduction is an exothermic reaction that must be cooled using an ice bath. Once dichlorosilanes are added to the flask, the reaction mixture can warm to room temperature to ensure complete silane conversion. The progress is monitored using GCMS. Upon completion of the reaction, hexanes are added to extract the organic products, and the excess hydride is quenched with DI water. The solids are separated by filtration. The crude mixture is concentrated and then passed through a silica chromatography column to isolate the pure *meta*-silane.

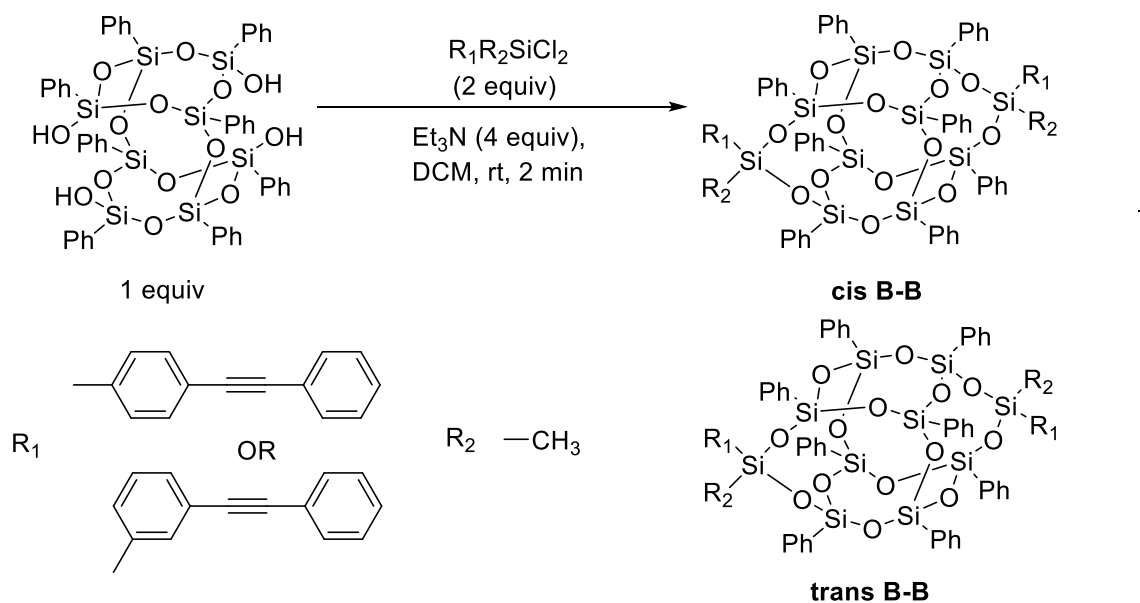
The conversion of these silanes back to chlorosilanes was attempted using various chlorinating agents. GCMS analyzed the reaction mixture. It was found that the triple bond of ethynyl was chlorinated along with the Si-H silane bonds. The capping of silanes directly to $\text{DDPh}_8\text{T}_8(\text{OH})_4$ was somewhat explored. The reaction yield was poor (<10%), and NMR analysis of the reaction mixture indicated that the cages were scrambled/broken due to the reaction conditions used.

3.3.5 Summary

Isomeric para/meta dichlorosilanes were synthesized using t-butyl lithium as a metalation reagent. This route yielded better results than the Grignard reagent route or the n-butyl lithium route. An excess of t-butyl lithium reagent is used to ensure complete conversion. The byproduct formed in the reaction is in a gaseous state at room temperature and hence can be easily separated. To improve the shelf life of chlorosilanes and yield, LiAlH_4 is used as a reducing agent to convert chlorosilanes to silanes to improve the shelf life and yield. The silanes can be purified using column chromatography, which yields better than sublimation/ distillation. Multiple reaction pathways were studied to convert silanes back to chlorosilanes, but in most cases, the ethynyl bond gets chlorinated, leading to undesired side products. Hence, one-pot synthesis of dichlorosilanes was a better reaction pathway than converting chlorosilanes to silanes and back to chlorosilanes.

3.4 Capping of DDPPh₈T₈(OH)₄

DDPh₈T₈(OH)₄ can be capped using various chlorosilanes to get up to four functional groups on the silicon core moiety. Depending on the type of side groups used, the DDSQ structures can be used as coupling agents or as nano-fillers to improve the mechanical properties of thermosets. The functionalized DDSQ structure can also be incorporated as the polymer backbone using monomeric functional units as capping reagents, followed by a polymerization reaction.



Scheme 3-11 : Reaction pathway for capping of DDPPh₈T₈(OH)₄ using dichlorosilanes

3.5 Separation of DDPPh₈T₈ isomers

Fractional crystallization can be used to isolate nearly pure *trans* and enriched *cis* DDSQ-2((R₁)(R₂)) isomers. In order to facilitate the separation of the mixture, the compounds were dissolved in DCM, and the addition of hexanes resulted in the crystallization and precipitation of the *trans* isomers. This step led to the enrichment of *cis* isomer in the mother liquor. The thermal behavior of nearly pure isomers was studied using DSC. The melting point of nearly pure *cis* isomer was 270 °C which was 33 °C lower than that of nearly pure *trans* isomer (303 °C). The entropy at

melting was higher for *trans* isomers indicating that the packing in *trans* isomers was more ordered than *cis*, leading to a higher melting point. A eutectic mixture was formed upon mixing the isomers with a mass fraction of *trans* isomer equal to 0.3. This eutectic mixture had a melting point of

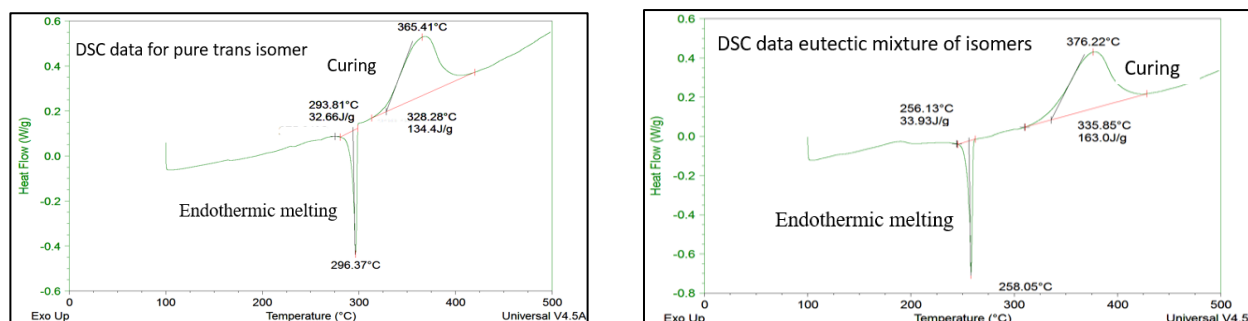


Figure 3-5 : DSC data for mixture of isomers

about 250 °C, lower than the melting temperatures of nearly pure *cis* and *trans* isomers. The heat of fusion is the same, while the heat of reaction for curing is higher for the eutectic mixture, indicating a higher degree of curing. The TGA data show that the isomeric mixture can withstand thermal degradation up to almost 500 °C.

3.6 Experimental details

3.6.1 General Information

All manipulations were done under a nitrogen atmosphere using standard Schlenk techniques except otherwise stated. All commercially available chemicals were used as received unless otherwise indicated. 1-Bromo-4-iodobenzene ($\text{C}_6\text{H}_4\text{BrI}$), 1-bromo-3-iodobenzene ($\text{C}_6\text{H}_4\text{BrI}$), ethynylbenzene (C_8H_6), cuprous iodide (CuI), Bis(triphenylphosphine)palladium(II) dichloride ($\text{PdCl}_2(\text{PPh}_3)_2$), magnesium turnings, n-butyl lithium (2.5M solution in hexanes), tertbutyl lithium (1.6M solution in hexanes), methyl trichlorosilane (MeSiCl_3), Karstedt's catalyst, styrene trimethoxysilane, methyldichlorosilane, vinyl cyanate, boron trichloride (1.0M in hexanes), deuterated chloroform with 1 vol % tetramethylsilane (CDCl_3 -1%TMS), were purchased from Sigma-Aldrich. Graphene nanoplatelet was obtained from XG Sciences. $\text{DDPh}_8\text{T}_8(\text{OH})_4$ was obtained from Hybrid Plastics. Triethylamine (Et_3N) was purchased from Avantor and distilled over calcium hydride before use. Tetrahydrofuran (THF), dichloromethane (DCM), and methanol (MeOH) n-hexanes were purchased from Sigma-Aldrich. THF was distilled over benzophenone and sodium metal at 50 °C under nitrogen. Toluene was distilled over calcium hydride at a temperature of 120 °C. The other solvents were used as purchased without further purification, and the glassware was oven dried. All ^1H , ^{13}C , and ^{29}Si NMR were acquired on an Agilent DirectDrive2 500 MHz NMR spectrometer equipped with a OneProbe operating at 500 MHz for ^1H NMR, 126 MHz for ^{13}C NMR, and 99 MHz for ^{29}Si NMR using CDCl_3 and recorded at 25 °C. ^1H -NMR spectra were recorded with 8 scans, a relaxation delay of 1s, and a pulse angle of 45° and referenced to the residual protonated solvent in CDCl_3 (7.24 ppm). ^{13}C -NMR spectra were collected with 254 scans, a relaxation delay of 0.1 s, and a pulse angle of 45°. ^{29}Si NMR spectra were recorded with either 256 scans, a relaxation delay of 25 s, and a pulse angle 45°. Column

chromatography was performed on EMD Millipore silica gel 60 columns of 40– 63 Å silica, 230– 400 mesh. Thin-layer chromatography (TLC) was performed on plates of EMD 250-µm silica 60-F254.

3.6.2 Synthesis procedure for *meta* Br-phenyl ethynyl benzene

To a 100 mL oven-dried round bottom flask CuI (0.0673 g, 0.353 mmol, 0.1 mol %), a varying quantity of Pd(PPh₃)₂Cl₂ (m mol % / m = 0.05, 0.1, 0.2, 0.5) and a stir bar was added. A rubber septum was used to seal the flask and flush it with nitrogen. The flask was placed in an oil bath preheated to 60 °C. THF (50 mL) was added to the flask fitted with a condenser. The reactants 1-bromo-3-iodobenzene (2.25 mL, 17.6 mmol, one equiv) and ethynylbenzene (2.15 mL, 19.4 mmol, 1.1 equiv) were charged into the flask. Finally, triethylamine (2 equiv) was charged to the flask. The contents of the reaction flask were stirred at room temperature. The mixture turned from light yellow to dark brown as the reaction progressed. The formation of triethylammonium chloride salt precipitate was observed. At time intervals of 1 hr, 0.1 mL of the reaction mixture was drawn out and quenched in 1.5 mL of methanol. GCMS then analyzed the quenched products. At the end of the reaction time (3 h), the solvent was evaporated using a rotary evaporator, and the resulting liquid mixture was stirred with DI water (30 mL) and extracted using DCM (50 mL). The solvent was evaporated to obtain a yellow liquid. The crude product was further purified using silica column chromatography. A glass preparatory chromatography column, 60 cm long and 4 cm internal diameter, with a 500 mL round top reservoir, was packed with Si-gel, resulting in a packing height of about 75% of the total column height.

n-Hexanes used as mobile phase were flushed through the packed bed under pressure generated by a dry N₂ stream. The mobile phase was passed through the column multiple times until no air bubbles or dry space was observed. A concentrated solution of the crude mixture with n-hexanes

was gently injected from the top of the wet Si-gel bed and pushed into the packed bed until no solution was observed above the packed bed. The column was then gently charged with 500 mL of n-hexanes and flushed using the N₂ stream. Fractions of 20 mL were collected at the bottom of the column until the n-hexanes reached the top of the bed. Each fraction was seated on 5 cm TLC plates of Si-gel supported on aluminum. Fractions were eluted with n-hexanes and then analyzed under a 245 nm UV lamp. Similar fractions were combined and dried.

¹³C NMR (126 MHz, Chloroform-*d*) δ 134.32, 131.69, 131.38, 130.15, 129.79, 128.64, 128.43, 125.30, 122.74, 122.18, 90.68, 87.80.

¹H NMR (500 MHz, Chloroform-*d*) δ 7.70 (t, *J* = 1.7 Hz, 1H), 7.57 – 7.50 (m, 2H), 7.50 – 7.44 (m, 2H), 7.41 – 7.33 (m, 3H), 7.22 (t, *J* = 7.9 Hz, 1H).

3.6.3 Synthesis of Grignard Reagent

To a 100 mL round bottom flask were added activated Mg (0) turnings (0.2 g, 8.5 mmol, 1.1 equiv) and a stir bar. The Mg (0) turnings were stirred under a reduced pressure atmosphere for 2 h, after which the contents were put under an N₂ atmosphere. 1-Bromo-3-(phenyl ethynyl) benzene (2 g, 7.7 mmol, 1 equiv) was dissolved in 20 mL freshly distilled THF and injected into the flask containing the Mg (0) turnings. This reaction mixture was stirred for 3 h. The color of the solution turned from colorless to dark green. An aliquot of the reaction mixture (0.1 mL) was dissolved in 1.5 mL of methanol to be analyzed by GCMS. The GCMS analysis showed only one peak with an *m/z* of 178, suggesting that complete Grignard formation was achieved.

3.6.4 Synthesis of lithiation reagent

Using n-butyl lithium as a reagent

To a 100 mL round bottom flask, a stir bar, 1-bromo-3-(phenyl ethynyl) benzene (2 g, 7.7 mmol, 1 equiv) was dissolved in 20 mL freshly distilled THF was added. The flask was flushed with N₂

and was placed in a dry ice and acetone bath to maintain the reaction temperature at $-78\text{ }^{\circ}\text{C}$. A 25 mL syringe flushed with N_2 was used to dropwise add the solution of n-butyl lithium (3.4 mL, 1.1 equiv, 2.5 M in hexanes) to the flask. This mixture was stirred for 3 h, and the initial colorless solution turned dark brown. An aliquot of the reaction mixture (0.1 mL) was dissolved in 1.5 mL of methanol to be analyzed by GCMS. The GCMS analysis showed only one peak with an m/z of 178, suggesting complete lithiated agent formation was achieved.

Using t-butyl lithium as a reagent

To a 100 mL round bottom flask, a stir bar and 1-Bromo-3-(phenyl ethynyl) benzene (2 g, 0.0077 mol, 1 equiv) was dissolved in 20 mL freshly distilled THF was added. The flask was flushed with N_2 and was placed in a dry ice and acetone bath to maintain the reaction temperature at $-78\text{ }^{\circ}\text{C}$. A solution of t-butyl lithium (10 mL, 2.1 equiv, 1.6 M in hexanes) was added to the flask. This mixture was stirred for 3 h, and the initial colorless solution turned dark brown. An aliquot of the reaction mixture (0.1 mL) was dissolved in 1.5 mL of methanol to be analyzed by GCMS. The GCMS analysis showed only one peak with an m/z of 178, suggesting complete lithiated agent formation was achieved.

3.6.5 Synthesis of PEP dichlorosilane

In a 500 mL round bottom flask equipped with a stir bar under an N_2 atmosphere, MeSiCl_3 (1 mL, 0.0085 mol, 1.1 equiv) and 40 mL THF were added. The MeSiCl_3 was freshly distilled over CaH_2 at $66\text{ }^{\circ}\text{C}$. The organometallic solution (Grignard/lithiated) was cannula transferred into the 500 mL flask containing MeSiCl_3 while maintaining both flasks at $-78\text{ }^{\circ}\text{C}$ during the transfer. The reaction was removed from the dry ice and acetone bath and warmed to room temperature. Aliquots of the reaction mixture (0.1 mL) were dissolved in 1.5 mL of methanol and were analyzed by GCMS at

certain time intervals. The reaction mixture was stirred for 6-9 h, and upon completion, GCMS analysis showed complete conversion.

It should be noted that the initial color of the solution was colorless, which turned red-brown upon the addition of organometallic solution and finally yellow-green upon completion of the reaction. At the end of the reaction, the solvent and MeSiCl_3 were evaporated, leaving behind a yellow solid mass. Fresh hexanes (~150 mL) were added to the powder creating a slurry. This slurry was filtered through a medium frit funnel using hexanes (~200 mL) to aid transfer and wash the solid on the frit. The solvent from the filtrate was evaporated. The solid mass obtained is then subjected to reduced pressure (0.01 torr) conditions to isolate the pure dichlorosilane. The dichlorosilanes obtained were stored under an N_2 atmosphere to be used for subsequent reactions.

3.6.6 Synthesis of silanes

A 500 mL round bottom flask of lithium aluminum hydride (0.9 g, 0.024 mol, 3.5 equiv) and a stir bar were added under the N_2 atmosphere. The flask was kept in an ice bath Methyl-phenyl ethynyl phenyl dichlorosilane (2 g, 0.0068 mol, 1 equiv) and THF (50 mL) were charged to the flask. The reaction mixture was stirred for 3 h. Then, hexanes (~150 mL) were added to the flask, stirring the reaction mass for 0.5 h. Then the reaction mixture was put in an ice bath, and DI water was added drop-wise to quench the excess hydride forming H_2 , LiOH , and $\text{Al}(\text{OH})_3$ salts. This slurry was filtered through a medium frit funnel using hexanes (~200 mL) to aid transfer and wash the solid on the frit. The solvent from the filtrate evaporated, leaving a crude yellow mixture behind. This crude mixture was further purified using silica column chromatography. A glass preparatory chromatography column, 60 cm in length 4 cm internal diameter, with a 500 mL round top reservoir, was packed with Si-gel, resulting in a packing height of about 75% of the total column height.

n-Hexanes used as mobile phase were flushed through the packed bed under pressure generated by a dry N₂ stream. The mobile phase was passed through the column multiple times until no air bubbles or dry space was observed. A concentrated solution of the crude mixture with n-hexanes was gently injected from the top of the wet Si-gel bed and pushed into the packed bed until no solution was observed above the packed bed. The column was then gently charged with 500 mL of n-hexanes and flushed using the N₂ stream. Fractions of 20 mL were collected at the bottom of the column until the n-hexanes reached the top of the bed. Each fraction was sealed on 5 cm TLC plates of Si-gel supported on aluminum. Fractions were eluted with n-hexanes and then analyzed under a 245 nm UV lamp. Similar fractions were combined and dried.

3.6.7 Capping of DDPPh₈T₈(OH)₄

To a 250 mL round bottom flask were added DDPPh₈T₈(OH)₄ (1.5 g, 0.0014 mol, 0.5 equiv), dichloro(methyl)((phenylethynyl)phenyl) silane (1 g, 0.0028 mol, 2 equiv), and a stir bar under N₂ atmosphere. Freshly distilled DCM (~50 mL) was then added. Et₃N (0.8 mL, 0.0056 mol, 2.0 equiv) was added dropwise to this solution. Upon addition of the triethylamine, a white precipitate was observed. The reaction mixture was stirred for 5 min, after which the solvent was evaporated, and THF was added to create a slurry. This slurry was filtered through a medium frit funnel to obtain the crude product in the filtrate. This filtrate was further concentrated and purified by silica column chromatography (DCM mobile phase) to afford the desired product. It should be noted that this is a mixture of the *cis* and *trans* isomers.

para- DDSQ (Si(Me)(PEP))₂: ²⁹Si NMR (99 MHz, Chloroform-*d*) δ -30.84, -78.36, -79.23, -79.51, -79.74. *meta*- DDSQ (Si(Me)(PEP))₂: ²⁹Si NMR (99 MHz, Chloroform-*d*) δ -31.28, -78.14, -79.02, -79.32, -79.58.

REFERENCES

- (1) Baney, R. H.; Itoh, M.; Sakakibara, A.; Suzuki, T. Silsesquioxanes. *Chem. Rev.* 1995, 95 (5), 22. <https://doi.org/10.1021/cr00037a012>.
- (2) Gnanasekaran, D.; Madhavan, K.; Reddy, B. S. R. Developments of Polyhedral Oligomeric Silsesquioxanes (PaSS), Pass Nanocomposites and Their Applications: A Review. 28.
- (3) Han, D.; Wen, T.; Han, G.; Deng, Y.; Deng, Y.; Zhang, Q.; Fu, Q. Synthesis of Janus POSS Star Polymer and Exploring Its Compatibilization Behavior for PLLA/PCL Polymer Blends. *Polymer* 2018, 136, 84–91. <https://doi.org/10.1016/j.polymer.2017.12.050>.
- (4) Han, D.; Zhang, Q.; Chen, F.; Fu, Q. Using POSS–C₆₀ Giant Molecules as a Novel Compatibilizer for PS/PMMA Polymer Blends. *RSC Adv.* 2016, 6 (23), 18924–18928. <https://doi.org/10.1039/C6RA00218H>.
- (5) Fina, A.; Monticelli, O.; Camino, G. POSS-Based Hybrids by Melt/Reactive Blending. *J. Mater. Chem.* 2010, 20 (42), 9297. <https://doi.org/10.1039/c0jm00480d>.
- (6) Schoen, B. Aminophenyl Double Decker Silsesquioxanes: Spectroscopic Elucidation, Physical and Thermal Characterization, and Their Applications, Michigan State University.
- (7) Dannatt, J. E. Advancing Frontiers in Reactive and Selective Iridium C–H Borylation Catalysis and Targeted Silsesquioxane Synthesis, Michigan State University.
- (8) Chinchilla, R.; Nájera, C. The Sonogashira Reaction: A Booming Methodology in Synthetic Organic Chemistry †. *Chem. Rev.* 2007, 107 (3), 874–922. <https://doi.org/10.1021/cr050992x>.

APPENDIX

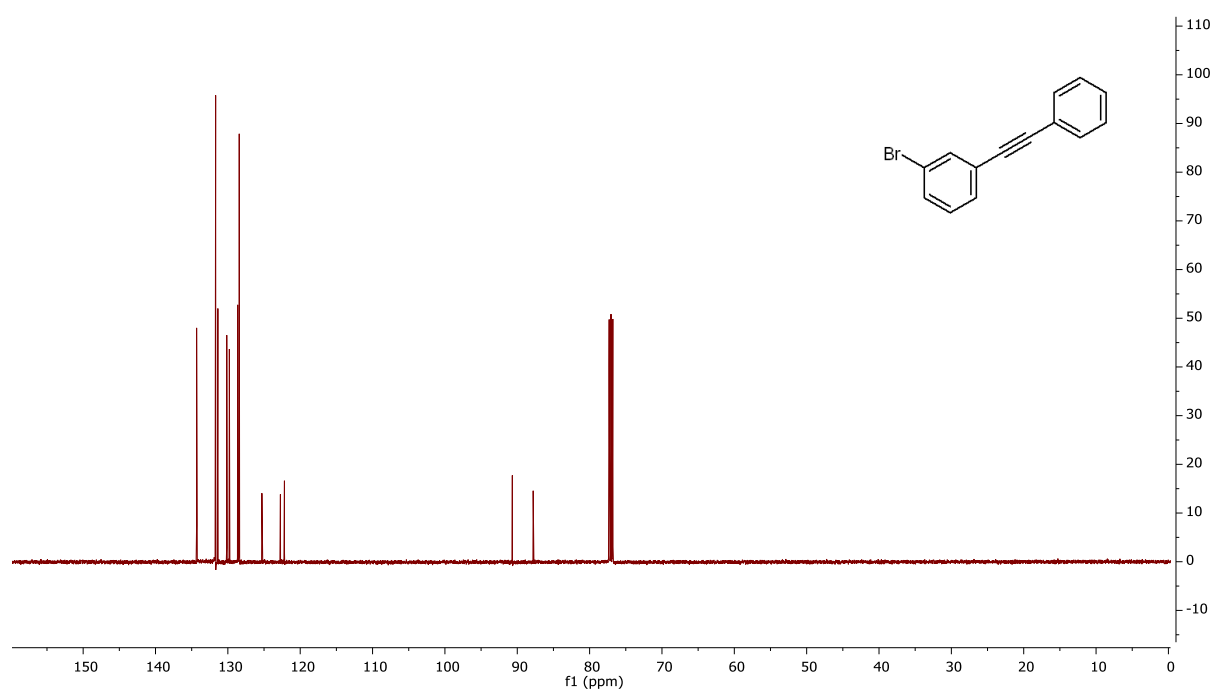


Figure 3-6 : ^1H NMR (CDCl_3 , 99 MHz)

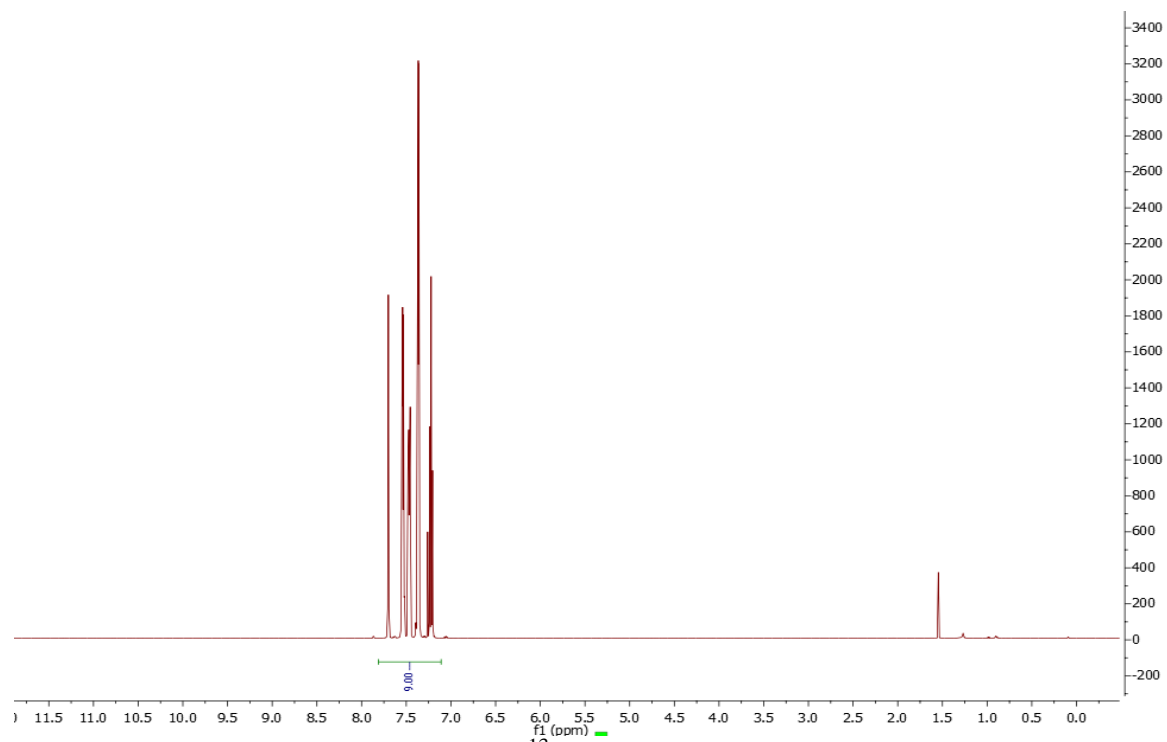


Figure 3-7 : ^{13}C -NMR (CDCl_3 , 126 MHz)

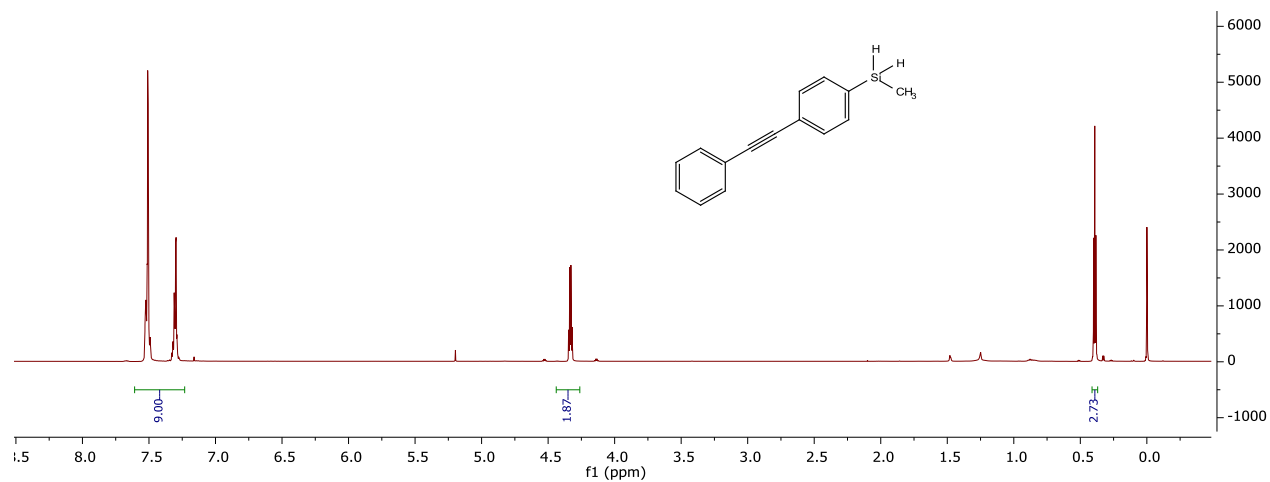


Figure 3-8 : ^1H NMR (CDCl_3 , 99 MHz)

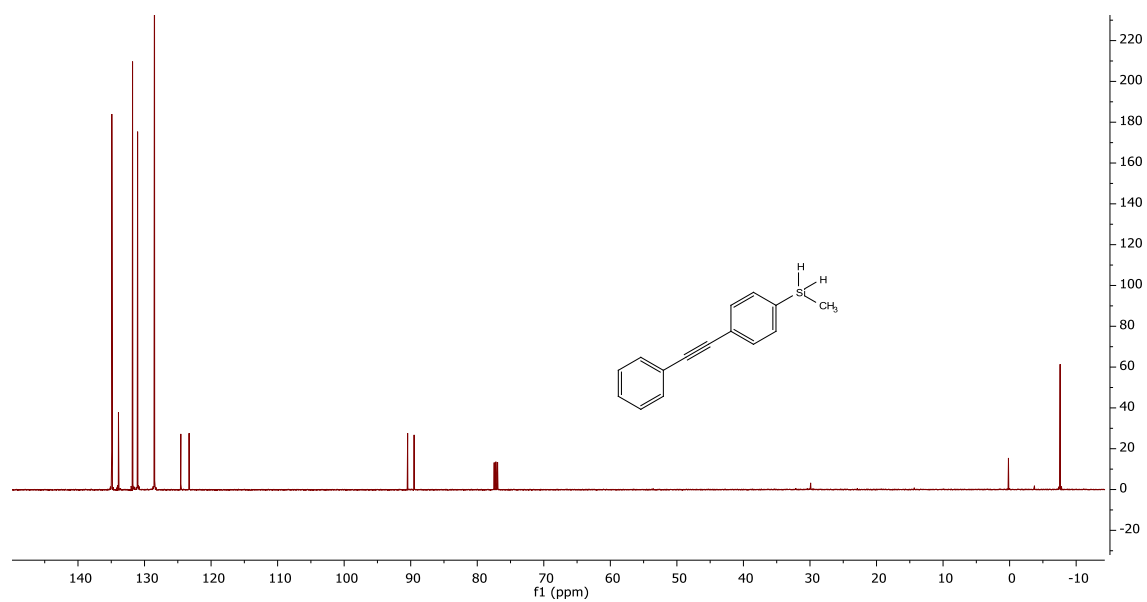


Figure 3-9 : ^{13}C -NMR (CDCl₃, 126 MHz)

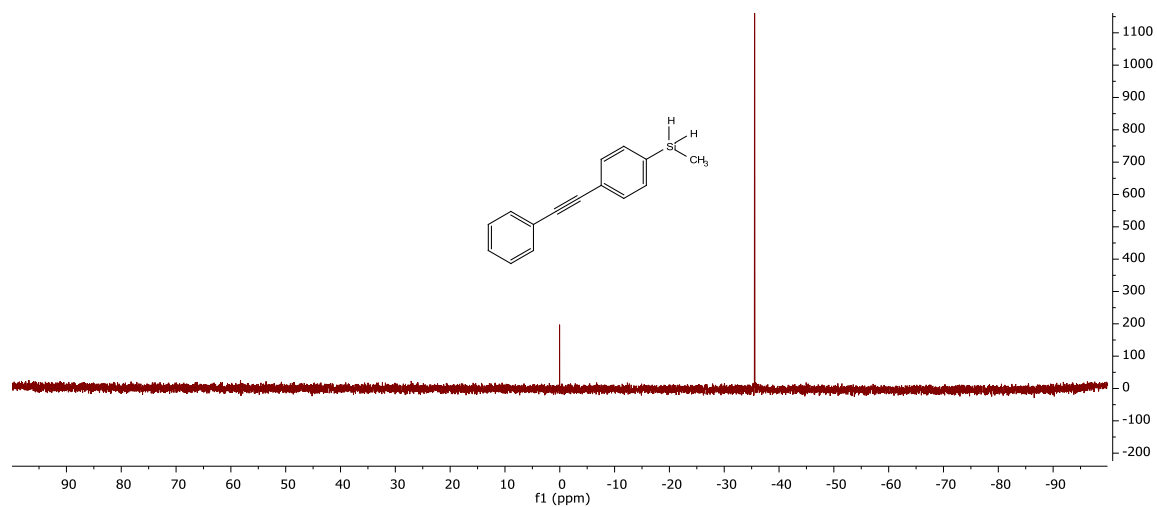


Figure 3-10 : ^1H -NMR (CDCl_3 , 500 MHz)

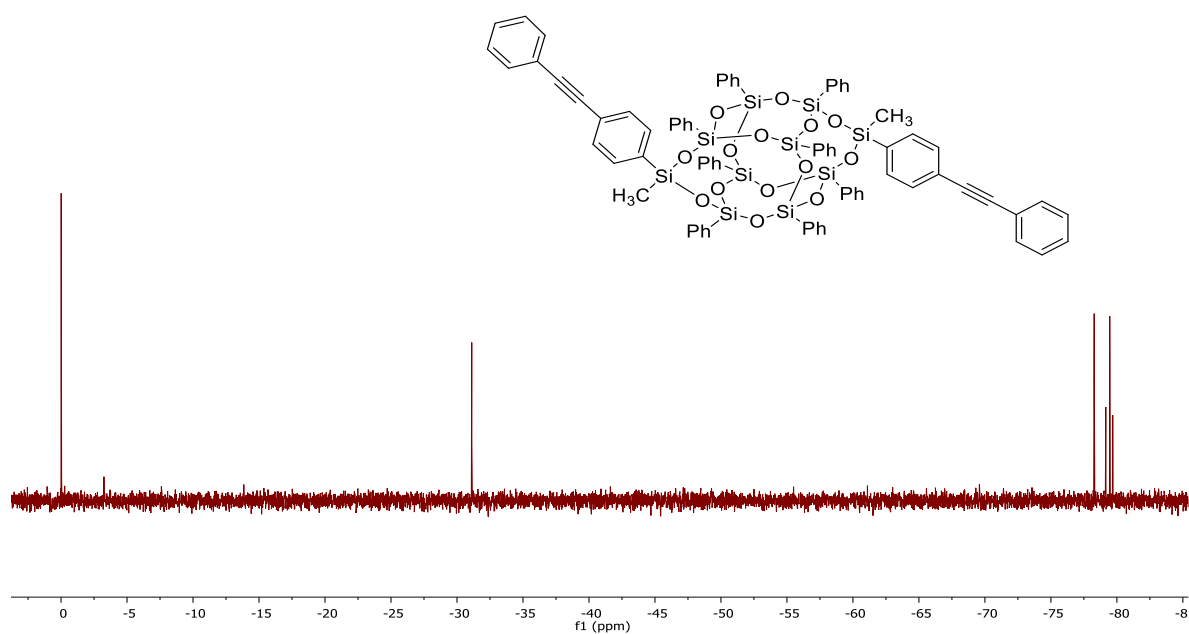


Figure 3-11 : $^{29}\text{Si}\{^1\text{H}\}$ -NMR (CDCl_3 , 99 MHz)

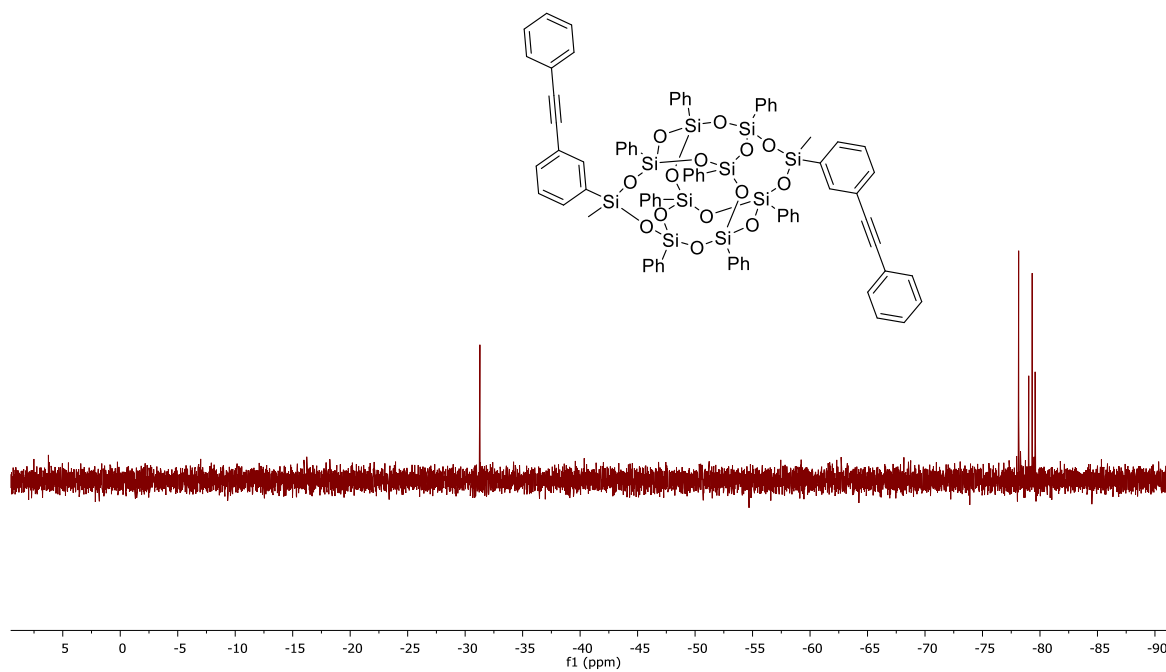
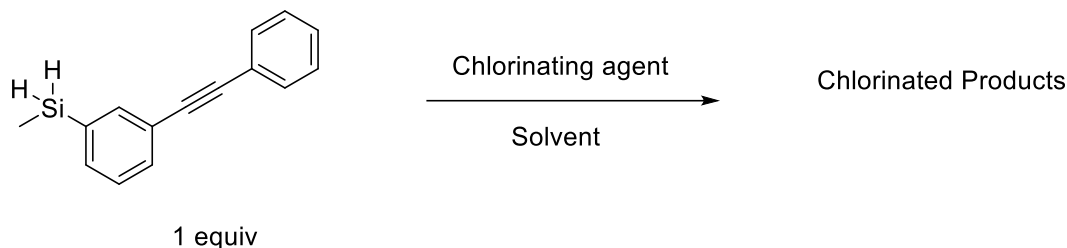


Figure 3-12 : $^{29}\text{Si}\{^1\text{H}\}$ -NMR (CDCl_3 , 99 MHz)

Converting silanes to dichlorosilanes

Upon successful isolation of pure silane, the next step is converting the silane back to chlorosilane for side-capping of $\text{DDPh}_8\text{T}_8(\text{OH})_4$. In order to achieve this moiety, various chlorinating agents can be used. The list of the chlorinating agents and the reaction condition is given in Scheme 3-12. The first reagent used for the attempted conversion was Boron trichloride (BCl_3).



Scheme 3-12 : Reaction pathway for dichlorosilane synthesis from silane

BCl_3 is a colorless gas usually available as a 1.0 molar solution in heptane. It is highly reactive towards water decomposing readily to give off HCl gas and needs to be handled carefully. The reaction progress was monitored by quenching a sample aliquot in methanol and then analyzed by GCMS. As shown in Table 3-1, after 5 min of reaction time, there were no products formed. The dechlorinated product and the initial reactant and undesired side product- tetrachlorinated silane- were observed as time progressed. After 3 h, no traces of the desired product were found, but there was still a finite amount of reactant and various fragments of the chlorinated products.

Trichloroisocyanuric acid (TCCA) or 1,3,5-trichloro-1,3,5-triazine-2,4,6-trione is a white crystalline powder with a strong chlorine smell. It is an excellent chlorinating agent for ketones, alkenes and an oxidizing agent for secondary alcohols, aldehydes, and ethers. The choice of solvent is essential while using TCCA. At temperatures above 0°C , TCCA can chlorinate ether solvents such as THF to give undesired side products. In order to avoid this formation of side products, the reaction must be carried at below 0°C . Initially, it was assumed that the reactivity of TCCA decreases as the chlorine atoms get replaced by hydrogen atoms, and hence the ratio of equivalents

of 'Cl' in TCCA to the equivalents of 'H' in reactants was kept at 3:1. As seen from Table 3-1, the first set of experiments was carried out using 2.2 equivalents of TCCA with THF as solvent at 0 °C. The reaction progress was monitored by quenching a sample aliquot in methanol and then analyzed by GCMS.

At the end of 5 min, mono- and di-chlorinated products were observed in the mass spectrum. Tetra-chlorinated products were also observed. This problem is because the TCCA can chlorinate the triple bond present in the reactant. The reaction was completed by testing the following sample at 20 min, but di- and tetra-chlorinated products were observed. These results lead to the conclusion that the kinetics of the undesired reaction is as fast as the kinetics of the desired reaction. The reaction was cooled to slow down the undesired reaction, two different reaction conditions: 0 °C and -78 °C, were tested to achieve the goal. On testing both reaction conditions at the end of 20 min, the ratio of area under the peak in the mass spectrum for tetra- to di-chlorinated products decreased, but the tetra-chlorinated products were still observed. The next step was to decrease the ratio of equivalents of 'Cl' in TCCA to the equivalents of 'H' in reactants to 3:2. The reaction completion time increased from 20 min to 40 min. On inspecting the mass spectrum at the end of the reaction, undesired tetra-chlorinated products were still observed, but the area under the peak had further decreased compared to previous reaction conditions. Decreasing the ratio of equivalents of 'Cl' in TCCA to the equivalents of 'H' in reactants to 1:1, the reaction yielded only mono and dichlorinated products even after 100 min.

Table 3-1 : List of chlorinating agents for converting silane to dichlorosilanes.

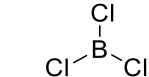
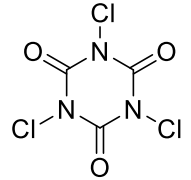
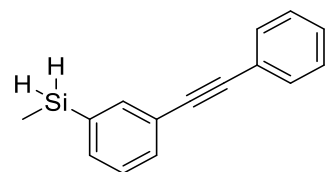
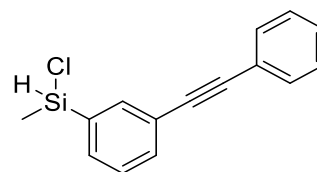
Chlorinating agent	Equivalents of reagent	Reaction conditions	Product(s) obtained
 Boron trichloride	2.2	0 °C, THF, 5 min	Reactant
		0 °C, THF, 15 min	Reactant, mono, and dichlorinated products, fragments of reactant
		0 °C, THF, 180 min	Reactant, fragments of reactant
 Trichloroisocyanuric acid	2.2	rt, THF, 5 min	Reactant, di- and tetrachlorinated products
		rt, THF, 20 min	di- and tetrachlorinated products
		0 °C, THF, 5 min	Reactant, mono-, di- and tetrachlorinated products
		0 °C, THF, 20 min	di- and tetrachlorinated products
		-78 °C, THF, 5 min	Reactant, mono-, di- and tetrachlorinated products
		-78 °C, THF, 20 min	di- and tetrachlorinated products
	1.1	rt, diethyl ether, 5 min	Reactant, mono- and dichlorinated, and products.
		rt, diethyl ether, 20 min	Reactant, mono-, di- and tetrachlorinated products
		rt, diethyl ether, 40 min	di- and tetrachlorinated products.

Table 3-1 (cont'd)

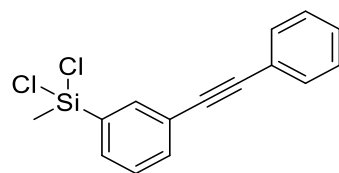
	0.66	rt, diethyl ether, 20 min	mono- and dichlorinated products.
		rt, diethyl ether, 100 min	mono- and dichlorinated products.
Cu^{2+} Cl^- Cl^- cupric chloride Cu^+ I^- Cuprous Iodide	10 0.07	rt, diethyl ether, 60 min	mono and di- chlorinated products
		rt, diethyl ether, 180 min	mono and di- chlorinated products
		rt, diethyl ether, 2880 min	mono and di- chlorinated products
	10	rt, diethyl ether, 360 min	mono and di- chlorinated products
	0.2	rt, diethyl ether, 630 min	mono and di- chlorinated products



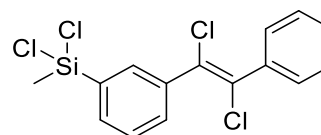
Reactant



monochlorinated product



dichlorinated product



tetrachlorinated product

Figure 3-13 : List of products and byproducts formed during the chlorination reaction

4 EFFECTS OF USING BULKY CAPPING GROUPS

4.1 Introduction

Polyhedral Oligomeric Double-decker-shaped silsesquioxanes (DDSQ) are cage-like silsesquioxanes with a 3-dimensional well-defined inorganic core with an inert organic corona compatible with the surrounding polymeric matrix and containing well-defined reactive sites. The incompletely condensed DDSQ tetrol, when capped with two equivalents of dichlorosilanes, forms a capped DDSQ structure. This capping provides up to four additional reactive sites, which can impart polarity to the compounds to improve the separation of isomers, increase the miscibility with the polymeric matrix, or improve the nanocomposites' thermal and rheological characteristics.¹⁻⁹

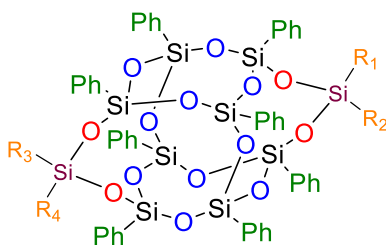
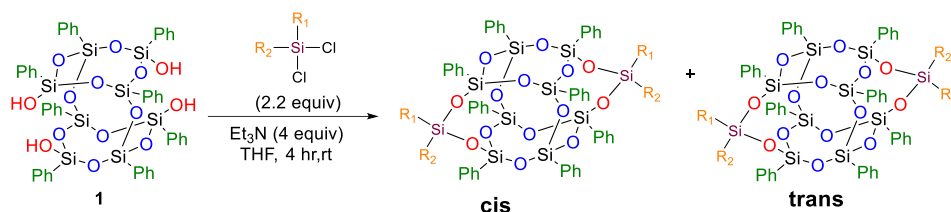


Figure 4-1 : DDSQ tetrol capped with 4 different functional groups

Adding functionalized DDSQ to polymeric matrices without using solvents is an environmentally friendly method to integrate these cage structures to form polymeric nanocomposites. This step can be achieved by melting the nanostructured cage silsesquioxanes and mixing them with the polymeric material. Solid nanostructured materials are usually considered amorphous solids with a low solid-to-liquid transition temperature for more efficient mixing.¹⁰⁻¹⁵ The previous work reported on changing the peripheral structures of capped DDSQ structures has been reported by Vogelsang and Schoen.^{11-14,16-20} The work done has been summarized in Scheme 4-1. Although most of the work done focuses on using DDSQ structures with phenyl rings as peripheral groups, there has been some work done on corner capped heptaphenyl POSS-(phenylethynylphthalimide). This structure did not exhibit melting characteristics. So, the focus was shifted to using phenyl

DDSQ tetrol as a starting reagent. Using two different functional groups on chlorosilanes leads to the formation of *cis* and *trans* isomers. Usually, one functional group is smaller, such as a methyl group, whereas the other group is a bulkier functional group. The bulkier functional groups used in the previous work are phenylethynylphthalimides, phenylethynylphenyl, aniline, and phenyl.



Scheme 4-1 : Reaction Scheme for capping of DDSQ tetrol with difunctional dichlorosilane

It was hypothesized that the melting of DDSQ-2(R_1R_2) was caused by higher entropy as compared to POSS- R_1 because the as-synthesized DDSQ-2(R_1R_2) products contain *cis* and *trans* isomers about the inorganic core.

To verify this hypothesis that increasing the entropy of the functional groups affects the melting characteristics of the caged structures and to take advantage of the effect of isomers on the melting characteristics of the DDSQ cage structures, an analogous series of DDSQ cage structures were synthesized. The thermal characteristics of these compounds were studied using Differential Scanning Calorimetry (DSC).

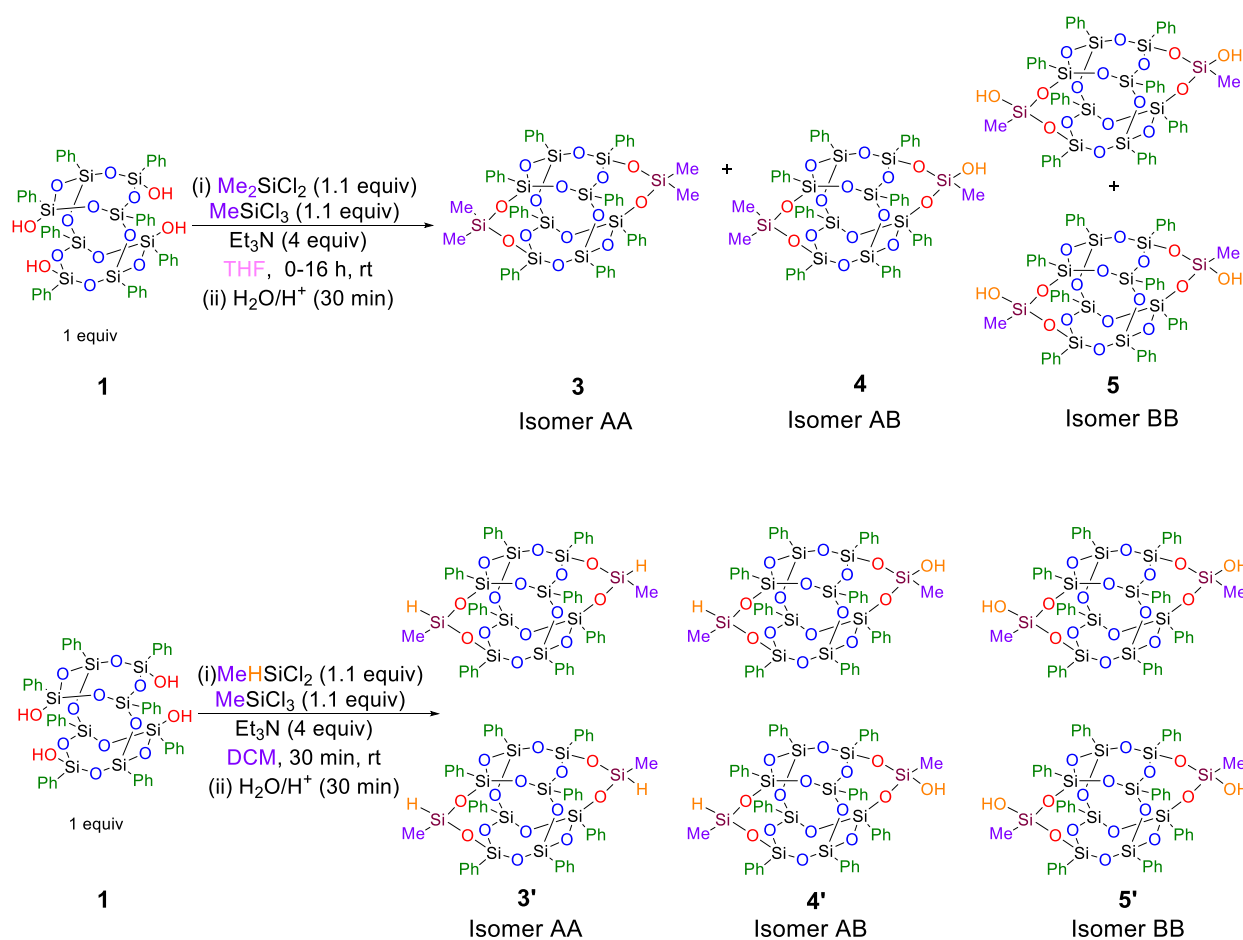
4.2 Synthesis of isomers of capped DDSQ structures

The series synthesis started via DDSQ tetrol capping using two equivalents of methyl trichlorosilane as a capping agent. The two ‘Cl’ functional groups on the chlorosilane react with the hydroxyl group on the DDSQ. The remaining third ‘Cl’ functional group is hydrolyzed to an -OH group in the subsequent step, as depicted in Scheme 4-2.



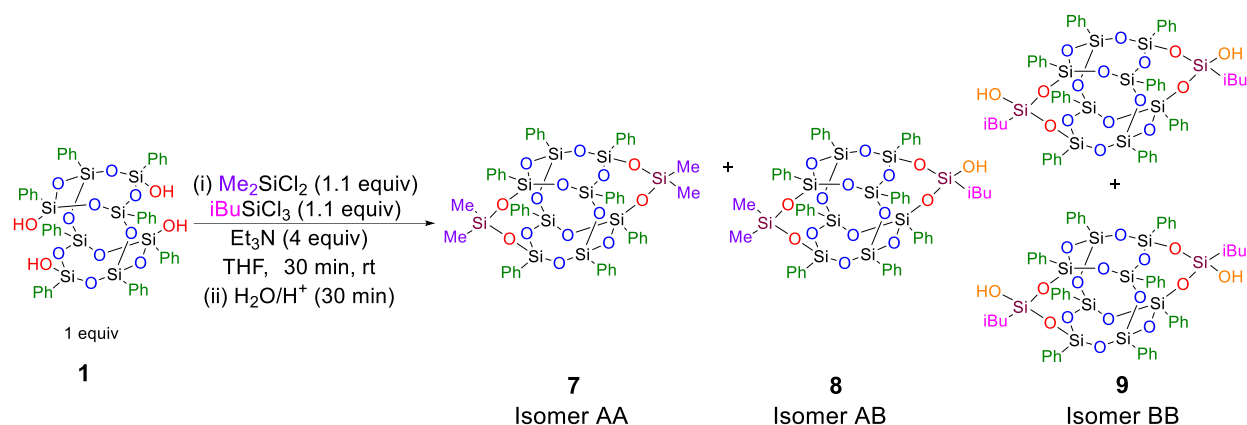
To begin with, the functional groups attached to the cage structures are small non-bulky groups such as methyl or hydrogen groups. Hence, there are two types of chlorosilanes used in this reaction; the first set is methyl hydrogen dichlorosilane and methyl trichlorosilane, whereas the second set is dimethyl dichlorosilane and methyl trichlorosilane. This addition leads to the formation of 3 major groups of isomeric compounds. Each isomeric group may have *cis* and *trans* isomers depending on the functional groups used in chlorosilanes. Isomer AA has been capped with the first type of dichlorosilane on both sides; isomer AB has been capped on either side by functional groups from both the dichlorosilanes and isomer BB has been capped with the second type of dichlorosilane on both sides.

The asymmetrically capped AB isomer has been isolated using column chromatography based on the polarity differences of the isomers. The AB isomer is then further used to extend one side of the functional groups while the other side of the cage has constant functional groups. The extension leads to asymmetry on the ends of the cages, leading to increased system entropy.



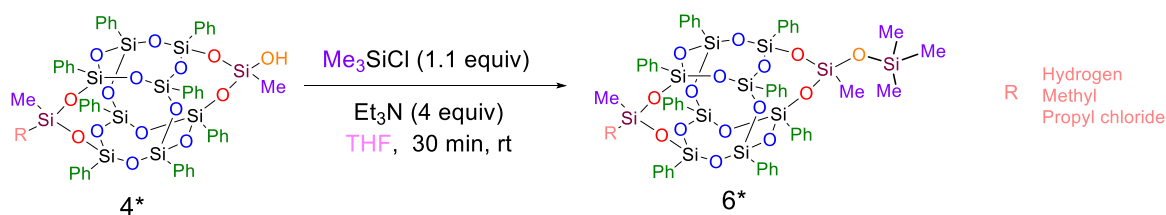
Scheme 4-3 : Capping of DDSQ tetrol using two different chlorosilanes to obtain an isomer mixture

Like compound **4**, compound **8** was synthesized starting with dimethyl dichlorosilane and isobutyl trichlorosilane. The resulting asymmetric AB product forms an analogous compound to the **4** synthesized previously.



Scheme 4-4 : Capping of DDSQ tetrol with RSiCl₂ type chlorosilanes

It has been found that the presence of hydroxy groups in the cage system might render them unsuitable to be analyzed with DSC. The extension of the side chain of capped DDSQ cages can be easily done using chlorosilane. The silanol group on the cage structure reacts with the chlorosilane to add an 'M' silicon onto the cage, as seen in Scheme 4-5.



Scheme 4-5 : Capping of the hydroxyl group with a dichlorosilane

²⁹Si NMR analysis of the product has been shown in Figure 4-2. The silicon NMR depicts seven groups of silicon atoms present in compound **6**. There are 1 group of 'M' silicon atoms, two groups of 'D' silicon atoms, and 4 types of 'T' silicon atoms. The red 'M' silicon atom comes around 10.0 ppm, the green 'D' silicon atom comes around -15 ppm, the yellow 'D' silicon atom comes around -64 ppm, and the remaining four groups of 'T' silicon atoms show up between -78.5 ppm to -80 ppm. A similar methodology can be used to modify the hydroxyl groups on the cage shown in Scheme 4-5.

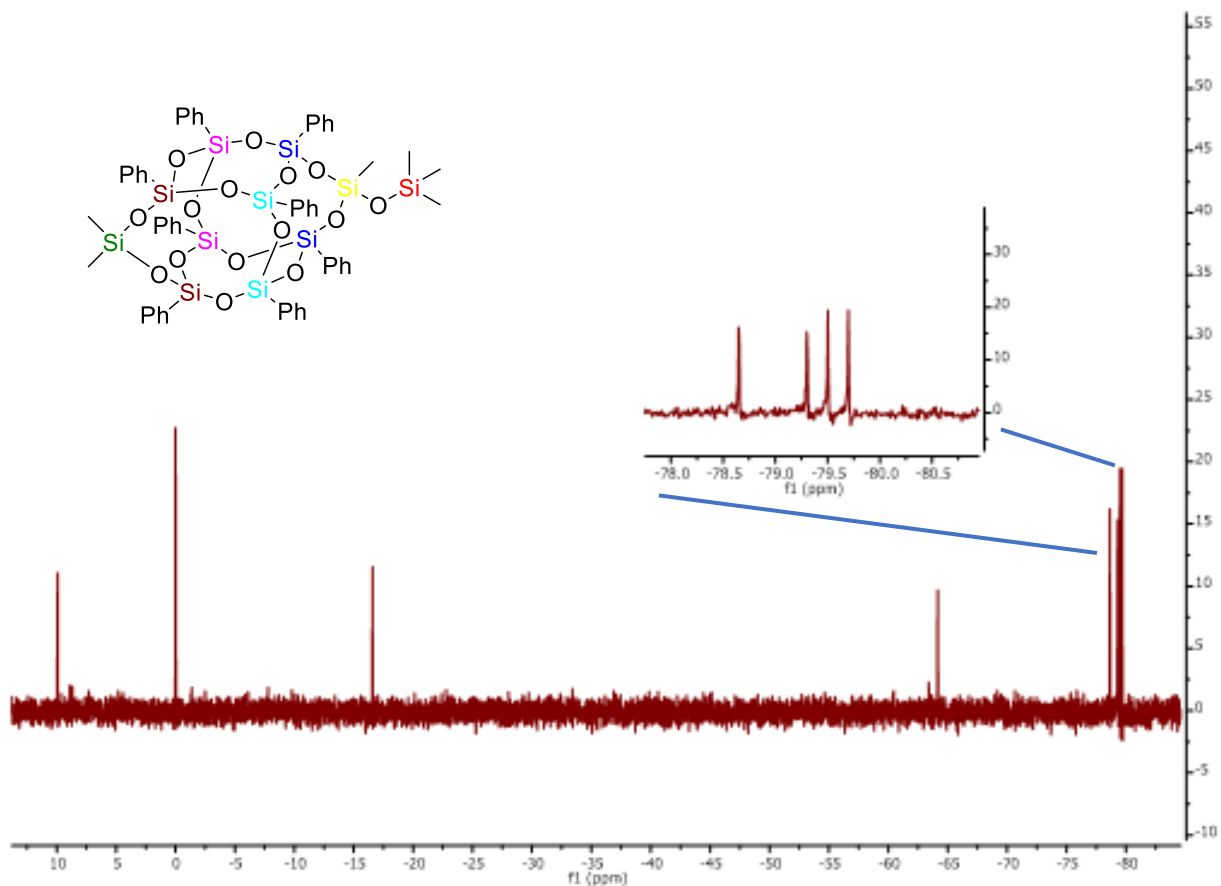


Figure 4-2 : ^{29}Si NMR analysis

4.3 Thermal Analysis using DSC

DSC analysis was performed to study the thermal characteristics of the synthesized series of analogous cage-like structures. Melting behavior, as expressed in DSC trace for pure compounds, is usually observed as a single sharp endothermic peak in which the onset temperature (T_{onset}) is very similar to the peak temperature (T_{peak}).¹¹ Presence of isomers usually broadens the solid-to-liquid transition peak.¹⁷ Table 4-1 depicts the melting temperatures, enthalpy, and entropy for 6 isomer mixtures synthesized using Scheme 4-3. The asymmetric isomer has a lower entropy as compared to the symmetrical isomers. **5'** has the highest entropy in the set of isomers. It means the isomer with hydroxyl groups has a more ordered crystal structure than any other isomer.

Table 4-1 : DSC obtained experimental values for DDSQ-2(R₁R₂).

Compound	T _{peak} (°C)	T _m (°C)	ΔH _m (kJ/mol)	ΔS _m (J/mol K)
3'	279 (Major)	276	39.7	144
5'	267	262	40.6	155
4'	286	282	31.7	111
6 isomer mixture	287 (Broad peak)	272	33.2	122

This value might be attributed to hydrogen bonding contributing to a more ordered crystal structure. Also, the 6-isomer mixture exhibits a broad solid-to-liquid transition peak of about 15 °C indicating that although the individual isomers do show a sharp melting transition, the mixture of isomers eventually disrupts the ordered packing leading to glassy like solid to liquid transition temperatures.

Table 4-2 : Experimental values obtained for DDSQ-2[(RMe)(MeOH)] by DSC.

Compound R (4*)	T _{peak} (°C)	T _m (°C)	ΔH _m (kJ/mol)	ΔS _m (J/mol K)
Hydrogen	286	282	33.6	119
Methyl	290	290	39.5	137
Propyl chloride	223 (Major)	219	28.6	131

4* is the analogous series of compounds where the R group keeps increasing in size from hydrogen to methyl to propyl chloride group. 4* with the methyl group has the sharpest melting point, with the onset and peak temperatures being the same. The enthalpy and entropy are the highest amongst

the series of compounds. In the case when the 'R' group is a hydrogen atom, the system has the lowest entropy overall in the system. The melting point is almost similar to that of the methyl group as the 'R' substituent, but the enthalpy is lower than that of the 'R' substituents. The system with propyl chloride with the substituent has the lowest melting point of the three compounds. Correspondingly, it also has the lowest enthalpy of the three compounds.

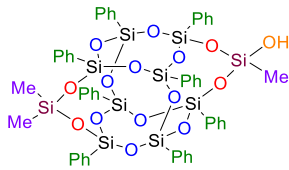
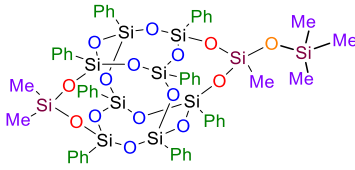
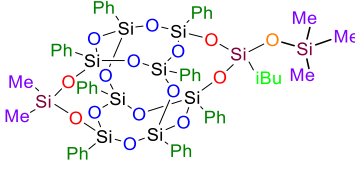
Table 4-3 : Experimental values obtained for DDSQ-2[(RMe)(MeOTMS)] by DSC.

Compound R (6*)	T_{peak} (°C)	T_m (°C)	ΔH_m (kJ/mol)	ΔS_m (J/mol K)
Hydrogen	206	200	37	185
Methyl	210	206	38.7	188
Propyl chloride	208 (Broad)	190	19.5	103

6* is the analogous series of compounds where the hydroxy group on 4* has been modified by shielding it via reaction with trimethylchlorosilane (TMSCl). The 'R' group keeps increasing from hydrogen to methyl to propyl chloride group. As seen from Table 4-3, the melting point of the compounds where the 'R' group is either a hydrogen atom or methyl group, the melting point of the system drops by almost 80 °C by adding a bulky TMS group on the cages. This instance is the first indication that increasing the asymmetry on one side of the cage leads to a significant swing in the melting temperature of the compounds. Surprisingly, the enthalpy and entropy for 6* in the case where the 'R' group is an H or Me is higher than the corresponding values in 4*. However, the solid-to-liquid transition temperature changes by about 20 ° when the 'R' group is propyl

chloride. The nature of the peak changes to a relatively broad peak with about a 15 °C difference between the onset and peak points.

Table 4-4 : Experimental values obtained for DDSQ-2[(Me₂)(RR')] by DSC.

Compound R (6*)	T _{peak} (°C)	T _m (°C)	ΔH _m (kJ/mol)	ΔS _m (J/mol K)
	290	290	39.5	137
	210	206	38.7	188
	152 (Broad)	138	21.6	157

The last comparison system of the capped cages studied in this work is based on Scheme 4-5. In this case, the isobutyl group has replaced the methyl group. Upon DSC analysis of the system, having two bulky groups, such as isobutyl and OTMS groups, on one side of the cage versus smaller groups, such as methyl groups, on the other side, vastly changes the thermal characteristics. The solid-to-liquid transition characteristics change from a sharp peak at 290 °C for the case with (Me)(OH) on one side to a broad peak around 145 °C where the functional groups are (iBu)(OTMS). The system's enthalpy drops as the size of the functional groups increases.

To summarize, a series of compounds with the increasing bulkiness of the functional groups was synthesized. The initial series had a reactive silanol functional group present in the cages. This

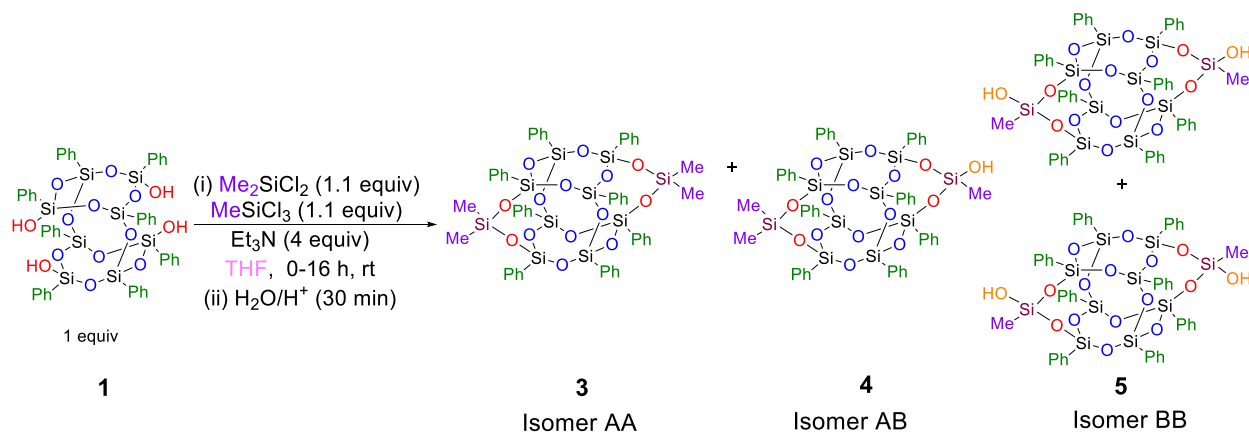
functional group's presence affected the cages' thermal characteristics studies. To circumnavigate the silanol group's decomposition problem, the silanol group was protected with trimethylsilyl chloride. This protection helps to improve the thermal stability of the cage system and, at the same time, provides another system of compounds with a bulky side group leading to the formation of asymmetry in the cage. DSC analysis shows that bulky groups reduce the solid-to-liquid transition temperature from 290 °C to 145 °C. The enthalpy of the system also reduces with increasing size. Although the system shows solid-to-liquid transition temperatures lowering, the system still does not exhibit a glassy substance-like solid-to-liquid transition characteristic. A new class of modified DDSQ-like cage systems needs to be developed that will inherently modify the structure of the core cage rather than modifying the peripheral organic corona. The next chapter synthesized and explored a new series of DDSQ-like cage structures.

4.4 Experimental details

4.4.1 General Information

All manipulations were done under a nitrogen atmosphere using standard Schlenk techniques except otherwise stated. All commercially available chemicals were used as received unless otherwise indicated. Methylchlorosilane, methyl trichlorosilane, dimethyl dichlorosilane, methyl (propyl chloride) dichlorosilane, trimethylchlorosilane, isobutyl trichlorosilane deuterated chloroform with 1 vol % tetramethylsilane (CDCl_3 -1%TMS), were purchased from Sigma-Aldrich. Graphene nanoplatelet was obtained from XG Sciences. $\text{DDPh}_8\text{T}_8(\text{OH})_4$ was obtained from Hybrid Plastics. Triethylamine (Et_3N) was purchased from Avantor and distilled over calcium hydride before use. Tetrahydrofuran (THF), dichloromethane (DCM), and methanol (MeOH) n-hexanes were purchased from Sigma-Aldrich. THF was distilled over benzophenone and sodium metal at 50 °C under nitrogen. The other solvents were used as purchased without further purification, and the glassware was oven dried. All ^1H , ^{13}C , and ^{29}Si NMR were acquired on an Agilent DirectDrive2 500 MHz NMR spectrometer equipped with a OneProbe operating at 500 MHz for ^1H NMR, 126 MHz for ^{13}C NMR, and 99 MHz for ^{29}Si NMR using CDCl_3 and recorded at 25 °C. ^1H -NMR spectra were recorded with 8 scans, a relaxation delay of 1s, and a pulse angle of 45° and referenced to the residual protonated solvent in CDCl_3 (7.24 ppm). ^{13}C -NMR spectra were collected with 254 scans, a relaxation delay of 0.1 s, and a pulse angle of 45°. ^{29}Si NMR spectra were recorded with either 256 scans, a relaxation delay of 25 s, and a pulse angle 45°. Column chromatography was performed on EMD Millipore silica gel 60 columns of 40– 63 Å silica, 230–400 mesh. Thin-layer chromatography (TLC) was performed on plates of EMD 250- μm silica 60-F254.

4.4.2 Synthesis of isomeric mixtures



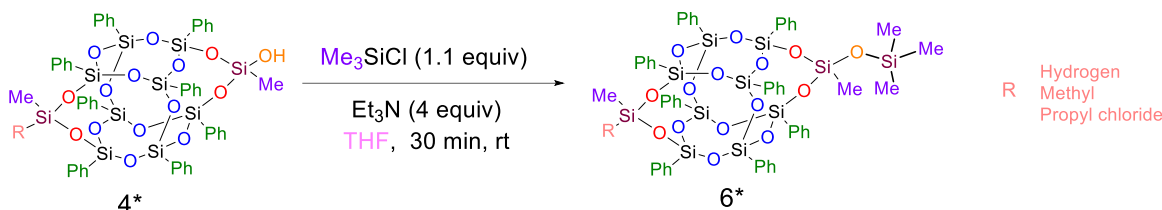
Scheme 4-6 : Reaction scheme for synthesis of 6 isomeric mixture

To a 250 mL round bottom flask was added DDPH₈T₈(OH)₄ (2.15 g, 0.002 mol, 1 equiv), methyl trichlorosilane (0.48 g, 0.002 mol, 1 equiv), dimethyldichlorosilane (0.40 g, 0.002 mol, 1 equiv) and a stir bar. The flask was placed under an N₂ atmosphere, and freshly distilled DCM (~50 mL) was added. Et₃N (0.815 g, 0.008 mol, 4 equiv) was added dropwise to this solution. Upon complete addition of the triethylamine, the white-colored reaction mixture turned colorless. The reaction mixture was stirred for 30 min. Dilute HCl solution (10 mL) was then added to the reaction flask, and the contents were stirred for 2 hours, after which the solvent was removed using a rotary evaporator. THF (~15 mL) was added to create a slurry. This slurry was filtered through a medium frit funnel to obtain the crude product. The products were isolated using silica column chromatography. A glass preparatory chromatography column, 60 cm in length 4 cm internal diameter, with a 500 mL round top reservoir, was packed with Si-gel, resulting in a packing height of about 75% of the total column height. DCM used as a mobile phase was flushed through the packed bed under pressure generated by a dry N₂ stream. The mobile phase was passed through the column multiple times until no air bubbles or dry space was observed.

A concentrated solution of the product mixture with DCM was gently injected from the top of the wet Si-gel bed and pushed into the packed bed until no solution was observed above the packed bed. The column was then gently charged with 500 mL of DCM and flushed using the N₂ stream. Fractions of 20 mL were collected at the bottom of the column until the DCM reached the top of the bed. Each fraction was seated on 5 cm TLC plates of Si-gel supported on aluminum. Fractions were eluted with DCM and then analyzed under a 245 nm UV lamp. Similar fractions were combined and dried. The asymmetrically capped DDSQ compound is eluted out as the second batch of fractions from the column. The yield is 48 %.

¹H NMR (500 MHz, Chloroform-*d*) δ 7.56 (ddt, J = 13.5, 8.1, 1.3 Hz, 8H), 7.44 (dq, J = 8.1, 1.5 Hz, 8H), 7.39 (tq, J = 7.8, 1.3 Hz, 4H), 7.36 – 7.29 (m, 4H), 7.25 (td, J = 1.8 Hz, 8H), 7.22 – 7.14 (m, 9H), 2.65 (d, J = 1.7 Hz, 1H), 0.35 (d, J = 0.9 Hz, 3H), 0.31 (d, J = 1.0 Hz, 6H). ²⁹Si{¹H} NMR (99 MHz, Chloroform-*d*) δ -79.40, -79.28, -78.65, -78.49, -54.01, -16.36.

4.4.3 Synthesis of protected TMS cages



Scheme 4-7 : Reaction scheme for synthesis of protected TMS cages

To a 250 mL round bottom flask was added $\text{DDPh}_8\text{T}_8(\text{Me}_2)(\text{MeOH})$ (1.05 g, 0.001 mol, 1 equiv), trichloromethyl silane (0.48 mL, 0.005 mol, 5 equiv), and a stir bar. The flask was placed under an N_2 atmosphere, and freshly distilled DCM (~50 mL) was added. Et_3N (0.102 g, 0.001 mol, 1.0 equiv) was added dropwise to this solution. Upon complete addition of the triethylamine, the white-colored reaction mixture turned colorless. The reaction mixture was stirred for 30 min, and the solvent was removed using a rotary evaporator. THF (~ 15 mL) was added to create a slurry. This slurry was filtered through a medium frit funnel to obtain the crude product. The products were isolated using silica column chromatography. The yield is 95 %

^1H NMR (500 MHz, Chloroform-*d*) δ 7.55 (td, $J = 8.3, 1.4$ Hz, 8H), 7.42 (dddd, $J = 7.6, 4.6, 2.9, 1.4$ Hz, 9H), 7.40 – 7.37 (m, 3H), 7.37 – 7.30 (m, 4H), 7.29 – 7.23 (m, 9H), 7.18 (q, $J = 7.5$ Hz, 8H), 0.30 (d, $J = 1.6$ Hz, 6H), 0.26 (s, 3H), 0.03 (s, 8H). $^{29}\text{Si}\{^1\text{H}\}$ NMR (99 MHz, Chloroform-*d*) δ -79.70, -79.50, -79.30, -78.65, -64.15, -16.59, 9.92.

REFERENCES

- (1) Agaskar, P. A. New Synthetic Route to the Hydridospherosiloxanes Oh-H₈Si₈O₁₂ and D5h-H₁₀Si₁₀O₁₅. *Inorg. Chem.* 1991, *30* (13), 2707–2708. <https://doi.org/10.1021/ic00013a002>.
- (2) Feher, F. J.; Weller, K. J. Polyhedral Aluminosilsesquioxanes as Models for Aluminosilicates: Unique Synthesis of Anionic Aluminum/Silicon/Oxygen Frameworks. *Organometallics* 1990, *9* (10), 2638–2640. <https://doi.org/10.1021/om00160a003>.
- (3) Li, G.; Wang, L.; Ni, H.; Jr, C. U. P. Polyhedral Oligomeric Silsesquioxane (POSS) Polymers and Copolymers: A Review.
- (4) Feher, F. J. Polyhedral Oligometallasilsesquioxanes (POMSS) as Models for Silica-Supported Transition-Metal Catalysts. Synthesis and Characterization of (C₅Me₅)Zr[(Si₇O₁₂)(c-C₆H₁₁)₇]. *J. Am. Chem. Soc.* 1986, *108* (13), 3850–3852. <https://doi.org/10.1021/ja00273a062>.
- (5) Wu, J.; Mather, P. T. POSS Polymers: Physical Properties and Biomaterials Applications. *Polymer Reviews* 2009, *49* (1), 25–63. <https://doi.org/10.1080/15583720802656237>.
- (6) Baney, R. H.; Itoh, M.; Sakakibara, A.; Suzuki, T. Silsesquioxanes.
- (7) Scott, D. W. Thermal Rearrangement of Branched-Chain Methylpolysiloxanes ¹. *J. Am. Chem. Soc.* 1946, *68* (3), 356–358. <https://doi.org/10.1021/ja01207a003>.
- (8) Martynova, T. N.; Chupakhina, T. I. Heterofunctional Oligoorganylsilsesquioxanes. *Journal of Organometallic Chemistry* 1988, *345* (1–2), 10–18. [https://doi.org/10.1016/0022-328X\(88\)80229-8](https://doi.org/10.1016/0022-328X(88)80229-8).
- (9) Shockey, E. G.; Bolf, A. G.; Jones, P. F.; Schwab, J. J.; Chaffee, K. P.; Haddad, T. S.; Lichtenhan, J. D. Functionalized Polyhedral Oligosilsesquioxane (POSS) Macromers: New Graftable POSS Hydride, POSS α-Olefin, POSS Epoxy, and POSS Chlorosilane Macromers and POSS-Siloxane Triblocks. *Appl. Organometal. Chem.* 1999, *13* (4), 311–327. [https://doi.org/10.1002/\(SICI\)1099-0739\(199904\)13:4<311::AID-AOC847>3.0.CO;2-1](https://doi.org/10.1002/(SICI)1099-0739(199904)13:4<311::AID-AOC847>3.0.CO;2-1).
- (10) Vahabi, H.; Eterradosi, O.; Ferry, L.; Longuet, C.; Sonnier, R.; Lopez-Cuesta, J.-M. Polycarbonate Nanocomposite with Improved Fire Behavior, Physical and Psychophysical Transparency. *European Polymer Journal* 2013, *49* (2), 319–327. <https://doi.org/10.1016/j.eurpolymj.2012.10.031>.
- (11) Schoen, B. Aminophenyl Double Decker Silsesquioxanes: Spectroscopic Elucidation, Physical and Thermal Characterization, and Their Applications, Michigan State University.
- (12) Schoen, B. W.; Holmes, D.; Lee, A. Identification and Quantification of *Cis* and *Trans* Isomers in Aminophenyl Double-Decker Silsesquioxanes Using ¹H-²⁹Si GHMBC NMR: Quantification of *Cis* and *Trans* Isomers in Double-Decker Silsesquioxanes. *Magn. Reson. Chem.* 2013, *51* (8), 490–496. <https://doi.org/10.1002/mrc.3962>.

- (13) Vogelsang, D. F.; Dannatt, J. E.; Schoen, B. W.; Maleczka, R. E.; Lee, A. Phase Behavior of Cis–Trans Mixtures of Double-Decker Shaped Silsesquioxanes for Processability Enhancement. *ACS Appl. Nano Mater.* 2019, 2 (3), 1223–1231. <https://doi.org/10.1021/acsanm.8b02114>.
- (14) Schoen, B. W.; Lira, C. T.; Lee, A. Separation and Solubility of Cis and Trans Isomers in Nanostructured Double-Decker Silsesquioxanes. *J. Chem. Eng. Data* 2014, 59 (5), 1483–1493. <https://doi.org/10.1021/je4010245>.
- (15) Guo, T.; Wang, B. Isothermal Cold Crystallization and Melting Behaviors of Poly(Lactic Acid)/Epoxy Vinyl Polyhedral Oligomeric Silsesquioxanes Nanocomposites. *Polymer-Plastics Technology and Engineering* 2014, 53 (9), 917–926. <https://doi.org/10.1080/03602559.2014.886061>.
- (16) Vogelsang, D. F.; Maleczka, R. E.; Lee, A. HPLC Characterization of Cis and Trans Mixtures of Double-Decker Shaped Silsesquioxanes. *Silicon* 2019, 11 (1), 5–13. <https://doi.org/10.1007/s12633-018-0045-4>.
- (17) Vogelsang, D. F.; Maleczka, R. E.; Lee, A. Phase Behavior of Selected Condensed Double-Decker Shaped Silsesquioxane Compounds. *Silicon* 2022, 14 (13), 7555–7565. <https://doi.org/10.1007/s12633-021-01470-0>.
- (18) Vogelsang, D. F.; Maleczka, R. E.; Lee, A. Predictive Liquid Chromatography Separation for Mixtures of Functionalized Double-Decker Shaped Silsesquioxanes Based on HPLC Chromatograms. *Ind. Eng. Chem. Res.* 2019, 58 (1), 403–410. <https://doi.org/10.1021/acs.iecr.8b05490>.
- (19) Suarez, D. F. V. Separation and Characterization of Closed Functionalized Double-Decker Shaped Silsesquioxanes, Michigan State University, 2018.
- (20) Vogelsang, D. F.; Dannatt, J. E.; Maleczka, R. E.; Lee, A. Separation of Asymmetrically Capped Double-Decker Silsesquioxanes Mixtures. *Polyhedron* 2018, 155, 189–193. <https://doi.org/10.1016/j.poly.2018.08.016>.

APPENDIX

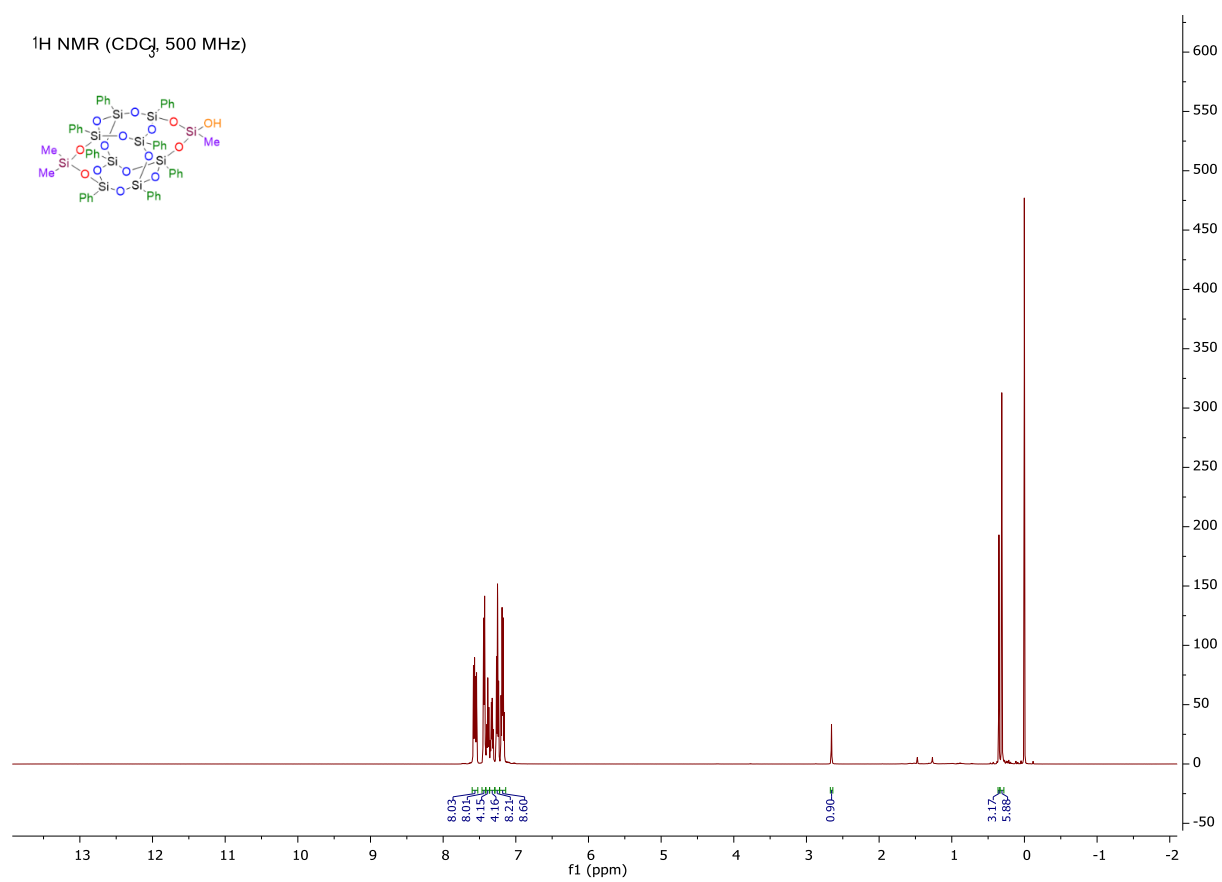


Figure 4-3 : ^1H -NMR (CDCl_3 , 500 MHz)

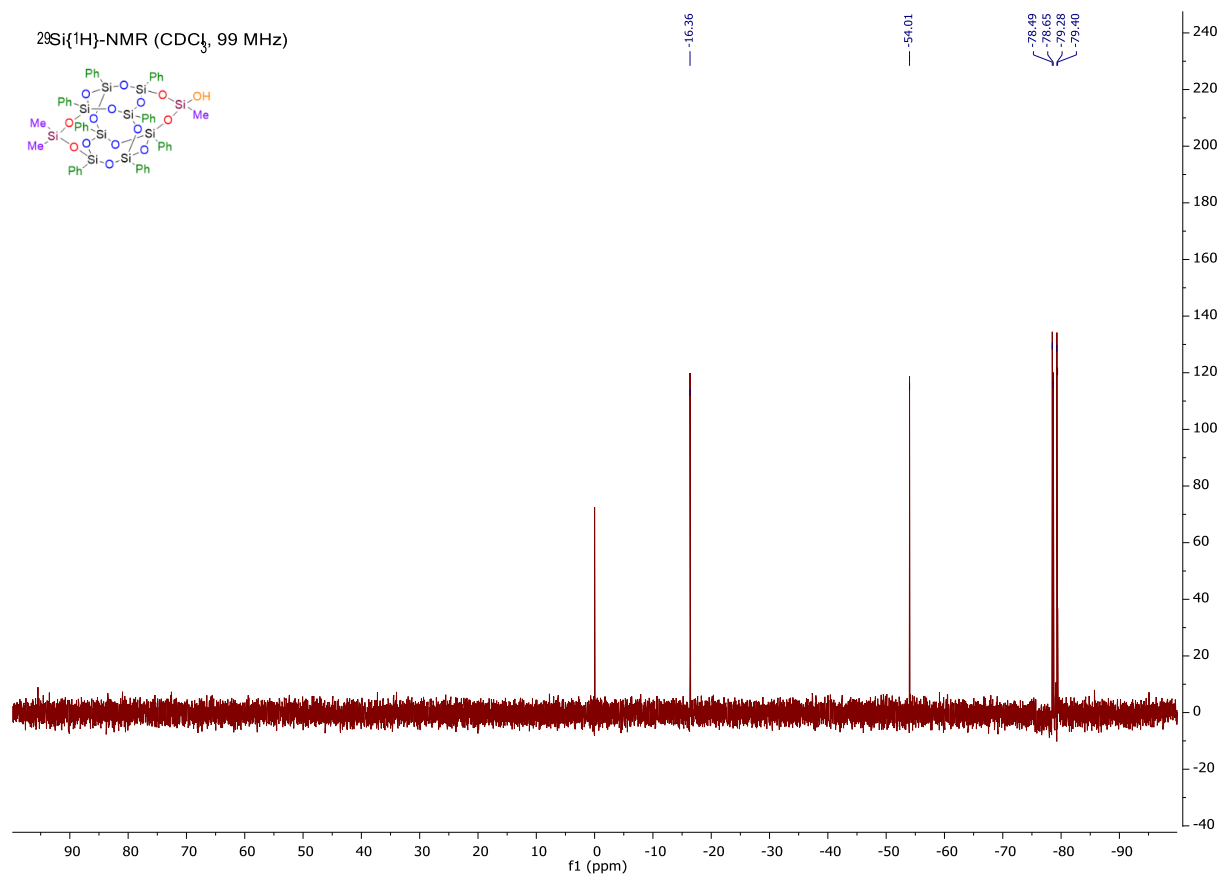
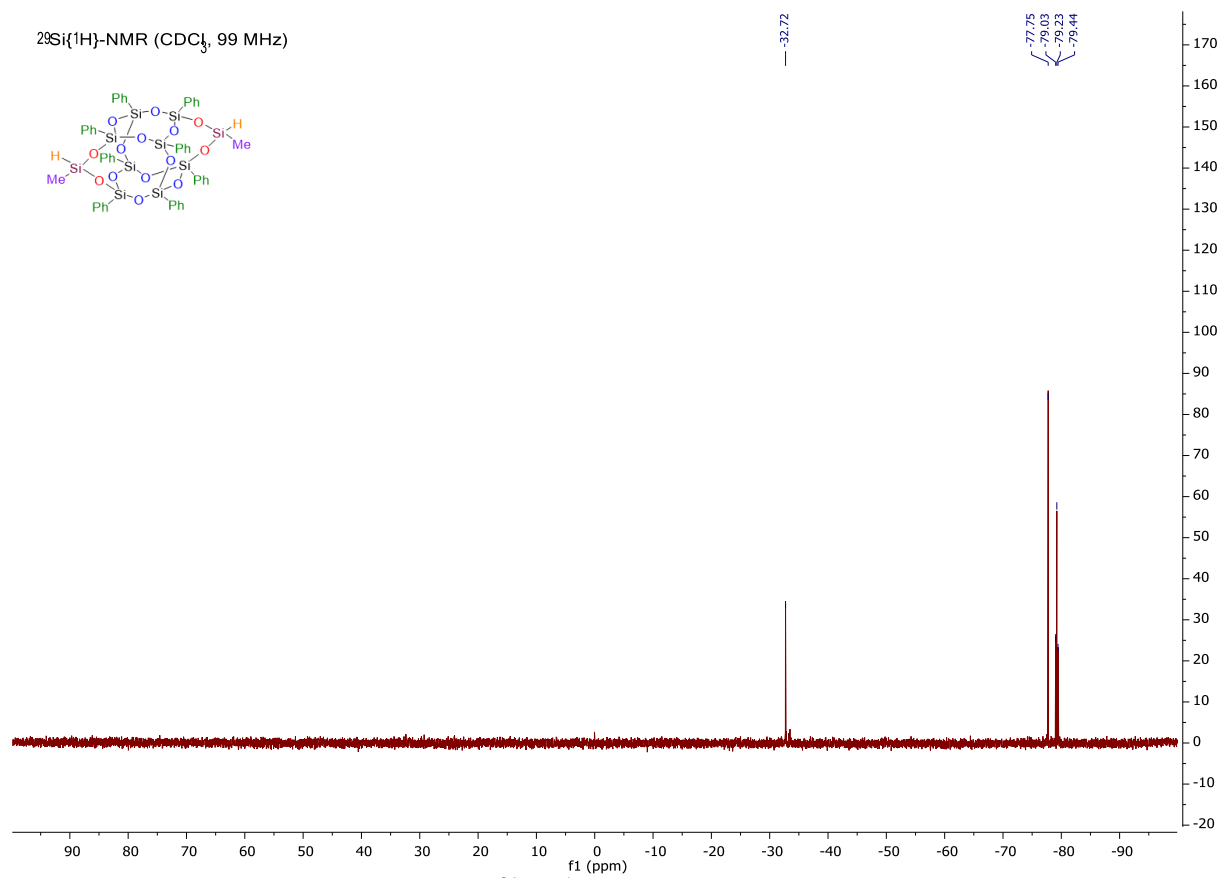


Figure 4-4 : $^{29}\text{Si}\{^1\text{H}\}$ -NMR (CDCl_3 , 99 MHz)



^1H NMR (CDCl_3 , 500 MHz)

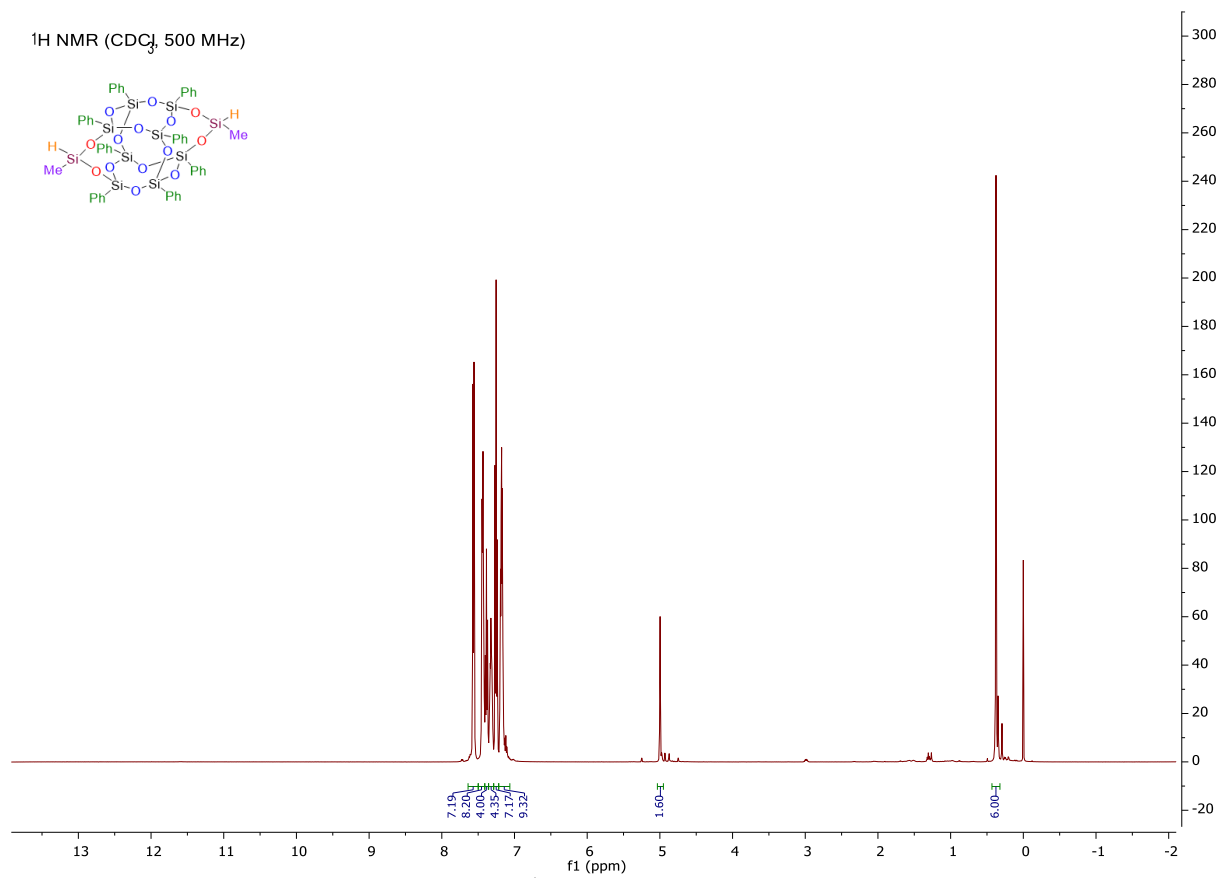


Figure 4-6 : ^1H -NMR (CDCl_3 , 500 MHz)

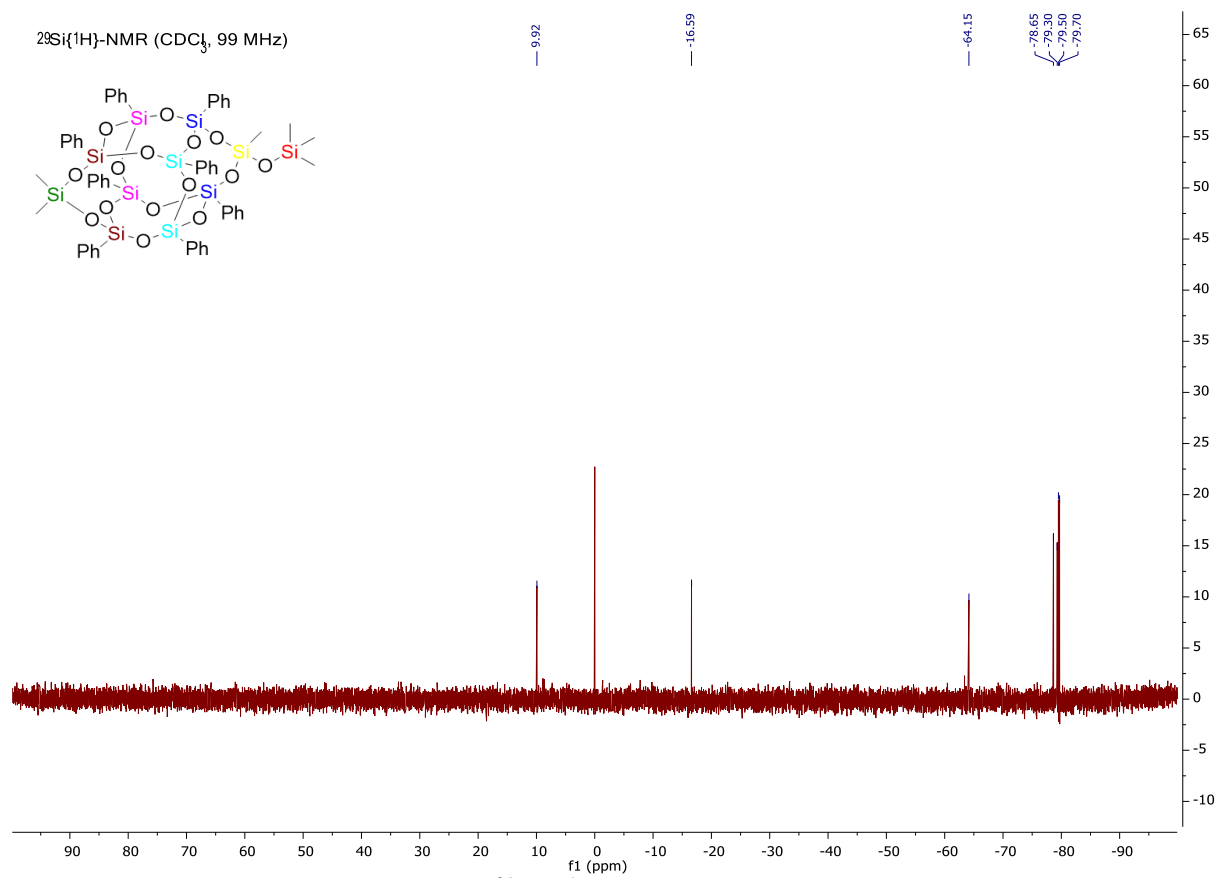


Figure 4-7 : $^{29}\text{Si}\{^1\text{H}\}$ -NMR (CDCl_3 , 99 MHz)

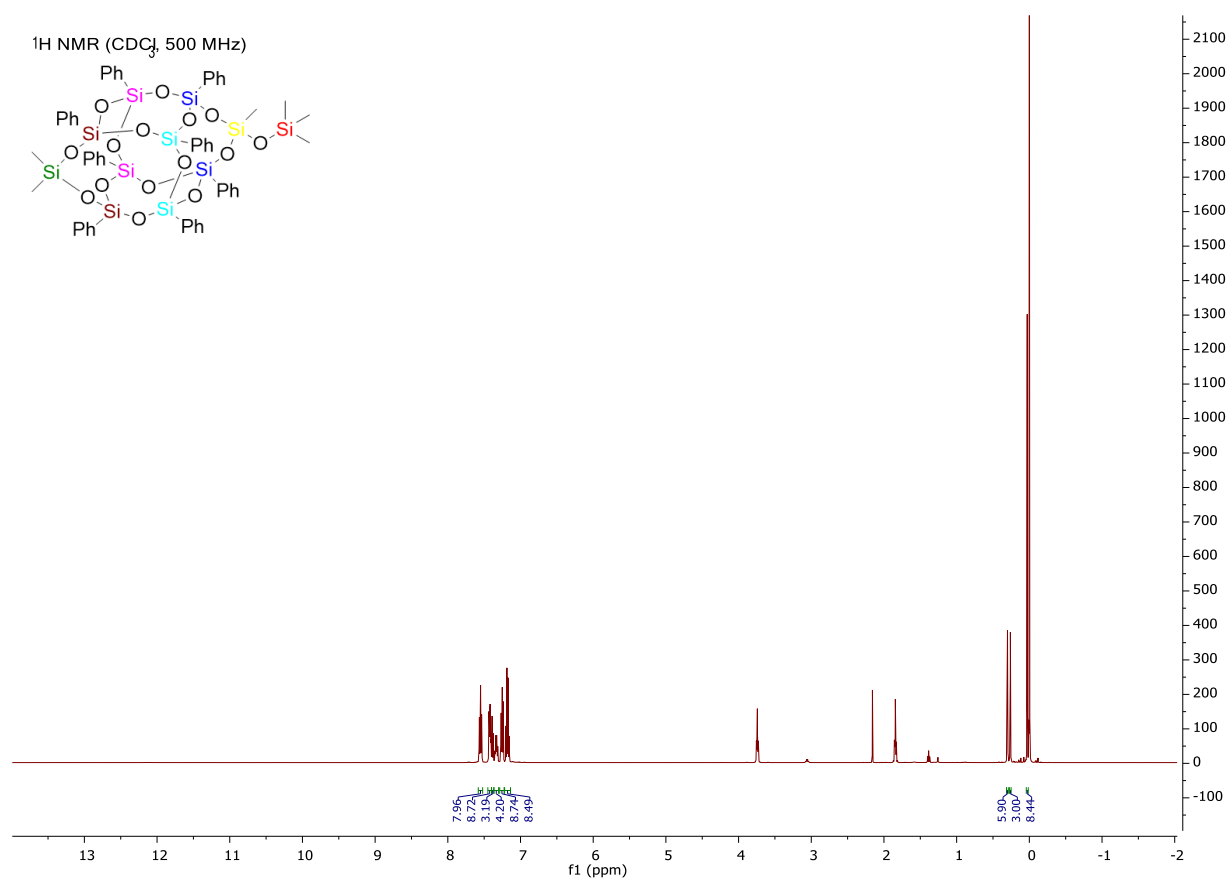


Figure 4-8 : ¹H-NMR (CDCl₃, 500 MHz)

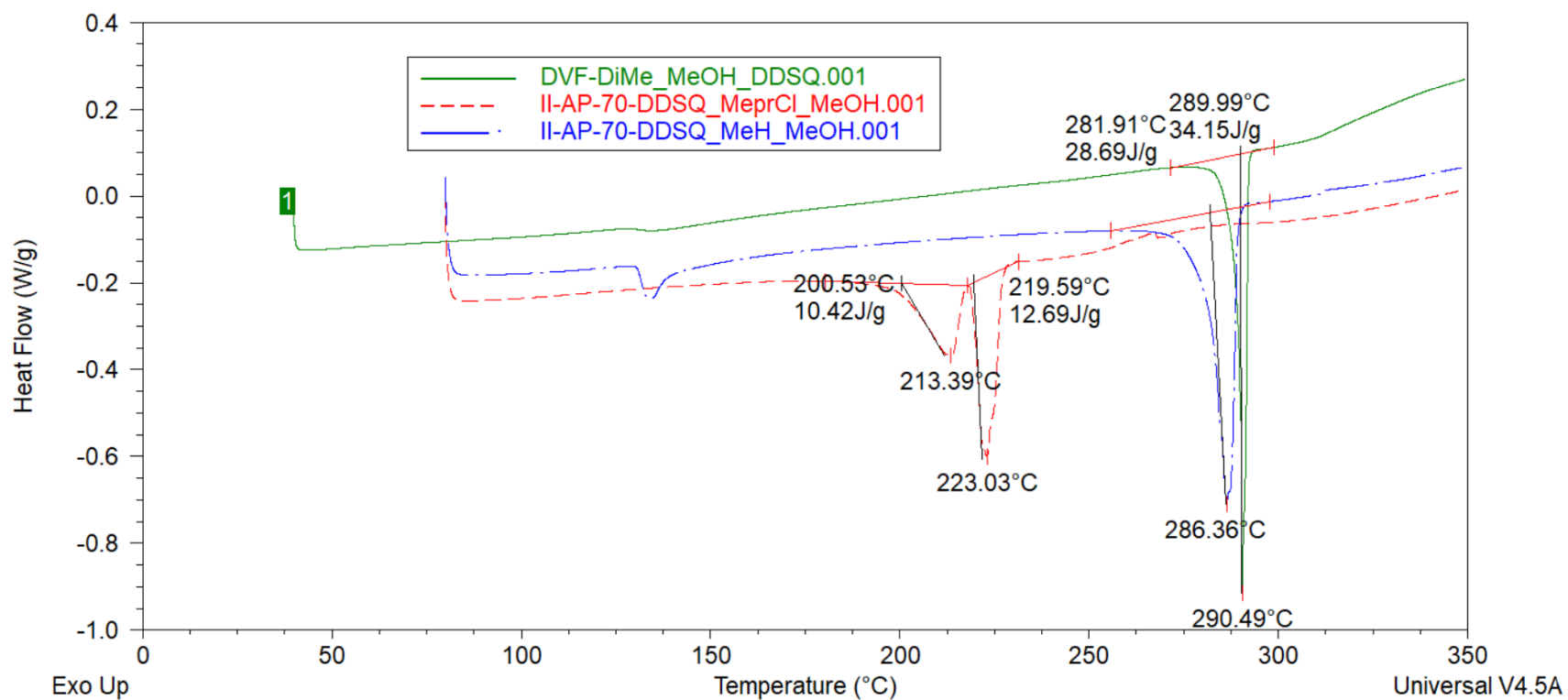


Figure 4-9 : DSC data for heating cycles (R)DDSQ(MeOH).

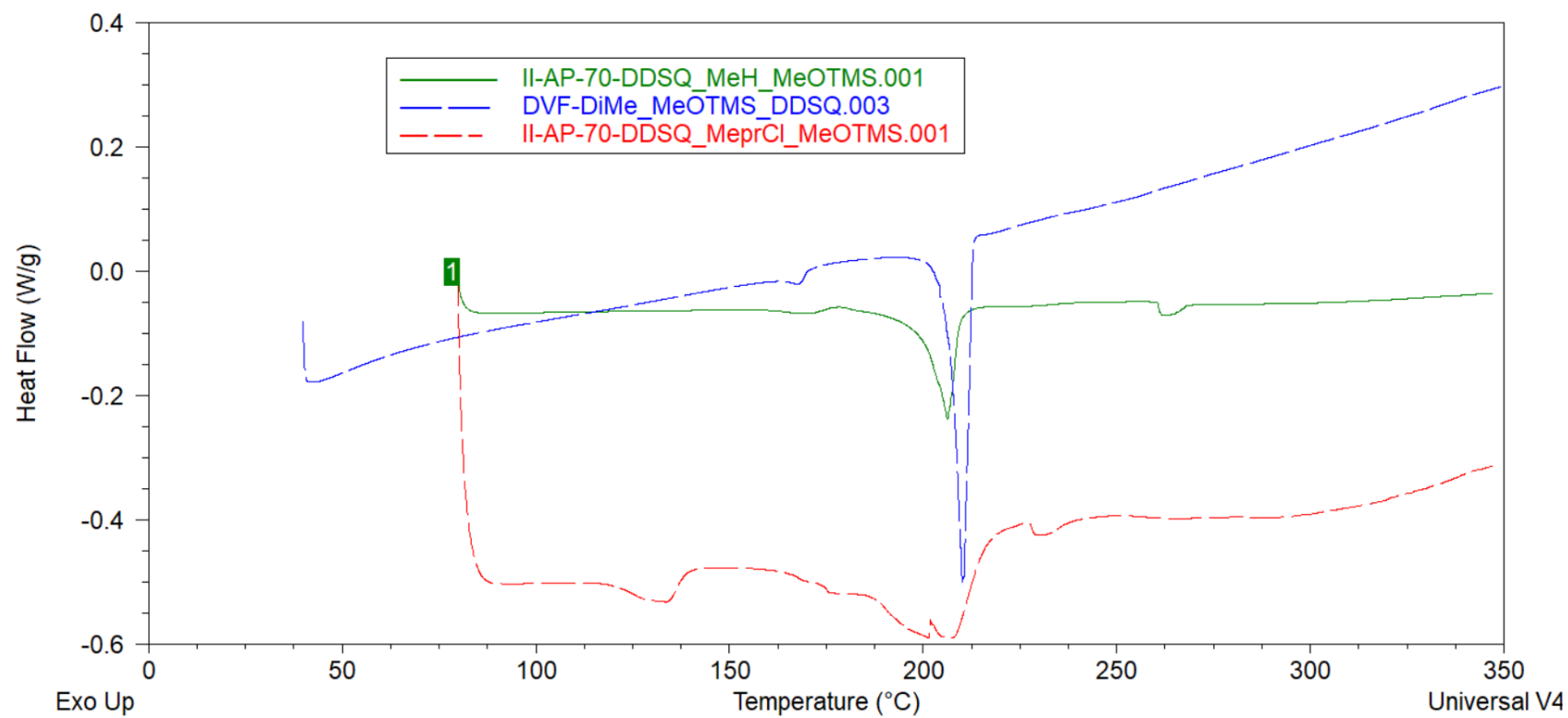


Figure 4-10 : DSC data for heating cycles (R)DDSQ(MeOTMS).

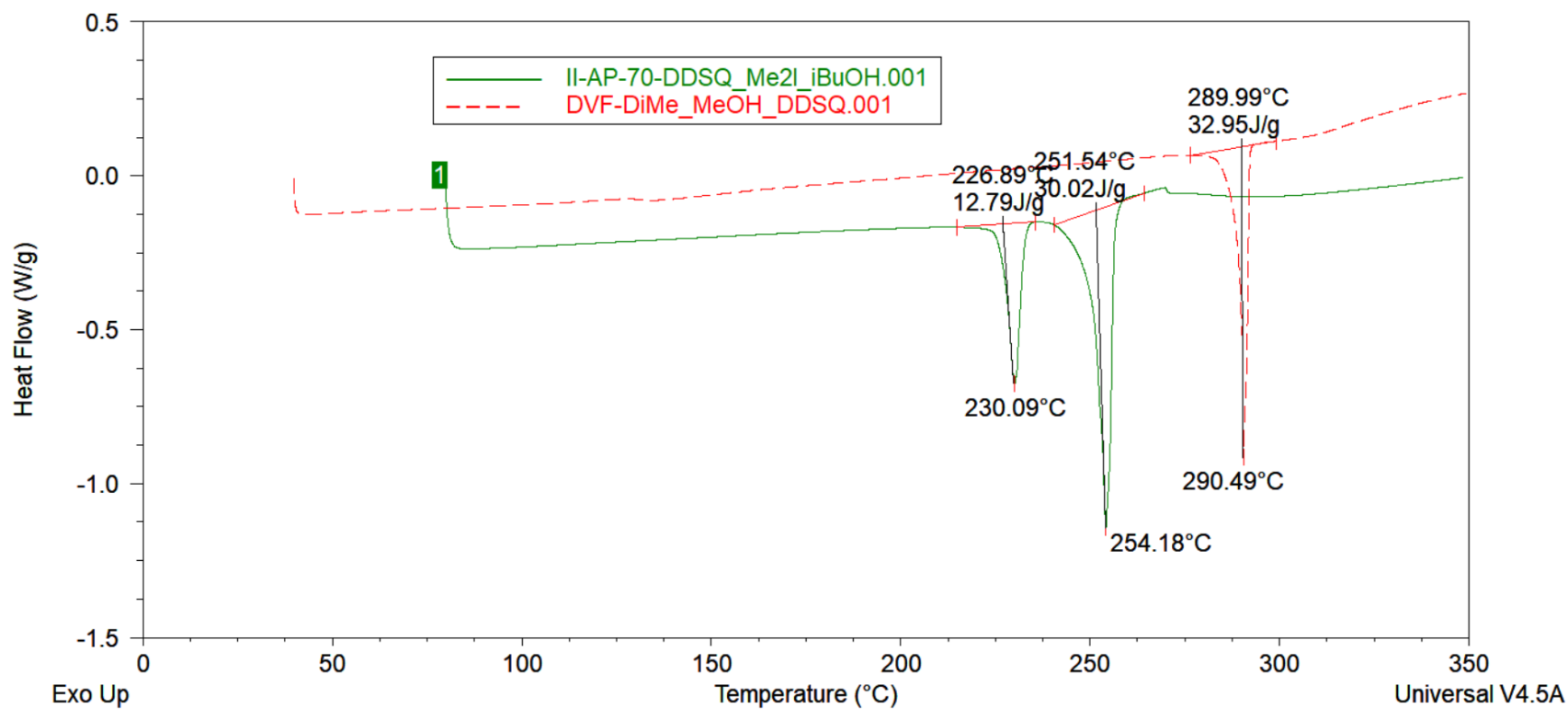


Figure 4-11 : DSC data for heating cycles for (Me₂)DDSQ(ROH)

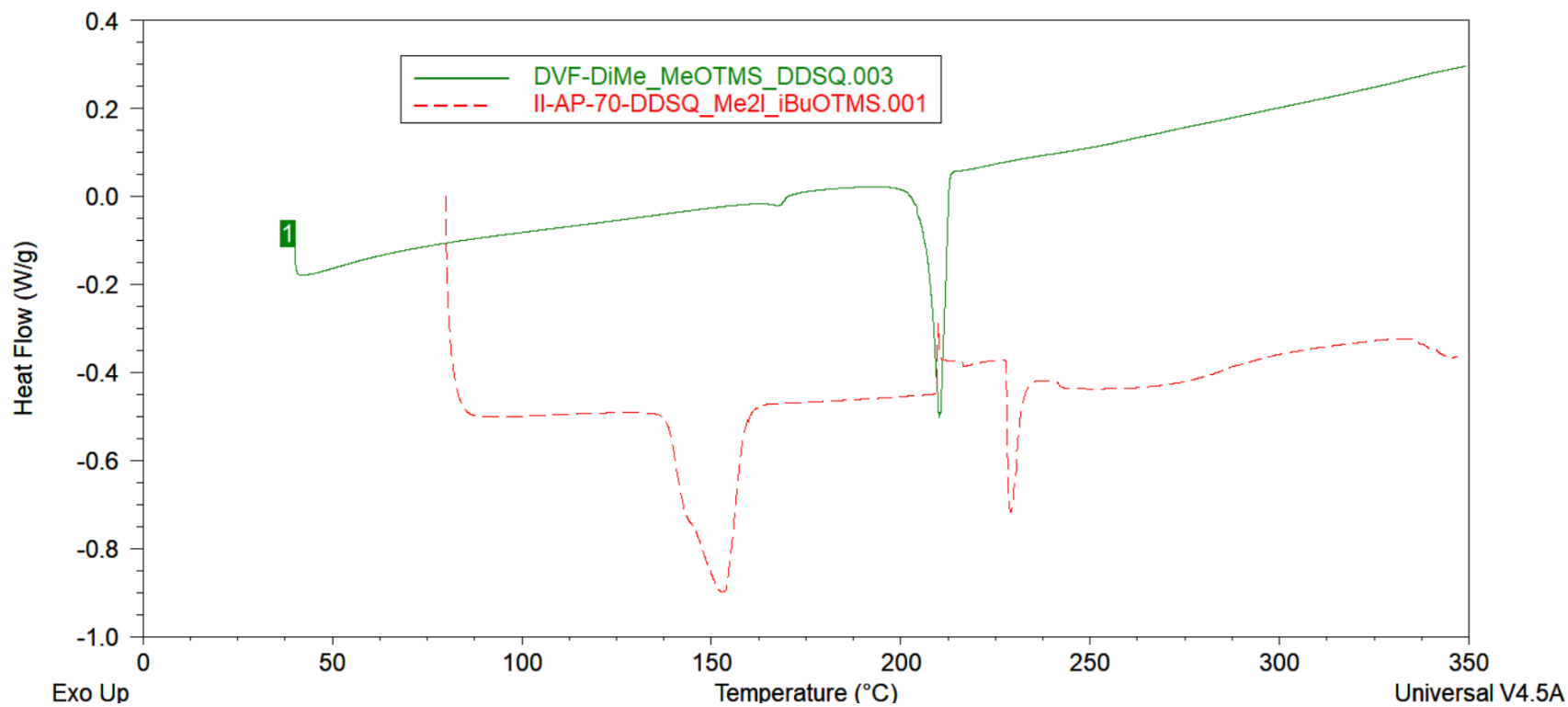


Figure 4-12 : DSC data for heating cycles for (Me₂)DDSQ(ROTMS)

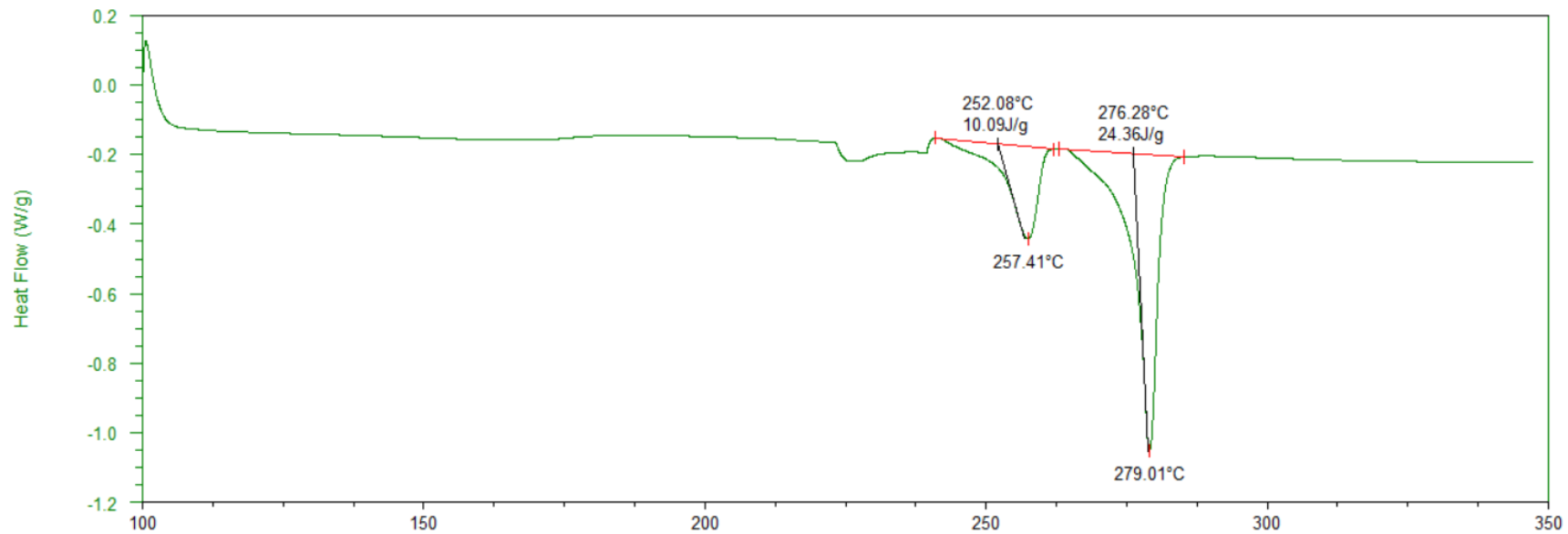


Figure 4-13 : DSC data for heating cycle for (MeH)DDSQ(MeH)

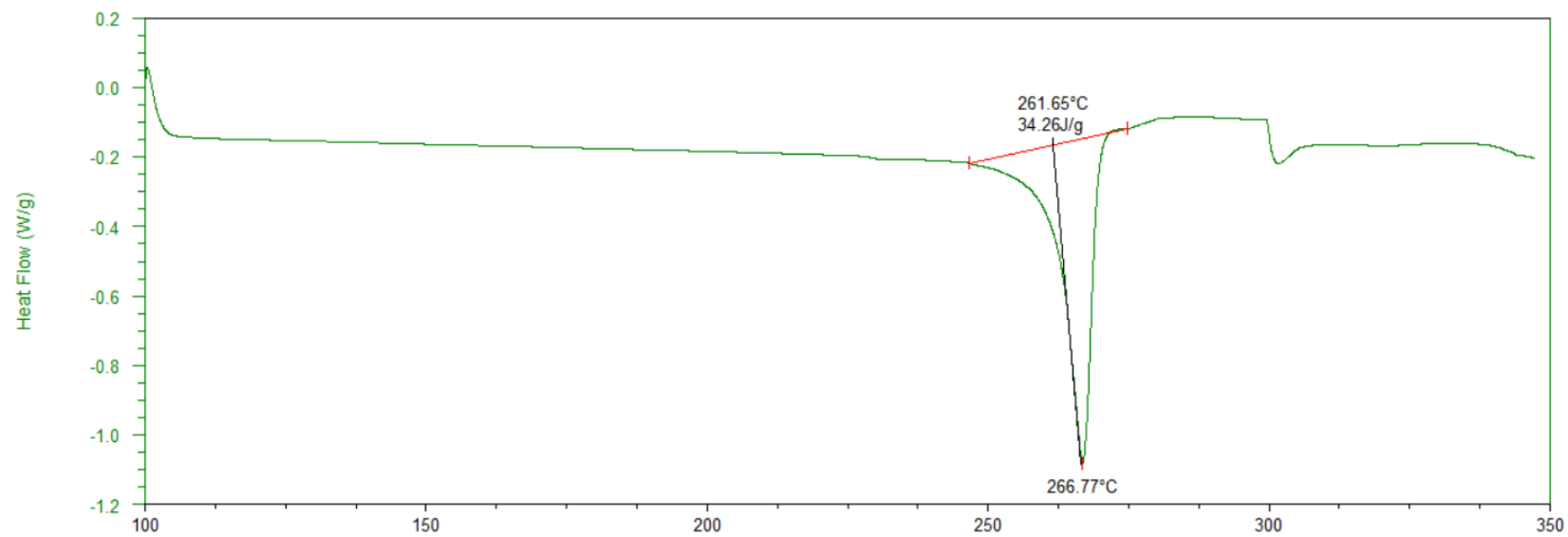


Figure 4-14 : DSC data for heating cycle for (MeOH)DDSQ(MeOH)

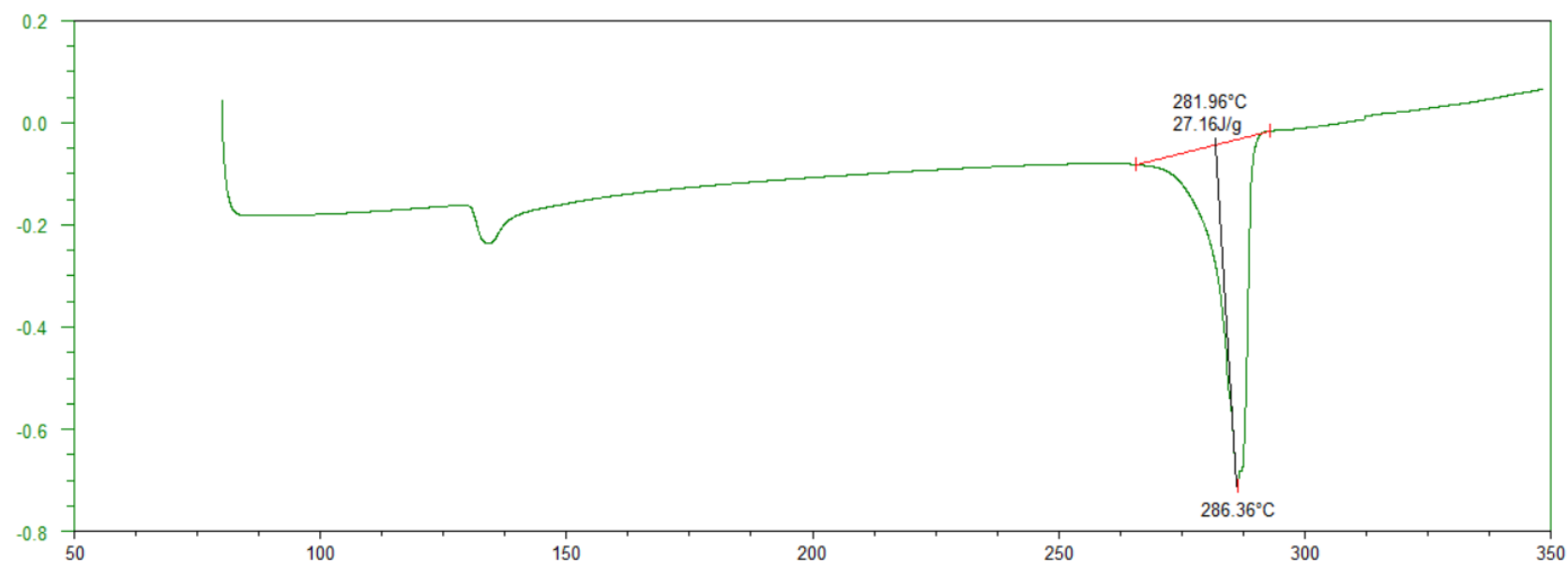


Figure 4-15 : DSC data for heating cycle for (MeH)DDSQ(MeOH)

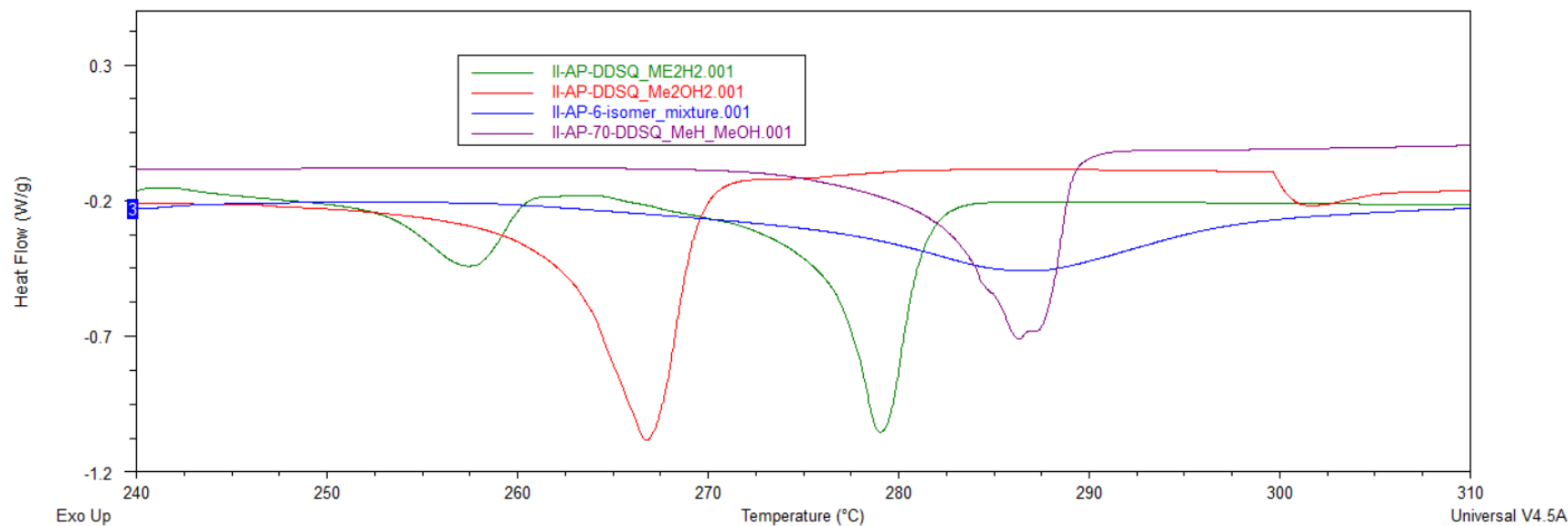
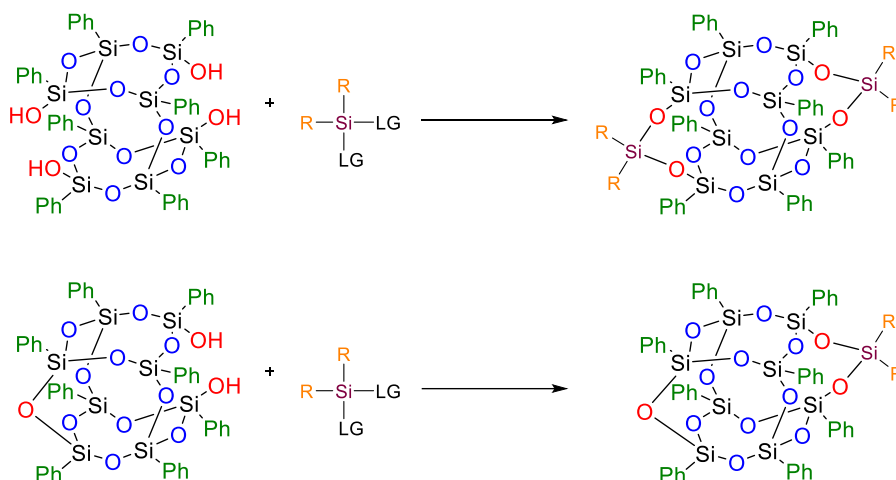


Figure 4-16 : Overlaid graph for the (MeR')DDSQ(MeR'') isomeric system

5 SOLVENT EFFECT FOR CAPPING OF DDPh₈T₈(OH)₄

5.1 Introduction

Incompletely condensed phenyl double-decker-shaped silsesquioxane can be functionalized using difunctional dichlorosilanes or dialkoxysilanes. Although there is a vast potential for side-capped



Scheme 5-1 : Reaction for capping of DDSQ tetrol using chlorosilanes

DDSQs, significant research has not been performed on the synthesis of side-capped DDSQs.¹ The most commonly used reaction scheme is in Scheme 5-1. Functionally capped SQs synthesized have a unique ability to be a part of the main chain or be a cross-linker between the polymer chains or act as pendants on the backbone of the polymer chain.²⁻⁶

The type of solvent used in the reaction plays a vital role in the rate of the reaction. Studies have suggested that depending on the type of reaction, changing the solvent from non-polar to polar solvent with either increase or decrease the rate of reaction.⁷ The specific interaction of solvent and the reactant molecules and the interaction between solvent and transition states dictate the solvent effect on reactivity in a homogeneous media.⁸⁻¹² When the magnitude of solvent in elementary reaction changes, the reaction rate will also change. This chapter explicitly discusses the effect of good and poor solvents on the reactant DDSQ tetrol. Tetrahydrofuran (THF) acts as a good solvent for DDSQ tetrol, where the solubility of DDSQ in THF is 80 mg / mL, whereas

5.2 DDSQ tetrol capping reaction using a good solvent

Reaction scheme showing the synthesis of compound **2** from compound **1**.

Compound **1** (a cage-like siloxane structure with phenyl groups and hydroxyl groups) reacts with a chlorosilane reagent (R-Si-Cl_2) in the presence of Et_3N (4 equiv) in THF, 0 - 2 hr, rt.

The reaction conditions are: (2.2 equiv) R-Si-Cl_2 , Et_3N (4 equiv), THF, 0 - 2 hr, rt.

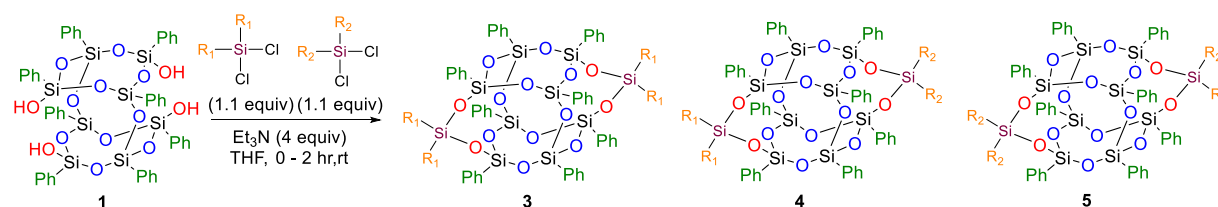
The product is compound **2**, which is a modified cage-like siloxane structure where the hydroxyl groups have been replaced by the R-Si-Cl_2 groups.

1, difunctional dichlorosilane and triethylamine are entirely soluble in THF. The solution is evident at the start of the reaction. As the reaction progresses, the chlorosilane reacts with the hydroxy groups, forming the product (**2**) and hydrochloric acid as a by-product. However, it has been found that the hydrochloric acid produced in the reaction can cause cleavage of the DDSQ cage. So, to neutralize the by-product, a base - triethylamine is used in the reaction. The neutralization reaction produces triethylammonium chloride salt, which is not soluble in THF, forming a white precipitate as the reaction progresses.

113

conversion. Me_2SiCl_2 has a smaller size and leads to complete conversion within minutes. The progress of reactions can be monitored using NMR analysis.

In another set of reactions, an equimolar mixture of two different chlorosilanes was used to synthesize asymmetrically capped DDSQ compounds, as seen in Scheme 5-3. This methodology helped to synthesize compounds with two different functional groups on either side of the cage structure. These asymmetrical structures are then used in various applications to cross-link the two

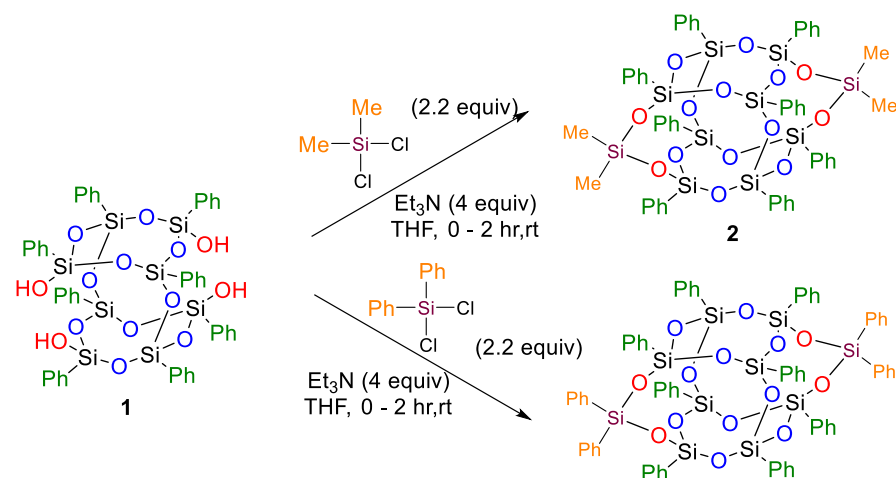


Scheme 5-3 : Capping of DDSQ tetrol using equimolar chlorosilanes as capping reagents.

polymeric chains to form a networked structure. Upon using an equimolar mixture of chlorosilanes as capping reagents, a mixture of 3 isomers of products was obtained. According to the probability distribution theory, if the dichlorosilanes have equal reactivity for the DDSQ tetrol, the ratio of isomers should be 25:50:25; that is, the yield of symmetrical products obtained from each chlorosilane should be 25%.

In contrast, the ratio of the asymmetrical product should be 50% in the final product composition. However, the ratio of the isomers was not the same as expected from the statistical distribution. The symmetrical product obtained from less bulky chlorosilane has a higher yield than the one obtained from the bulkier chlorosilane.

The time required to achieve complete conversion for various chlorosilanes was studied to determine the deviation in ratios from the statistical distribution. Two different types of chlorosilanes were selected for this study. Ph_2SiCl_2 and Me_2SiCl_2 were the chlorosilanes used to cap the DDSQ tetrol, as shown in Scheme 5-4.



Scheme 5-4 : Reaction scheme used to study the time required to achieve complete conversion to product.

The capping reaction can be followed by using NMR analysis. An aliquot was removed from the reaction mixture and quenched with methanol to prepare the sample for NMR analysis. Post-quenching deuterated chloroform was added to the quenched product, and an NMR of the sample was taken. The phenyl region can be monitored to figure out the changes in the cage structure, as

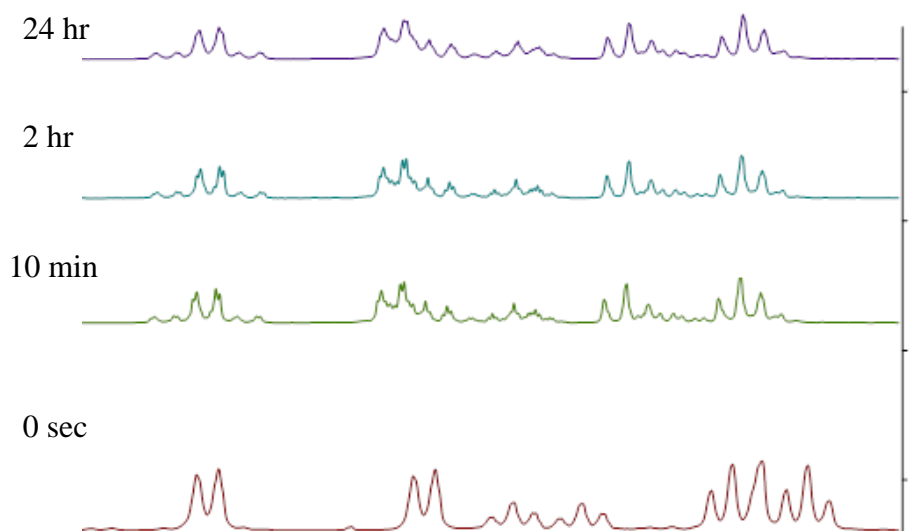


Figure 5-1: Reaction progress monitoring using NMR analysis for DDSQ tetrol capping with Me_2SiCl_2 using THF as a solvent

seen in Figure 5-1. As seen from the NMR analysis, there is no apparent change in the phenyl region after 1 min of the reaction time. The NMR sample taken after 2 hours almost matches the

NMR sample taken at 1 minute, indicating that the reaction reached complete conversion in that time. Similar studies were conducted using Ph_2SiCl_2 chlorosilanes. It was found that the reaction

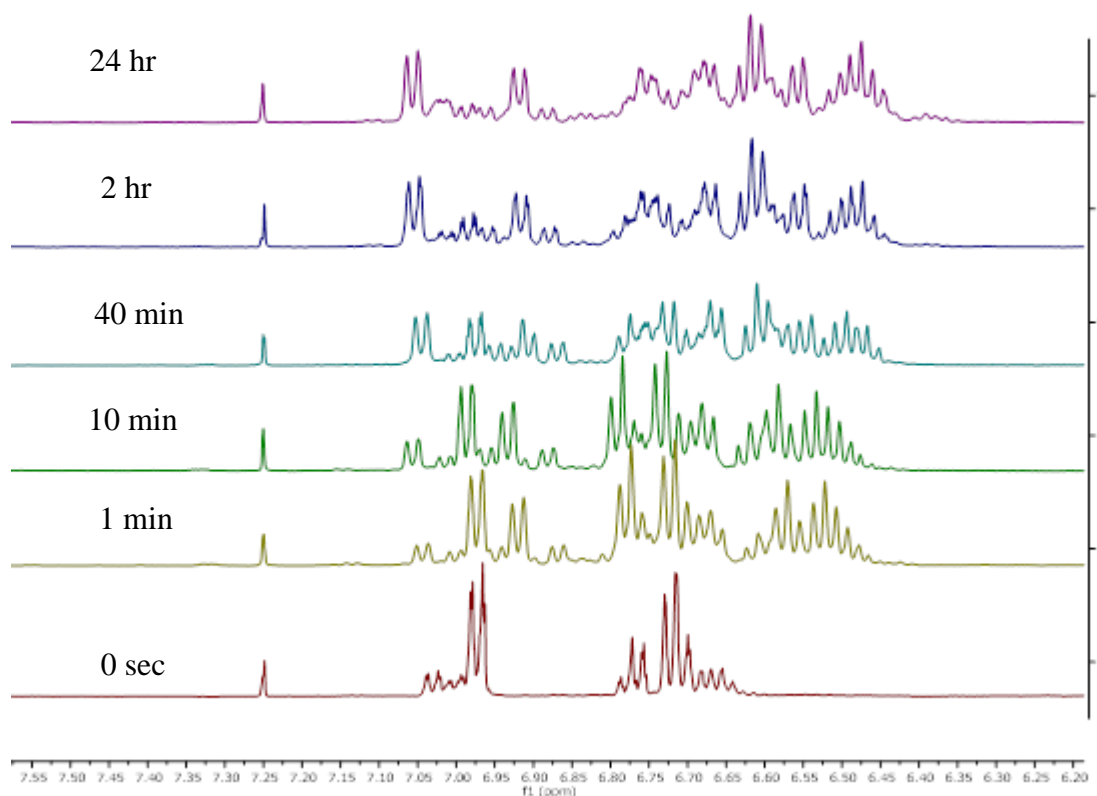


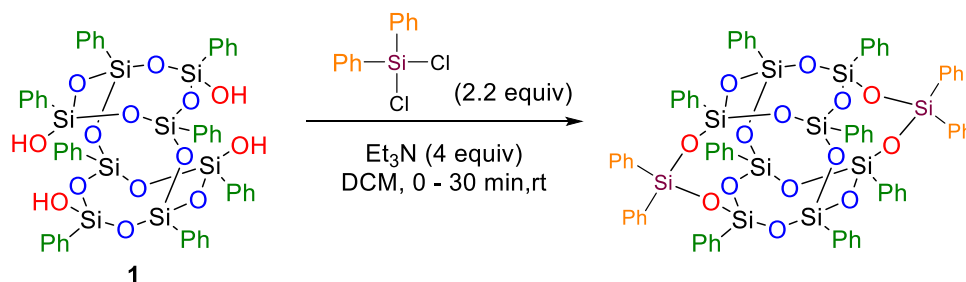
Figure 5-2 : Reaction progress monitoring using NMR analysis for DDSQ tetrol capping with Ph_2SiCl_2 using THF as a solvent

takes longer to reach completion. Figure 5-2 shows a zoomed-in picture of the phenyl region of DDSQ. As can be seen from the spectra, peaks at 6.97 ppm disappear as the reaction progresses. The peaks completely vanished in 2 hours—also, the peak position and intensities at 6.78 ppm changed as the reaction progressed. The doublet peak disappears, and a new singlet appears upfield to the original peaks. There was no change in the peak positions and intensities when the reaction was monitored from 2 to 24 hours, indicating reaction completion in 2 hours. This critical difference in the time required for the capping of the two chlorosilanes accounts for the differences in the ratio of the isomeric products. DCM was proposed as an alternative solvent for the capping

reaction to solve this issue and ensure the reaction time remains unchanged irrespective of the type of chlorosilanes used.

5.3 DDSQ tetrol capping reaction using a poor solvent

Dichloromethane (DCM) acts as a poor solvent for DDSQ tetrol. The solubility of tetrol in DCM is approximately 0.2 mg / mL. This solubility is almost 400 times less than tetrol's solubility in THF (80 mg / mL). As a result, the starting reaction mixture is a suspension in DCM compared to being a clear solution in THF. Another essential difference between the two reactions is that the by-product triethylammonium salt formed during the reaction is soluble in DCM, which is insoluble in THF. The dichlorosilane used in the reaction total miscibility with the solvent. This fact helps to monitor the reaction visually. As the reaction progresses, the suspension turns into a clear solution. Adding a base to the suspended solution of DDSQ tetrol in DCM helps solubilize the DDSQ tetrol. It has been seen that the amount of base required to solubilize tetrol in DCM entirely is one equivalent per equivalent of the hydroxy group. Any lower amount of addition of base will not completely solubilize the tetrol. The reaction scheme for capping DDSQ tetrol with dichlorosilane is shown in Scheme 5-5



Scheme 5-5 : Reaction scheme for DDSQ tetrol capping using Ph_2SiCl_2

To verify the differences in the time required for the capping reaction for the Ph_2SiCl_2 reaction, aliquots were taken out at certain times, quenched with methanol, and then NMR analysis was done to monitor the changes in the peaks. The NMR analysis is shown in Figure 5-3. ^{29}Si NMR has been used to monitor the progress of the reaction. Spectra 1 depicts the NMR for the starting

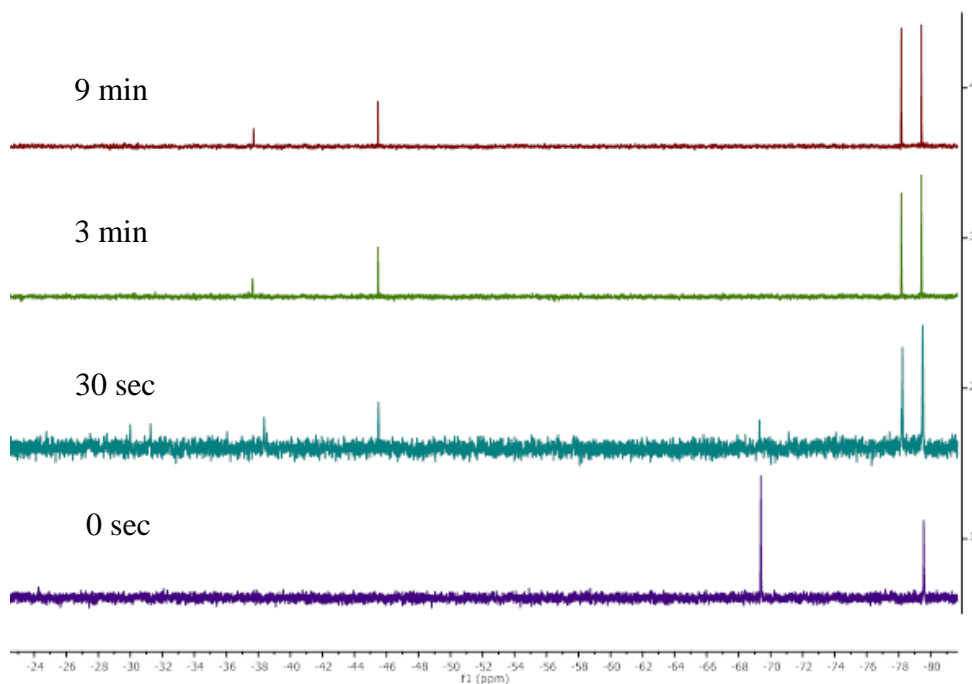


Figure 5-3 : Reaction progress monitoring using NMR analysis for DDSQ tetrol capping with Ph_2SiCl_2 using DCM as a solvent.

material DDSQ tetrol; spectra 2 depicts the progress of the reaction after 30 seconds. The peak intensity at -69 ppm represents the silicon atom connected to the hydroxyl group. This peak will diminish in intensity as the product is formed. The peak at -78 ppm starts to increase in intensity, and this peak refers to the silicon atom that was previously connected to the hydroxy group, which is now connected with the silicon peak of the dichlorosilane. The peak -45 ppm also starts to appear, depicting the product's 'D' Silicon peak. Peaks at -38 ppm depict the silicon peaks obtained from quenched chlorosilane. Spectra 3 shows the progress of the reaction after 3 minutes. Spectra 4 shows the progress of the reaction after 9 minutes.

As seen from these spectra, the peak at -69 ppm completely vanishes, which leads to the conclusion that the reaction reaches completion within 3 minutes as opposed to the reaction done in THF, where the time required is 120 minutes. The difference in reactivity can be attributed to the difference in pKa of triethylamine in two different solvents. Triethylamine has a higher pKa value in DCM as compared to THF. This change in pKa results in a higher level of deprotonation of tetrol in the presence of DCM solvent than that in THF. Consequently, a higher reactant activity in DCM solvent than in THF solvent. As a result, we get a faster reaction in DCM as a solvent medium than in THF. Various chlorosilanes and mixtures of chlorosilanes were used to cap DDSQ tetrol using DCM solvent. Detailed information on the procedure and NMR spectra have been given in the SI.

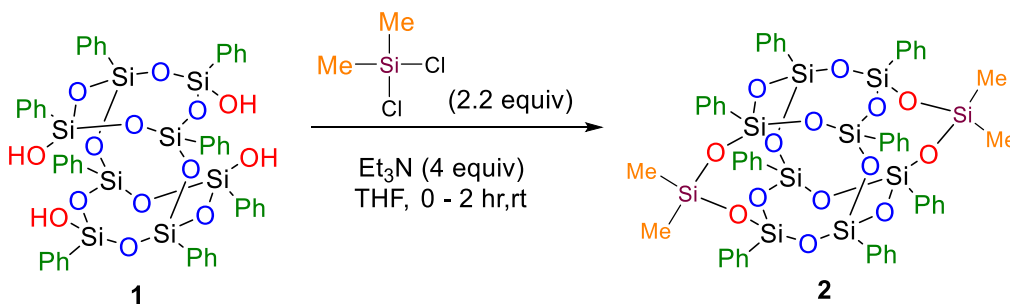
In conclusion, a new method for capping DDSQ tetrol with chlorosilanes has been proposed. The reaction time has been reduced to 5 minutes irrespective of the type of chlorosilane or mixture of chlorosilanes used in the reaction. The increased activity of the reactant in DCM can be attributed to the difference in pKa values of triethylamine in DCM vs. THF.

5.4 Experimental Details

5.4.1 General Information

All manipulations were done under a nitrogen atmosphere using standard Schlenk techniques except otherwise stated. All commercially available chemicals were used as received unless otherwise indicated. Methyl trichlorosilane (MeSiCl_3), dimethyl dichlorosilane (Me_2SiCl_2), diphenyl dichlorosilane (Ph_2SiCl_2), methyl cyanopropyl dichlorosilane $\text{Me}(\text{C}_3\text{H}_6\text{CN})\text{SiCl}_2$, deuterated chloroform with 1 vol % tetramethylsilane (CDCl_3 -1%TMS), were purchased from Sigma-Aldrich. Graphene nanoplatelet was obtained from XG Sciences. $\text{DDPh}_8\text{T}_8(\text{OH})_4$ was obtained from Hybrid Plastics. Triethylamine (Et_3N) was purchased from Avantor and distilled over calcium hydride before use. Tetrahydrofuran (THF), dichloromethane (DCM), and methanol (MeOH) n-hexanes were purchased from Sigma-Aldrich. THF was distilled over benzophenone and sodium metal at 50 °C under nitrogen. Toluene was distilled over calcium hydride at a temperature of 120 °C. The other solvents were used as purchased without further purification, and the glassware was oven dried. All ^1H , ^{13}C , and ^{29}Si NMR were acquired on an Agilent DirectDrive2 500 MHz NMR spectrometer equipped with a OneProbe operating at 500 MHz for ^1H NMR, 126 MHz for ^{13}C NMR, and 99 MHz for ^{29}Si NMR using CDCl_3 and recorded at 25 °C. ^1H -NMR spectra were recorded with 8 scans, a relaxation delay of 1s, and a pulse angle of 45° and referenced to the residual protonated solvent in CDCl_3 (7.24 ppm). ^{13}C -NMR spectra were collected with 254 scans, a relaxation delay of 0.1 s, and a pulse angle of 45°. ^{29}Si NMR spectra were recorded with either 256 scans, a relaxation delay of 25 s, and a pulse angle 45°. Column chromatography was performed on EMD Millipore silica gel 60 columns of 40– 63 Å silica, 230– 400 mesh. Thin-layer chromatography (TLC) was performed on plates of EMD 250- μm silica 60-F254.

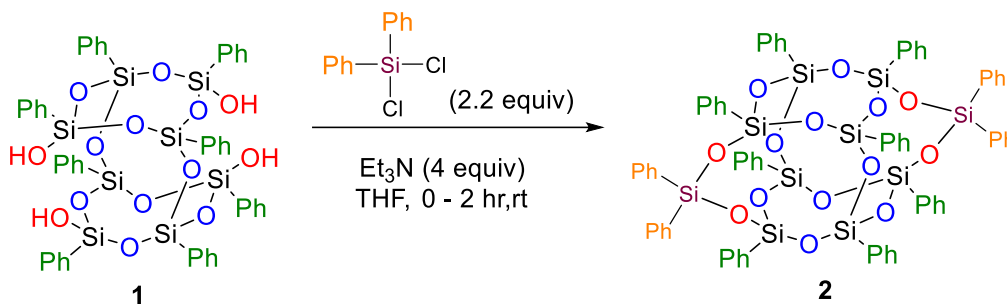
5.4.2 Synthesis of 9,9,19,19-tetramethyl-1,3,5,7,11,13,15,17-octaphenyl-2,4,6,8,10,12,14,16,18,20,21,22,23,24-tetradeca-1,3,5,7,9,11,13,15,17,19-decasilapentacyclo[11.7.1.13,11.15,17.17,15]tetracosane



Scheme 5-6 : Synthesis of capped DDSQ (Me)₄

To a 100 mL round bottom flask were added $\text{DDPh}_8\text{T}_8(\text{OH})_4$ (2 g, 0.0018 mol, 1 equiv), dichlorodimethylsilane (0.50 mL, 0.0041 mol, 2.2 equiv), and a stir bar under N_2 atmosphere. Freshly distilled THF (~30 mL) was then added. A clear solution was formed. Et_3N (1.05 mL, 0.0074 mol, 4 equiv) was added dropwise to this solution. Upon the addition of the triethylamine, the solution turned milky white. The reaction mixture was stirred for 120 min, after which a slurry was formed. This slurry was filtered through a medium frit funnel to obtain the crude product in the filtrate. The filtrate was concentrated to obtain white powder. This powder was washed with methanol (~60 mL) for 30 min. The slurry was again filtered through a medium frit funnel to obtain the product as a white powder (2.12 g, 96% yield). ^1H NMR (500 MHz, Chloroform- d) δ 7.54 (d, J = 6.9 Hz, 8H), 7.40 (dd, J = 23.5, 7.2 Hz, 13H), 7.33 (t, J = 7.5 Hz, 5H), 7.24 (d, J = 7.5 Hz, 6H), 7.18 (t, J = 7.5 Hz, 9H), 0.30 (s, 12H). $^{13}\text{C}\{^1\text{H}\}$ NMR (126 MHz, Chloroform- d) δ 134.04, 133.92, 132.12, 131.07, 127.77, 127.62, 0.53. $^{29}\text{Si}\{^1\text{H}\}$ NMR (99 MHz, Chloroform- d) δ -16.55, -78.63, -79.61.

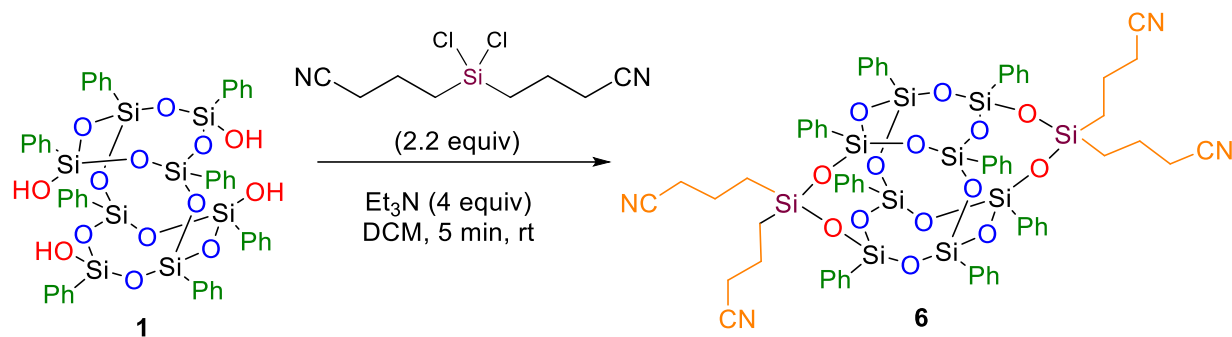
5.4.3 Synthesis of 1,3,5,7,9,9,11,13,15,17,19,19-dodecaphenyl-2,4,6,8,10,12,14,16,18,20,21,22,23,24-tetradeca-1,3,5,7,9,11,13,15,17,19-decasilapentacyclo[11.7.1.13,11.15,17.17,15]tetracosane



Scheme 5-7 : Synthesis of capped DDSQ (Ph)₄

To a 100 mL round bottom flask were added DDPh₈T₈(OH)₄ (2 g, 0.0018 mol, 1 equiv), dichlorodiphenylsilane (0.79 mL, 0.0041 mol, 2.2 equiv), and a stir bar under N₂ atmosphere. Freshly distilled THF (~30 mL) was then added. A clear solution was formed. Et₃N (1.05 mL, 0.0074 mol, 4 equiv) was added dropwise to this solution. Upon the addition of the triethylamine, the solution turned milky white. The reaction mixture was stirred for 120 min, after which a slurry was formed. This slurry was filtered through a medium frit funnel to obtain the crude product in the filtrate. The filtrate was concentrated to obtain crude white powder. The crude and purified by silica column chromatography (DCM mobile phase) to afford the desired product. ¹H NMR (500 MHz, Chloroform-*d*) δ 7.71 – 7.65 (m, 8H), 7.54 – 7.51 (m, 8H), 7.40 – 7.35 (m, 8H), 7.31 – 7.27 (m, 4H), 7.22 (q, *J* = 7.5 Hz, 18H), 7.18 – 7.14 (m, 8H), 7.11 – 7.06 (m, 8H). ¹³C NMR (126 MHz, Chloroform-*d*) δ 127.40, 127.78, 127.82, 130.11, 130.19, 130.41, 130.49, 131.56, 134.03, 134.10, 134.27, 134.58. ²⁹Si{¹H} NMR (99 MHz, Chloroform-*d*) δ -79.40, -78.14, -45.47.

5.4.4 Synthesis of 4,4',4'',4'''-(1,3,5,7,11,13,15,17-octaphenyl-2,4,6,8,10,12,14,16,18,20,21,22,23,24-tetradeca-1,3,5,7,9,11,13,15,17,19-decasilapentacyclo[11.7.1.13,11.15,17.17,15]tetracosane-9,9,19,19-tetrayl)tetrabutananitrile

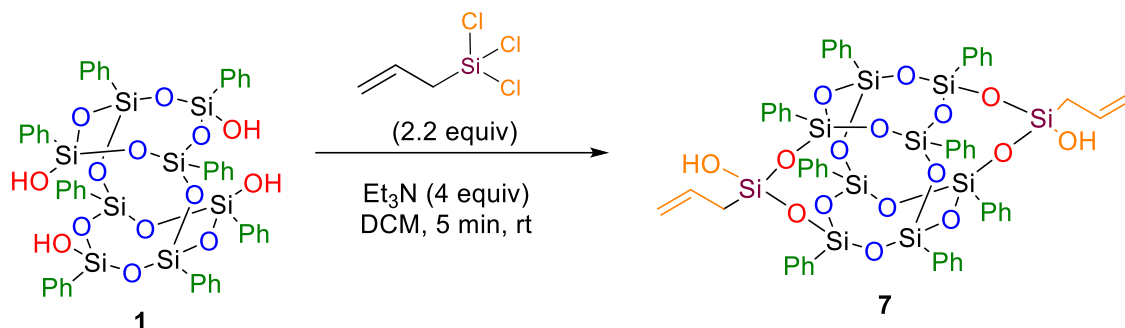


Scheme 5-8 : Synthesis of capped DDSQ (propylCN)₄

To a 100 mL round bottom flask were added $\text{DDPh}_8\text{T}_8(\text{OH})_4$ (2 g, 0.0018 mol, 1 equiv), bis(cyanopropyl)dichlorosilane (0.83 mL, 0.0041 mol, 2.2 equiv), and a stir bar under N_2 atmosphere. Freshly distilled DCM (~30 mL) was then added. A cloudy solution was formed. Et_3N (1.05 mL, 0.0074 mol, 4 equiv) was added dropwise to this solution. Upon the addition of the triethylamine, the solution turned clear. The reaction mixture was stirred for 5 min, after which the solvent evaporated. Fresh THF (~50 mL) was added, and a slurry was formed. This slurry was filtered through a medium frit funnel to obtain the crude product in the filtrate. The filtrate was concentrated to obtain white powder. This powder was washed with methanol (~60 mL) for 30 min. The slurry was again filtered through a medium frit funnel to obtain the product as a white powder (2.45 g, 94% yield).

^1H NMR (500 MHz, Chloroform-*d*) δ 7.51 – 7.47 (m, 8H), 7.42 (qd, J = 9.3, 8.1, 4.8 Hz, 16H), 7.32 – 7.23 (m, 18H), 2.18 (t, J = 6.9 Hz, 8H), 1.80 – 1.67 (m, 9H), 0.96 – 0.81 (m, 8H). ^{13}C NMR (126 MHz, Chloroform-*d*) δ 14.84, 19.20, 20.07, 119.19, 128.02, 128.13, 130.17, 130.89, 133.70, 133.86. $^{29}\text{Si}\{^1\text{H}\}$ NMR (99 MHz, Chloroform-*d*) δ -79.15, -78.19, -22.23.

5.4.5 Synthesis of 9,19-diallyl-1,3,5,7,11,13,15,17-octaphenyl-2,4,6,8,10,12,14,16,18,20,21,22,23,24-tetradeca-1,3,5,7,9,11,13,15,17,19-decasilapentacyclo[11.7.1.13,11.15,17.17,15]tetracosane-9,19-diol



Scheme 5-9 : Synthesis of capped DDSQ (allyl OH)₂

To a 100 mL round bottom flask were added $\text{DDPh}_8\text{T}_8(\text{OH})_4$ (2 g, 0.0018 mol, 1 equiv), allyl trichlorosilane (0.57 mL, 0.0041 mol, 2.2 equiv), and a stir bar under N_2 atmosphere. Freshly distilled DCM (~30 mL) was then added. A cloudy solution was formed. Et_3N (1.05 mL, 0.0074 mol, 4 equiv) was added dropwise to this solution. Upon the addition of the triethylamine, the solution turned clear. The reaction mixture was stirred for 5 min, after which the solvent evaporated. Fresh THF (~50 mL) was added, and a slurry was formed. This slurry was filtered through a medium frit funnel to obtain the crude product in the filtrate. The filtrate was concentrated to obtain white powder. This powder was washed with methanol (~60 mL) for 30 min. The slurry was again filtered through a medium frit funnel to obtain the product as a white powder (2.45 g, 94% yield).

^1H NMR (500 MHz, Chloroform-*d*) δ 7.62 – 7.55 (m, 8H), 7.48 – 7.32 (m, 16H), 7.31 – 7.16 (m, 16H), 5.88 – 5.77 (m, 2H), 4.93 (dp, $J = 17.0, 1.7$ Hz, 2H), 4.79 (dq, $J = 10.1, 1.9, 1.2$ Hz, 2H), 3.75 – 3.71 (m, 2H), 1.87 – 1.78 (m, 6H). $^{29}\text{Si}\{^1\text{H}\}$ NMR (99 MHz, Chloroform-*d*) δ -79.39, -79.28, -79.16, -78.78, -60.76.

REFERENCES

- (1) *Applications of Polyhedral Oligomeric Silsesquioxanes*; Hartmann-Thompson, C., Ed.; Advances in Silicon Science; Springer Netherlands: Dordrecht, 2011; Vol. 3. <https://doi.org/10.1007/978-90-481-3787-9>.
- (2) Constable, G. S.; Lesser, A. J.; Coughlin, E. B. Morphological and Mechanical Evaluation of Hybrid Organic–Inorganic Thermoset Copolymers of Dicyclopentadiene and Mono- or Tris(Norbornenyl)-Substituted Polyhedral Oligomeric Silsesquioxanes. *Macromolecules* 2004, 37 (4), 1276–1282. <https://doi.org/10.1021/ma034989w>.
- (3) Fu, B. X.; Lee, A.; Haddad, T. S. Styrene–Butadiene–Styrene Triblock Copolymers Modified with Polyhedral Oligomeric Silsesquioxanes. *Macromolecules* 2004, 37 (14), 5211–5218. <https://doi.org/10.1021/ma049753m>.
- (4) Feher, F. J.; Budzichowski, T. A.; Rahimian, K.; Ziller, J. W. Reactions of Incompletely-Condensed Silsesquioxanes with Pentamethylantimony: A New Synthesis of Metallasilsesquioxanes with Important Implications for the Chemistry of Silica Surfaces. *J. Am. Chem. Soc.* 1992, 114 (10), 3859–3866. <https://doi.org/10.1021/ja00036a038>.
- (5) Gilman, J. W.; Schlitzer, D. S.; Lichtenhan, J. D. Low Earth Orbit Resistant Siloxane Copolymers. *J. Appl. Polym. Sci.* 1996, 60 (4), 591–596. [https://doi.org/10.1002/\(SICI\)1097-4628\(19960425\)60:4<591::AID-APP12>3.0.CO;2-2](https://doi.org/10.1002/(SICI)1097-4628(19960425)60:4<591::AID-APP12>3.0.CO;2-2).
- (6) Wright, M. E.; Schorzman, D. A.; Feher, F. J.; Jin, R.-Z. Synthesis and Thermal Curing of Aryl-Ethynyl-Terminated Co POSS Imide Oligomers: New Inorganic/Organic Hybrid Resins. *Chem. Mater.* 2003, 15 (1), 264–268. <https://doi.org/10.1021/cm020238h>.
- (7) Parker, A. J. Protic-Dipolar Aprotic Solvent Effects on Rates of Bimolecular Reactions. *Chem. Rev.* 1969, 69 (1), 1–32. <https://doi.org/10.1021/cr60257a001>.
- (8) Ghosh, K. K. Kinetic Solvent Effect on the Hydrolysis of N-Benzylbenzohydroxamic Acid in Some Binary Aqueous Solvent Mixtures. *Journal of Molecular Liquids* 1999, 81 (2), 135–145. [https://doi.org/10.1016/S0167-7322\(99\)00062-8](https://doi.org/10.1016/S0167-7322(99)00062-8).
- (9) Schmeer, G.; Steinkirchner, J. Investigations on Substituent and Solvent Effects of Solvolysis Reactions. VIII. The Influence of Water and Nonaqueous Solvents on the Imidazolysis of 4-Nitrophenyl Acetate.
- (10) Seliverstova, T. S.; Kushner, M. A.; Matusevich, L. G. Kinetics and Mechanism of the Hydrolysis of Benzyl Ether Bonds in Aqueous–Organic Media. *Russ. J. Phys. Chem.* 2020, 94 (2), 310–316. <https://doi.org/10.1134/S0036024420020302>.
- (11) Habibi-Yangjeh, A.; Nooshyar, M. Prediction of Solvent Effects on Rate Constant of [2+2] Cycloaddition Reaction of Diethyl Azodicarboxylate with Ethyl Vinyl Ether Using Artificial Neural Networks. *Bulletin of the Korean Chemical Society* 2005, 26 (1), 139–145. <https://doi.org/10.5012/BKCS.2005.26.1.139>.

- (12) Iglesias, E. Solvent Effects versus Concentration Effects in Determining Rates of Base-Catalyzed Keto-Enol Tautomerization. *New J. Chem.* 2005, 29 (4), 625.
<https://doi.org/10.1039/b415220d>.

APPENDIX

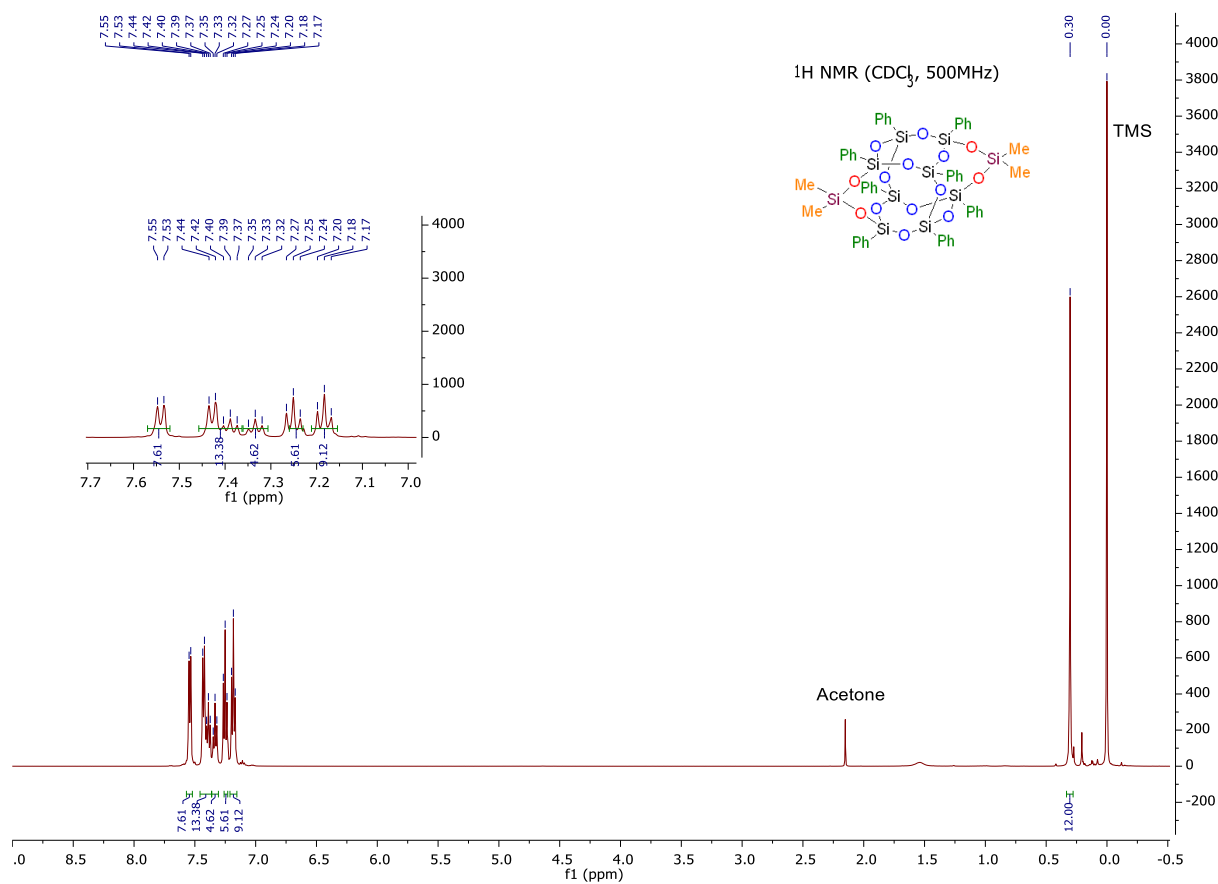


Figure 5-4 : ¹H-NMR (CDCl₃, 500 MHz)

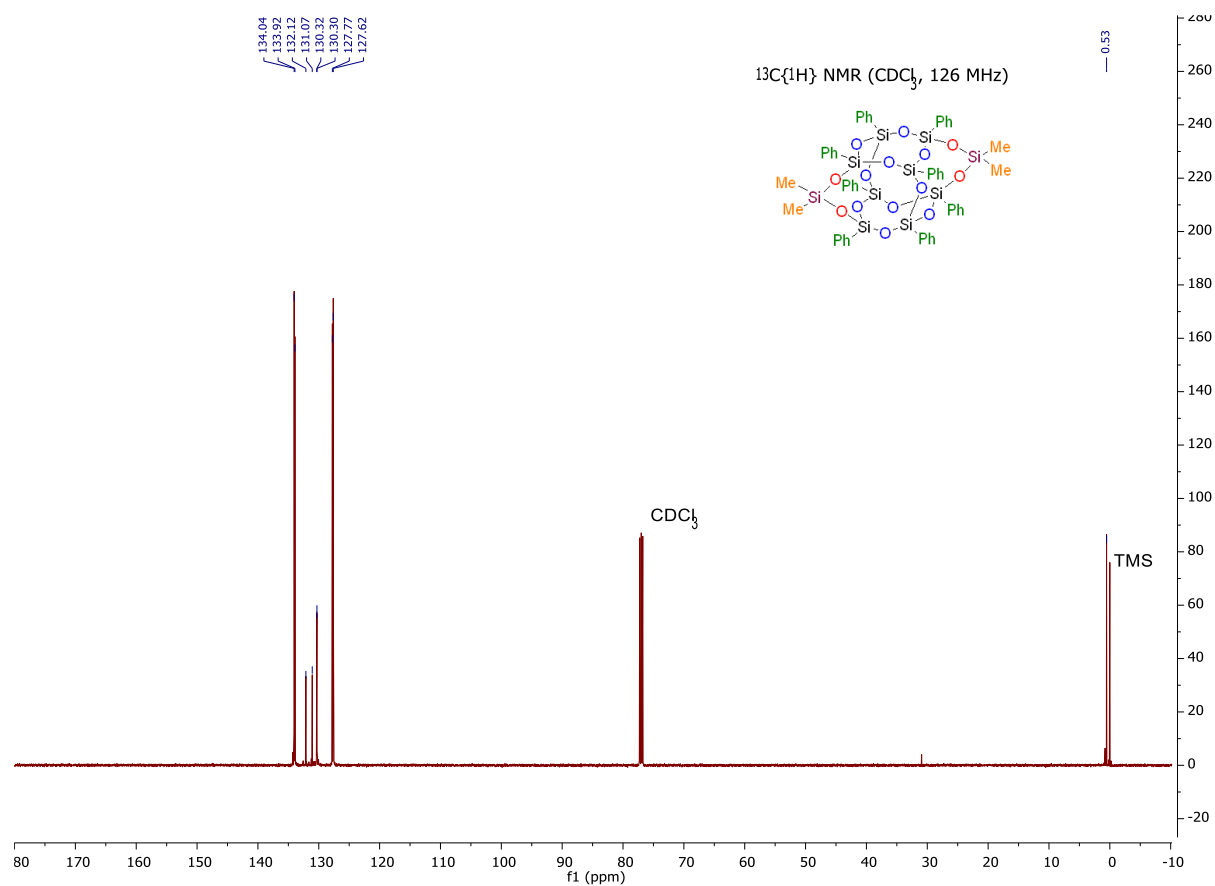


Figure 5-5 : ^{13}C -NMR (CDCl_3 , 126 MHz)

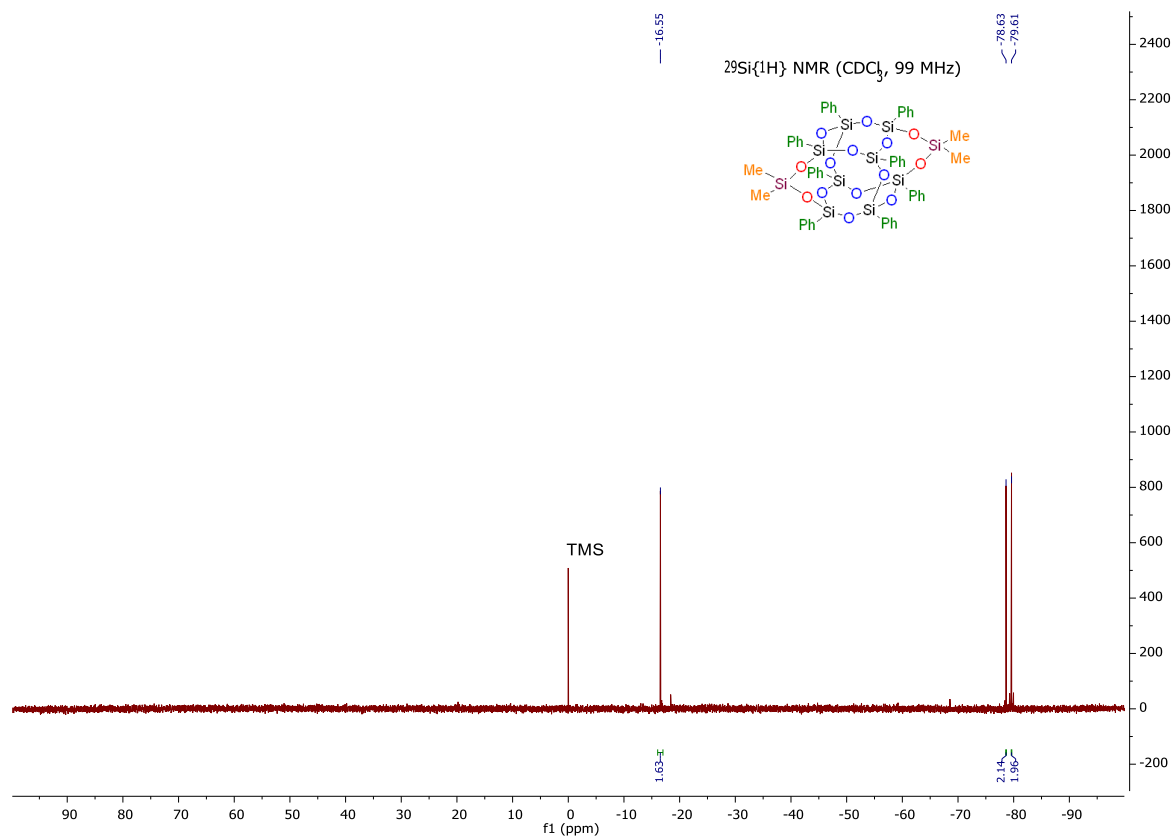


Figure 5-6 : $^{29}\text{Si}\{^1\text{H}\}$ -NMR (CDCl_3 , 99 MHz)

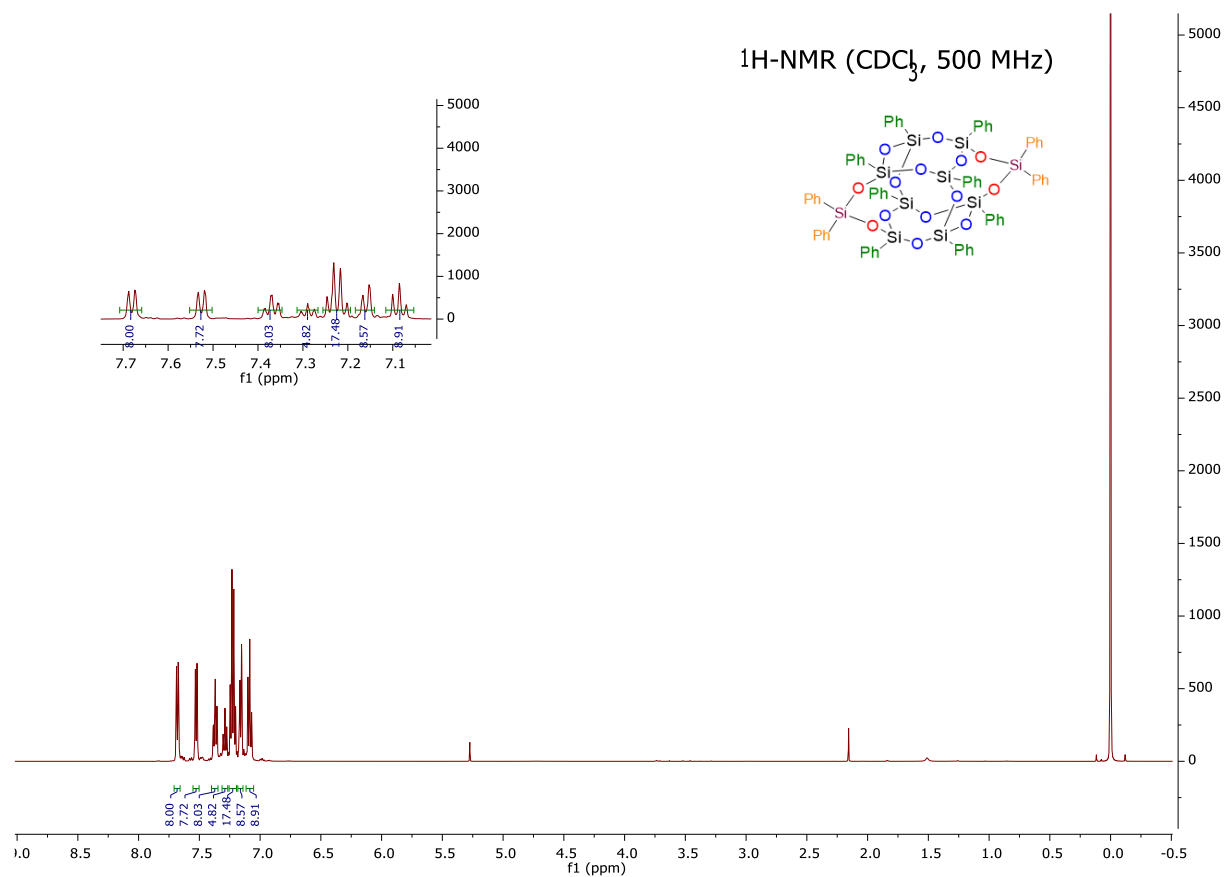


Figure 5-7 : $^1\text{H-NMR}$ (CDCl_3 , 500 MHz)

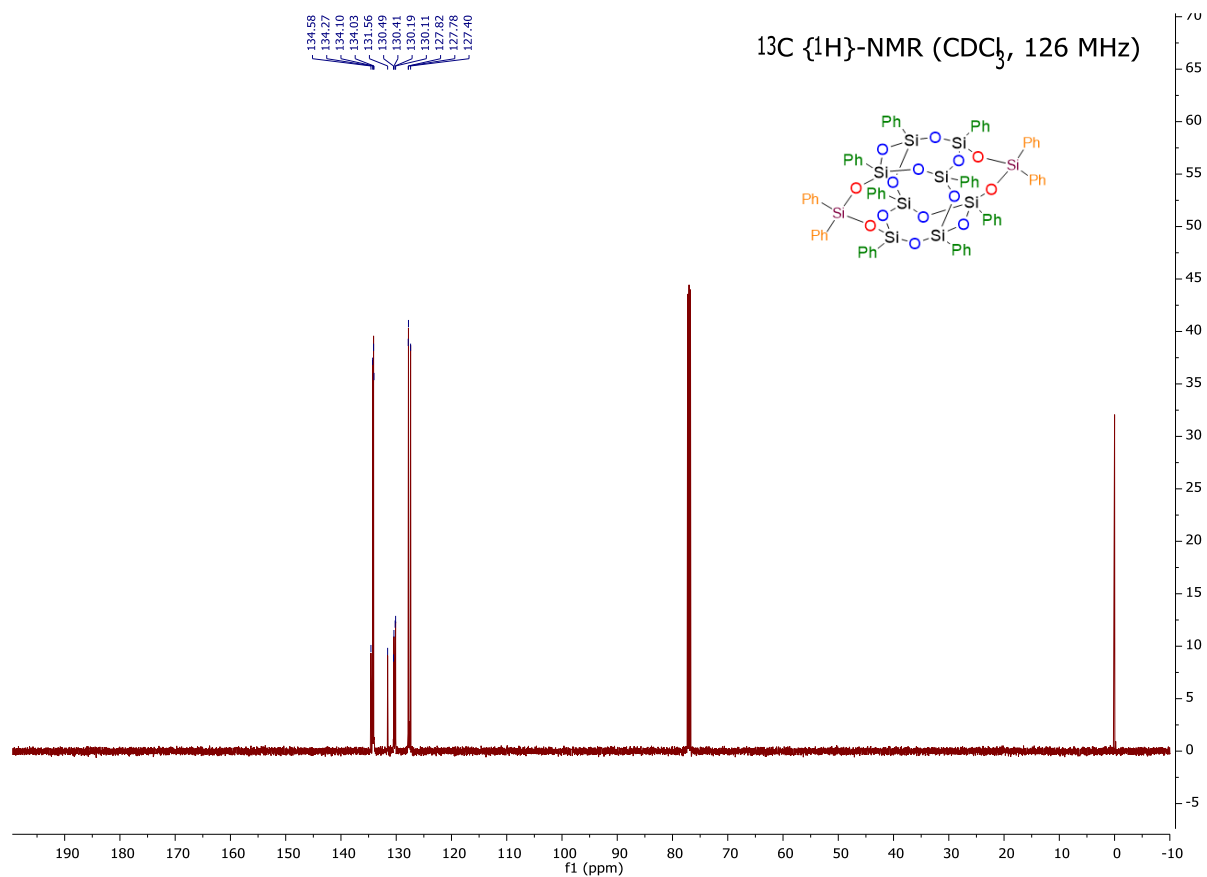


Figure 5-8 : ^{13}C -NMR (CDCl_3 , 126 MHz)

$^{29}\text{Si}\{^1\text{H}\}$ -NMR (CDCl_3 , 99 MHz)

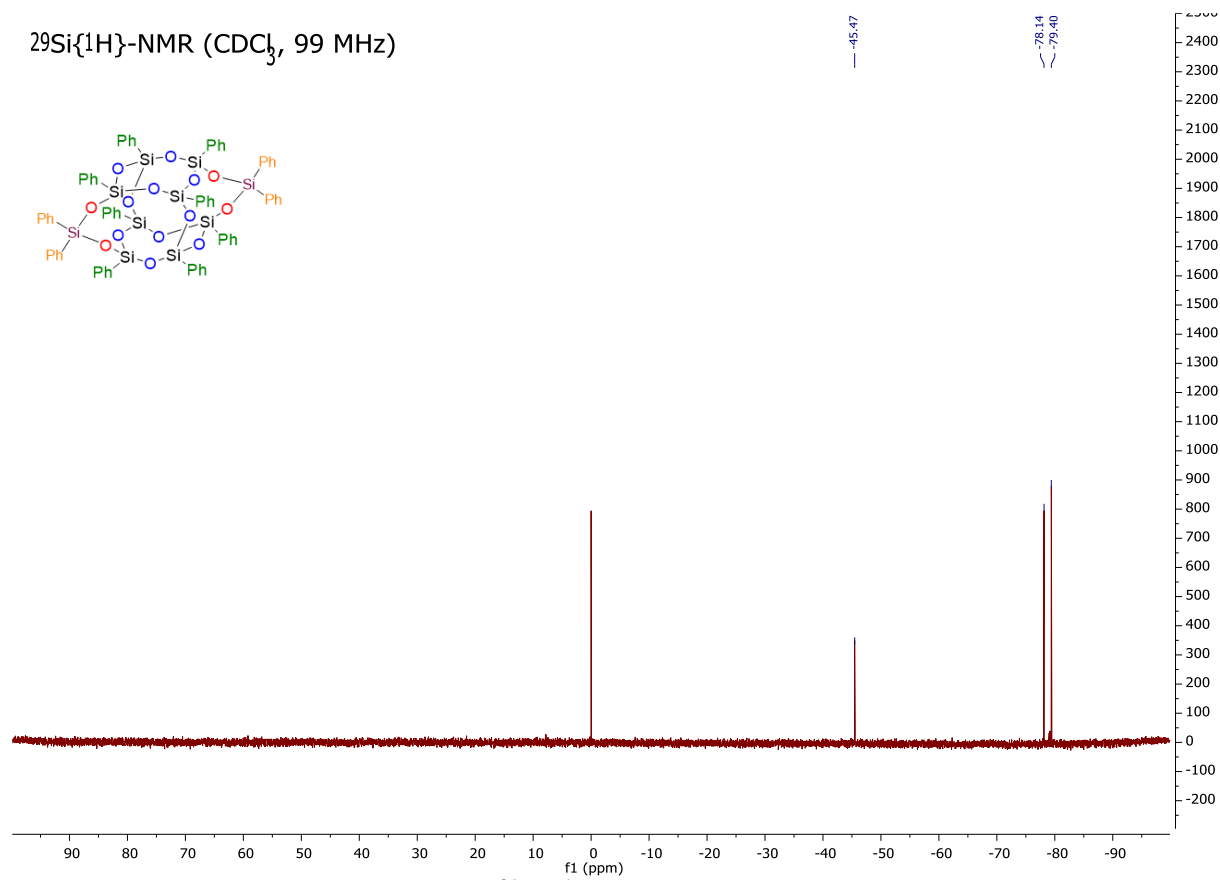


Figure 5-9 : $^{29}\text{Si}\{^1\text{H}\}$ -NMR (CDCl_3 , 99 MHz)

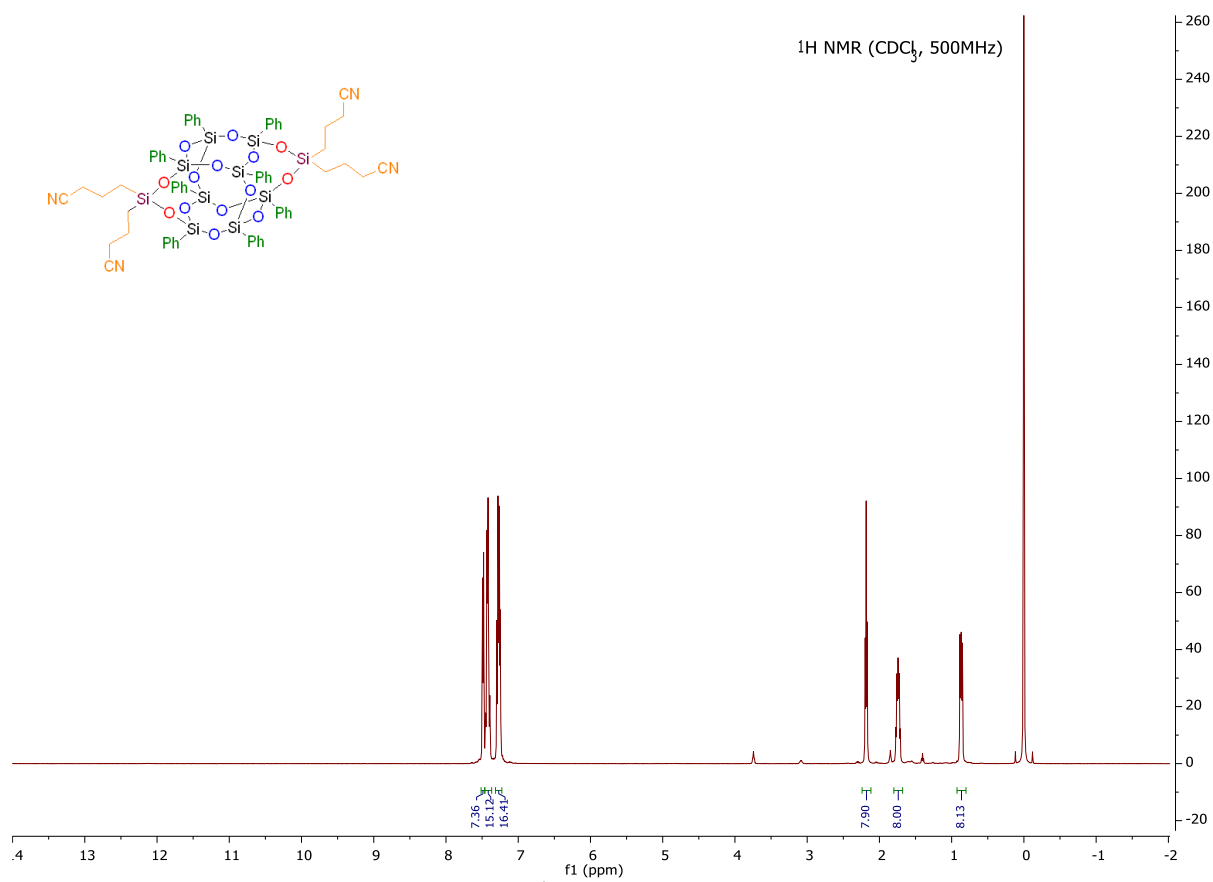
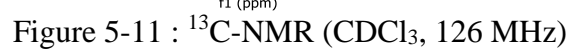


Figure 5-10 : ¹H-NMR (CDCl₃, 500 MHz)



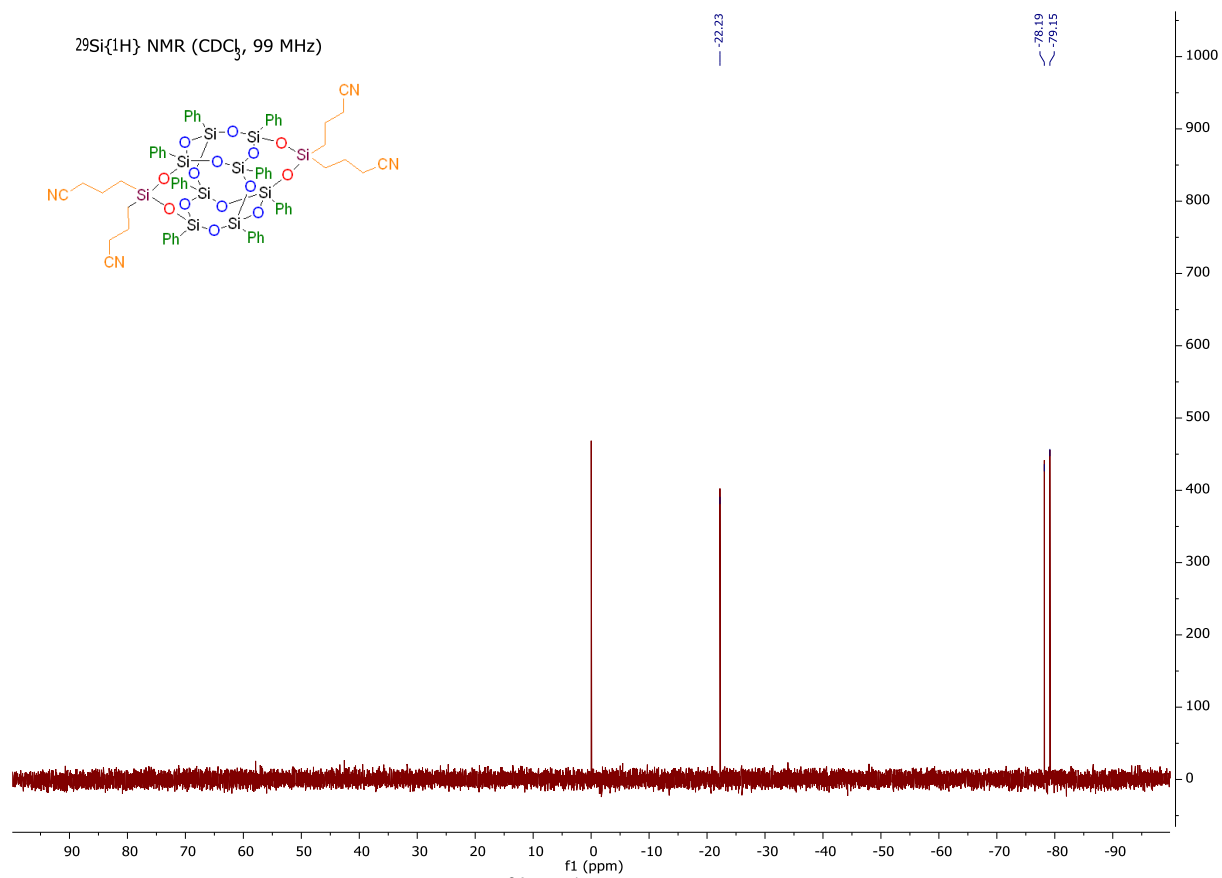


Figure 5-12 : $^{29}\text{Si}\{^1\text{H}\}$ -NMR (CDCl_3 , 99 MHz)

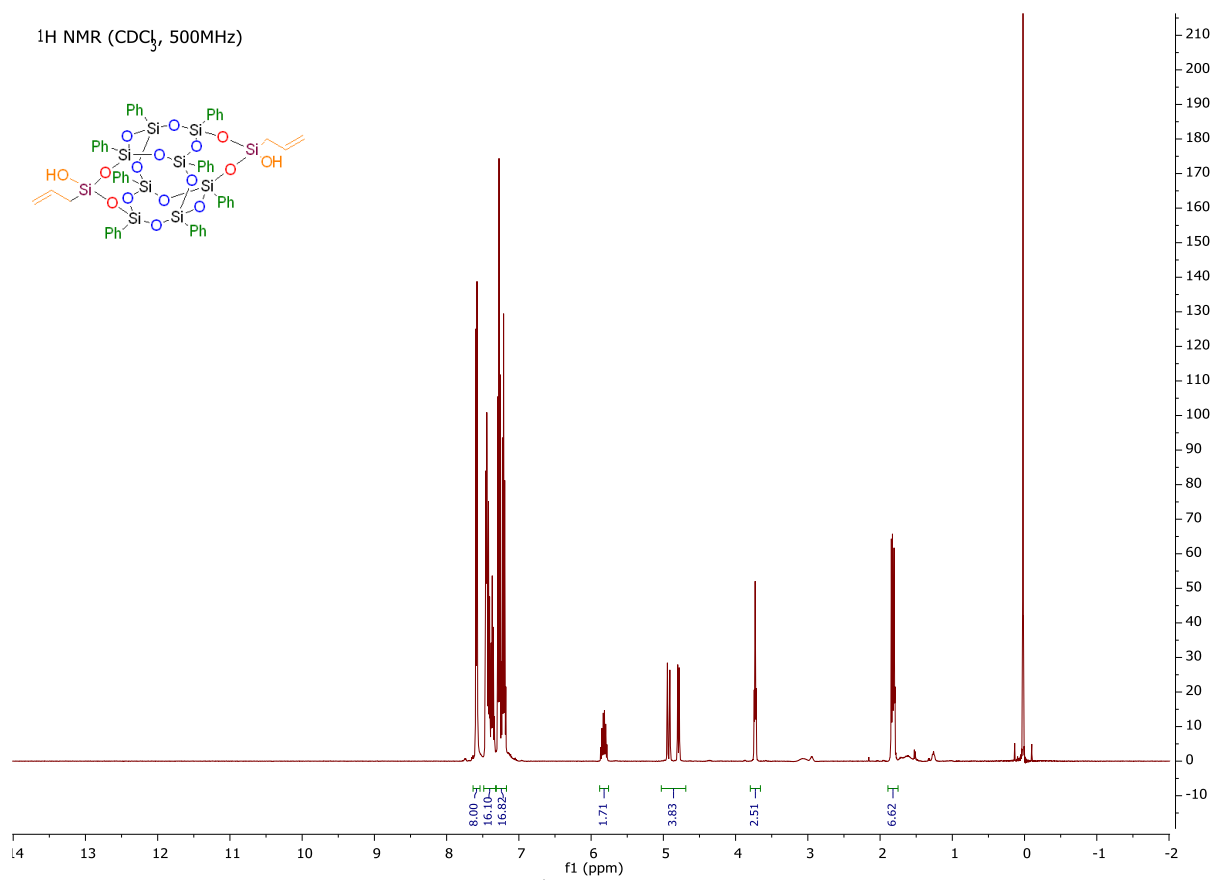


Figure 5-13 : ^1H -NMR (CDCl_3 , 500 MHz)

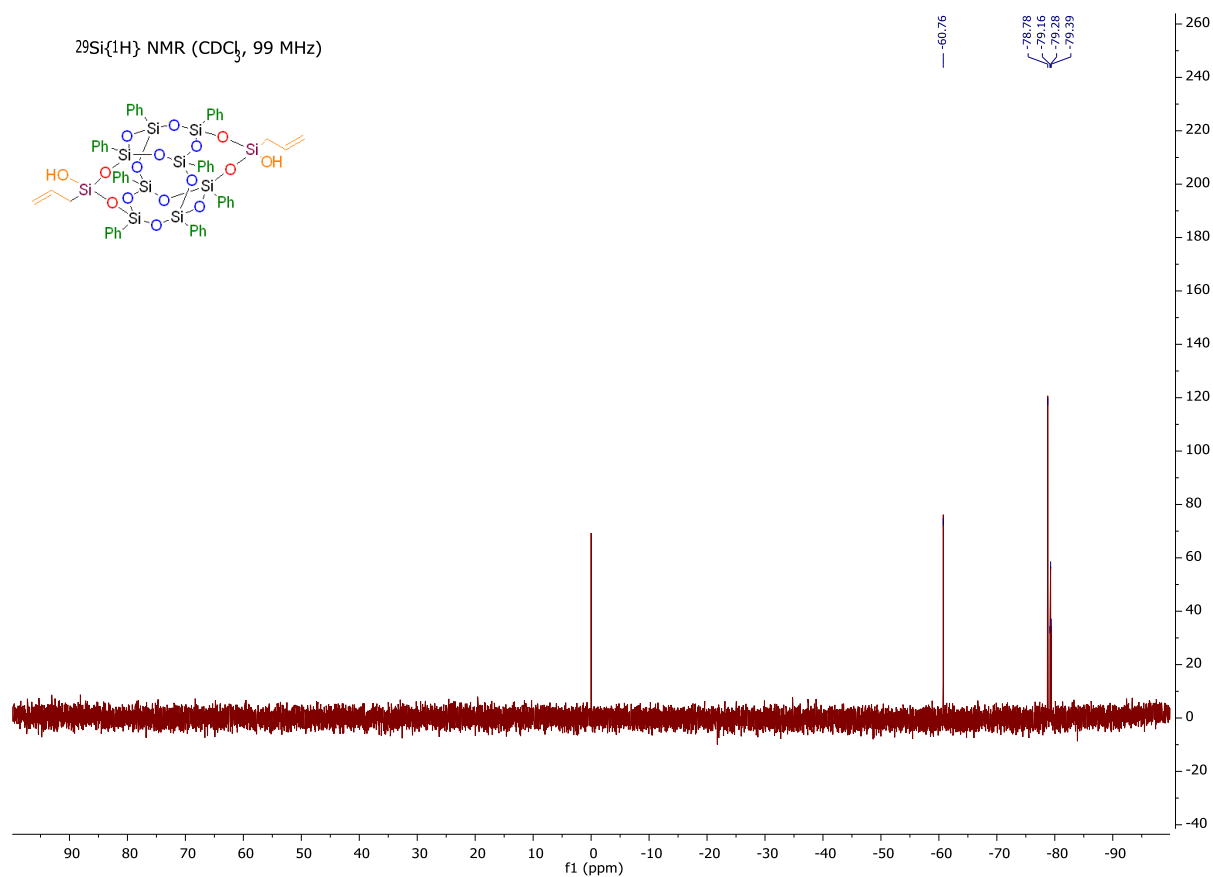


Figure 5-14 : $^{29}\text{Si}\{^1\text{H}\}$ -NMR (CDCl_3 , 99 MHz)

6 INCOMPLETELY CONDENSED CAGE-LIKE SILSESQUIOXANES

6.1 Introduction

Polyhedral oligomeric silsesquioxane (POSS) has been among the most promising hybrid organic-inorganic nanofillers in academic and industrial research due to its ease of functionalization, multifunctional nanostructure, and high thermal stability. The compounds' thermal behavior and crystal packing structures have been studied in detail. Wang et al. synthesized a series of alkylated cage silsesquioxanes and found that the size of attached alkyl chains effectively tuned the intermolecular forces between the cage structures.¹ Blanco et al. mono aryl halide substituted POSS cage structures and found an improvement in solubility and thermal properties of the synthesized POSS cage structures.² Wang et al. extensively reviewed the enhancement of POSS's thermal, mechanical, and optical properties modified using various corona groups.³ It was found that functionalizing the incompletely condensed octaphenyl double-decker silsesquioxane tetrasilanol, $\text{DDPh}_8\text{T}_8(\text{OH})_4$, with reactive dichlorosilanes forms a condensed, hybrid molecule with reactive organic groups on the opposite edge of the inorganic $\text{SiO}_{1.5}$, SQ, core surrounded by phenyl moiety.⁴⁻¹² Vogelsang et al. found that the *cis/trans* isomers formed during the capping of $\text{DDPh}_8\text{T}_8(\text{OH})_4$ can be isolated by using a combination of selective solvent fractional crystallization and liquid chromatography.¹³⁻¹⁷ On separation of the *cis* and *trans* isomers, it is found that *trans* isomers have higher melting temperatures than the *cis* isomers. Increasing the size of groups attached to the cage lowers the melting temperature. The *cis-trans* isomer mixture exhibits eutectic melting.

On the contrary, a few studies on unsymmetrical/asymmetrical silsesquioxane or siloxane cages. This fact is mainly due to the difficulties in obtaining a perfect Janus cage using simple hydrolytic condensation techniques. Due to the unique physical and chemical properties related to the different types, quantities, and functionality of the organic groups present in the single molecule,

the synthesis of asymmetrical cage structures has become an essential subject in the field of silicon chemistry.^{18–23}

So far, most of the studies and modifications on POSS/DDSQ cage have been on changing the corona groups of the system. This study focuses on tailoring the core Si-O-Si cage to study the

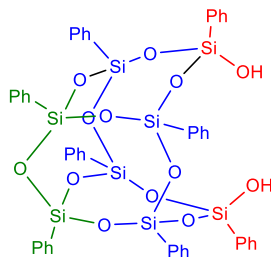
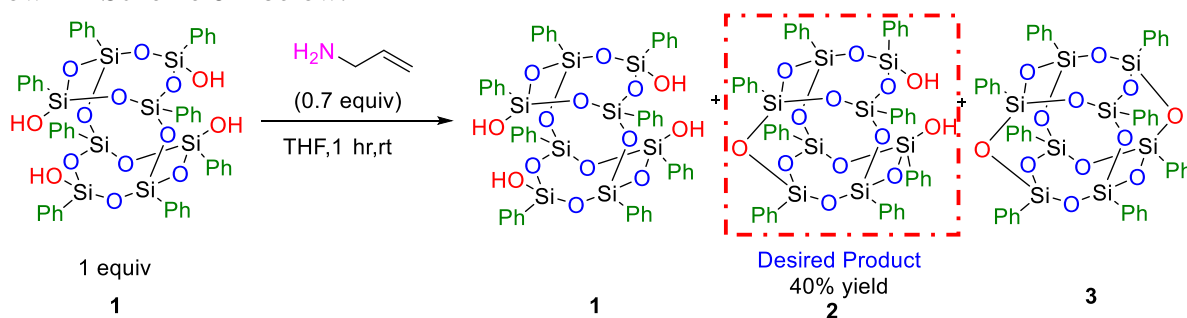


Figure 6-1 : The structure of Side Open $\text{Ph}_8\text{T}_8(\text{OH})_2$

effects on thermal properties and the crystal packing of the system. To facilitate that, an asymmetrical closed cage silsesquioxane structure with one edge closed and silanol groups on the other end.

6.2 Synthesis of Incompletely Condensed Cage diol

The starting material $\text{SOPh}_8\text{T}_8(\text{OH})_2$ was synthesized via base-mediated partial cage closure of $\text{DDPh}_8\text{T}_8(\text{OH})_4$. Allyl amine was used for the condensation reaction of tetra-silanol cages, as shown in Scheme 6-1 below.



Scheme 6-1 : Reaction scheme for synthesis of $\text{SOPh}_8\text{T}_8(\text{OH})_2$

A per pass yield of 40% desired $\text{SOPh}_8\text{T}_8(\text{OH})_2$ compound was isolated from the condensation reaction shown above. The by-product of the reaction is a condensed silanol cage which can be separated using simple filtration techniques and is recycled to resynthesize $\text{DDPh}_8\text{T}_8(\text{OH})_4$ via

NaOH mediated route as shown by Barry et al. The uncondensed starting material can also be separated via filtration to be reused in the reaction. The synthesis does not require any complex work-up steps. The by-products produced in the reaction can be converted back to the starting material, thus making the synthesis an atom-efficient and green chemistry reaction.

The condensation reaction synthesizing diol produces a partially or fully condensed cage. The amount of allyl amine used in the reaction must be optimized to get the desired cage's maximum yield, like diol. The conditions used for optimization have been illustrated in Table 6-1.

Table 6-1 : Reaction optimization conditions for the synthesis of $\text{SOPh}_8\text{T}_8(\text{OH})_2$

	Compound	mmol	Time	$\text{DDPh}_8\text{T}_8(\text{OH})_4$	$\text{SOPh}_8\text{T}_8(\text{OH})_2$	DDPh_8T_8
		[Weight (g)]	hr	Weight %	Weight %	Weight %
A	$\text{DDPh}_8\text{T}_8(\text{OH})_4$	1.87 [2]	2	0	1	99
	Allylamine	1.34 [0.076]				
B	$\text{DDPh}_8\text{T}_8(\text{OH})_4$	1.87 [2]	1	5	19	76
	Allylamine	1.34 [0.076]				
C	$\text{DDPh}_8\text{T}_8(\text{OH})_4$	7.48 [8]	1	21	37	42
	Allylamine	1.34 [0.076]				

The best reaction conditions for optimum yield of the desired product are using 0.1 mL of allyl amine for every 8 g of $\text{DDPh}_8\text{T}_8(\text{OH})_4$ used in the reaction. Once the desired diol has been synthesized, the next step is capping the diol with different dichlorosilanes to obtain an analogous

series of compounds, as previously done by Vogelsang et al.¹³, which has been shown in Scheme

6-2

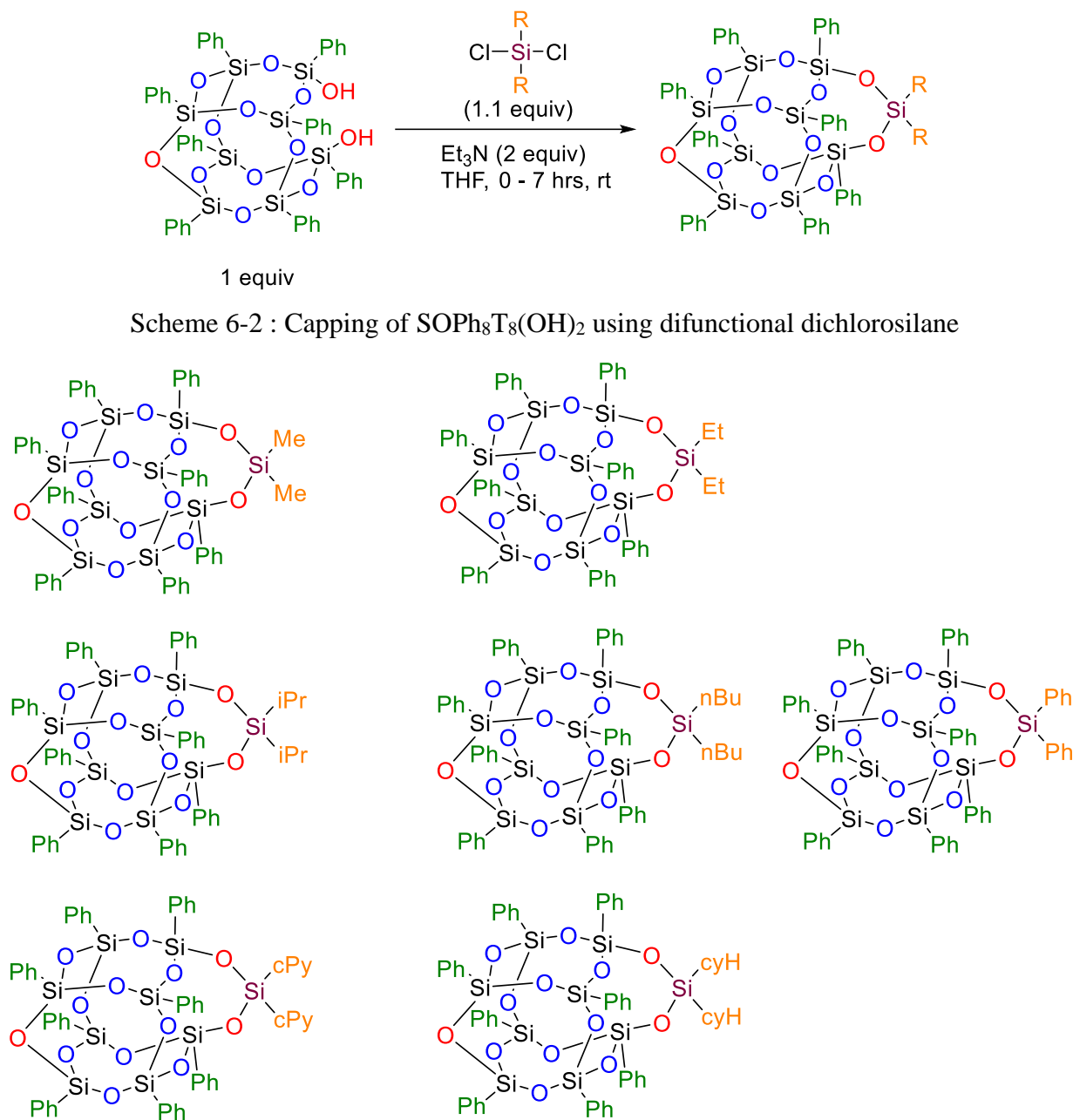


Figure 6-2 : The series of compounds synthesized in this work

The analogous series of compounds synthesized in this work has been shown in Figure 6-2

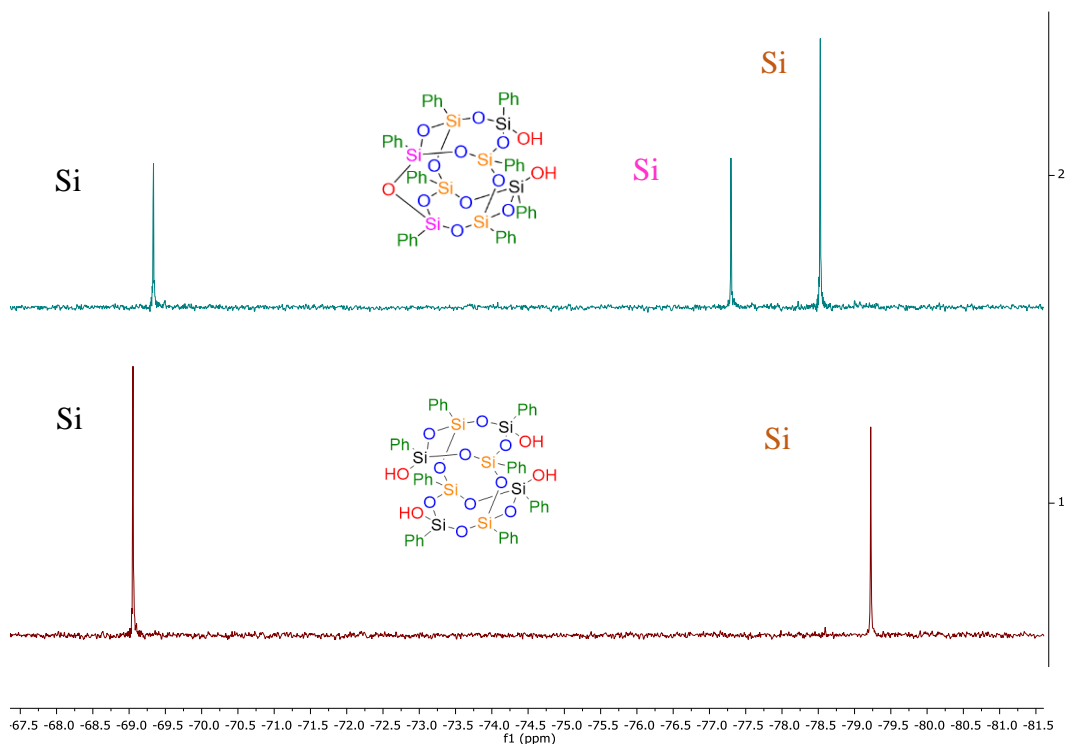


Figure 6-3 : ^{29}Si NMR comparison between $\text{SOPh}_8\text{T}_8(\text{OH})_2$ and $\text{DDPh}_8\text{T}_8(\text{OH})_4$

To verify the synthesis of $\text{SOPh}_8\text{T}_8(\text{OH})_2$ and to study the behavior of the molecules in solution, Proton (^1H), Carbon (^{13}C), and Silicon (^{29}Si), NMR analysis was performed. As seen in Figure 6-3, the silicon atoms for **2** can be classified into 3 different types, as depicted by the color of the silicon atoms. The 8 T-silicon atoms on the core cage are divided in the ratio 2:4:2 based on the bond connectivity and nuclear environment around these atoms. A noticeable difference can also be observed for the magnetic environment phenyl groups attached to these T-silicon atoms. Similarly, the silicon atoms for **1** can be classified into 2 different types as depicted by the color of the silicon atoms. The 8 T-silicon atoms on the core cage are divided in the ratio 1:1. The T-silicon atoms directly attached to the hydroxy groups (shown in black color) have a different magnetic environment than the silicon atoms internal to the cage (shown in orange color). The ^1H NMR comparative analysis for **1** and **2** has been shown in

Figure 6-4. The splitting pattern of the phenyl protons for **1** was more uniform than that of **2**, denoting more symmetry in the structure of **1** compared to **2**. This change in splitting pattern can be attributed to the presence of 2 types of phenyl rings in **1** versus 3 types of phenyl rings in **2**.

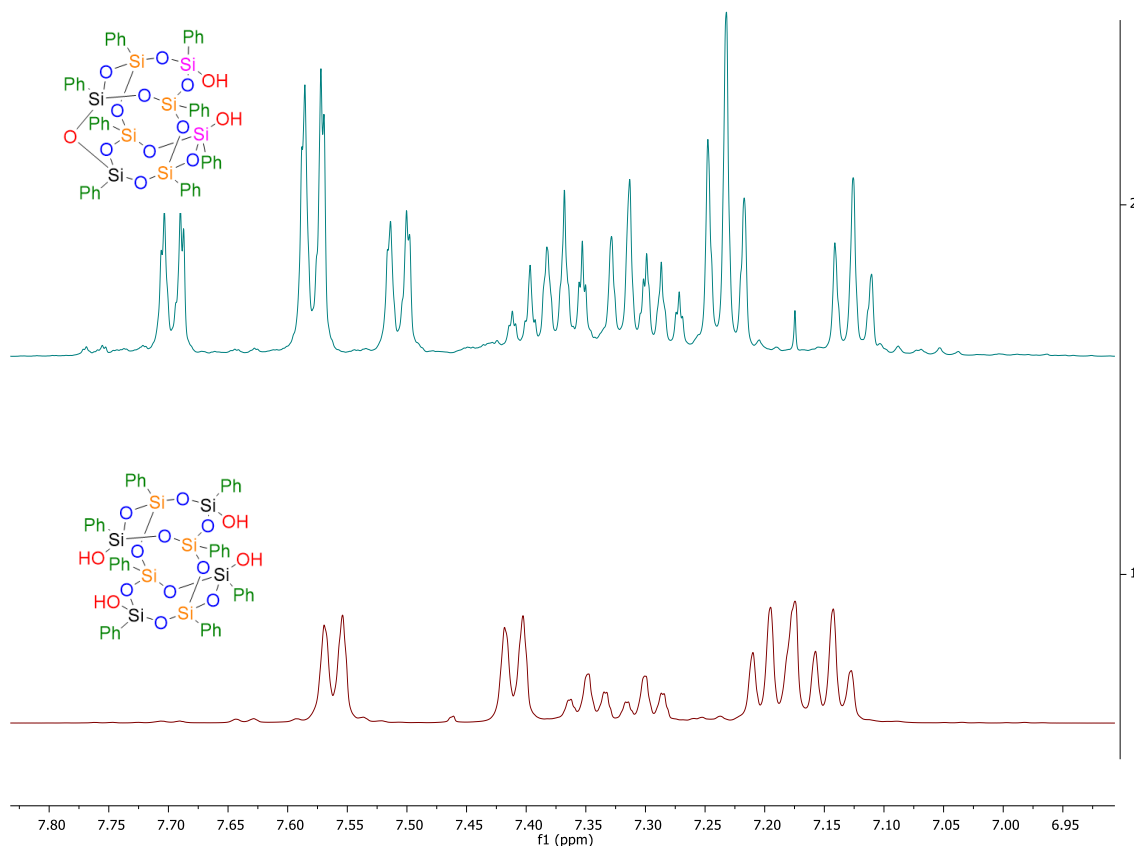


Figure 6-4 : ^1H NMR comparison between $\text{SOPh}_8\text{T}_8(\text{OH})_2$ and $\text{DDPh}_8\text{T}_8(\text{OH})_4$

The detailed synthesis procedures of the analogous series of compounds and the NMR data are provided in the chapter's supplementary information attached. For comparison, $\text{SOPh}_8\text{T}_8\text{Me}_2$ and $\text{SOPh}_8\text{T}_8\text{Ph}_2$ have been taken as model compounds, and their thermal properties have been studied.

6.3 Thermal properties of model compounds

Detailed thermal studies have been performed to study the impact of the difference in the crystal packing and the consequence of cage structure variation on the isomers' thermal properties. The DSC analysis performed on the two isomers revealed a significant difference in their melting

points, as seen in Table 6-2. The DSC thermograms have been shown in SI. In the case of **4**, ΔH_m and ΔS_m obtained from DSC are 29.8 kJ/mol and 60.4 J/mol K, respectively. However, in the case of $\text{SOPh}_8\text{T}_8\text{Me}_2$, ΔH_m and ΔS_m values obtained are 58.5 kJ/mol and 107 J/mol K, respectively.

Table 6-2 : Thermal Parameters for $\text{SOPh}_8\text{T}_8\text{Me}_2$ and $\text{SOPh}_8\text{T}_8\text{Ph}_2$ based on DSC analysis.

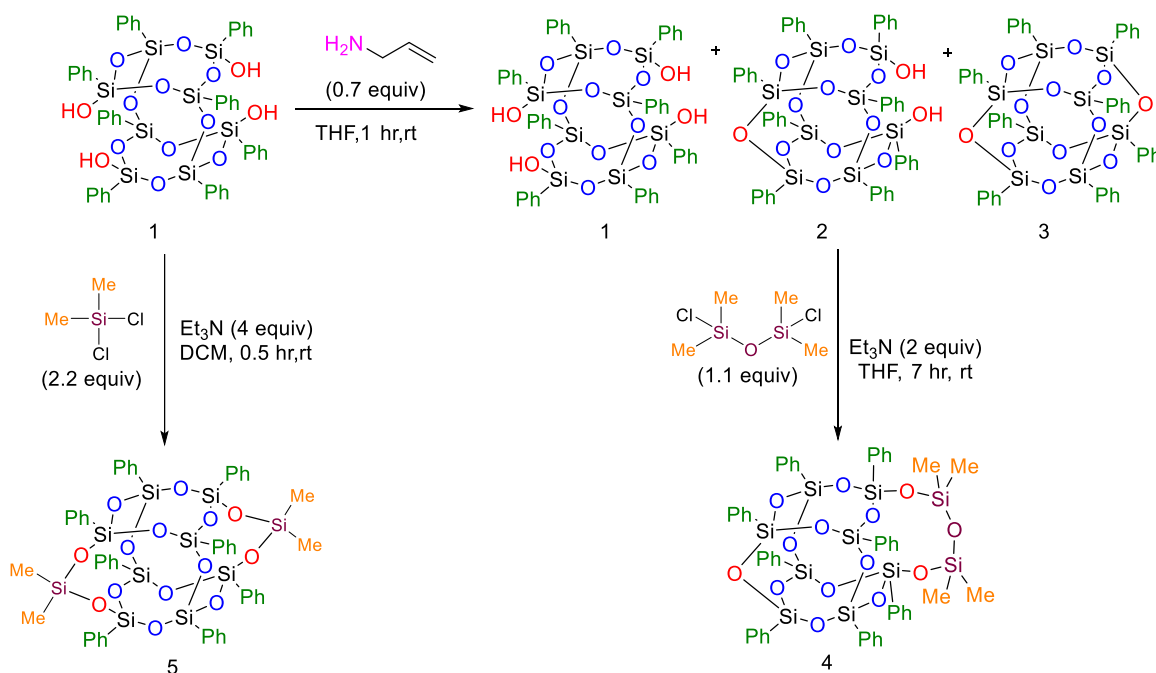
	$\text{SOPh}_8\text{T}_8\text{Me}_2$	$\text{SOPh}_8\text{T}_8\text{Ph}_2$
1 st heating cycle	Sharp melting peak (274 °C)	Broad melting peak (267 °C)
1 st cooling cycle	Broad recrystallization at 236 °C	No recrystallization peak was observed during cooling
2 nd heating cycle	Sharp melting peak like the first heating cycle	Cold recrystallization, as well as a melting peak, was observed
ΔH_m (kJ/mol)	58.5	21
ΔS_m^* (J/ (mol K))	107	38.9

A change in entropy of melting (ΔS_m) is directly related to the ability to disrupt the intermolecular packing of the compounds. More significant the entropy changes at melting, the more compact the crystal packing. The cooling cycles also showed a significant difference in the recrystallization kinetics of the two isomers. A broad recrystallization peak was observed for $\text{SOPh}_8\text{T}_8\text{Me}_2$. The enthalpy of recrystallization observed from the DSC thermogram was 46.3 kJ/mol.

However, interestingly, $\text{SOPh}_8\text{T}_8\text{Ph}_2$ did not exhibit any recrystallization peak even at low cooling rates (2 °C/min). A second heating cycle was performed on the isomers to verify the compounds' thermal stability during the DSC runs. $\text{SOPh}_8\text{T}_8\text{Me}_2$ exhibited a melting peak in the same temperature range as was obtained in the first heating cycle. $\text{SOPh}_8\text{T}_8\text{Ph}_2$ exhibited an interesting thermogram in that a recrystallization peak was observed around 152 °C and a melting peak at the same temperature range as obtained in the first heating cycle.

6.4 Synthesis and Characterization of constitutional isomers

Structural isomer (or constitutional isomer in the IUPAC nomenclature) is the most radical type of isomerism. Although two compounds have the same number of atoms, their chemical and physical properties are entirely different since they have logically distinct bonds. In this work, constitutional isomerism of cage-like silsesquioxanes has been investigated. Precisely, edge-open octaphenyl silsesquioxane diol condensed with tetramethyl dichlorosiloxane, **4**, and double-decker-shaped silsesquioxane tetraol condensed with dimethyl dichlorosilanes, **5**, form structural isomers. The characteristics of these two condensed derivatives were examined by Nuclear Magnetic Resonance (NMR) to confirm their structure. Physical and thermal characteristics were investigated using differential scanning calorimetry, thermogravimetric analysis, synchrotron X-ray, and rheometry.



Scheme 6-3 : Synthesis of constitutional isomers

To verify the synthesis and the purity of the two structural isomers **4** and **5** and to study the behavior of the molecules in solution, Proton (^1H), Carbon (^{13}C), and Silicon (^{29}Si), NMR analysis was

performed. As seen in Figure 6-5, the silicon atoms for **4** can be classified into 4 different types, as depicted by the color of the silicon atoms. The methyl groups attached to D-silicon atoms (depicted by the marron color) have a similar magnetic environment. The 8 T-silicon atoms on the core cage are divided in the ratio 2:4:2 based on the bond connectivity and nuclear environment around these atoms. A noticeable difference can also be observed for the magnetic environment phenyl groups attached to these T-silicon atoms. Similarly, the silicon atoms for **5** can be classified into 3 different types as depicted by the color of the silicon atoms. The D-silicon atoms are located on either side of the cage as compared to **4**, where the D-silicon atoms are on one side.

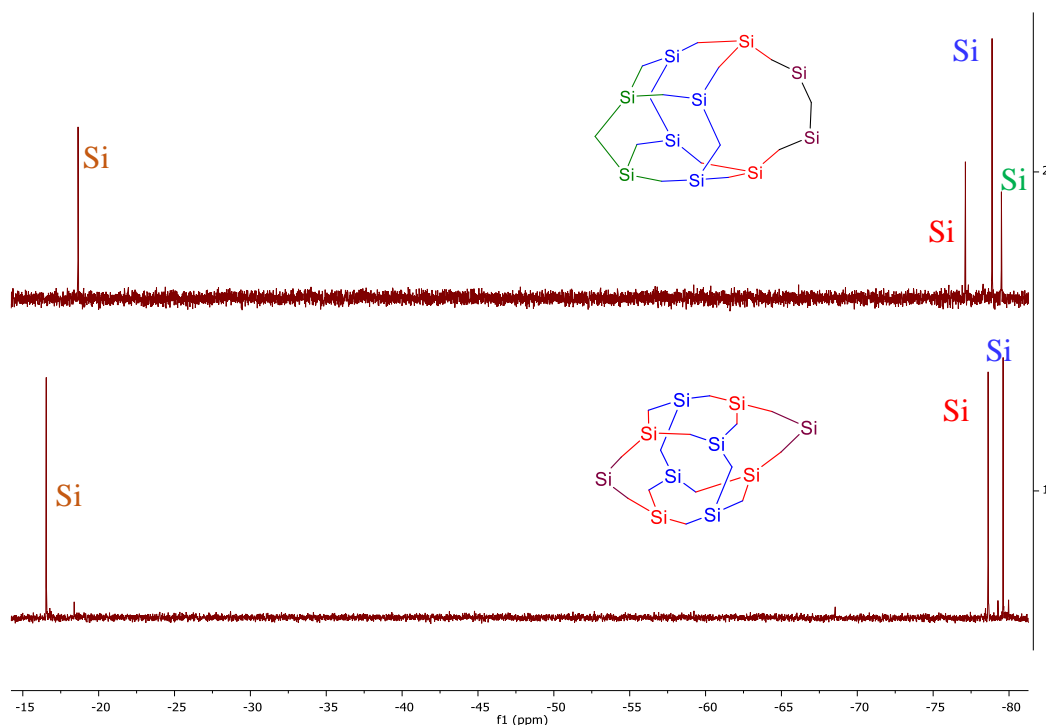


Figure 6-5 : ^{29}Si NMR comparison between isomers **4** and **5**

The 8 T-silicon atoms on the core cage are divided in the ratio 1:1. The T-silicon atoms directly attached to the D-silicon atoms (shown in blue color) have a different magnetic environment than the silicon atoms internal to the cage (shown in red color).

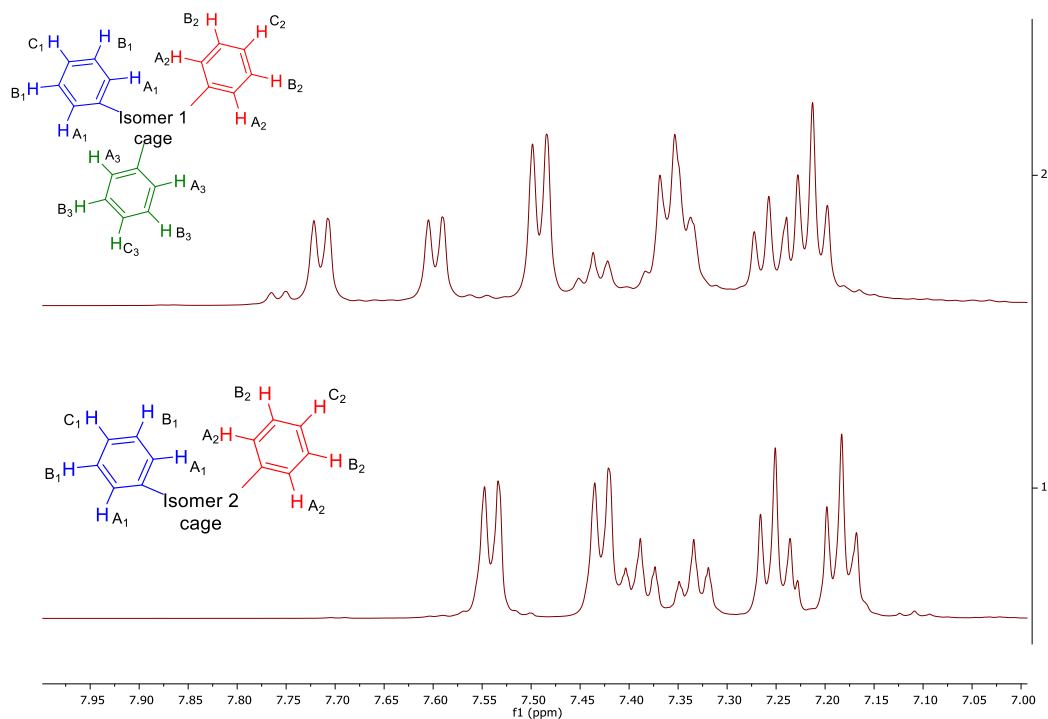


Figure 6-6 : Comparative ^1H NMR of the phenyl region for 4 and 5

Upon studying the comparative analysis of ^1H NMR (Figure 6-6) for isomer 1 (**4**) and isomer 2 (**5**), it is evident that there are 12 protons for the four methyl groups attached to the D-Si atoms and 40 protons in the phenyl groups which are attached to T-Si atoms on the silsesquioxane cage. The chemical shift of the methyl group protons for **4** (0.23 ppm) was upshifted compared to that of **5** (0.30 ppm). The splitting pattern of the phenyl protons for **5** was more uniform than that of **4**, denoting more symmetry in the structure of **5** compared to **4**. This pattern can be attributed to 2 types of phenyl rings in **5** versus 3 in **4**.

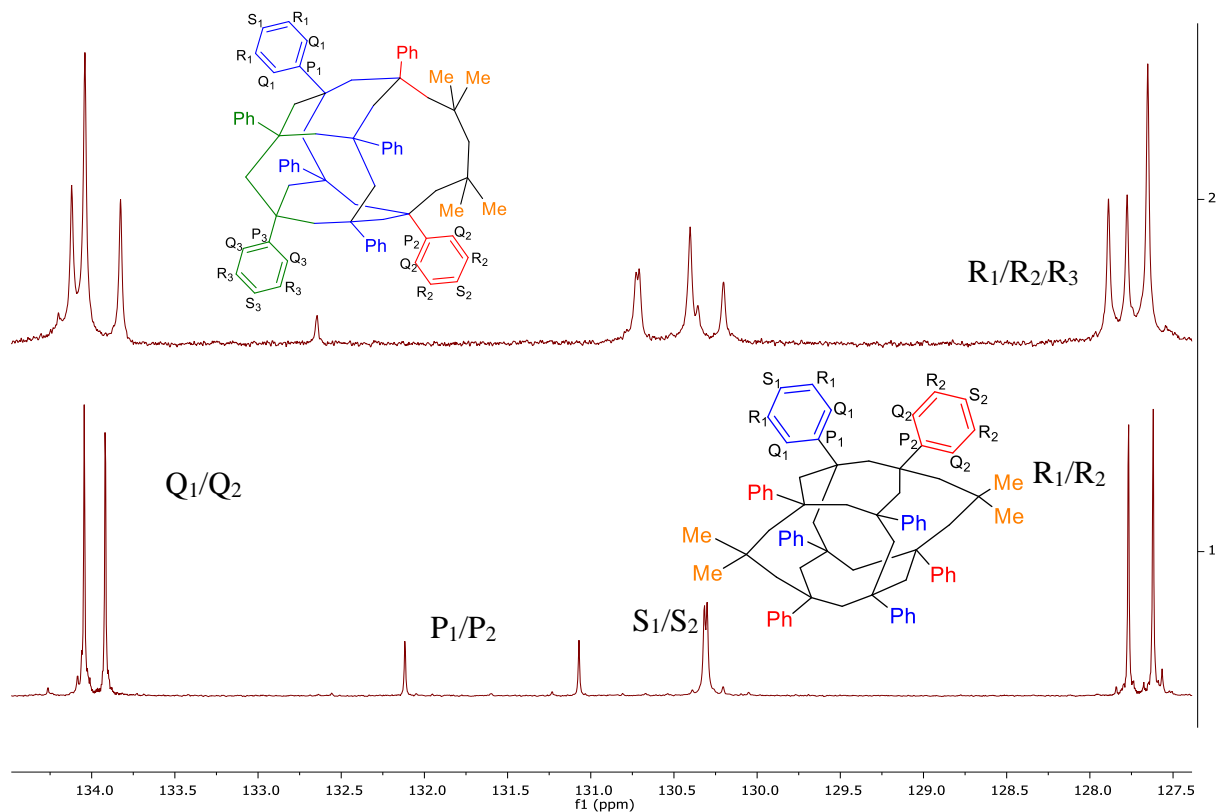


Figure 6-7 : Comparative ^{13}C NMR of the phenyl region for 4 and 5

The ^{13}C NMR analysis of the isomers depicts the difference in the uniformity of cages between the isomers. The distribution of carbon atoms in phenyl rings for **4** and **5** are as labeled in Figure 6-7. The type of atoms connected to phenyl rings (or the silicon atoms) and the number of atoms are the same, but the chemical shifts of the carbon atoms are different. The phenyl rings' steric position, shielding, and deshielding effects can explain the differences in the NMR spectra. The splitting pattern of carbon atoms in the phenyl region for **4** indicates the *meta* and *ortho* region carbon atoms in the ratio of 1:2:1, whereas that ratio is 1:1 for isomer **5**. It can also be seen that the chemical shifts of *ortho* carbon > *para* carbon > *meta* carbon are due to the difference in electron densities. ^{29}Si NMR shows the most discrepancies in the structure of the two isomers, as seen in Figure 6-5. The D-Si NMR peak for **4** (-18.64 ppm) is upshifted compared to **5** (-15.65 ppm). This shift indicates that the phenyl rings less effectively shield the D-Si atoms on the

silsesquioxane cage for **5**. In the case of the T-Si region of the silsesquioxane cages for **5** exhibits only two peaks at -78.63 ppm, corresponding to four Si atoms attached to the D-Si atoms, and at -79.61 ppm, corresponding to four interior cage Si atoms. For **4**, this T-Si region has 3 peaks indicating the presence of 3 distinct types of Si atom environments and a more distorted cage structure. The peak at -77.13 ppm corresponds to two T-Si atoms connected to the D-Si atoms. The next peak denotes the interior four T-Si atoms at -78.88 ppm. The peak at -79.50 ppm corresponds to two T-Si atoms on the opposite end of the cage structure. Thus, it can be concluded that the phenyl rings have different angles of orientation on the silsesquioxane cage for the two constitutional isomers even in a solution, thus leading to a significant difference in the atomic packing structure of the cages.

The crystal structure of each compound was obtained by X-ray diffraction from a solution-grown single crystal. The crystal packing structures of the two isomers are vastly different (Refer to Appendix for detailed crystal structure).

Table 6-3 : Parameters for isomers from X-ray diffraction analysis

Isomer 1 (4)		Isomer 2 (5)	
Formula	C ₅₂ H ₅₂ O ₁₄ Si ₁₀	Formula	C ₅₂ H ₅₂ O ₁₄ Si ₁₀
CCDC #	2189474	CCDC #	1832148
Volume	5742.3 Å ³	Volume	5852.3 Å ³
Crystal System	monoclinic	Crystal System	tetragonal
Space Group	P2 ₁ /n	Space Group	P4 ₂ /m
D _{calc}	1.37 g.cm ⁻³	D _{calc}	1.34 g.cm ⁻³
a	10.9 Å	a	14.9 Å
b	21.3 Å	b	14.9 Å
c	24.6 Å	c	26.2 Å
α	90°	α	90°
β	93.5°	β	90°
γ	90°	γ	90°

The parameters for the two isomer components from X-ray diffraction analysis have been shown in Table 6-3

It is evident from the analysis that **4** has a less symmetrical monoclinic crystal system, whereas **5** has a tetragonal crystal system. **4** has a volume (5742.3 \AA^3) lower than that of **5** (5852.3 \AA^3), but the density of **5** (1.34 g.cm^3) was reported lower than that of **4** (1.37 g.cm^3). This anomalous behavior can be attributed to the fact that **4** has a more distorted cage structure, thus effectively

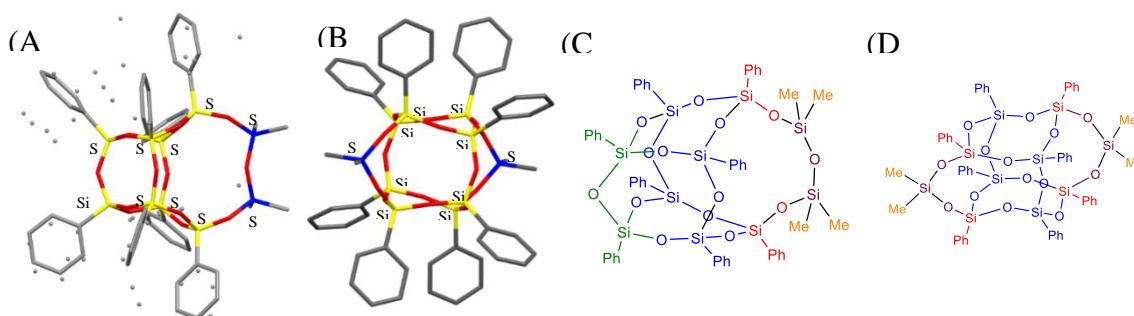


Figure 6-8 : (A),(B) Crystal structure for isomers of tetramethyl capped Ph_8T_8 (C),(D) Analogous chemdraw structure for isomers of tetramethyl capped Ph_8T_8

helping it pack better in a crystal lattice than **5**.

From the analysis of the intramolecular configuration of the crystal structure of the isomers, the distances between various Si atoms (D-Si, T-Si) were extracted. The isomers have the same chemical formula yet different packing. For **4**, the longest distance is between T-Si and D-Si atoms ($\text{Si(T)}_9\text{-Si(D)}_2 - 7.69 \text{ \AA}$). Since the cage is asymmetrically skewed, the distance between the second pair of T-Si and D-Si atoms ($\text{Si(T)}_{10}\text{-Si(D)}_1 - 7.69 \text{ \AA}$) is slightly smaller. Similar findings can be seen in the case of two different pairs of T-Si - T-Si atoms. ($\text{Si(T)}_9\text{-Si(T)}_{10} - 3.06 \text{ \AA}$; $\text{Si(T)}_3\text{-Si(T)}_6 - 5.69 \text{ \AA}$). The distance between the pair of D-Si atoms ($\text{Si(D)}_1\text{-Si(D)}_2$) is almost three times smaller than that of the corresponding isomer. The findings in Figure 6-8 also suggest that the phenyl groups bonded to T-Si twist asymmetrically to accommodate the D-Si atoms affecting the overall crystallographic packing density.

For **5**, three significant bond distances have been identified. The longest distance can be found between the two D-Si atoms (8.54 Å) on either side of the cage. The other notable distances between two T-Si atoms (4.55 Å) and D-Si – T-Si atoms (6.83 Å) have also been noted. Interestingly, the cage displays axial symmetry, and the bond distances remain the same across the similar atoms in the cage, as seen in Figure 6-8.

6.5 Thermal and Rheological Property of isomers: TGA, DSC, and Viscosity

Detailed thermal studies have been performed to study the impact of the difference in crystal packing and the consequence of variation in cage structure on the thermal properties of the isomers. These thermal studies provide insights into the solid-liquid transition temperatures, thermal stability, and the phase behavior of these constitutional isomers. TGA analysis was performed on

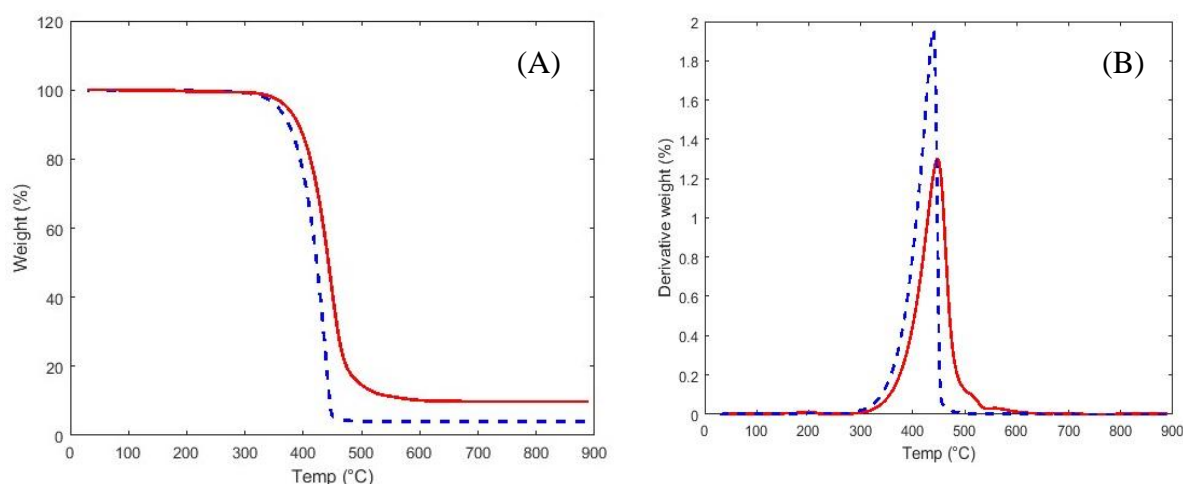


Figure 6-9 : TGA analysis for isomers **4** and **5**. The solid red line indicates compound **4** whereas the dotted blue line indicates compound **5**. (A) Weight loss vs temperature curves for the two isomers. (B) Derivatized weight loss curves for the two isomers

two isomers to verify the vaporization behavior, as shown in Figure 6-9. The thermograms show that the onset of weight loss is almost identical. To further analyze the thermograms, derivatized weight loss versus temperature was plotted. The slope of the derivatized peak indicates the compounds' evaporation rate.

The rate of evaporation for **4** is slower than the rate of evaporation for **5**. This rate is indicated by the sharp slope of the derivative weight peak for **5**. **4** indicated a secondary peak around 550 °C, whereas no secondary peak was observed for **5**. This secondary indicates a more complex weight loss mechanism for **4** than **5**. The final residual weight loss for **5** was higher than **4**. **4** exhibited complete evaporation without residue in the TGA pan, whereas **5** left behind black solid mass residue (~ 10 wt. %). Although the number of Si atoms is the same for both isomers, there is a difference in the types of Si bonds. **4** exhibits a peculiar D-Si to D-Si bonding which is absent in **5**. Also, the number of D-Si to T-Si bonds in **4** is half the number in **5**. This difference in bonding can be a possible explanation for the complex weight loss mechanism exhibited by **4**.

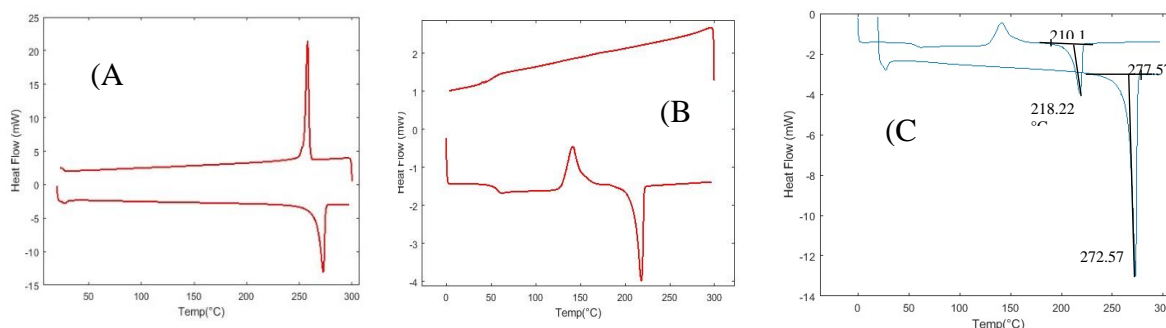


Figure 6-10 : DSC analysis for isomers **4** and **5**. (A) DSC heating and cooling curve for compound **5**. (B) DSC heating and cooling curve for compound **4** (C) Comparative heating curves for compounds **4** and **5**

The DSC analysis performed on the two isomers revealed a significant difference in their melting points, as seen in Table 6-4. Despite having the same number of bonds and atoms, a difference of 60 °C in the melting points of the compounds deserves to be investigated in further detail. Our group has demonstrated various examples of symmetrically capped $\text{DDSQPh}_8\text{T}_8(\text{OH})_4$ and the effect of various alkyl/cyclic/aromatic groups on the thermal properties of the compounds.¹³ We calculated the thermodynamic properties from the DSC thermogram, as seen in Table 6-4. The DSC thermograms have been shown in SI. In the case of **4**, ΔH_m and ΔS_m obtained from DSC are

29.8 kJ/mol and 60.4 J/mol K, respectively. However, in the case of **5**, ΔH_m and ΔS_m values obtained are 55.5 kJ/mol and 101 J/mol K, respectively. A change in entropy of melting (ΔS_m) is directly related to the ability to disrupt the intermolecular packing of the compounds. It has been found that the more significant the entropy change at melting, the more compact the crystal packing for a given molecule. Considering this ΔS_m value, we can conclude that **5** is more ordered and stable.

Table 6-4 : Thermal Parameters for isomers 1 and 2 based on DSC analysis

	5	4
1 st heating cycle	Sharp melting peak (276 °C)	Broad melting peak (220 °C)
1 st cooling cycle	Rapid recrystallization at 225 °C	No recrystallization peak was observed during cooling
2 nd heating cycle	Sharp melting peak like the first heating cycle	Cold recrystallization, as well as a melting peak, was observed
ΔH_m (kJ/mol)	55.5	29.8
ΔS_m^* (J/ (mol K))	101	60.4

The cooling cycles also showed a significant difference in the recrystallization kinetics of the two isomers. A rapid recrystallization peak with undercooling was observed for **5**. The enthalpy of recrystallization observed from the DSC thermogram was 56.4 kJ/mol. However, interestingly, **4** did not exhibit any recrystallization peak even at low cooling rates (2 °C/min). A second heating cycle was performed on the isomers to verify the compounds' thermal stability during the DSC runs. **5** exhibited a melting peak in the same temperature range as was obtained in the first heating cycle. **4** exhibited an interesting thermogram in that a recrystallization peak was observed around 140 °C, and a melting peak was observed at the same temperature range as obtained in the first heating cycle.

6.6 Rheological data

Rheological data was calculated for compound **4**. The effect of temperature on the viscosity of compound **4** was studied. The temperature range varied from 220 °C to 240 °C, and the corresponding viscosity of the compound was measured. It was found that the viscosity of the compound hard varied between 1 Pa.s to 4 Pa.s, as seen in Figure 6-11 below.

The effect of shear rate versus viscosity was studied at constant temperature. The temperature was set at 230 °C, which was above the solid-to-liquid transition temperature of the compound. It was found that as the shear rate changed from 0.001 s⁻¹ to 1 s⁻¹, the viscosity of the compounds changed by two orders of magnitude, i.e., compound **4** exhibits shear thinning behavior. This behavior is unusual for isolated pure compounds. This behavior is usually seen in non-Newtonian materials. This behavior in compound **4** can be attributed to the molecule's shape. Due to the structure's non-symmetrical nature, the molecules' orientation significantly affects the compound's viscosity.

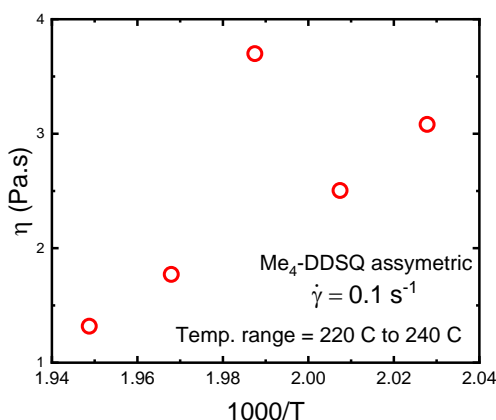


Figure 6-11 : Effect of temperature on viscosity of compound **4**

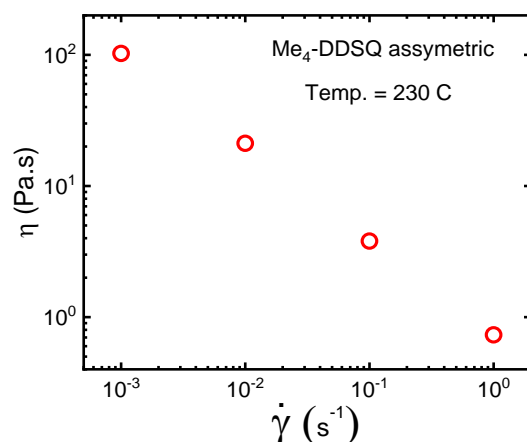


Figure 6-12 : Effect of shear rate on viscosity with constant temperature at 230 °C

To summarize, a novel strategy was developed to synthesize structural isomers to examine the effect of inorganic core on the thermal and crystal packing of cage-like silsesquioxane compounds. The synthesized isomers have the same number of atoms, the same types, and the number of bonds. **4** exhibits a 20 % faster weight loss rate and has a higher residual weight at 900 °C. The melting temperature of **5** (272 °C) was almost 60 °C higher than **4**, and the heat of fusion for **4** was half that of **5**. The entropy of melting for **5** was 40 % higher than that of **4**. This value indicates a more compact and symmetrical packing for **5** over **4**. Single crystal X-ray analysis indicates the symmetrical tetragonal crystal packing for **5**, whereas **4** has more asymmetrical monoclinic crystal packing. It is interesting to note that although **5** has a lower asymmetry than **4**, it has a higher density than **4**. Although this work demonstrated that the inorganic core could affect properties, additional work is still needed to fully understand the effects of Si_(T) vs. Si_(D) atoms on the silsesquioxane cages.

6.7 Experimental Details

6.7.1 General Information

All manipulations were done under a nitrogen atmosphere using standard Schlenk techniques except otherwise stated. All commercially available chemicals were used as received unless otherwise indicated. Allyl amine ($\text{C}_3\text{H}_7\text{N}$), dimethyl dichlorosilane ($\text{C}_2\text{H}_6\text{Cl}_2\text{Si}$), 1,3-dichloro-1,1,3,3-tetramethyldisiloxane ($\text{C}_4\text{H}_{12}\text{Cl}_2\text{OSi}_2$), triethylamine ($\text{C}_6\text{H}_{15}\text{N}$) deuterated chloroform with 1 vol % tetramethylsilane (CDCl_3 -1%TMS), were purchased from Sigma-Aldrich. 1,3,5,7,9,11,14,17-octaphenyl-2,4,6,8,10,12,13,15,16,18-decaoxa-1,3,5,7,9,11,14,17-octasilatricyclo[7.3.3.3^{3,7}]octadecane-5,11,14,17-tetraol ($\text{DDPh}_8\text{T}_8(\text{OH})_4$) was obtained from Hybrid Plastics. Tetrahydrofuran (THF), dichloromethane (DCM), and methanol (MeOH) were purchased from Sigma-Aldrich. THF was distilled over benzophenone and sodium metal at 70 °C under nitrogen. Toluene was distilled over calcium hydride at a temperature of 120 °C. The other solvents were used as purchased without further purification, and the glassware was oven dried. All ^1H , ^{13}C , and ^{29}Si NMR were acquired on an Agilent DirectDrive2 500 MHz NMR spectrometer equipped with a OneProbe operating at 500 MHz for ^1H NMR, 126 MHz for ^{13}C NMR, and 99 MHz for ^{29}Si NMR using CDCl_3 and recorded at 25 °C. ^1H -NMR spectra were recorded with 8 scans, a relaxation delay of 1s, and a pulse angle of 45° and referenced to the residual protonated solvent in CDCl_3 (7.24 ppm). ^{13}C -NMR spectra were collected with 254 scans, a relaxation delay of 0.1 s, and a pulse angle of 45°. ^{29}Si NMR spectra were recorded with either 256 scans, a relaxation delay of 25 s, and a pulse angle 45°.

For crystallographic analysis, 0.5 g of each compound was dissolved in DCM and slowly evaporated for three days to get crystals. The crystal was kept at a temperature of 173 K during

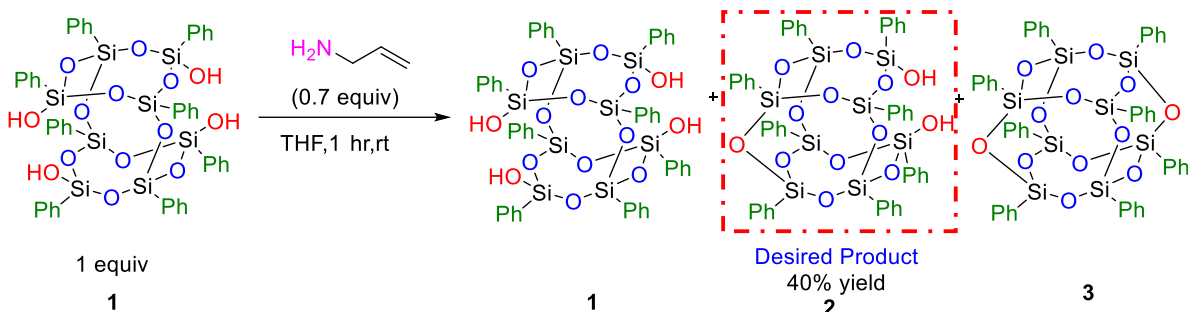
data collection. The crystals obtained were mounted on a nylon loop with paratone oil and analyzed on a Bruker APEX-II CCD diffractometer.

For differential scanning calorimetry (DSC) experiments, TA Instruments Q2000 equipped with a mechanical cooler was used. The temperature was equilibrated to 50 °C for 2 min, a constant heating rate of 10 K/min up to a determined temperature above melting. A second heating ramp with the same rate as the first was used to verify the reproducibility and possible thermal degradation that may occur during the first heating cycle. Cooling traces were obtained from the above complete melting at a constant cooling rate of 5 K/min up to 50 °C. No thermal degradation was observed.

Thermogravimetric analysis was run in a TGA Q50 apparatus from TA instruments. A platinum pan was loaded with a sample weight of 8 mg \pm 0.2 mg. The samples were equilibrated at 323.15 K and heated to 1073.15 K at a rate of 20 K/min. The experiment used a dry nitrogen stream at a 100 ml/min flow rate.

Rheological measurements were performed on an Anton Paar MCR302 Rheometer with a CTD 600 oven. The temperature control accuracy was \pm 0.1 K. Small amplitude oscillatory shear (SAOS) tests were performed on a pair of 4 mm diameter parallel plates at a temperature range from 373 K to 453 K.

6.7.2 Synthesis of 1,3,5,7,9,11,13,15-octaphenyl-2,4,6,8,10,12,14,16,17,18,19-undecaoxa-1,3,5,7,9,11,13,15-octasilatetracyclo[9.5.1.1^{3,9}.1^{5,15}]nonadecane-7,13-diol

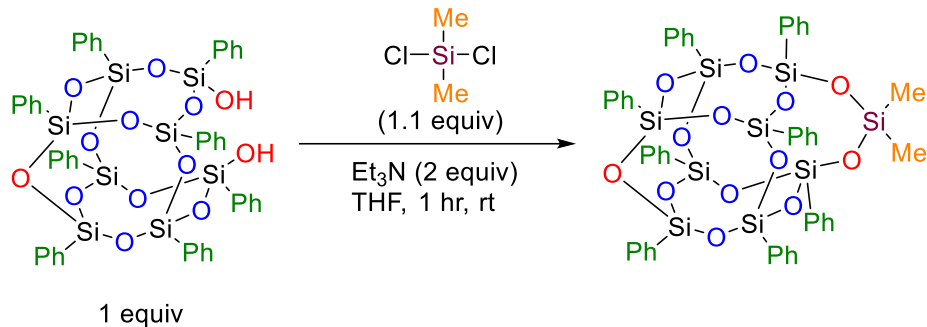


Scheme 6-4 : Synthesis of SOPh₈T₈(OH)₂

To a 500 mL round bottom flask were added DDPPh₈T₈(OH)₄ (8 g, 0.0075 mol, 1 equiv), allylamine (0.1 mL, 0.0013 mol, 0.18 equiv), and a stir bar under N₂ atmosphere. Freshly distilled DCM (200 mL) was then added. A clear solution was formed. The reaction mixture was stirred for 60 minutes, and a white slurry was observed. The solvent was evaporated, and THF (~ 200 mL) was added to recreate a slurry. This slurry was filtered through a medium frit funnel to obtain the crude product mixture in the filtrate. The filtrate was concentrated to obtain white powder. CHCl₃ (2x200 mL) was added to recreate a slurry. This slurry was filtered through a medium frit funnel to obtain the product in the filtrate. The solvent was evaporated, and the product was obtained as a white powder (2.64 g, 33% yield).

¹H NMR (500 MHz, Chloroform-d) δ 7.74 – 7.70 (m, 4H), 7.60 (td, J = 8.3, 1.4 Hz, 12H), 7.46 – 7.33 (m, 14H), 7.28 (d, J = 7.6 Hz, 6H), 7.27 – 7.20 (m, 4H), 3.75 – 3.71 (m, 1H), 1.85 – 1.81 (m, 1H). ¹³C{¹H} NMR (126 MHz, Chloroform-d) δ 127.76, 127.88, 130.20, 130.36, 130.64, 130.79, 130.87, 134.15, 134.18. ²⁹Si{¹H} NMR (99 MHz, Chloroform-d) δ -78.57, -78.32, -77.36, -69.27.

6.7.3 Synthesis of 17,17-dimethyl-1,3,5,7,9,11,13,15-octaphenyl-2,4,6,8,10,12,14,16,18,19,20,21,22-tridecaoxa-1,3,5,7,9,11,13,15,17-nonasilapentacyclo[9.7.1.13,9.15,15.17,13]docosane

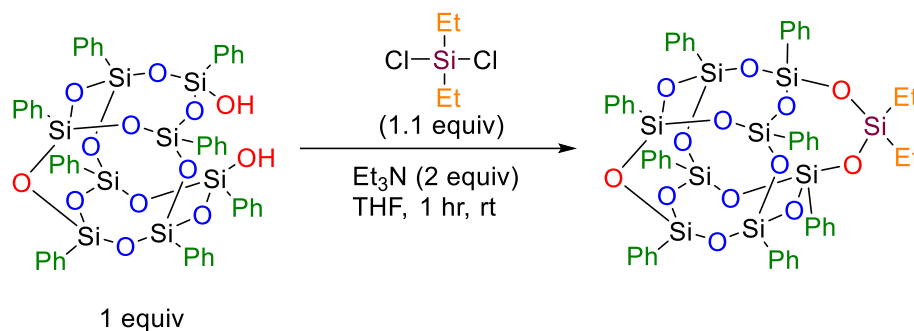


Scheme 6-5 : Synthesis of a capped SOPh₈T₈ (Me)₂

To a 100 mL round bottom flask were added SOPh₈T₈(OH)₂ (1 g, 0.95 mmol, 1 equiv), dimethyl dichlorosilane (0.13 mL, 1 mmol, 1.1 equiv), and a stir bar under N₂ atmosphere. Freshly distilled THF (~30 mL) was then added. A clear solution was obtained. Et₃N (0.26 mL, 0.0019 mol, 2.0 equiv) was added dropwise to this solution. The reaction mixture was stirred for 7 hr, after which the solvent was evaporated, and then fresh THF (~ 60 mL) was added to create a slurry. This slurry was filtered through a medium frit funnel to obtain the crude product in the filtrate. The filtrate was concentrated to obtain white powder. Methanol (~ 60 mL) was added to the reaction flask, stirring the slurry for 2 hours. The slurry was again filtered through a medium frit funnel to obtain the product as a white powder (0.89 g, 85% yield).

¹H NMR (500 MHz, Chloroform-d) δ 7.74 – 7.69 (m, 5H), 7.60 (d, J = 6.9 Hz, 14H), 7.41 (d, J = 15.4 Hz, 4H), 7.37 – 7.23 (m, 20H), 0.31 (s, 6H). ¹³C{¹H} NMR (126 MHz, Chloroform-d) δ 0.55, 127.75, 127.81, 127.84, 130.36, 130.55, 130.61, 130.73, 133.89, 134.11, 134.19. ²⁹Si{¹H} NMR (99 MHz, Chloroform-d) δ -79.31, -79.00, -77.48, -16.99.

6.7.4 Synthesis of 17,17-diethyl-1,3,5,7,9,11,13,15-octaphenyl-2,4,6,8,10,12,14,16,18,19,20,21,22-tridecaoxa-1,3,5,7,9,11,13,15,17-nonasilapentacyclo[9.7.1.13.9.15,15.17,13]docosane

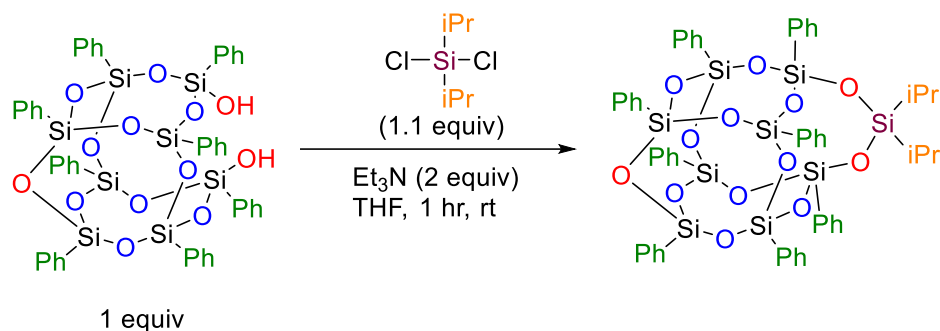


Scheme 6-6 : Synthesis of a capped SPh₈T₈ (Et)₂

To a 100 mL round bottom flask were added SPh₈T₈(OH)₂ (1 g, 0.95 mmol, 1 equiv), diethyl dichlorosilane (0.13 mL, 1 mmol, 1.1 equiv), and a stir bar under N₂ atmosphere. Freshly distilled THF (~30 mL) was then added. A clear solution was obtained. Et₃N (0.26 mL, 0.0019 mol, 2.0 equiv) was added dropwise to this solution. The reaction mixture was stirred for 7 hr, after which the solvent was evaporated, and then fresh THF (~ 60 mL) was added to create a slurry. This slurry was filtered through a medium frit funnel to obtain the crude product in the filtrate. The filtrate was concentrated to obtain white powder. Methanol (~ 60 mL) was added to the reaction flask, stirring the slurry for 2 hours. The slurry was again filtered through a medium frit funnel to obtain the product as a white powder (0.85 g, 80% yield).

¹H NMR (500 MHz, Chloroform-d) δ 7.73 (d, J = 7.2 Hz, 5H), 7.60 (d, J = 7.2 Hz, 11H), 7.47 – 7.13 (m, 28H), 1.01 (q, J = 9.7, 8.7 Hz, 6H), 0.72 (q, J = 7.7 Hz, 4H). ¹³C{¹H} NMR (126 MHz, Chloroform-d) δ 6.32, 6.92, 127.75, 127.80, 127.85, 130.32, 130.53, 130.67, 130.72, 133.88, 134.08, 134.19. ²⁹Si{¹H} NMR (99 MHz, Chloroform-d) δ -79.50, -78.98, -77.42, -17.22.

6.7.5 Synthesis of 17,17-diisopropyl-1,3,5,7,9,11,13,15-octaphenyl-2,4,6,8,10,12,14,16,18,19,20,21,22-tridecaoxa-1,3,5,7,9,11,13,15,17-nonasilapentacyclo[9.7.1.1^{3,9}.1^{5,15}.1^{7,13}]docosane

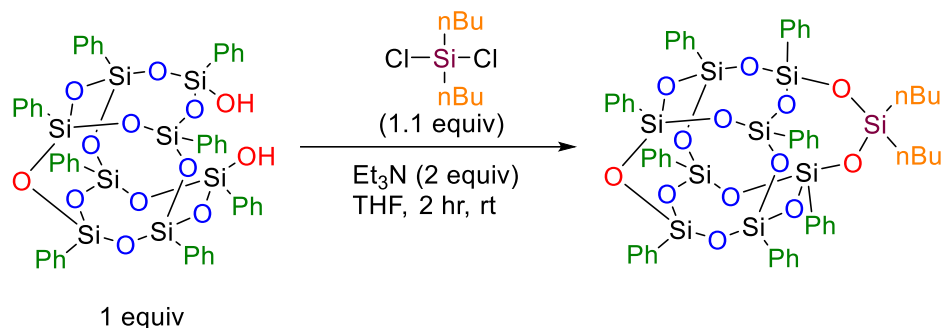


Scheme 6-7 : Synthesis of a capped SPh₈T₈ (iPr)₂

To a 100 mL round bottom flask were added SPh₈T₈(OH)₂ (1 g, 0.95 mmol, 1 equiv), diisopropyl dichlorosilane (0.19 mL, 1 mmol, 1.1 equiv), and a stir bar under N₂ atmosphere. Freshly distilled THF (~30 mL) was then added. A clear solution was obtained. Et₃N (0.26 mL, 0.0019 mol, 2.0 equiv) was added dropwise to this solution. The reaction mixture was stirred for 1 hr, after which the solvent was evaporated, and then fresh THF (~ 60 mL) was added to create a slurry. This slurry was filtered through a medium frit funnel to obtain the crude product in the filtrate. The filtrate was concentrated to obtain white powder. Methanol (~ 60 mL) was added to the reaction flask, stirring the slurry for 2 hours. The slurry was again filtered through a medium frit funnel to obtain the product as a white powder (0.81 g, 74.3% yield).

¹H NMR (500 MHz, Chloroform-d) δ 7.78 – 7.70 (m, 4H), 7.63 – 7.56 (m, 9H), 7.46 – 7.32 (m, 16H), 7.27 (m, 13H), 1.05 (m, 14H). ¹³C{¹H} NMR (126 MHz, Chloroform-d) δ 12.89, 16.77, 127.79, 127.82, 127.89, 130.32, 130.43, 130.55, 130.72, 130.76, 132.13, 133.93, 134.10, 134.23. ²⁹Si{¹H} NMR (99 MHz, Chloroform-d) δ -80.07, -79.10, -77.48, -19.94.

6.7.6 Synthesis of 17,17-dibutyl-1,3,5,7,9,11,13,15-octaphenyl-2,4,6,8,10,12,14,16,18,19,20,21,22-tridecaoxa-1,3,5,7,9,11,13,15,17-nonasilapentacyclo[9.7.1.1^{3,9}.1^{5,15}.1^{7,13}]docosane

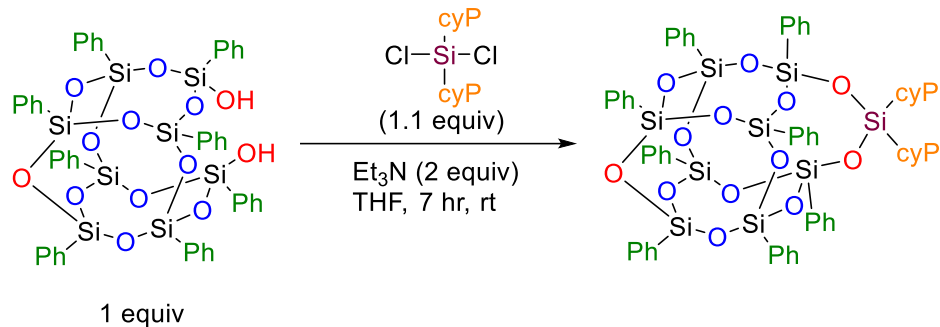


Scheme 6-8 : Synthesis of a capped SPh₈T₈ (nBu)₂

To a 100 mL round bottom flask were added SPh₈T₈(OH)₂ (1 g, 0.95 mmol, 1 equiv), dibutyl dichlorosilane (0.22 mL, 1 mmol, 1.1 equiv), and a stir bar under N₂ atmosphere. Freshly distilled THF (~30 mL) was then added. A clear solution was obtained. Et₃N (0.26 mL, 0.0019 mol, 2.0 equiv) was added dropwise to this solution. The reaction mixture was stirred for 2 hr, after which the solvent was evaporated, and then fresh THF (~ 60 mL) was added to create a slurry. This slurry was filtered through a medium frit funnel to obtain the crude product in the filtrate. The filtrate was concentrated to obtain white powder. Methanol (~ 60 mL) was added to the reaction flask, stirring the slurry for 2 hours. The slurry was again filtered through a medium frit funnel to obtain the product as a white powder (0.68 g, 61% yield).

¹H NMR (500 MHz, Chloroform-d) δ 7.77 – 7.70 (m, 4H), 7.63 – 7.57 (m, 9H), 7.46 – 7.32 (m, 12H), 7.32 – 7.19 (m, 12H), 1.47 – 1.37 (m, 4H), 1.29 (dt, J = 7.7, 7.3 Hz, 5H), 0.76 (s, 1H), 0.75 – 0.68 (m, 8H). ¹³C{¹H} NMR (126 MHz, Chloroform-d) δ 15.41, 24.86, 26.09, 127.71, 127.77, 127.84, 130.28, 130.39, 130.52, 130.66, 130.71, 132.14, 133.89, 134.10, 134.19. ²⁹Si{¹H} NMR (99 MHz, Chloroform-d) δ -79.66, -78.98, -77.44, -18.61.

6.7.7 Synthesis of 17,17-dicyclopentyl-1,3,5,7,9,11,13,15-octaphenyl-2,4,6,8,10,12,14,16,18,19,20,21,22-tridecaoxa-1,3,5,7,9,11,13,15,17-nonasilapentacyclo[9.7.1.1^{3,9}.1^{5,15}.1^{7,13}]docosane

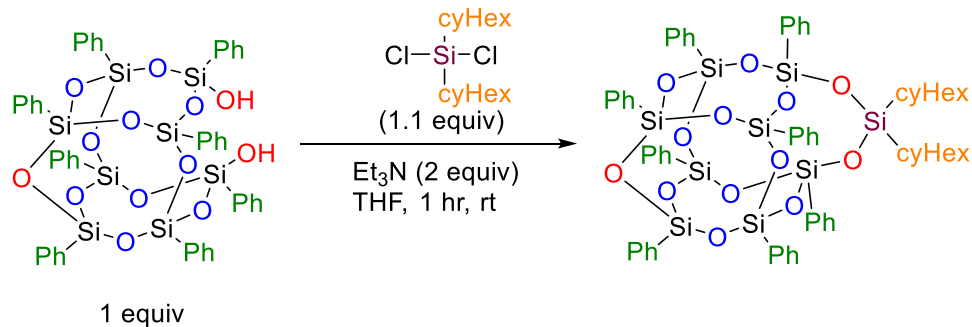


Scheme 6-9 : Synthesis of a capped SOPh₈T₈ (cyP)₂

To a 100 mL round bottom flask were added SOPh₈T₈(OH)₂ (1 g, 0.95 mmol, 1 equiv), dicyclopentyl dichlorosilane (0.13 mL, 1 mmol, 1.1 equiv), and a stir bar under N₂ atmosphere. Freshly distilled THF (~30 mL) was then added. A clear solution was obtained. Et₃N (0.26 mL, 0.0019 mol, 2.0 equiv) was added dropwise to this solution. The reaction mixture was stirred for 7 hr, after which the solvent was evaporated, and then fresh THF (~60 mL) was added to create a slurry. This slurry was filtered through a medium frit funnel to obtain the crude product in the filtrate. The filtrate was concentrated to obtain white powder. Methanol (~60 mL) was added to the reaction flask, stirring the slurry for 2 hours. The slurry was again filtered through a medium frit funnel to obtain the product as a white powder (0.66 g, 58% yield).

¹H NMR (500 MHz, Chloroform-d) δ 7.72 (d, J = 19.2 Hz, 5H), 7.66 – 7.51 (m, 9H), 7.51 – 7.31 (m, 14H), 7.31 – 6.85 (m, 14H), 1.76 (s, 4H), 1.48 (s, 11H), 1.00 (s, 2H). ¹³C{¹H} NMR (126 MHz, Chloroform-d) δ 24.92, 27.02, 27.13, 127.72, 127.74, 127.85, 130.22, 130.41, 130.49, 130.71, 132.20, 133.84, 134.05, 134.19. ²⁹Si{¹H} NMR (99 MHz, Chloroform-d) δ -80.02, -79.02, -77.43, -20.62.

6.7.8 Synthesis of 17,17-dicyclohexyl-1,3,5,7,9,11,13,15-octaphenyl-2,4,6,8,10,12,14,16,18,19,20,21,22-tridecaoxa-1,3,5,7,9,11,13,15,17-nonasilapentacyclo[9.7.1.1^{3,9}.1^{5,15}.1^{7,13}]docosane

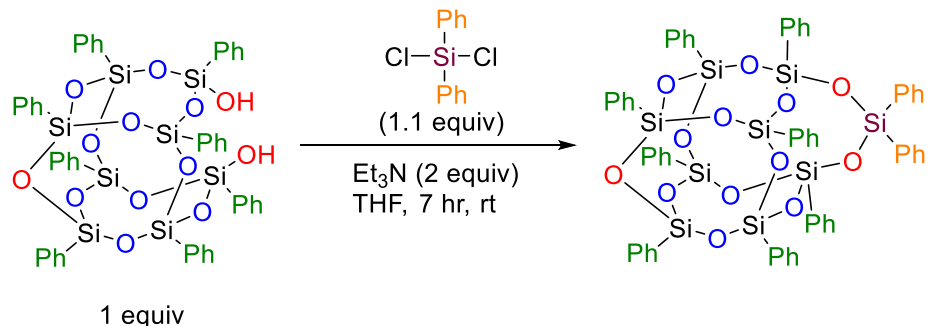


Scheme 6-10 : Synthesis of a capped SPh₈T₈ (cyhex)₂

To a 100 mL round bottom flask were added SPh₈T₈(OH)₂ (1 g, 0.95 mmol, 1 equiv), dicyclohexyl dichlorosilane (0.25 mL, 1 mmol, 1.1 equiv), and a stir bar under N₂ atmosphere. Freshly distilled THF (~30 mL) was then added. A clear solution was obtained. Et₃N (0.26 mL, 0.0019 mol, 2.0 equiv) was added dropwise to this solution. The reaction mixture was stirred for 7 hr, after which the solvent was evaporated, and then fresh THF (~60 mL) was added to create a slurry. This slurry was filtered through a medium frit funnel to obtain the crude product in the filtrate. The filtrate was concentrated to obtain white powder. Methanol (~60 mL) was added to the reaction flask, stirring the slurry for 2 hours. The slurry was again filtered through a medium frit funnel to obtain the product as a white powder (0.68 g, 59% yield).

¹H NMR (500 MHz, Chloroform-*d*) δ 7.78 – 7.69 (m, 4H), 7.59 (d, *J* = 7.7 Hz, 8H), 7.48 – 7.32 (m, 13H), 7.27 (q, *J* = 7.9 Hz, 14H), 1.79 (d, *J* = 7.8 Hz, 4H), 1.64 (d, *J* = 7.6 Hz, 6H), 1.30 (q, *J* = 12.0 Hz, 4H), 1.15 (d, *J* = 7.1 Hz, 6H), 0.85 (tt, *J* = 12.3, 3.0 Hz, 2H). ¹³C{¹H} NMR (126 MHz, Chloroform-*d*) δ 24.80, 26.51, 26.82, 27.64, 127.72, 127.75, 127.85, 130.23, 130.50, 130.71, 132.18, 133.94, 134.07, 134.19. ²⁹Si{¹H} NMR (99 MHz, Chloroform-*d*) δ -80.08, -78.96, -77.43, -24.19.

6.7.9 Synthesis of 17,17-diphenyl-1,3,5,7,9,11,13,15-octaphenyl-2,4,6,8,10,12,14,16,18,19,20,21,22-tridecaoxa-1,3,5,7,9,11,13,15,17-nonasilapentacyclo[9.7.1.1^{3,9}.1^{5,15}.1^{7,13}]docosane

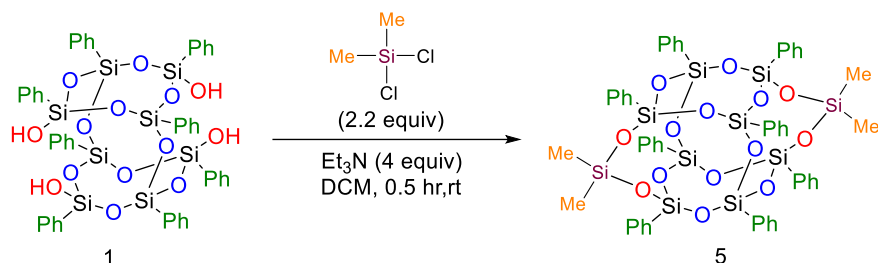


Scheme 6-11 : Synthesis of a capped SOPh₈T₈Ph₂

To a 100 mL round bottom flask were added SOPh₈T₈(OH)₂ (1 g, 0.95 mmol, 1 equiv), diphenyl dichlorosilane (0.22 mL, 1 mmol, 1.1 equiv), and a stir bar under N₂ atmosphere. Freshly distilled THF (~30 mL) was then added. A clear solution was obtained. Et₃N (0.26 mL, 0.0019 mol, 2.0 equiv) was added dropwise to this solution. The reaction mixture was stirred for 7 hr, after which the solvent was evaporated, and then fresh THF (~ 60 mL) was added to create a slurry. This slurry was filtered through a medium frit funnel to obtain the crude product in the filtrate. The filtrate was concentrated to obtain white powder. Methanol (~ 60 mL) was added to the reaction flask, stirring the slurry for 2 hours. The slurry was again filtered through a medium frit funnel to obtain the product as a white powder (0.75 g, 65% yield).

¹H NMR (500 MHz, Chloroform-*d*) δ 7.95 – 7.63 (m, 7H), 7.57 (d, *J* = 7.3 Hz, 4H), 7.47 (d, *J* = 7.3 Hz, 6H), 7.39 (m, 13H), 7.31 – 6.69 (m, 20H). ¹³C{¹H} NMR (126 MHz, Chloroform-*d*) δ 127.63, 127.80, 127.82, 127.85, 130.08, 130.28, 130.31, 130.45, 130.52, 130.75, 131.46, 134.02, 134.13, 134.18, 134.24. ²⁹Si{¹H} NMR (99 MHz, Chloroform-*d*) δ -78.81, -78.71, -77.35, -45.95.

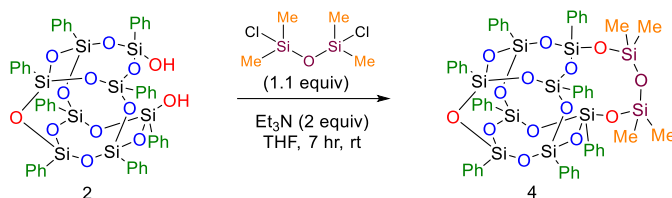
6.7.10 Synthesis of 9,9,19,19-tetramethyl-1,3,5,7,11,13,15,17-octaphenyl 2,4,6,8,10,12,14,16,18,20,21,22,23,24-tetradecaoxa-1,3,5,7,9,11,13,15,17,19-decasilapentacyclo[11.7.1.1^{3,11}.1^{5,17}.1^{7,15}] tetracosane



Scheme 6-12 : Synthesis of symmetrically capped DDSQ Me₄

To a 100 mL round bottom flask were added DDPh₈T₈(OH)₄ (2 g, 0.0018 mol, 1 equiv), dichloro dimethyl silane (0.50 mL, 0.0041 mol, 2.2 equiv), and a stir bar under N₂ atmosphere. Freshly distilled DCM (~30 mL) was then added. A white-colored solution was formed. Et₃N (1.05 mL, 0.0074 mol, 4 equiv) was added dropwise to this solution. Upon the addition of triethylamine, the solution turned colorless. The reaction mixture was stirred for 30 min, after which the solvent was evaporated, and THF (~60 mL) was added to create a slurry. This slurry was filtered through a medium frit funnel to obtain the crude product in the filtrate. The filtrate was concentrated to obtain white powder. This powder was washed with methanol (~60 mL) for 30 min. The slurry was again filtered through a medium frit funnel to obtain the product as a white powder (2.12 g, 96% yield). ¹H NMR (500 MHz, Chloroform-d) δ 7.54 (d, J = 6.9 Hz, 8H), 7.40 (dd, J = 23.5, 7.2 Hz, 13H), 7.33 (t, J = 7.5 Hz, 5H), 7.24 (d, J = 7.5 Hz, 6H), 7.18 (t, J = 7.5 Hz, 9H), 0.30 (s, 12H). ¹³C{¹H} NMR (126 MHz, Chloroform-d) δ 134.04, 133.92, 132.12, 131.07, 127.77, 127.62, 0.53. ²⁹Si{¹H} NMR (99 MHz, Chloroform-d) δ -16.55, -78.63, -79.61.

6.7.11 Synthesis of 17,17,19,19-tetramethyl-1,3,5,7,9,11,13,15-octaphenyl-2,4,6,8,10,12,14,16,18,20,21,22,23,24-tetradeca-1,3,5,7,9,11,13,15,17,19-decasilapentacyclo[9.9.1.1^{3,9}.1^{5,15}.1^{7,13}]tetracosane



Scheme 6-13 : Synthesis of SOPh₈T₈Me₄

To a 100 mL round bottom flask were added SOPh₈T₈(OH)₂ (2 g, 0.0019 mol, 1 equiv), 1,3-dichloro-1,1,3,3-tetramethyldisiloxane (0.41 mL, 0.002 mol, 1.1 equiv), and a stir bar under N₂ atmosphere. Freshly distilled THF (~30 mL) was then added. A clear solution was obtained. Et₃N (1.05 mL, 0.0074 mol, 2.0 equiv) was added dropwise to this solution. The reaction mixture was stirred for 7 hr, after which the solvent was evaporated, and then fresh THF (~ 60 mL) was added to create a slurry. This slurry was filtered through a medium frit funnel to obtain the crude product in the filtrate. The filtrate was concentrated to obtain white powder. Methanol (~ 60 mL) was added to the reaction flask, stirring the slurry for 2 hours. The slurry was again filtered through a medium frit funnel to obtain the product as a white powder (1.75 g, 78% yield).

¹H NMR (500 MHz, Chloroform-d) δ 7.71 (d, J = 7.0 Hz, 4H), 7.60 (d, J = 7.1 Hz, 4H), 7.49 (d, J = 7.2 Hz, 8H), 7.46 – 7.41 (m, 3H), 7.35 (t, J = 7.8 Hz, 11H), 7.27 (s, 2H), 7.22 (q, J = 7.5 Hz, 10H), 0.23 (s, 12H). ¹³C{¹H} NMR (126 MHz, Chloroform-d) δ 0.75, 127.65, 127.78, 127.89, 130.20, 130.40, 130.71, 130.73, 133.83, 134.04, 134.12. ²⁹Si{¹H} NMR (99 MHz, Chloroform-d) δ -79.50, -78.88, -77.13, -18.64.

REFERENCES

- (1) Wang, L.; Ishida, Y.; Maeda, R.; Tokita, M.; Hayakawa, T. Alkylated Cage Silsesquioxanes: A Comprehensive Study of Thermal Properties and Self-Assembled Structure. *RSC Adv.* 2014, 4 (66), 34981–34986. <https://doi.org/10.1039/C4RA04987J>.
- (2) Blanco, I.; Abate, L.; Bottino, F. A. Mono Substituted Octaphenyl POSSs: The Effects of Substituents on Thermal Properties and Solubility. *Thermochimica Acta* 2017, 655, 117–123. <https://doi.org/10.1016/j.tca.2017.06.019>.
- (3) Wang, M.; Chi, H.; K.S., J.; Wang, F. Progress in the Synthesis of Bifunctionalized Polyhedral Oligomeric Silsesquioxane. *Polymers* 2019, 11 (12), 2098. <https://doi.org/10.3390/polym11122098>.
- (4) Schoen, B. W.; Holmes, D.; Lee, A. Identification and Quantification of *Cis* and *Trans* Isomers in Aminophenyl Double-Decker Silsesquioxanes Using ^1H - ^{29}Si GHMBC NMR: Quantification of *Cis* and *Trans* Isomers in Double-Decker Silsesquioxanes. *Magn. Reson. Chem.* 2013, 51 (8), 490–496. <https://doi.org/10.1002/mrc.3962>.
- (5) Schoen, B. W.; Lira, C. T.; Lee, A. Separation and Solubility of *Cis* and *Trans* Isomers in Nanostructured Double-Decker Silsesquioxanes. *J. Chem. Eng. Data* 2014, 59 (5), 1483–1493. <https://doi.org/10.1021/je4010245>.
- (6) Moore, L. M. J.; Zavala, J. J.; Lamb, J. T.; Reams, J. T.; Yandek, G. R.; Guenther, A. J.; Haddad, T. S.; Ghiassi, K. B. Bis-Phenylethynyl Polyhedral Oligomeric Silsesquioxanes: New High-Temperature, Processable Thermosetting Materials. *RSC Adv.* 2018, 8 (48), 27400–27405. <https://doi.org/10.1039/C8RA05954C>.
- (7) Seurer, B.; Vij, V.; Haddad, T.; Mabry, J. M.; Lee, A. Thermal Transitions and Reaction Kinetics of Polyhedral Silsesquioxane Containing Phenylethynylphthalimides. *Macromolecules* 2010, 43 (22), 9337–9347. <https://doi.org/10.1021/ma101640q>.
- (8) Wei, K.; Wang, L.; Zheng, S. Organic–Inorganic Polyurethanes with 3,13-Dihydroxypropyloctaphenyl Double-Decker Silsesquioxane Chain Extender. *Polym. Chem.* 2013, 4 (5), 1491–1501. <https://doi.org/10.1039/C2PY20930F>.
- (9) Hoque, Md. A.; Kakihana, Y.; Shinke, S.; Kawakami, Y. Polysiloxanes with Periodically Distributed Isomeric Double-Decker Silsesquioxane in the Main Chain. *Macromolecules* 2009, 42 (9), 3309–3315. <https://doi.org/10.1021/ma900124x>.
- (10) Tanaka, T.; Hasegawa, Y.; Kawamori, T.; Kunthom, R.; Takeda, N.; Unno, M. Synthesis of Double-Decker Silsesquioxanes from Substituted Difluorosilane. *Organometallics* 2019, 38 (4), 743–747. <https://doi.org/10.1021/acs.organomet.8b00896>.
- (11) Mituła, K.; Dudziec, B.; Marciniak, B. Synthesis of Dialkenyl-Substituted Double-Decker Silsesquioxanes as Precursors for Linear Copolymeric Systems. *J Inorg Organomet Polym* 2018, 28 (2), 500–507. <https://doi.org/10.1007/s10904-017-0746-y>.

- (12) Walczak, M.; Januszewski, R.; Majchrzak, M.; Kubicki, M.; Dudziec, B.; Marciniec, B. Unusual Cis and Trans Architecture of Dihydrofunctional Double-Decker Shaped Silsesquioxane and Synthesis of Its Ethyl Bridged π -Conjugated Arene Derivatives. *New J. Chem.* 2017, 41 (9), 3290–3296. <https://doi.org/10.1039/C7NJ00255F>.
- (13) Vogelsang, D. F.; Dannatt, J. E.; Schoen, B. W.; Maleczka, R. E.; Lee, A. Phase Behavior of Cis–Trans Mixtures of Double-Decker Shaped Silsesquioxanes for Processability Enhancement. *ACS Appl. Nano Mater.* 2019, 2 (3), 1223–1231. <https://doi.org/10.1021/acsanm.8b02114>.
- (14) Vogelsang, D. F.; Maleczka, R. E.; Lee, A. Phase Behavior of Selected Condensed Double-Decker Shaped Silsesquioxane Compounds. *Silicon* 2022, 14 (13), 7555–7565. <https://doi.org/10.1007/s12633-021-01470-0>.
- (15) Vogelsang, D. F.; Maleczka, R. E.; Lee, A. Predictive Liquid Chromatography Separation for Mixtures of Functionalized Double-Decker Shaped Silsesquioxanes Based on HPLC Chromatograms. *Ind. Eng. Chem. Res.* 2019, 58 (1), 403–410. <https://doi.org/10.1021/acs.iecr.8b05490>.
- (16) Vogelsang, D. F.; Dannatt, J. E.; Maleczka, R. E.; Lee, A. Separation of Asymmetrically Capped Double-Decker Silsesquioxanes Mixtures. *Polyhedron* 2018, 155, 189–193. <https://doi.org/10.1016/j.poly.2018.08.016>.
- (17) Vogelsang, D. F.; Maleczka, R. E.; Lee, A. HPLC Characterization of Cis and Trans Mixtures of Double-Decker Shaped Silsesquioxanes. *Silicon* 2019, 11 (1), 5–13. <https://doi.org/10.1007/s12633-018-0045-4>.
- (18) Barry, B.-D.; Dannatt, J. E.; King, A. K.; Lee, A.; Maleczka, R. E. A General Diversity Oriented Synthesis of Asymmetric Double-Decker Shaped Silsesquioxanes. *Chem. Commun.* 2019, 55 (59), 8623–8626. <https://doi.org/10.1039/C9CC03972D>.
- (19) Naoki, O.; Yasunobu, E.; Nobuhiro, T.; Masafumi, U. Janus-Cube Octasilsesquioxane: Facile Synthesis and Structure Elucidation. *Angew. Chem. Int. Ed.* 2016, No. 55, 9336–9339. <https://doi.org/10.1002/anie.201602413>.
- (20) Vogelsang, D. F.; Dannatt, J. E.; Maleczka, R. E.; Lee, A. Separation of Asymmetrically Capped Double-Decker Silsesquioxanes Mixtures. *Polyhedron* 2018, 155, 189–193. <https://doi.org/10.1016/j.poly.2018.08.016>.
- (21) Sugiyama, T.; Shiba, H.; Yoshikawa, M.; Wada, H.; Shimojima, A.; Kuroda, K. Synthesis of Polycyclic and Cage Siloxanes by Hydrolysis and Intramolecular Condensation of Alkoxysilylated Cyclosiloxanes. *Chem. Eur. J.* 2019, 25 (11), 2764–2772. <https://doi.org/10.1002/chem.201805942>.
- (22) Asuncion, M. Z.; Ronchi, M.; Abu-Seir, H.; Laine, R. M. Synthesis, Functionalization and Properties of Incompletely Condensed “Half Cube” Silsesquioxanes as a Potential Route to Nanoscale Janus Particles. *Comptes Rendus Chimie* 2010, 13 (1–2), 270–281. <https://doi.org/10.1016/j.crci.2009.10.007>.

- (23) Uchida, T.; Egawa, Y.; Adachi, T.; Oguri, N.; Kobayashi, M.; Kudo, T.; Takeda, N.; Unno, M.; Tanaka, R. Synthesis, Structures, and Thermal Properties of Symmetric and Janus “Lantern Cage” Siloxanes. *Chem. Eur. J.* 2019, 25 (7), 1683–1686. <https://doi.org/10.1002/chem.201805200>.

APPENDIX

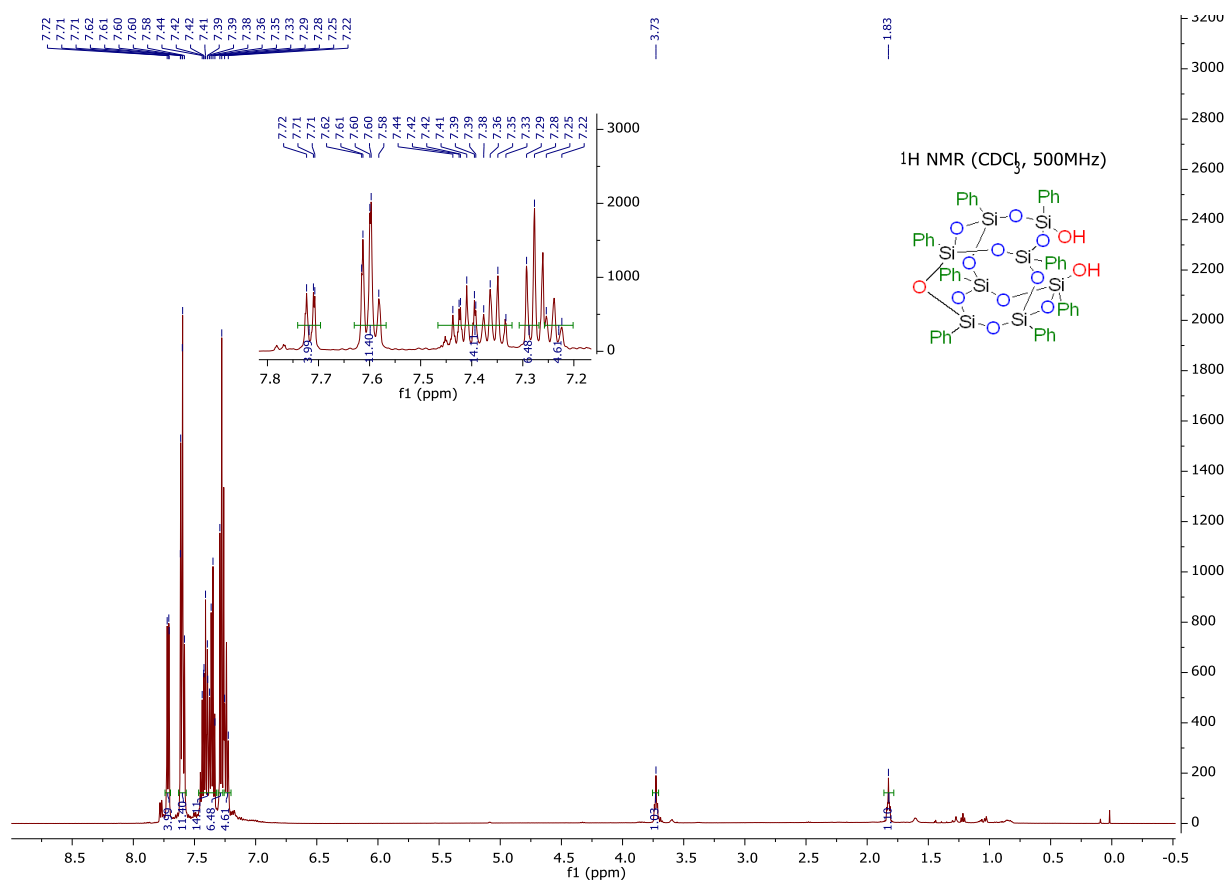


Figure 6-13 : ¹H-NMR (CDCl₃, 500 MHz)

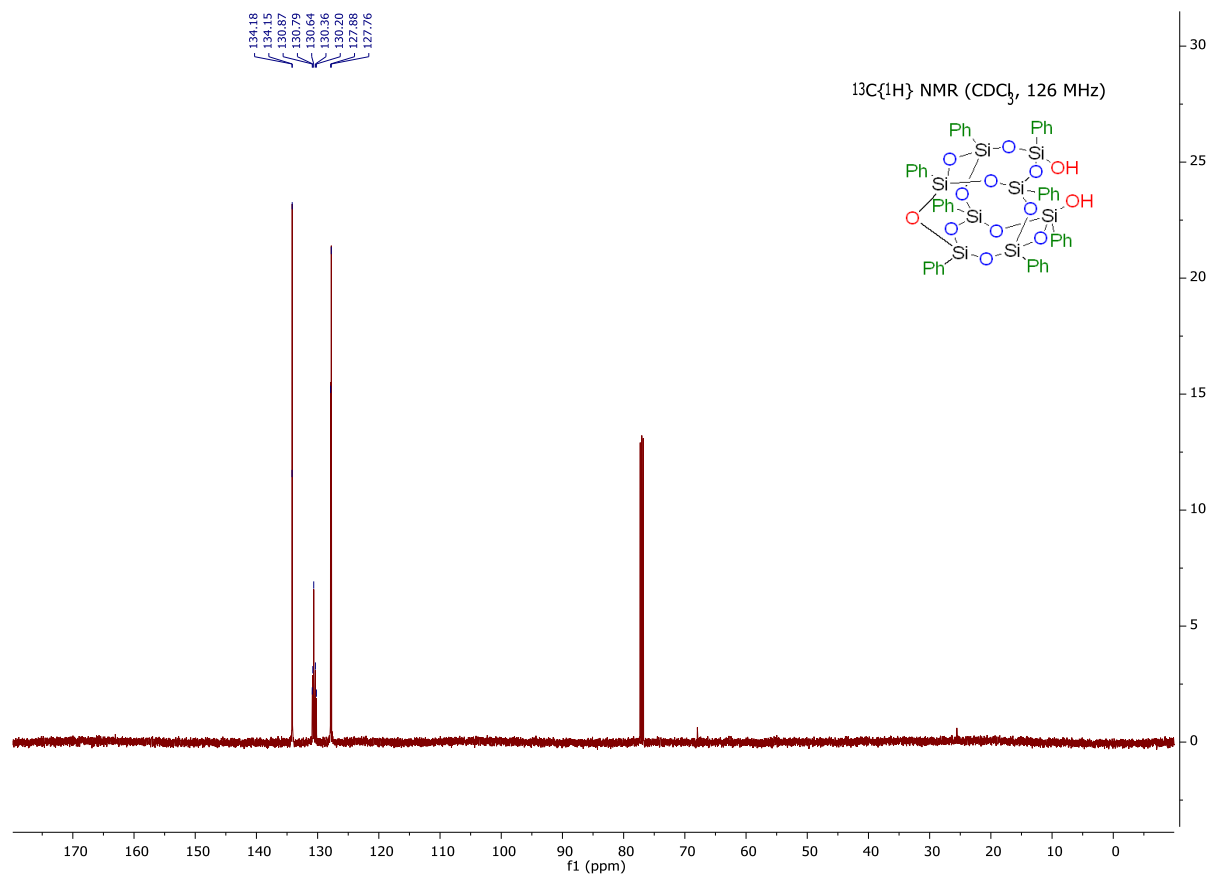


Figure 6-14 : ^{13}C -NMR (CDCl₃, 126 MHz)

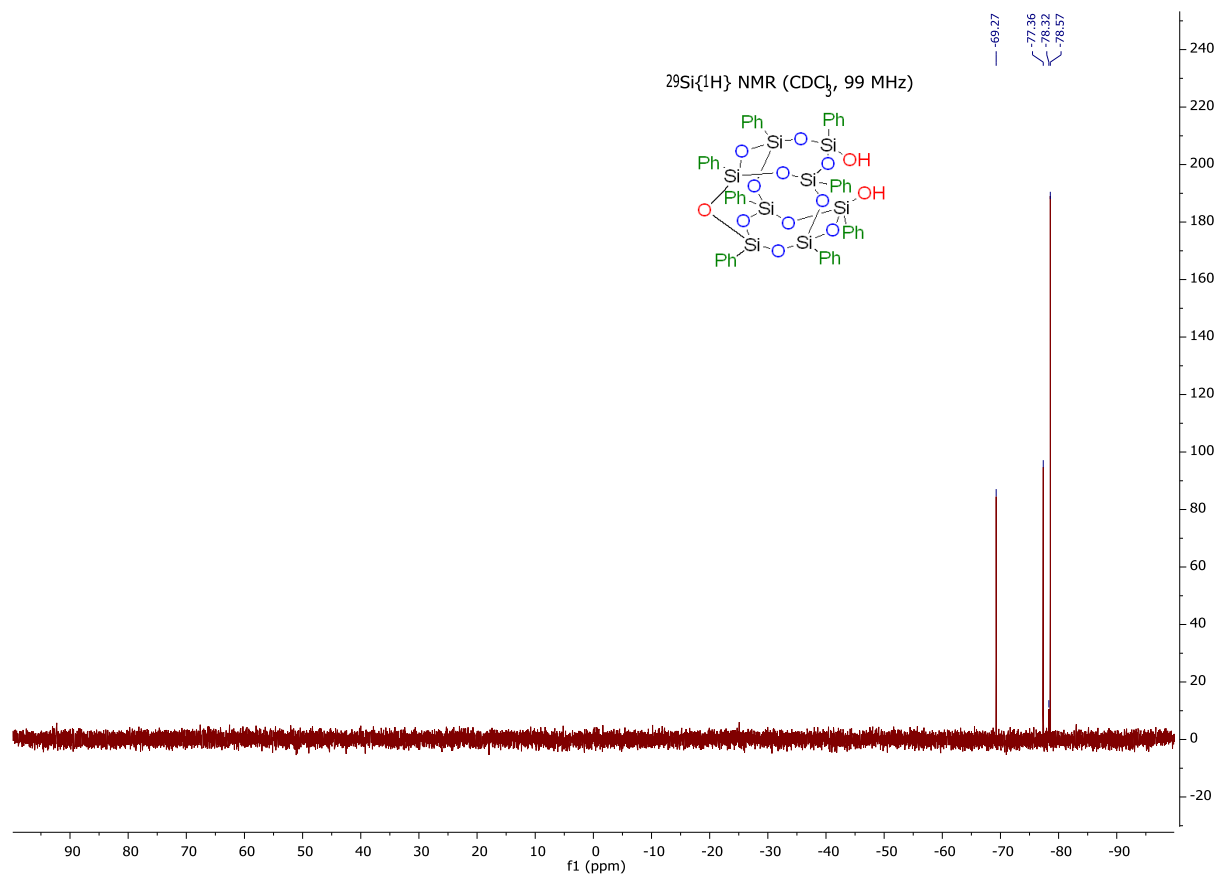


Figure 6-15 : $^{29}\text{Si}\{^1\text{H}\}$ -NMR (CDCl_3 , 99 MHz)

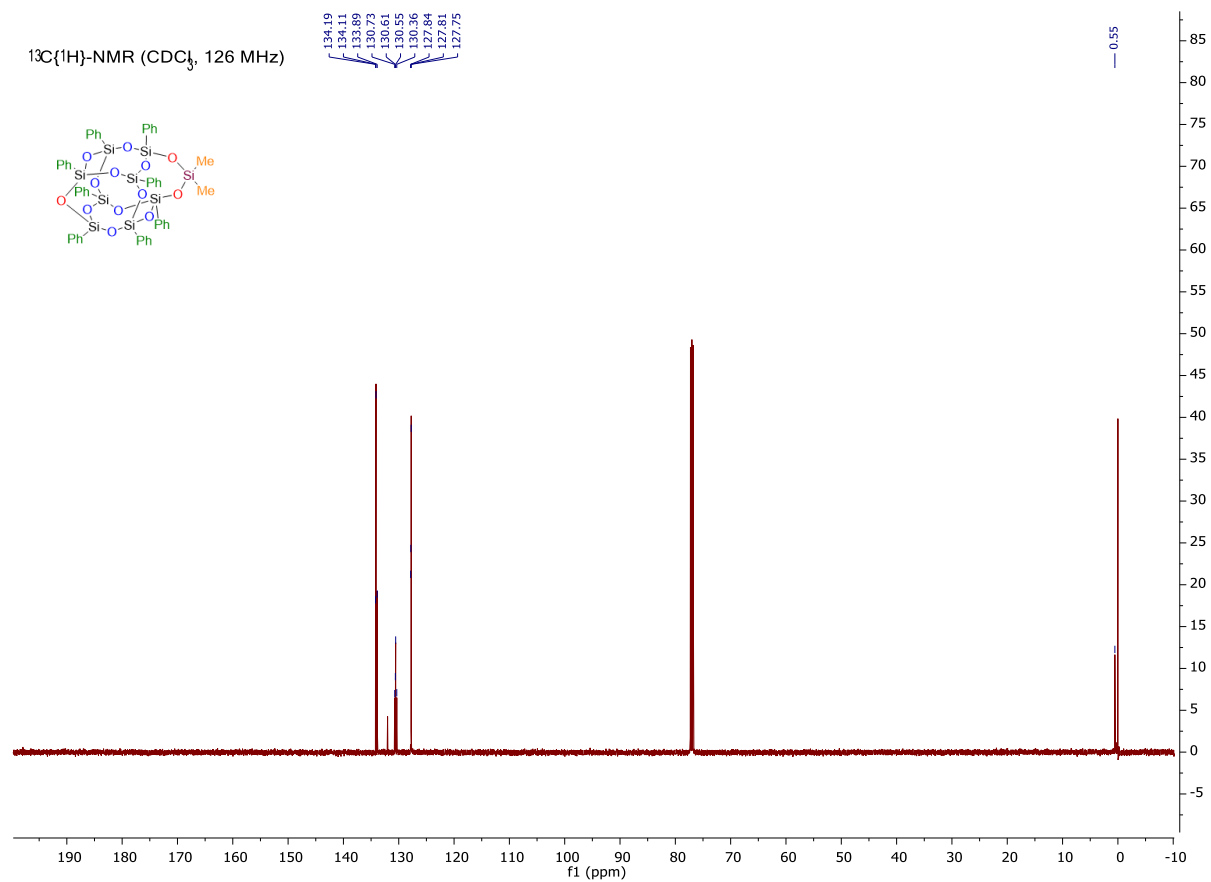


Figure 6-17 : $^{13}\text{C}\{^1\text{H}\}$ -NMR (CDCl_3 , 126 MHz)

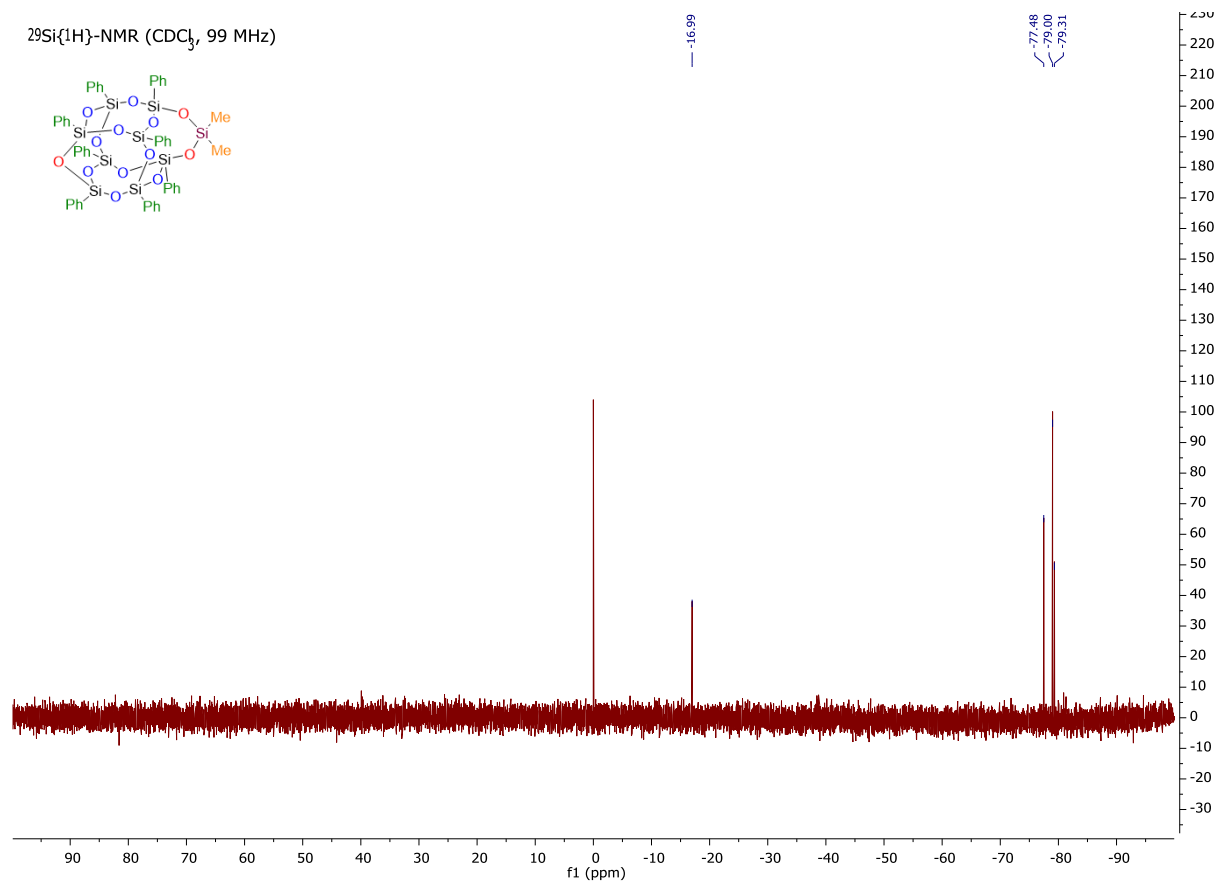


Figure 6-18 : $^{29}\text{Si}\{^1\text{H}\}$ -NMR (CDCl_3 , 99 MHz)

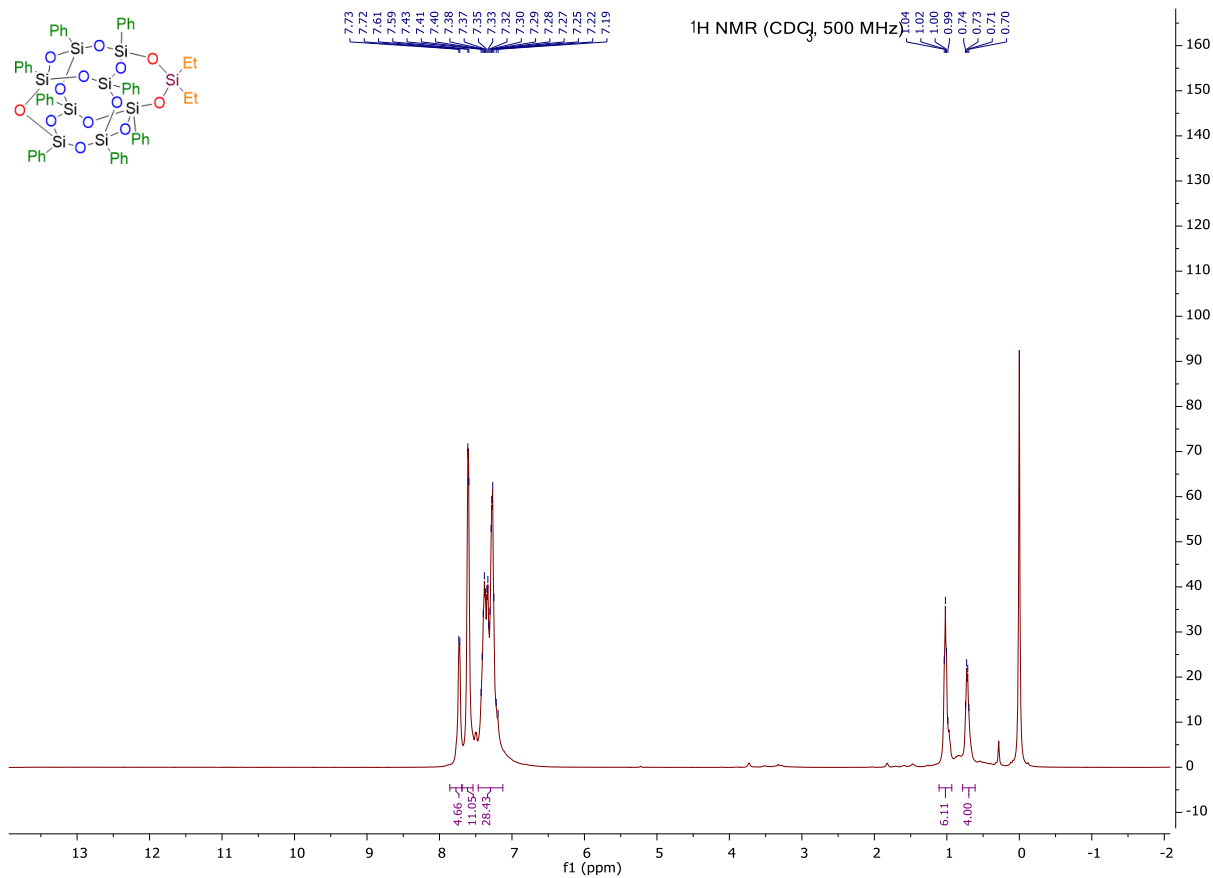


Figure 6-19 : ¹H-NMR (CDCl₃, 500 MHz)

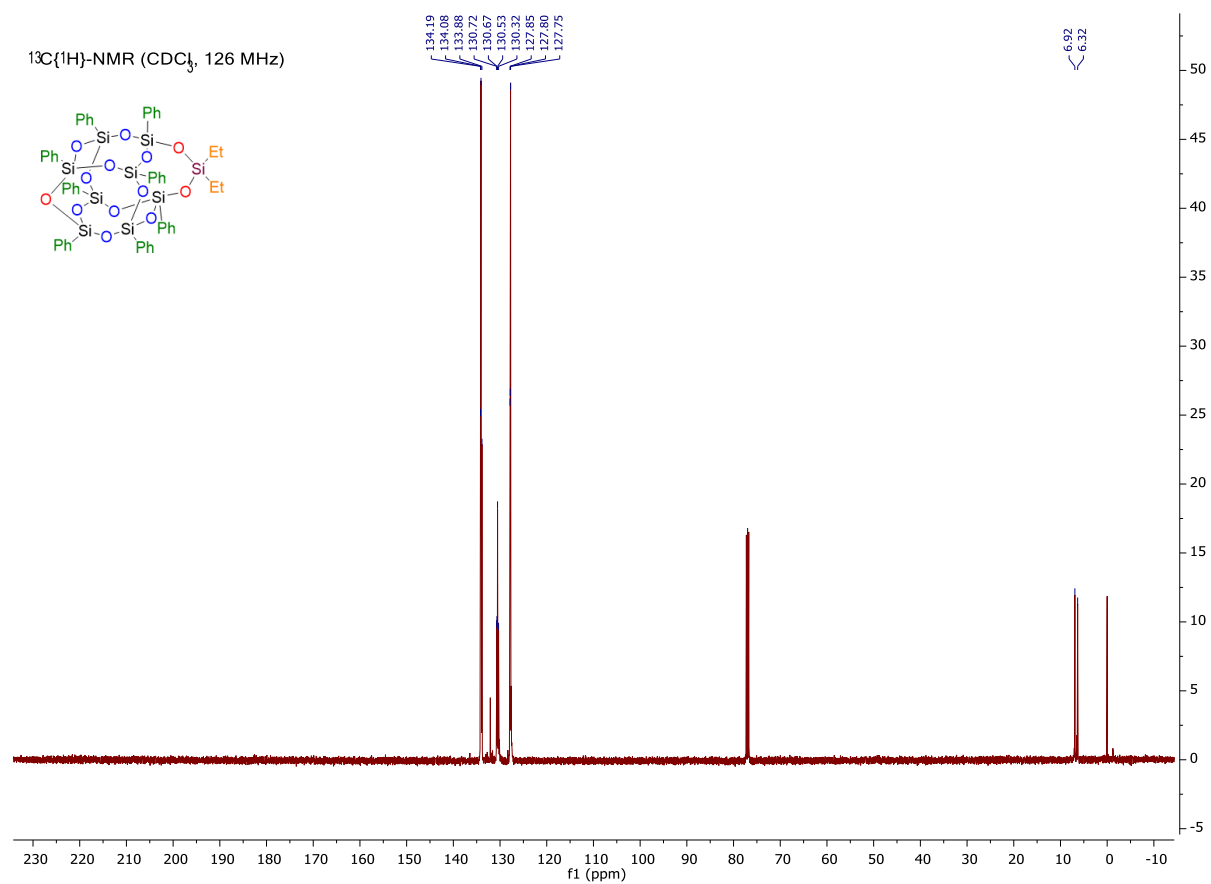


Figure 6-20 : ^{13}C -NMR (CDCl_3 , 126 MHz)

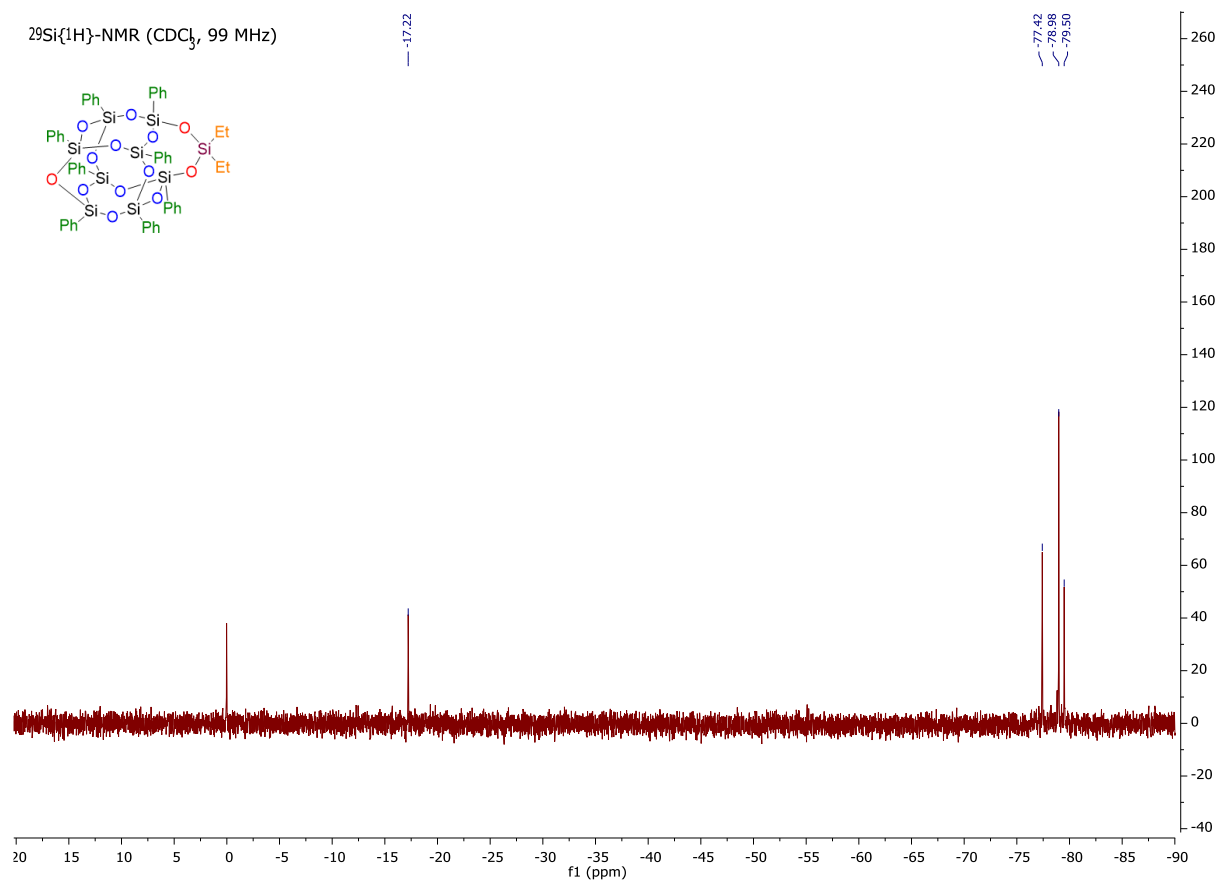


Figure 6-21 : $^{29}\text{Si}\{^1\text{H}\}$ -NMR (CDCl_3 , 99 MHz)

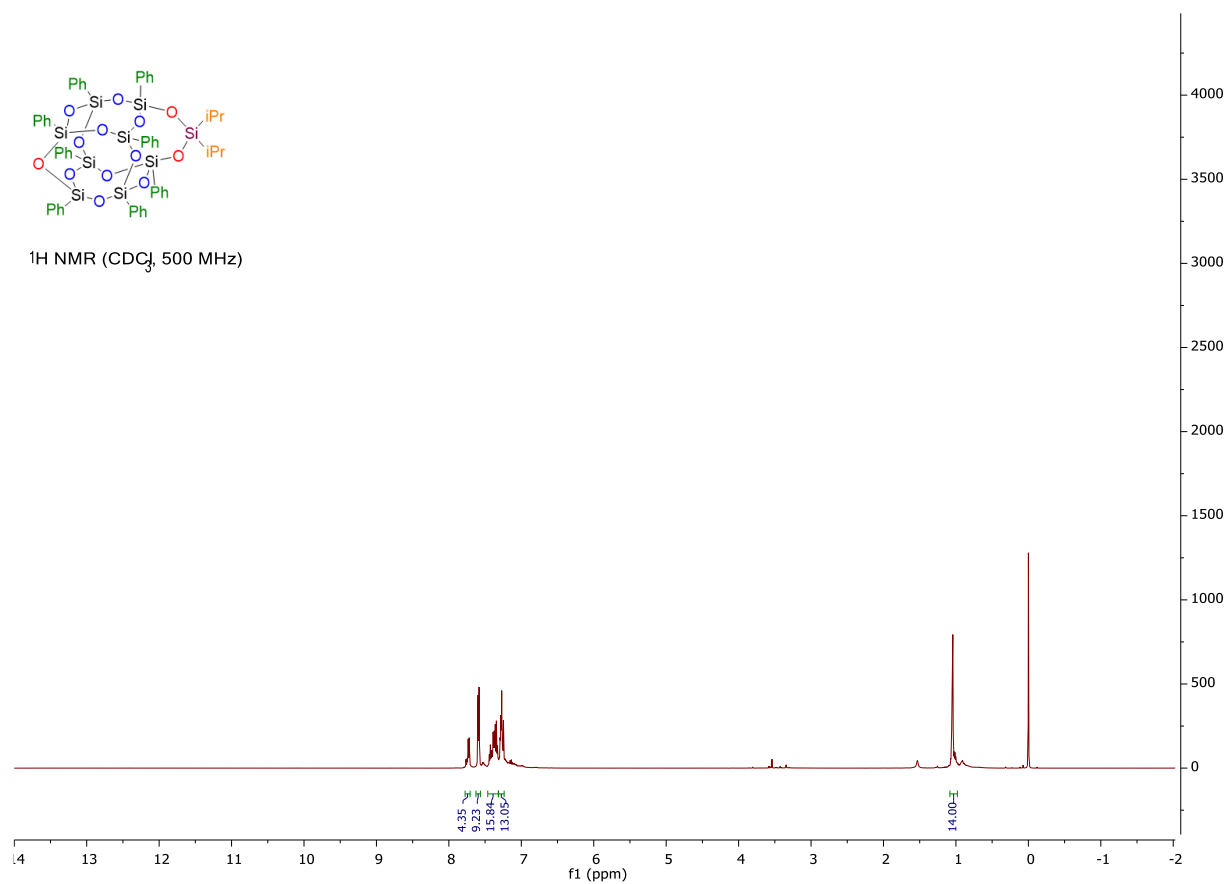


Figure 6-22 : ^1H -NMR (CDCl_3 , 500 MHz)

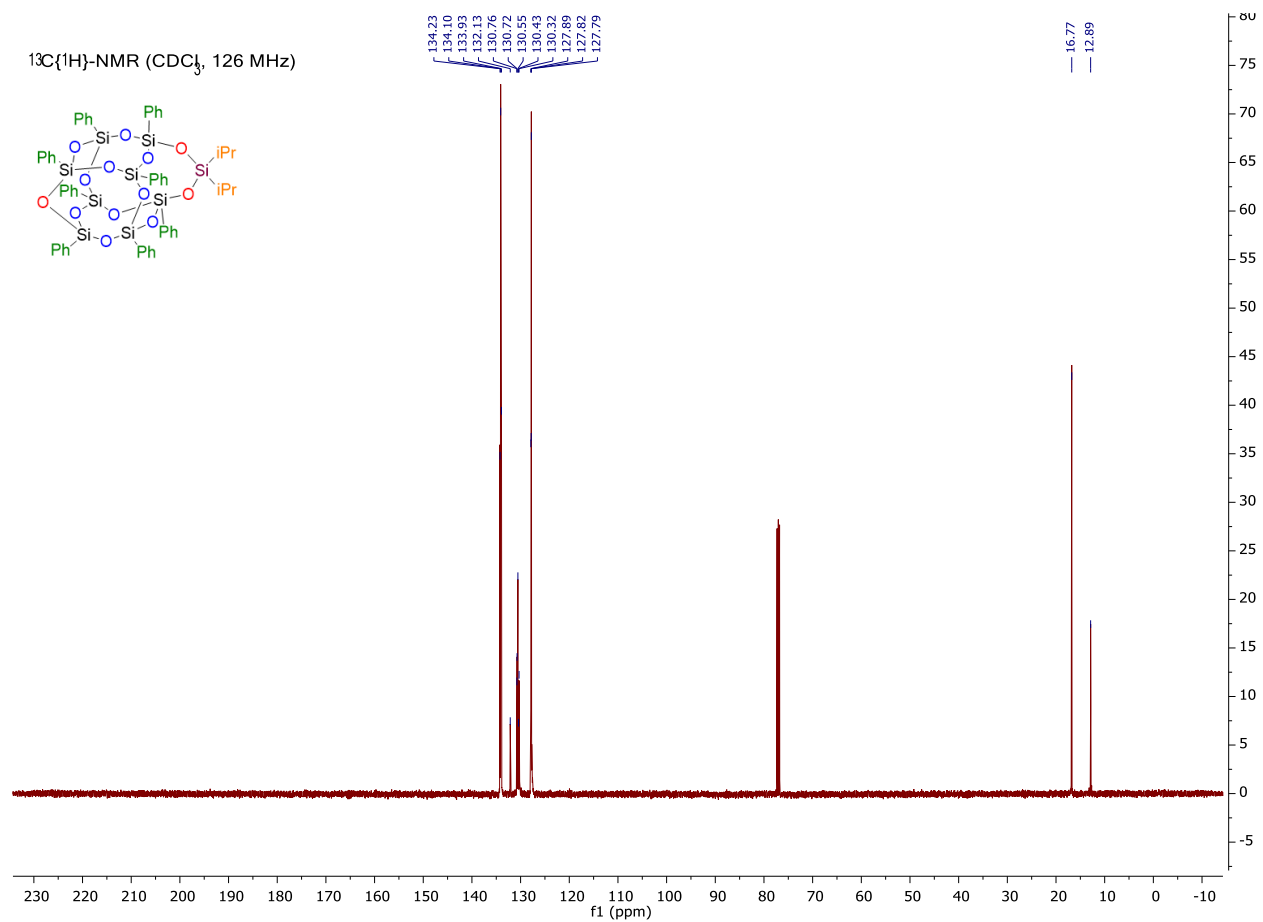


Figure 6-23 : ^{13}C -NMR (CDCl_3 , 126 MHz)

$^{29}\text{Si}\{^1\text{H}\}$ -NMR (CDCl_3 , 99 MHz)

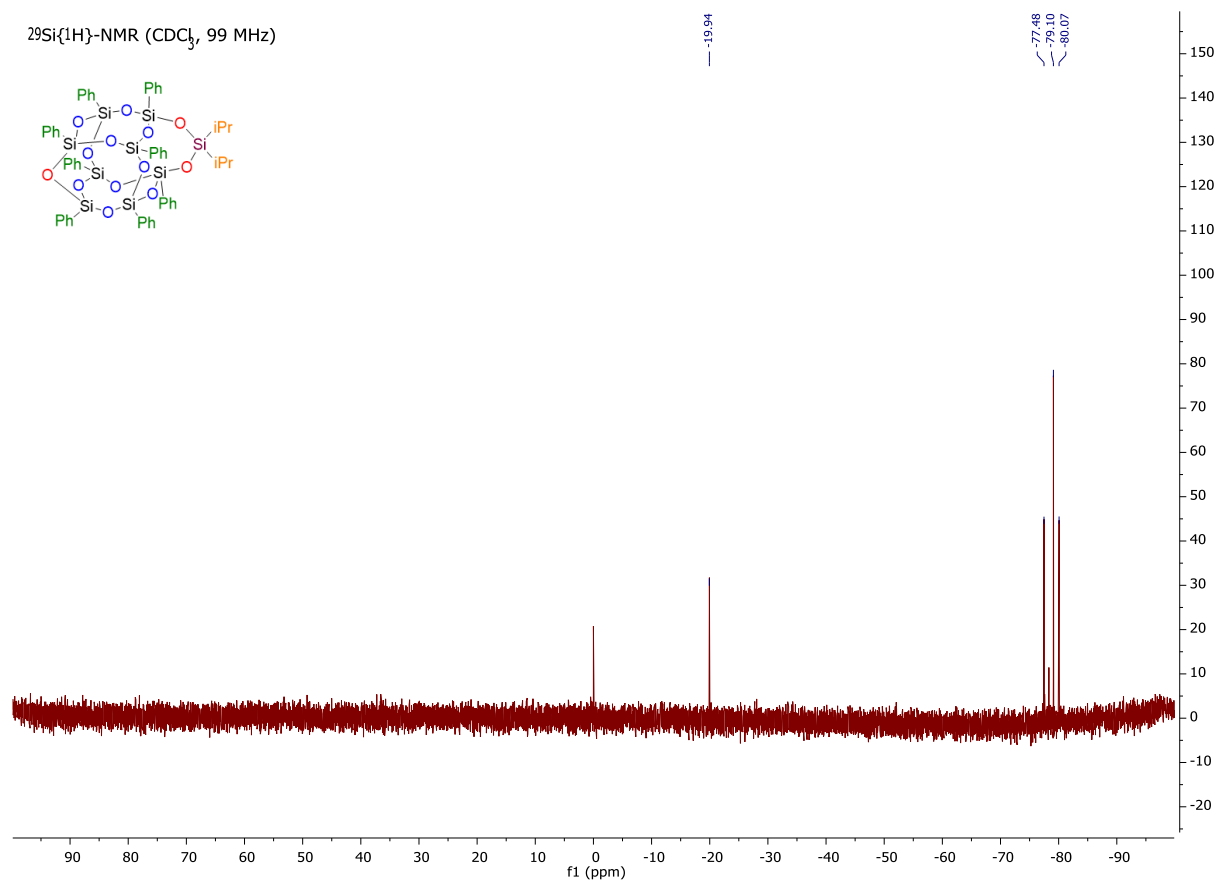


Figure 6-24 : $^{29}\text{Si}\{^1\text{H}\}$ -NMR (CDCl_3 , 99 MHz)

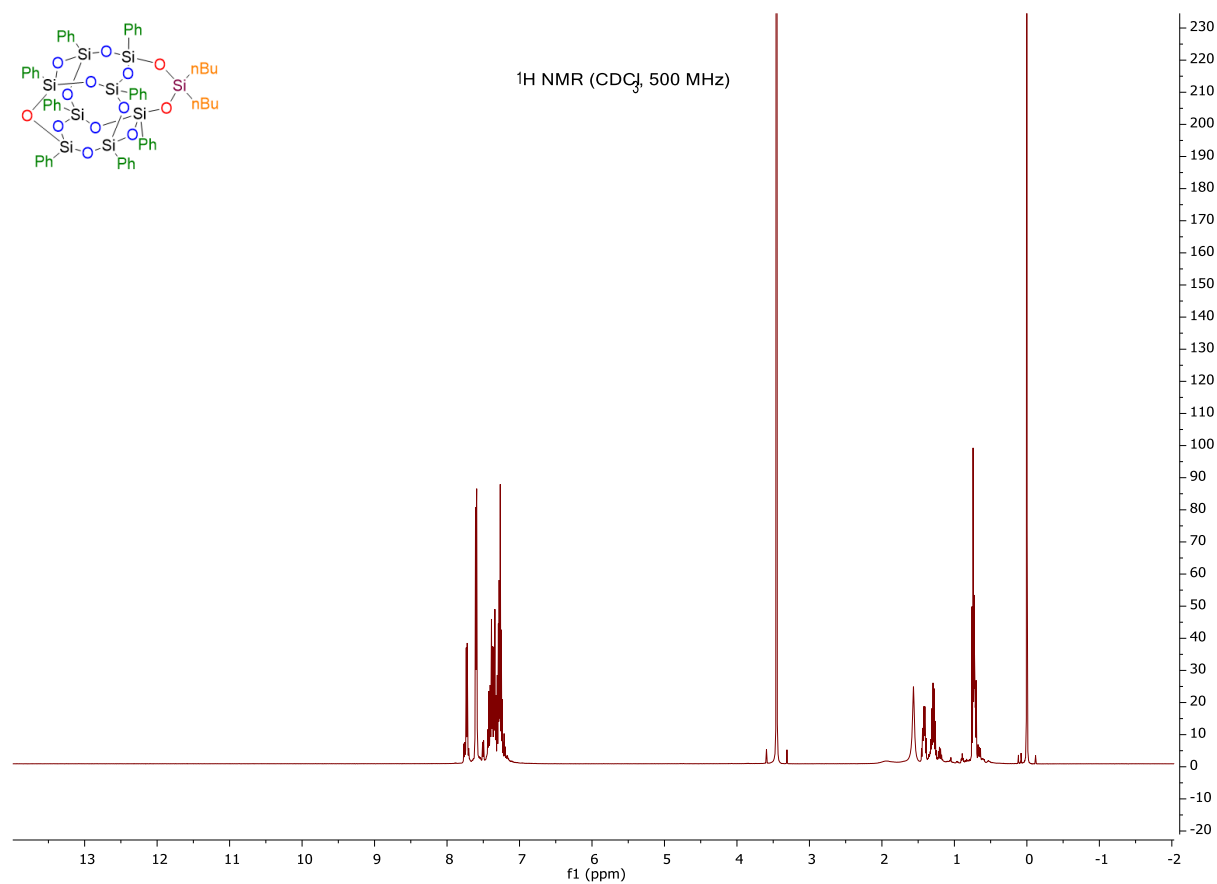


Figure 6-25 : ^1H -NMR (CDCl_3 , 500 MHz)

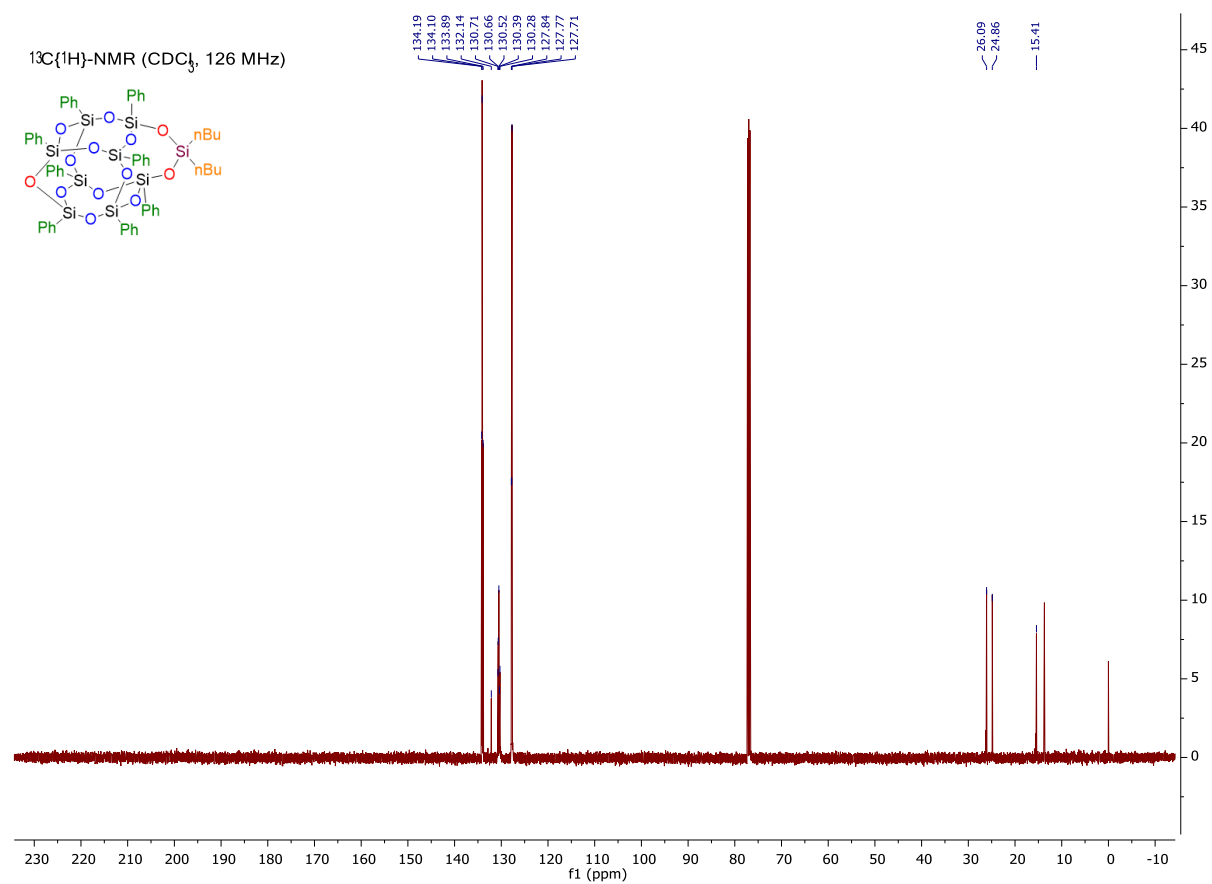


Figure 6-26 : ^{13}C -NMR (CDCl_3 , 126 MHz)

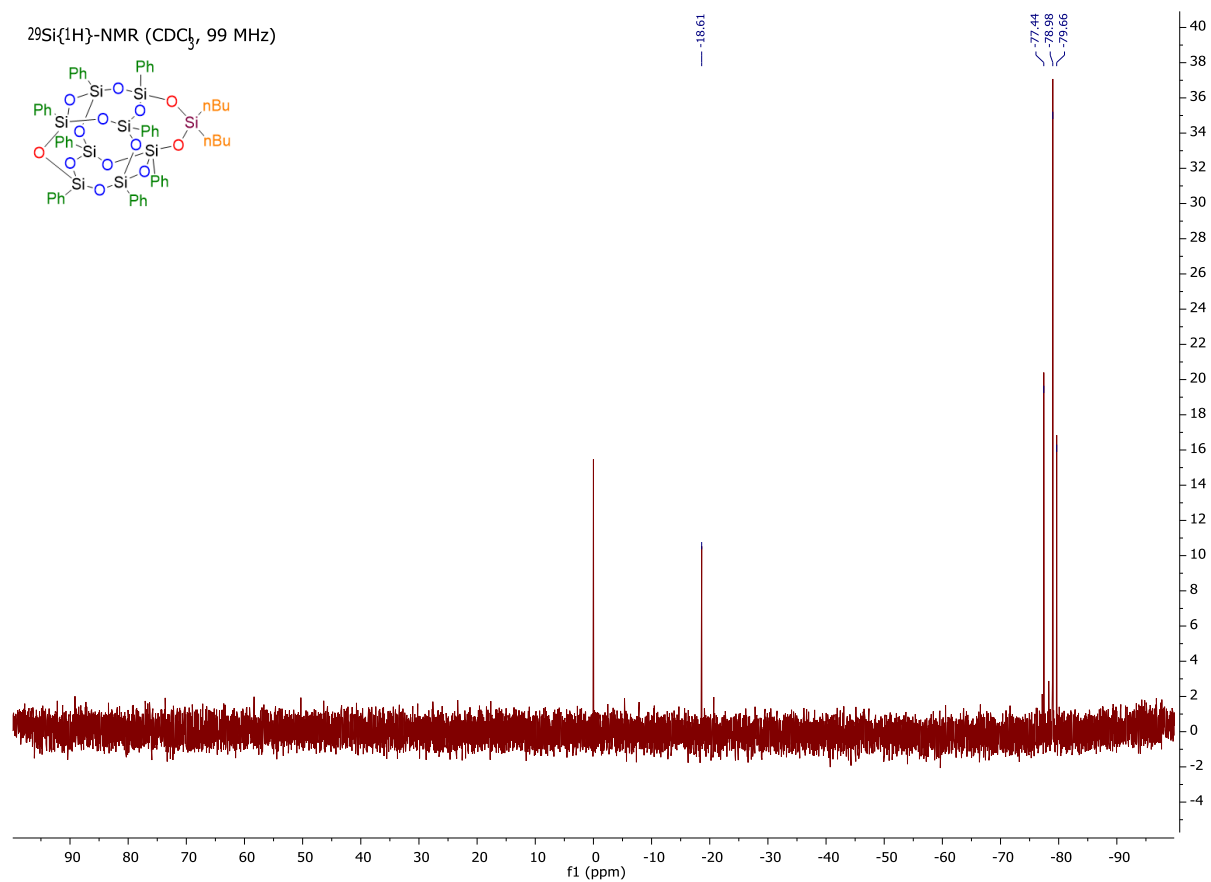


Figure 6-27 : $^{29}\text{Si}\{^1\text{H}\}$ -NMR (CDCl_3 , 99 MHz)

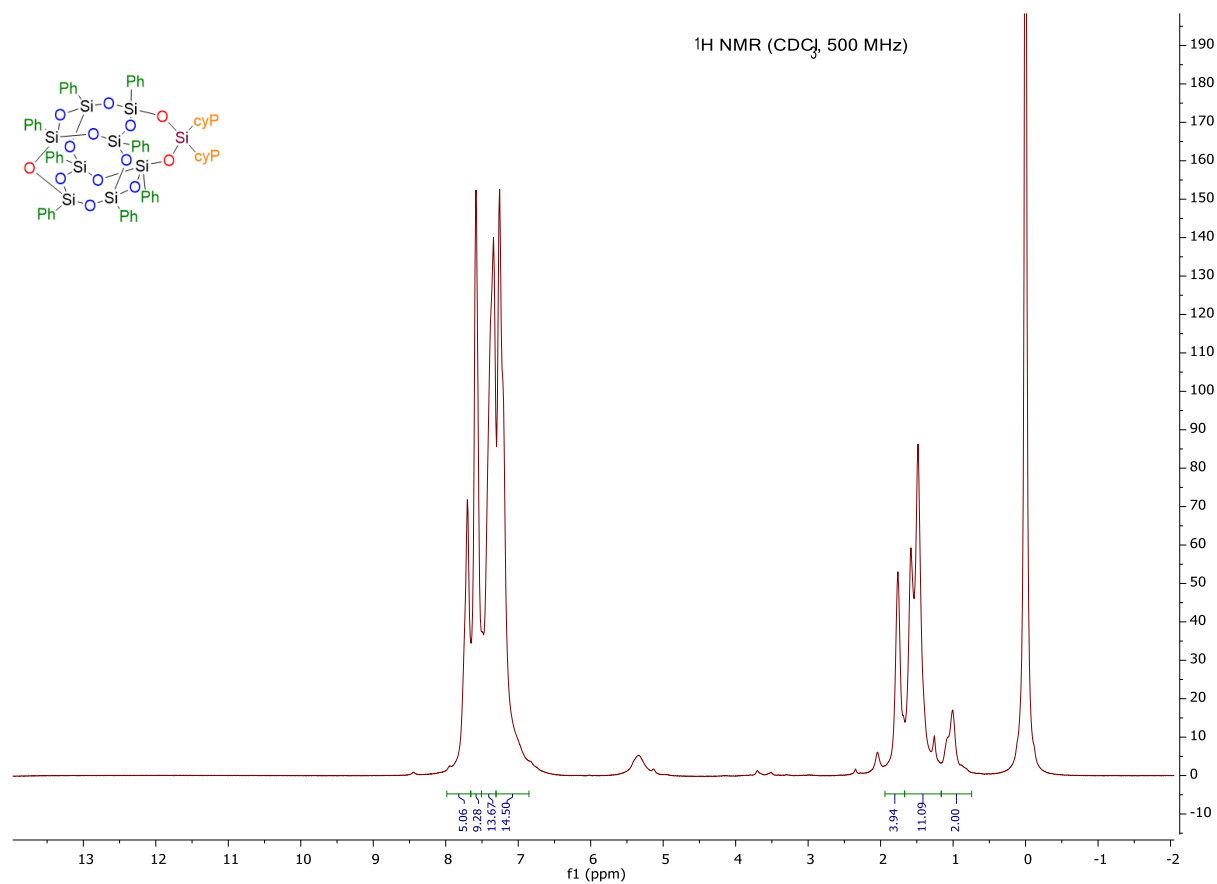


Figure 6-28 : ¹H-NMR (CDCl₃, 500 MHz)

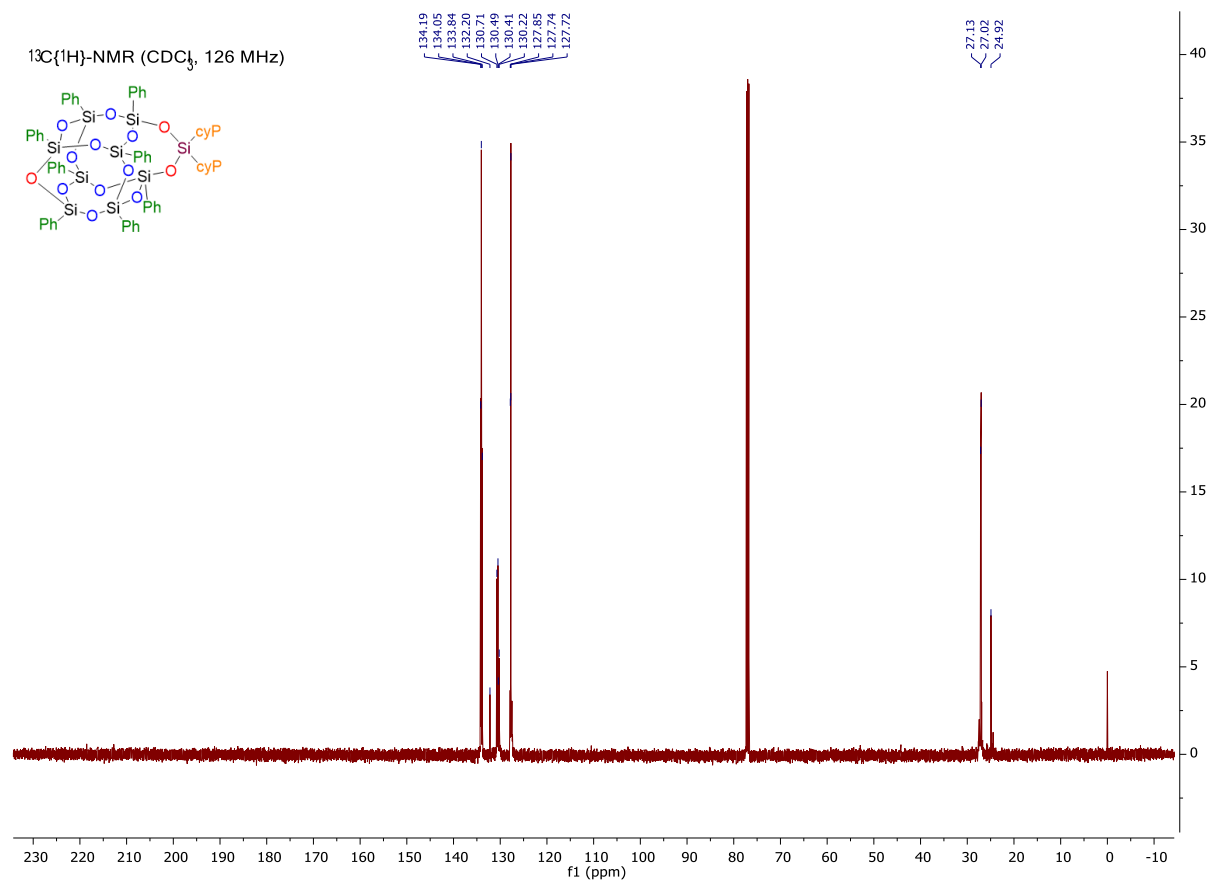


Figure 6-29 : ^{13}C -NMR (CDCl_3 , 126 MHz)

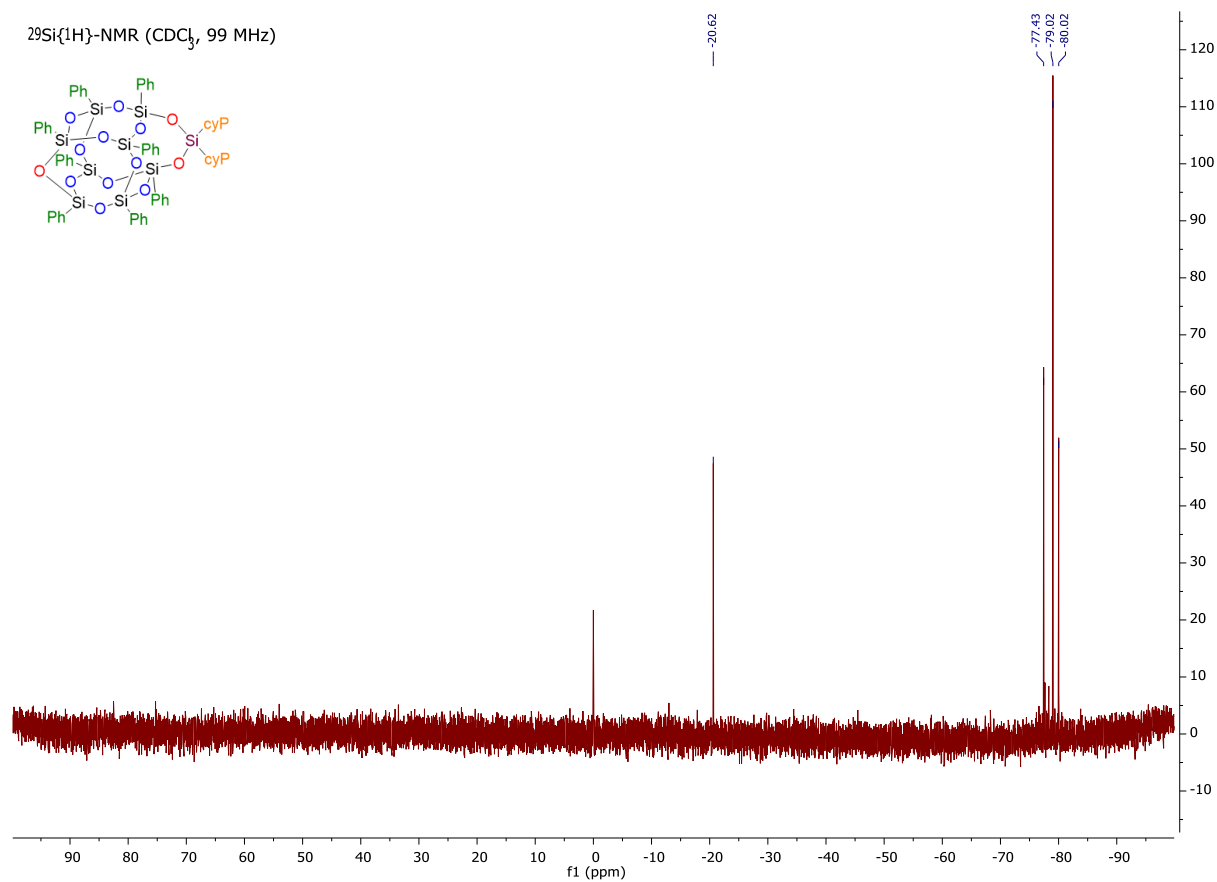


Figure 6-30 : $^{29}\text{Si}\{^1\text{H}\}$ -NMR (CDCl_3 , 99 MHz)

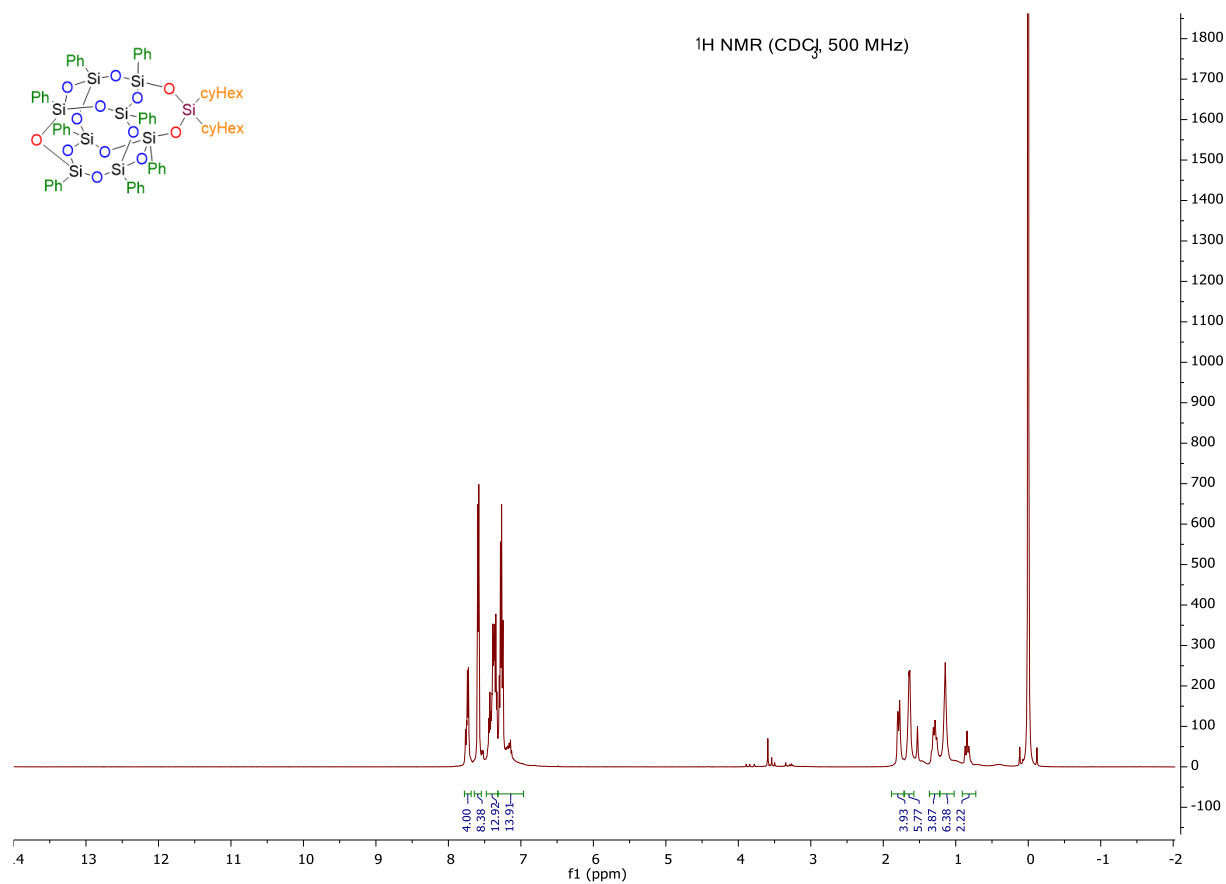


Figure 6-31 : ¹H-NMR (CDCl₃, 500 MHz)

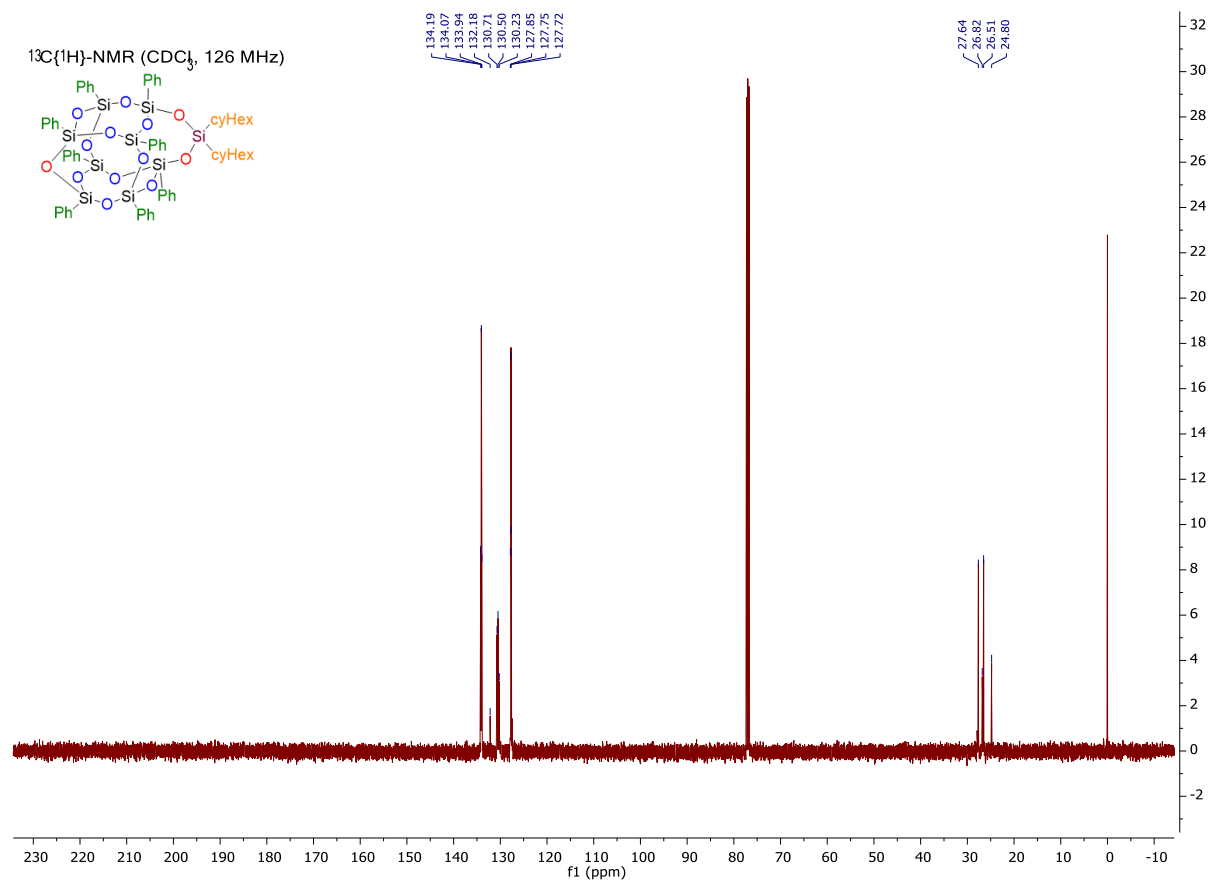


Figure 6-32 : ^{13}C -NMR (CDCl_3 , 126 MHz)

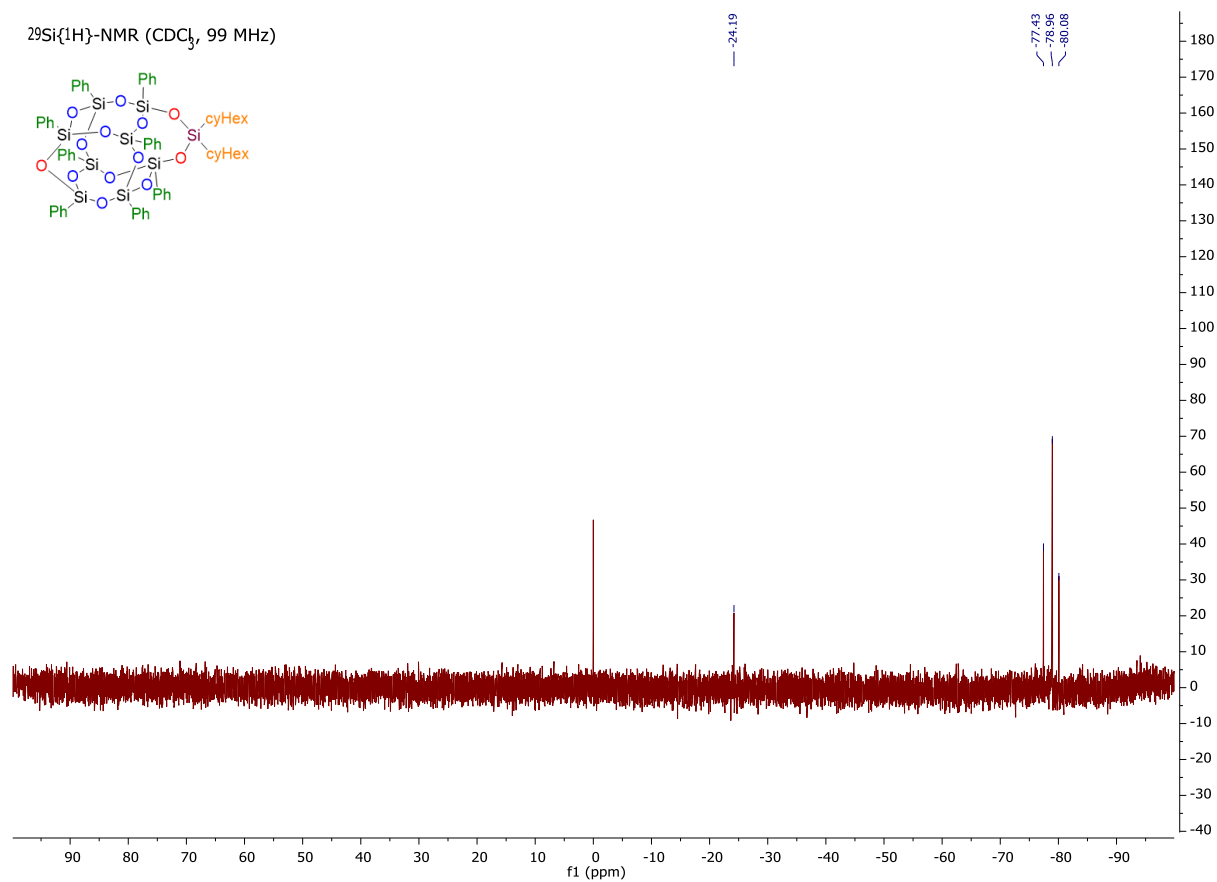


Figure 6-33 : $^{29}\text{Si}\{^1\text{H}\}$ -NMR (CDCl_3 , 99 MHz)

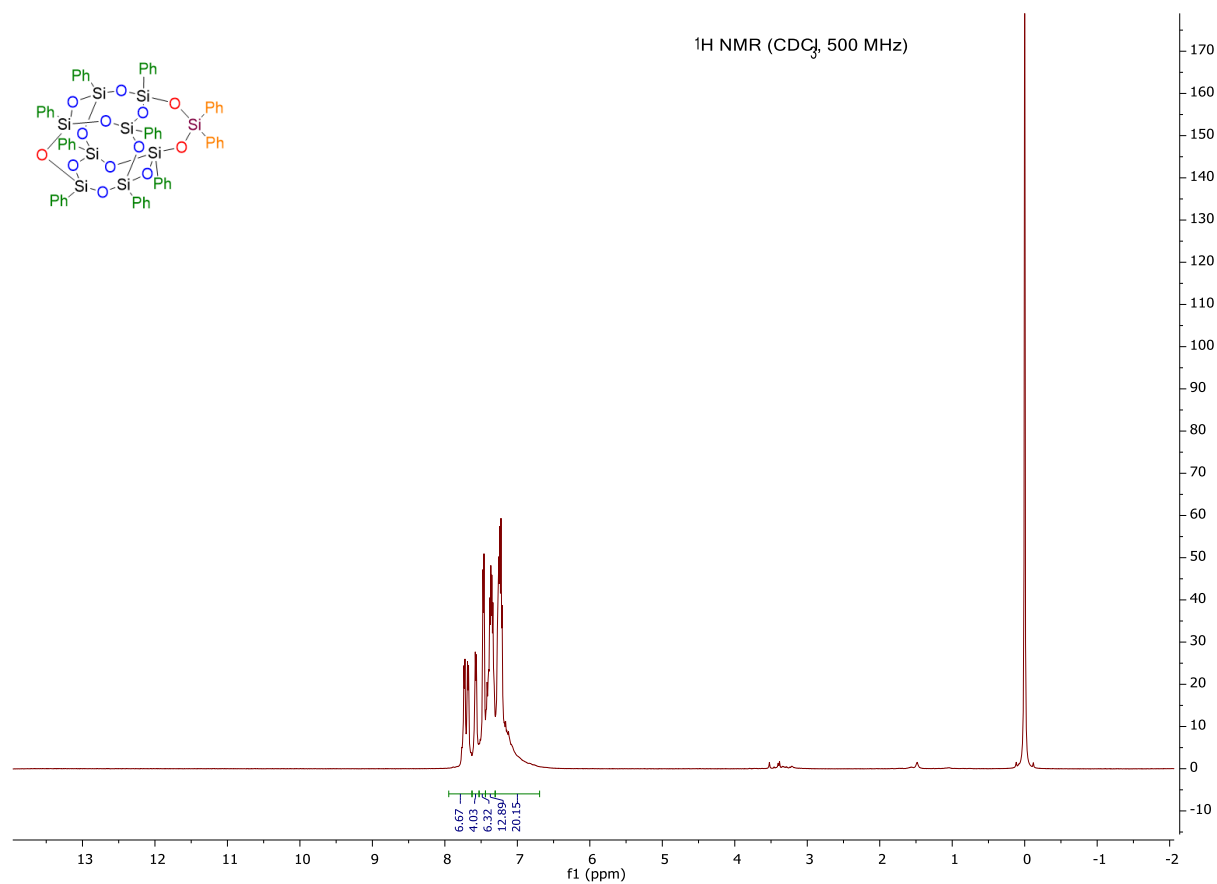


Figure 6-34 : ¹H-NMR (CDCl₃, 500 MHz)

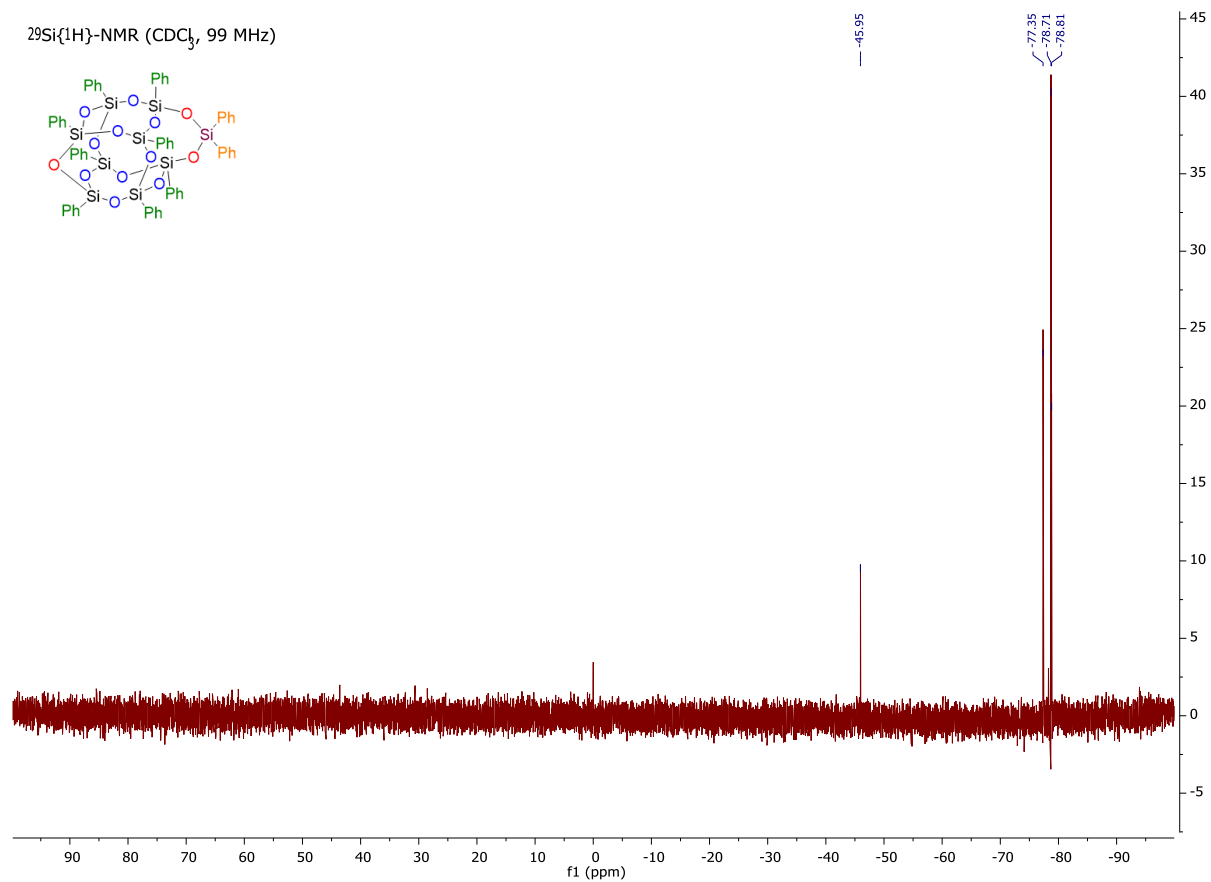


Figure 6-36 : $^{29}\text{Si}\{^1\text{H}\}$ -NMR (CDCl_3 , 99 MHz)

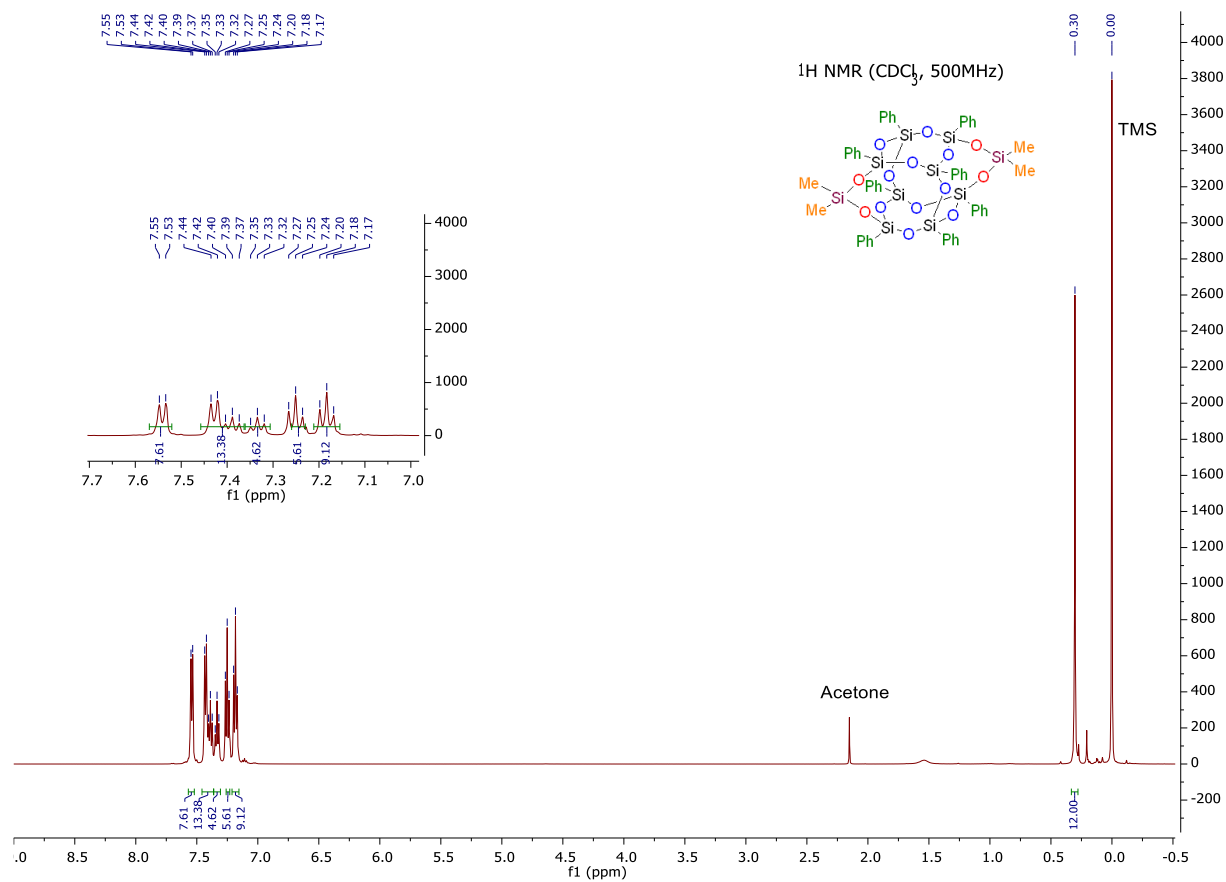


Figure 6-37 : ¹H-NMR (CDCl₃, 500 MHz) of **4**

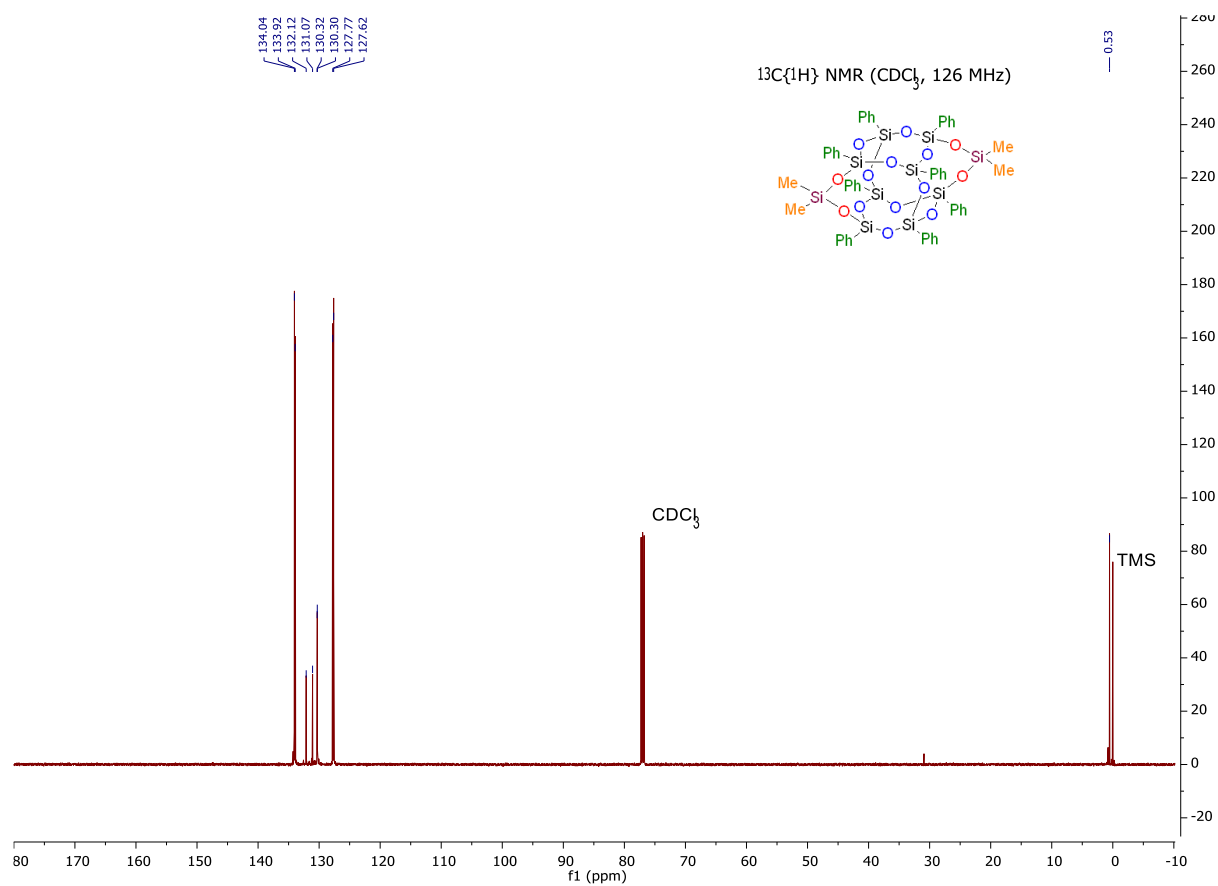


Figure 6-38 : $^{13}\text{C}\{^1\text{H}\}$ -NMR (CDCl_3 , 126 MHz)

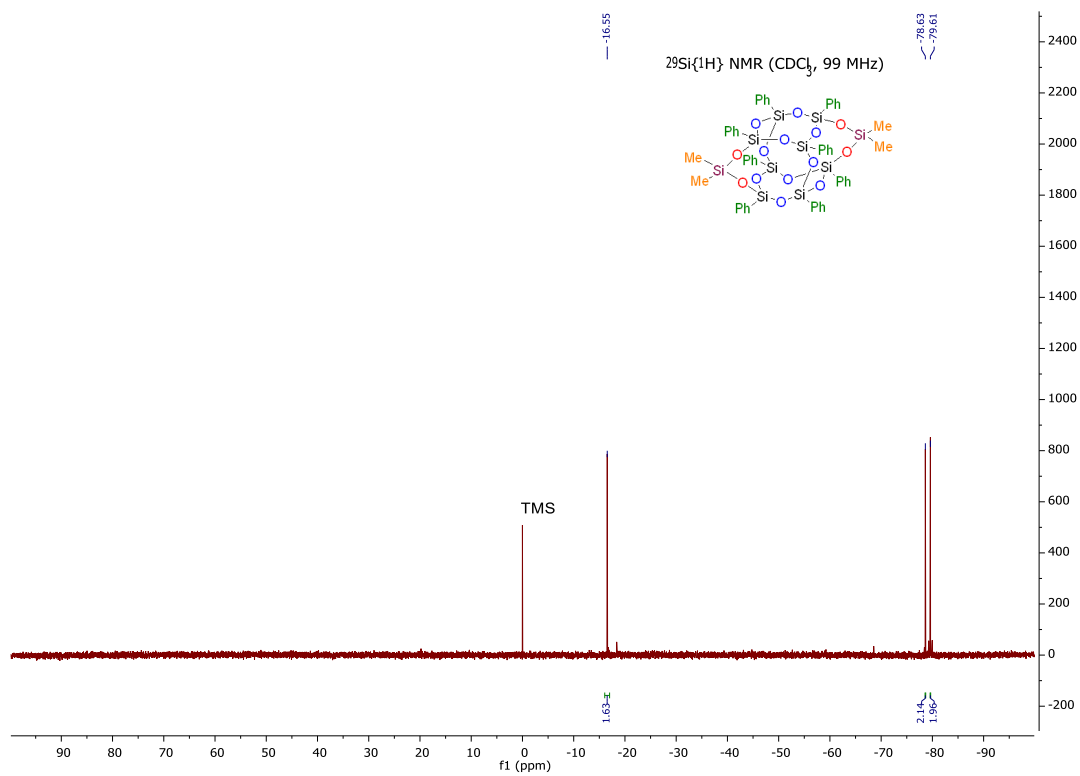


Figure 6-39 : $^{29}\text{Si}\{^1\text{H}\}$ -NMR (CDCl_3 , 99 MHz)

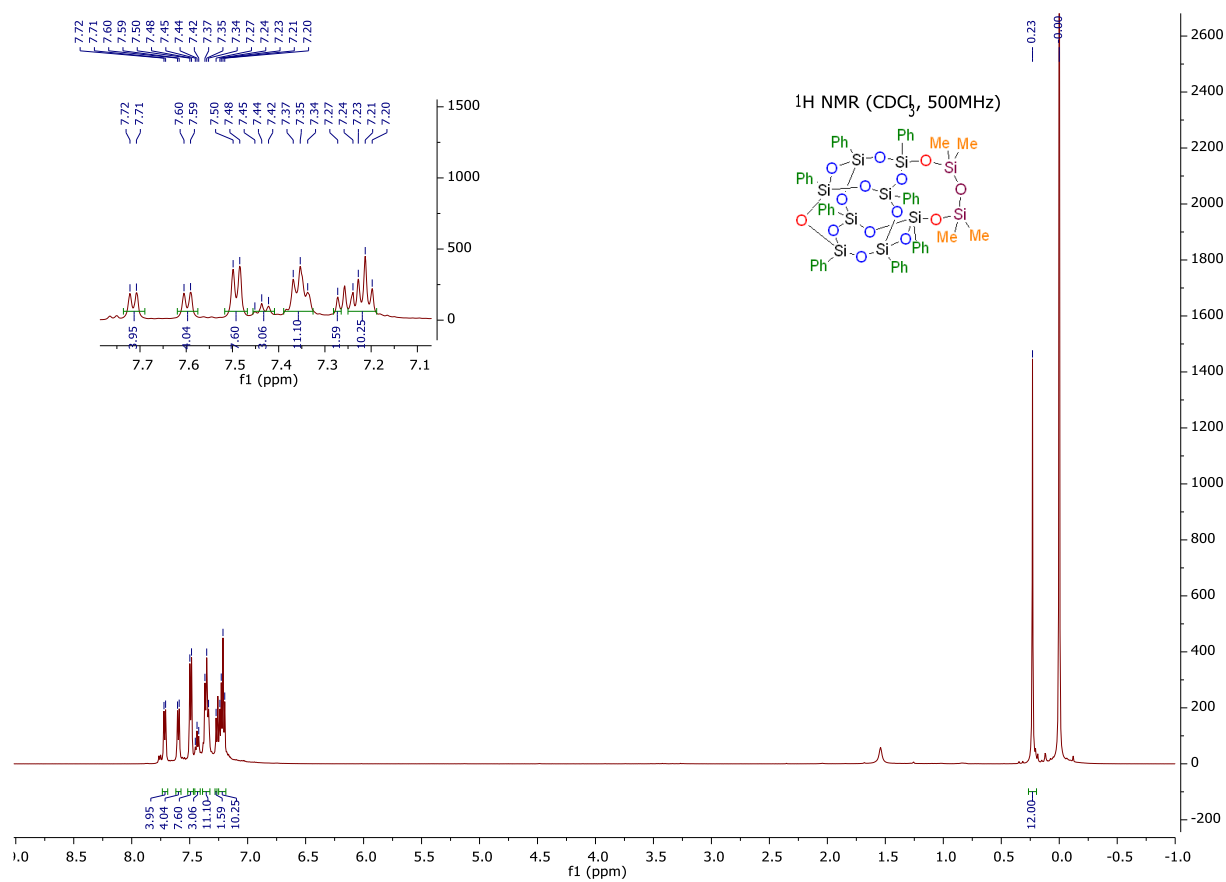


Figure 6-40 : ¹H-NMR (CDCl₃, 500 MHz) of **5**

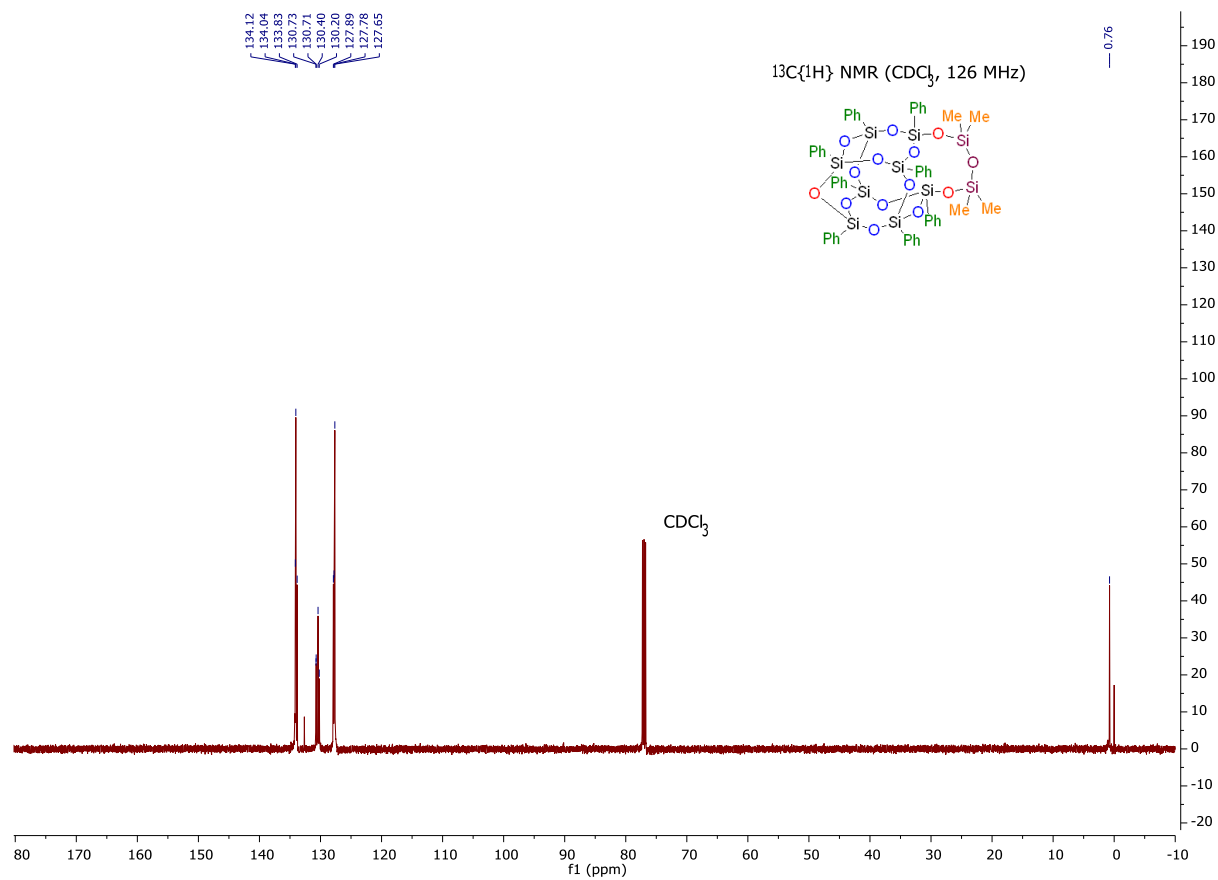


Figure 6-41 : $^{13}\text{C}\{^1\text{H}\}$ -NMR (CDCl_3 , 126 MHz)

Crystal structure data

Table 6-5 : Crystal structure data for compound **4**

Compound	AL722A
Formula	C ₅₂ H ₅₂ O ₁₄ Si ₁₀
CCDC	2189474
$D_{calc./}$ g cm ⁻³	1.367
m/mm^{-1}	2.693
Formula Weight	1181.83
Color	colorless
Shape	block-shaped
Size/mm ³	0.21×0.12×0.08
T/K	100.00(10)
Crystal System	monoclinic
Space Group	$P2_1/n$
$a/\text{\AA}$	10.93887(8)
$b/\text{\AA}$	21.34238(15)
$c/\text{\AA}$	24.64084(19)
$a/^\circ$	90
$b/^\circ$	93.4495(7)
$g/^\circ$	90
$V/\text{\AA}^3$	5742.26(7)
Z	4
Z'	1
Wavelength/ \AA	1.54184
Radiation type	Cu K $_{\alpha}$
$Q_{min}/^\circ$	2.741
$Q_{max}/^\circ$	80.432
Measured Refl's.	98144
Indep't Refl's	12415
Refl's $I \geq 2 \sigma(I)$	10850
R_{int}	0.0382
Parameters	899
Restraints	0
Largest Peak	0.744
Deepest Hole	-1.010
GooF	1.032
wR_2 (all data)	0.1260
wR_2	0.1192
R_1 (all data)	0.0575
R_1	0.0499

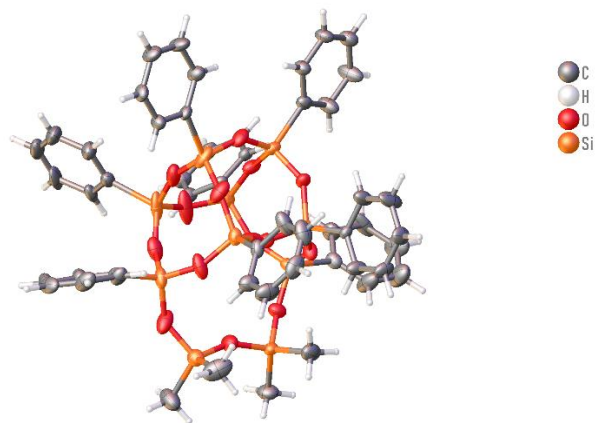


Figure 6-43 : Crystal structure data for compound 4

Table 6-6 : Bond Angles for Compound **4**

Atom	Atom	Atom	Angle/°
O1	Si1	O2	107.76(12)
O1	Si1	C1	109.08(13)
O1	Si1	C2	109.12(17)
O2	Si1	C1	108.83(15)
O2	Si1	C2	109.21(14)
C1	Si1	C2	112.7(2)
O1	Si2	O3	106.99(10)
O1	Si2	C3	109.20(13)
O1	Si2	C4	110.06(14)
O3	Si2	C3	108.01(12)
O3	Si2	C4	109.71(12)
C4	Si2	C3	112.68(15)
O2	Si3	O4	109.61(12)
O2	Si3	O10	107.80(12)
O2	Si3	C10A	109.21(16)
O2	Si3	C10B	109.06(17)
O4	Si3	O10	110.18(11)
O4	Si3	C10A	102.76(14)
O4	Si3	C10B	114.34(15)
O10	Si3	C10A	117.09(17)
O10	Si3	C10B	105.60(16)
O4	Si4	O5	107.22(10)
O4	Si4	O11	110.93(12)
O4	Si4	C20	109.67(11)
O5	Si4	O11	108.58(10)
O5	Si4	C20	111.66(10)
O11	Si4	C20	108.77(11)
O5	Si5	O12	108.28(9)
O5	Si5	C30A	116.81(13)
O5	Si5	C30B	106.71(14)
O6	Si5	O5	107.69(9)
O6	Si5	O12	110.29(10)
O6	Si5	C30A	102.82(12)
O6	Si5	C30B	117.76(14)
O12	Si5	C30A	110.73(13)
O12	Si5	C30B	105.75(12)
O3	Si6	O6	110.14(10)
O3	Si6	O7	109.12(10)
O3	Si6	C40A	109.61(15)
O3	Si6	C40B	109.19(14)
O6	Si6	C40A	118.43(15)
O6	Si6	C40B	100.07(14)
O7	Si6	O6	109.46(10)

Table 6-6 (cont'd)

O7	Si6	C40A	99.36(17)
O7	Si6	C40B	118.44(14)
O7	Si7	O8	107.18(15)
O7	Si7	O18	108.84(9)
O7	Si7	C50A	116.1(2)
O7	Si7	C50B	109.4(2)
O8	Si7	C50A	108.1(2)
O8	Si7	C50B	108.5(2)
O18	Si7	O8	111.40(13)
O18	Si7	C50A	105.3(2)
O18	Si7	C50B	111.4(2)
O8	Si8	O10	108.74(15)
O8	Si8	C60A	106.58(16)
O8	Si8	C60B	110.51(16)
O9	Si8	O8	109.48(13)
O9	Si8	O10	109.50(10)
O9	Si8	C60A	119.95(16)
O9	Si8	C60B	99.30(15)
O10	Si8	C60A	101.99(16)
O10	Si8	C60B	118.76(15)
O9	Si9	O11	108.68(12)
O9	Si9	O14	109.52(10)
O9	Si9	C70A	99.55(14)
O9	Si9	C70B	117.09(14)
O11	Si9	C70A	109.26(14)
O11	Si9	C70B	110.88(13)
O14	Si9	O11	108.94(11)
O14	Si9	C70A	120.16(15)
O14	Si9	C70B	101.32(12)
O12	Si10	C80A	111.1(2)
O12	Si10	C80B	106.4(2)
O14	Si10	O12	110.02(9)
O14	Si10	C80A	107.6(2)
O14	Si10	C80B	112.5(2)
O18	Si10	O12	108.08(9)
O18	Si10	O14	109.39(10)
O18	Si10	C80A	110.6(2)
O18	Si10	C80B	110.28(19)
Si1	O1	Si2	152.53(14)
Si3	O2	Si1	142.53(14)
Si6	O3	Si2	148.41(12)
Si4	O4	Si3	151.07(15)
Si5	O5	Si4	150.36(11)
Si5	O6	Si6	147.60(12)

Table 6-6 (cont'd)

Si7	O7	Si6	153.01(13)
Si7	O8	Si8	149.55(16)
Si8	O9	Si9	157.30(15)
Si8	O10	Si3	150.78(14)
Si4	O11	Si9	141.73(12)
Si5	O12	Si10	140.81(11)
Si9	O14	Si10	141.40(13)
Si7	O18	Si10	157.00(12)
C11A	C10A	Si3	120.6(2)
C11A	C10A	C15A	120.0
C15A	C10A	Si3	119.4(2)
C12A	C11A	C10A	120.0
C11A	C12A	C13A	120.0
C14A	C13A	C12A	120.0
C13A	C14A	C15A	120.0
C14A	C15A	C10A	120.0
C11B	C10B	Si3	120.5(2)
C11B	C10B	C15B	120.0
C15B	C10B	Si3	118.0(2)
C12B	C11B	C10B	120.0
C11B	C12B	C13B	120.0
C14B	C13B	C12B	120.0
C13B	C14B	C15B	120.0
C14B	C15B	C10B	120.0
C21	C20	Si4	122.37(19)
C21	C20	C25	118.0(2)
C25	C20	Si4	119.6(2)
C20	C21	C22	121.1(3)
C23	C22	C21	119.4(3)
C24	C23	C22	120.5(3)
C23	C24	C25	119.6(3)
C24	C25	C20	121.4(3)
C35A	C30A	Si5	120.40(18)
C35A	C30A	C31A	120.0
C31A	C30A	Si5	119.60(18)
C30A	C35A	C34A	120.0
C33A	C34A	C35A	120.0
C32A	C33A	C34A	120.0
C33A	C32A	C31A	120.0
C32A	C31A	C30A	120.0
C35B	C30B	Si5	122.29(18)
C35B	C30B	C31B	120.0
C31B	C30B	Si5	117.45(18)
C30B	C35B	C34B	120.0

Table 6-6 (cont'd)

C33B	C34B	C35B	120.0
C34B	C33B	C32B	120.0
C33B	C32B	C31B	120.0
C32B	C31B	C30B	120.0
C41A	C40A	Si6	120.2(2)
C41A	C40A	C45A	120.0
C45A	C40A	Si6	119.8(2)
C42A	C41A	C40A	120.0
C41A	C42A	C43A	120.0
C44A	C43A	C42A	120.0
C43A	C44A	C45A	120.0
C44A	C45A	C40A	120.0
C41B	C40B	Si6	123.3(2)
C41B	C40B	C45B	120.0
C45B	C40B	Si6	116.5(2)
C40B	C41B	C42B	120.0
C43B	C42B	C41B	120.0
C42B	C43B	C44B	120.0
C45B	C44B	C43B	120.0
C44B	C45B	C40B	120.0
C55A	C50A	Si7	119.7(4)
C55A	C50A	C51A	120.0
C51A	C50A	Si7	120.2(4)
C54A	C55A	C50A	120.0
C55A	C54A	C53A	120.0
C52A	C53A	C54A	120.0
C53A	C52A	C51A	120.0
C52A	C51A	C50A	120.0
C55B	C50B	Si7	118.2(4)
C55B	C50B	C51B	120.0
C51B	C50B	Si7	121.6(4)
C50B	C55B	C54B	120.0
C55B	C54B	C53B	120.0
C54B	C53B	C52B	120.0
C51B	C52B	C53B	120.0
C52B	C51B	C50B	120.0
C65A	C60A	Si8	122.4(3)
C65A	C60A	C61A	120.0
C61A	C60A	Si8	117.1(3)
C60A	C65A	C64A	120.0
C63A	C64A	C65A	120.0
C64A	C63A	C62A	120.0
C61A	C62A	C63A	120.0
C62A	C61A	C60A	120.0

Table 6-6 (cont'd)

C61B	C60B	Si8	126.7(2)
C61B	C60B	C65B	120.0
C65B	C60B	Si8	113.3(2)
C62B	C61B	C60B	120.0
C61B	C62B	C63B	120.0
C64B	C63B	C62B	120.0
C65B	C64B	C63B	120.0
C64B	C65B	C60B	120.0
C75A	C70A	Si9	120.8(2)
C75A	C70A	C71A	120.0
C71A	C70A	Si9	118.8(2)
C70A	C75A	C74A	120.0
C73A	C74A	C75A	120.0
C72A	C73A	C74A	120.0
C73A	C72A	C71A	120.0
C72A	C71A	C70A	120.0
C75B	C70B	Si9	125.64(18)
C75B	C70B	C71B	120.0
C71B	C70B	Si9	114.24(18)
C70B	C75B	C74B	120.0
C73B	C74B	C75B	120.0
C74B	C73B	C72B	120.0
C73B	C72B	C71B	120.0
C72B	C71B	C70B	120.0
C81A	C80A	Si10	118.5(4)
C81A	C80A	C85A	120.0
C85A	C80A	Si10	121.4(4)
C82A	C81A	C80A	120.0
C83A	C82A	C81A	120.0
C84A	C83A	C82A	120.0
C83A	C84A	C85A	120.0
C84A	C85A	C80A	120.0
C81B	C80B	Si10	118.8(4)
C81B	C80B	C85B	120.0
C85B	C80B	Si10	121.2(4)
C80B	C81B	C82B	120.0
C83B	C82B	C81B	120.0
C82B	C83B	C84B	120.0
C85B	C84B	C83B	120.0
C84B	C85B	C80B	120.0

Table 6-7 : Bond lengths for compound **4**

Atom	Atom	Length/Å
Si1	O1	1.612(2)
Si1	O2	1.628(2)
Si1	C1	1.845(3)
Si1	C2	1.852(4)
Si2	O1	1.6149(19)
Si2	O3	1.6310(18)
Si2	C3	1.843(3)
Si2	C4	1.841(3)
Si3	O2	1.615(2)
Si3	O4	1.6152(18)
Si3	O10	1.617(2)
Si3	C10A	1.894(3)
Si3	C10B	1.838(3)
Si4	O4	1.6072(19)
Si4	O5	1.6187(16)
Si4	O11	1.622(2)
Si4	C20	1.841(2)
Si5	O5	1.6186(16)
Si5	O6	1.6065(16)
Si5	O12	1.6194(16)
Si5	C30A	1.872(2)
Si5	C30B	1.855(2)
Si6	O3	1.6049(18)
Si6	O6	1.6183(17)
Si6	O7	1.616(2)
Si6	C40A	1.786(3)
Si6	C40B	1.965(3)
Si7	O7	1.602(2)
Si7	O8	1.610(2)
Si7	O18	1.6094(18)
Si7	C50A	1.871(6)
Si7	C50B	1.874(5)
Si8	O8	1.612(2)
Si8	O9	1.609(3)
Si8	O10	1.614(2)
Si8	C60A	1.828(3)
Si8	C60B	1.965(3)
Si9	O9	1.609(2)
Si9	O11	1.624(2)
Si9	O14	1.620(2)
Si9	C70A	1.809(3)
Si9	C70B	1.957(2)

Table 6-7 (cont'd)

Si10	O12	1.6215(16)
Si10	O14	1.6209(18)
Si10	O18	1.6151(17)
Si10	C80A	1.752(5)
Si10	C80B	1.973(5)
C10A	C11A	1.3900
C10A	C15A	1.3900
C11A	C12A	1.3900
C12A	C13A	1.3900
C13A	C14A	1.3900
C14A	C15A	1.3900
C10B	C11B	1.3900
C10B	C15B	1.3900
C11B	C12B	1.3900
C12B	C13B	1.3900
C13B	C14B	1.3900
C14B	C15B	1.3900
C20	C21	1.381(4)
C20	C25	1.398(4)
C21	C22	1.392(4)
C22	C23	1.384(5)
C23	C24	1.373(5)
C24	C25	1.378(4)
C30A	C35A	1.3900
C30A	C31A	1.3900
C35A	C34A	1.3900
C34A	C33A	1.3900
C33A	C32A	1.3900
C32A	C31A	1.3900
C30B	C35B	1.3900
C30B	C31B	1.3900
C35B	C34B	1.3900
C34B	C33B	1.3900
C33B	C32B	1.3900
C32B	C31B	1.3900
C40A	C41A	1.3900
C40A	C45A	1.3900
C41A	C42A	1.3900
C42A	C43A	1.3900
C43A	C44A	1.3900
C44A	C45A	1.3900
C40B	C41B	1.3900
C40B	C45B	1.3900
C41B	C42B	1.3900

Table 6-7 (cont'd)

C42B	C43B	1.3900
C43B	C44B	1.3900
C44B	C45B	1.3900
C50A	C55A	1.3900
C50A	C51A	1.3900
C55A	C54A	1.3900
C54A	C53A	1.3900
C53A	C52A	1.3900
C52A	C51A	1.3900
C50B	C55B	1.3900
C50B	C51B	1.3900
C55B	C54B	1.3900
C54B	C53B	1.3900
C53B	C52B	1.3900
C52B	C51B	1.3900
C60A	C65A	1.3900
C60A	C61A	1.3900
C65A	C64A	1.3900
C64A	C63A	1.3900
C63A	C62A	1.3900
C62A	C61A	1.3900
C60B	C61B	1.3900
C60B	C65B	1.3900
C61B	C62B	1.3900
C62B	C63B	1.3900
C63B	C64B	1.3900
C64B	C65B	1.3900
C70A	C75A	1.3900
C70A	C71A	1.3900
C75A	C74A	1.3900
C74A	C73A	1.3900
C73A	C72A	1.3900
C72A	C71A	1.3900
C70B	C75B	1.3900
C70B	C71B	1.3900
C75B	C74B	1.3900
C74B	C73B	1.3900
C73B	C72B	1.3900
C72B	C71B	1.3900
C80A	C81A	1.3900
C80A	C85A	1.3900
C81A	C82A	1.3900
C82A	C83A	1.3900
C83A	C84A	1.3900

C84A	C85A	1.3900
C80B	C81B	1.3900
C80B	C85B	1.3900
C81B	C82B	1.3900
C82B	C83B	1.3900
C83B	C84B	1.3900
C84B	C85B	1.3900

Table 6-8 : Crystal structure data for compound **5**

Compound	AL722C
Formula	C ₅₀ H ₄₈ O ₁₄ Si ₉
CCDC	2191689
$D_{calc.}/\text{g cm}^{-3}$	1.370
m/mm^{-1}	2.602
Formula Weight	1125.69
Color	colorless
Shape	irregular-shaped
Size/ mm^3	0.32×0.15×0.14
T/K	100.00(10)
Crystal System	triclinic
Space Group	$P-1$
$a/\text{\AA}$	13.9487(7)
$b/\text{\AA}$	14.6216(6)
$c/\text{\AA}$	15.1753(6)
$a/^\circ$	87.437(3)
$b/^\circ$	65.756(4)
$g/^\circ$	75.749(4)
$V/\text{\AA}^3$	2729.7(2)
Z	2
Z'	1
Wavelength/ \AA	1.54184
Radiation type	Cu K_α
$Q_{min}/^\circ$	3.125
$Q_{max}/^\circ$	89.674
Measured Refl's.	36882
Indep't Refl's	11537
Refl's $I \geq 2\sigma(I)$	8552
R_{int}	0.0530
Parameters	719
Restraints	31
Largest Peak	0.847
Deepest Hole	-0.716
GooF	1.051
wR_2 (all data)	0.2498
wR_2	0.2294
R_1 (all data)	0.1092
R_1	0.0866

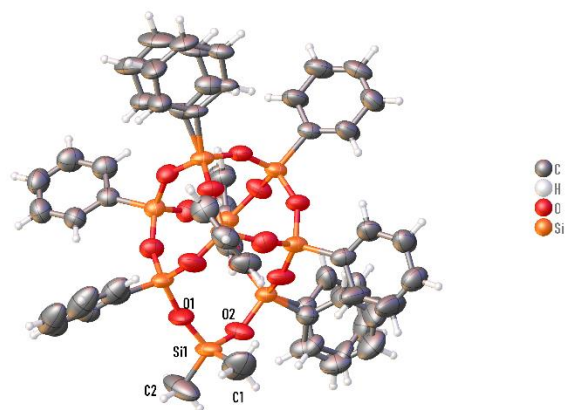


Figure 6-44 : Crystal structure data for compound **4**

Table 6-9 : Bond lengths for compound **5**

Atom	Atom	Length/Å
i1	O1	1.580(4)
Si1	O2	1.616(4)
Si1	C1	1.867(9)
Si1	C2	1.791(8)
Si2	O1	1.592(4)
Si2	O3	1.597(4)
Si2	O6	1.607(4)
Si2	C20	1.848(6)
Si3	O3	1.615(4)
Si3	O4	1.598(4)
Si3	O7	1.603(3)
Si3	C30	1.852(5)
Si4	O4	1.614(4)
Si4	O5	1.609(3)
Si4	O8	1.616(3)
Si4	C40	1.838(5)
Si5	O2	1.589(4)
Si5	O5	1.615(4)
Si5	O9	1.600(3)
Si5	C50	1.908(6)
Si5	C50B	1.798(7)
Si6	O6	1.609(3)
Si6	O10	1.629(3)
Si6	O13	1.611(4)
Si6	C60	1.833(5)
Si7	O7	1.617(3)
Si7	O10	1.609(4)
Si7	O11	1.609(4)
Si7	C70	1.847(5)
Si7	C70B	1.874(6)
Si8	O8	1.611(3)
Si8	O11	1.606(4)
Si8	O12	1.615(4)
Si8	C80	1.847(5)
Si9	O9	1.602(3)
Si9	O12	1.620(3)
Si9	O13	1.596(4)
Si9	C90	1.845(5)
C20	C21	1.385(8)
C20	C25	1.386(8)
C21	C22	1.389(9)
C22	C23	1.389(13)
C23	C24	1.377(14)

Table 6-9 (cont'd)

C24	C25	1.368(11)
C30	C31	1.385(7)
C30	C35	1.372(8)
C31	C32	1.399(8)
C32	C33	1.350(9)
C33	C34	1.376(9)
C34	C35	1.393(9)
C40	C41	1.385(7)
C40	C45	1.364(8)
C41	C42	1.379(9)
C42	C43	1.336(10)
C43	C44	1.357(9)
C44	C45	1.384(8)
C50	C55	1.3900
C50	C51	1.3900
C55	C54	1.3900
C54	C53	1.3900
C53	C52	1.3900
C52	C51	1.3900
C50B	C55B	1.3900
C50B	C51B	1.3900
C55B	C54B	1.3900
C54B	C53B	1.3900
C53B	C52B	1.3900
C52B	C51B	1.3900
C60	C61	1.388(7)
C60	C65	1.386(7)
C61	C62	1.388(8)
C62	C63	1.355(9)
C63	C64	1.381(9)
C64	C65	1.366(8)
C70	C75	1.3900
C70	C71	1.3900
C75	C74	1.3900
C74	C73	1.3900
C73	C72	1.3900
C72	C71	1.3900
C70B	C71B	1.3900
C70B	C75B	1.3900
C71B	C72B	1.3900
C72B	C73B	1.3900
C73B	C74B	1.3900
C74B	C75B	1.3900
C80	C81	1.409(7)

Table 6-9 (cont'd)

C80	C85	1.352(8)
C81	C82	1.375(8)
C82	C83	1.387(10)
C83	C84	1.340(9)
C84	C85	1.415(7)
C90	C91	1.396(6)
C90	C95	1.403(7)
C91	C92	1.390(8)
C92	C93	1.366(9)
C93	C94	1.380(8)
C94	C95	1.376(8)

Table 6-10 : Bond Angles for Compound **5**

Atom	Atom	Atom	Angle/°
O1	Si1	O2	110.8(2)
O1	Si1	C1	106.6(4)
O1	Si1	C2	111.6(4)
O2	Si1	C1	103.4(3)
O2	Si1	C2	111.8(3)
C2	Si1	C1	112.2(5)
O1	Si2	O3	109.5(2)
O1	Si2	O6	109.2(2)
O1	Si2	C20	109.3(2)
O3	Si2	O6	109.75(19)
O3	Si2	C20	109.1(3)
O6	Si2	C20	110.0(2)
O3	Si3	C30	110.3(2)
O4	Si3	O3	108.3(2)
O4	Si3	O7	110.1(2)
O4	Si3	C30	110.4(2)
O7	Si3	O3	109.4(2)
O7	Si3	C30	108.4(2)
O4	Si4	O8	109.19(19)
O4	Si4	C40	110.0(2)
O5	Si4	O4	107.6(2)
O5	Si4	O8	110.25(18)
O5	Si4	C40	110.1(2)
O8	Si4	C40	109.6(2)
O2	Si5	O5	109.8(2)
O2	Si5	O9	109.2(2)
O2	Si5	C50	110.3(3)
O2	Si5	C50B	102.8(3)
O5	Si5	C50	115.8(4)

Table 6-10 (cont'd)

O5	Si5	C50B	107.6(4)
O9	Si5	O5	108.15(18)
O9	Si5	C50	103.2(3)
O9	Si5	C50B	119.0(4)
O6	Si6	O10	109.54(19)
O6	Si6	O13	110.6(2)
O6	Si6	C60	109.9(2)
O10	Si6	C60	110.45(19)
O13	Si6	O10	107.47(19)
O13	Si6	C60	108.9(2)
O7	Si7	C70	106.4(4)
O7	Si7	C70B	114.7(4)
O10	Si7	O7	108.68(19)
O10	Si7	O11	110.12(19)
O10	Si7	C70	117.6(3)
O10	Si7	C70B	101.6(3)
O11	Si7	O7	108.9(2)
O11	Si7	C70	104.8(3)
O11	Si7	C70B	112.5(4)
O8	Si8	O12	109.28(19)
O8	Si8	C80	110.2(2)
O11	Si8	O8	109.27(19)
O11	Si8	O12	108.6(2)
O11	Si8	C80	109.9(2)
O12	Si8	C80	109.6(2)
O9	Si9	O12	109.8(2)
O9	Si9	C90	108.86(19)
O12	Si9	C90	109.81(19)
O13	Si9	O9	109.0(2)
O13	Si9	O12	108.3(2)
O13	Si9	C90	111.0(2)
Si1	O1	Si2	167.0(3)
Si5	O2	Si1	143.3(2)
Si2	O3	Si3	156.7(3)
Si3	O4	Si4	152.4(3)
Si4	O5	Si5	157.4(2)
Si2	O6	Si6	157.5(3)
Si3	O7	Si7	149.6(3)
Si8	O8	Si4	147.8(2)
Si5	O9	Si9	155.7(2)
Si7	O10	Si6	143.5(2)
Si8	O11	Si7	152.9(2)
Si8	O12	Si9	145.0(2)
Si9	O13	Si6	157.9(2)

Table 6-10 (cont'd)

C21	C20	Si2	120.9(4)
C21	C20	C25	118.3(6)
C25	C20	Si2	120.7(5)
C20	C21	C22	121.6(7)
C23	C22	C21	118.8(8)
C24	C23	C22	119.8(8)
C25	C24	C23	120.9(9)
C24	C25	C20	120.6(8)
C31	C30	Si3	120.9(4)
C35	C30	Si3	122.1(4)
C35	C30	C31	117.0(5)
C30	C31	C32	121.2(6)
C33	C32	C31	120.5(6)
C32	C33	C34	119.7(6)
C33	C34	C35	119.6(7)
C30	C35	C34	122.1(6)
C41	C40	Si4	120.8(5)
C45	C40	Si4	123.3(4)
C45	C40	C41	115.9(5)
C42	C41	C40	121.7(7)
C43	C42	C41	120.8(6)
C42	C43	C44	119.2(6)
C43	C44	C45	120.2(6)
C40	C45	C44	122.1(5)
C55	C50	Si5	119.2(5)
C55	C50	C51	120.0
C51	C50	Si5	120.8(5)
C50	C55	C54	120.0
C53	C54	C55	120.0
C52	C53	C54	120.0
C53	C52	C51	120.0
C52	C51	C50	120.0
C55B	C50B	Si5	121.0(6)
C55B	C50B	C51B	120.0
C51B	C50B	Si5	118.9(6)
C50B	C55B	C54B	120.0
C53B	C54B	C55B	120.0
C54B	C53B	C52B	120.0
C53B	C52B	C51B	120.0
C52B	C51B	C50B	120.0
C61	C60	Si6	121.0(4)
C65	C60	Si6	122.4(4)
C65	C60	C61	116.6(5)
C62	C61	C60	121.7(6)

Table 6-10 (cont'd)

C63	C62	C61	119.7(6)
C62	C63	C64	120.0(6)
C65	C64	C63	119.9(6)
C64	C65	C60	122.1(6)
C75	C70	Si7	122.5(5)
C75	C70	C71	120.0
C71	C70	Si7	117.4(5)
C70	C75	C74	120.0
C73	C74	C75	120.0
C74	C73	C72	120.0
C73	C72	C71	120.0
C72	C71	C70	120.0
C71B	C70B	Si7	116.9(5)
C71B	C70B	C75B	120.0
C75B	C70B	Si7	123.1(5)
C70B	C71B	C72B	120.0
C73B	C72B	C71B	120.0
C72B	C73B	C74B	120.0
C75B	C74B	C73B	120.0
C74B	C75B	C70B	120.0
C81	C80	Si8	118.3(4)
C85	C80	Si8	124.1(4)
C85	C80	C81	117.6(5)
C82	C81	C80	120.9(6)
C81	C82	C83	119.5(6)
C84	C83	C82	121.1(5)
C83	C84	C85	118.8(6)
C80	C85	C84	122.1(5)
C91	C90	Si9	121.8(4)
C91	C90	C95	117.2(5)
C95	C90	Si9	121.0(4)
C92	C91	C90	120.4(5)
C93	C92	C91	121.3(5)
C92	C93	C94	119.3(5)
C95	C94	C93	120.2(6)
C94	C95	C90	121.7(5)

Table 6-11 : Crystal structure data for SOPh₈T₈Et₂

Compound	AL722B
Formula	C ₅₂ H ₅₀ O ₁₃ Si ₉
CCDC	2189783
$D_{calc./} \text{ g cm}^{-3}$	1.401
m/mm^{-1}	2.629
Formula Weight	1135.73
Color	colorless
Shape	block-shaped
Size/mm ³	0.15×0.08×0.05
T/K	100.00(10)
Crystal System	monoclinic
Space Group	$P2_1/c$
$a/\text{\AA}$	14.17342(8)
$b/\text{\AA}$	16.35769(10)
$c/\text{\AA}$	23.54541(15)
$a/^\circ$	90
$b/^\circ$	99.4850(6)
$g/^\circ$	90
$V/\text{\AA}^3$	5384.24(6)
Z	4
Z'	1
Wavelength/ \AA	1.54184
Radiation type	Cu K $_{\alpha}$
$Q_{min}/^\circ$	3.161
$Q_{max}/^\circ$	80.286
Measured Refl's.	78522
Indep't Refl's	11693
Refl's $I \geq 2 \sigma(I)$	10615
R_{int}	0.0334
Parameters	694
Restraints	0
Largest Peak	0.668
Deepest Hole	-0.460
GooF	1.060
wR_2 (all data)	0.1013
wR_2	0.0989
R_1 (all data)	0.0385
R_1	0.0353

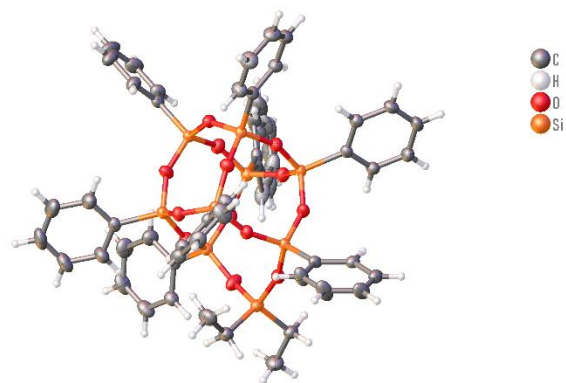


Figure 6-45 : Crystal structure data for SOPh₈T₈Et₂

Table 6-12 : Bond lengths for compound **6**

Atom	Atom	Length/Å
Si1	O1	1.6269(13)
Si1	O2	1.6404(13)
Si1	C1	1.857(2)
Si1	C3	1.8572(19)
Si2	O1	1.6108(12)
Si2	O3	1.6150(12)
Si2	O6	1.6129(12)
Si2	C10	1.8482(16)
Si3	O3	1.6128(12)
Si3	O4	1.6189(12)
Si3	O7	1.6230(12)
Si3	C20	1.8436(16)
Si4	O4	1.6196(12)
Si4	O5	1.6173(12)
Si4	O8	1.6239(12)
Si4	C30	1.8386(17)
Si5	O5	1.6118(12)
Si5	O6	1.6149(12)
Si5	O9	1.6200(12)
Si5	C40	1.8427(17)
Si6	O2	1.6037(13)
Si6	O10	1.6245(13)
Si6	O13	1.6144(14)
Si6	C50	1.8486(17)
Si7	O7	1.6234(12)
Si7	O10	1.6125(13)
Si7	O11	1.6112(12)
Si7	C60	1.8415(18)
Si8	O8	1.6170(12)
Si8	O11	1.6103(12)
Si8	O12	1.6117(13)
Si8	C70	1.8437(17)
Si9	O9	1.6176(12)
Si9	O12	1.6192(13)
Si9	O13	1.6095(14)
Si9	C80A	1.885(2)
Si9	C80B	1.791(6)
C1	C2	1.517(3)
C3	C4	1.534(3)
C10	C11	1.399(3)
C10	C15	1.396(2)
C11	C12	1.396(3)
C12	C13	1.379(3)

Table 6-12 (cont'd)

C13	C14	1.385(3)
C14	C15	1.399(2)
C20	C21	1.395(3)
C20	C25	1.391(2)
C21	C22	1.394(3)
C22	C23	1.370(3)
C23	C24	1.378(3)
C24	C25	1.393(3)
C30	C31	1.399(2)
C30	C35	1.397(2)
C31	C32	1.388(2)
C32	C33	1.389(3)
C33	C34	1.374(3)
C34	C35	1.396(3)
C40	C41	1.403(2)
C40	C45	1.399(2)
C41	C42	1.382(3)
C42	C43	1.390(3)
C43	C44	1.387(3)
C44	C45	1.392(3)
C50	C51	1.390(3)
C50	C55	1.396(2)
C51	C52	1.395(3)
C52	C53	1.389(4)
C53	C54	1.369(3)
C54	C55	1.390(3)
C60	C61	1.393(3)
C60	C65	1.390(3)
C61	C62	1.387(3)
C62	C63	1.373(4)
C63	C64	1.365(4)
C64	C65	1.395(3)
C70	C71	1.393(3)
C70	C75	1.393(2)
C71	C72	1.386(3)
C72	C73	1.385(4)
C73	C74	1.370(4)
C74	C75	1.389(3)
C80A	C85A	1.3900
C80A	C81A	1.3900
C85A	C84A	1.3900
C84A	C83A	1.3900
C83A	C82A	1.3900
C82A	C81A	1.3900

Table 6-12 (cont'd)

C80B	C85B	1.3900
C80B	C81B	1.3900
C85B	C84B	1.3900
C84B	C83B	1.3900
C83B	C82B	1.3900
C82B	C81B	1.3900

Table 6-13 : Bond angles for compound **6**

Atom	Atom	Atom	Angle/°
O1	Si1	O2	107.57(7)
O1	Si1	C1	111.19(9)
O1	Si1	C3	109.27(8)
O2	Si1	C1	109.01(9)
O2	Si1	C3	106.53(8)
C1	Si1	C3	113.02(9)
O1	Si2	O3	109.97(7)
O1	Si2	O6	108.86(7)
O1	Si2	C10	108.19(7)
O3	Si2	C10	110.55(7)
O6	Si2	O3	109.60(6)
O6	Si2	C10	109.64(7)
O3	Si3	O4	109.65(7)
O3	Si3	O7	107.82(6)
O3	Si3	C20	111.38(7)
O4	Si3	O7	110.38(6)
O4	Si3	C20	108.24(7)
O7	Si3	C20	109.38(7)
O4	Si4	O8	108.49(6)
O4	Si4	C30	110.44(7)
O5	Si4	O4	109.30(7)
O5	Si4	O8	108.40(6)
O5	Si4	C30	109.82(7)
O8	Si4	C30	110.34(7)
O5	Si5	O6	110.68(7)
O5	Si5	O9	109.45(6)
O5	Si5	C40	108.63(7)
O6	Si5	O9	108.22(7)
O6	Si5	C40	108.89(7)
O9	Si5	C40	110.97(7)
O2	Si6	O10	108.72(7)
O2	Si6	O13	109.61(8)
O2	Si6	C50	108.12(8)
O10	Si6	C50	110.78(7)

Table 6-13 (cont'd)

O13	Si6	O10	108.81(7)
O13	Si6	C50	110.78(8)
O7	Si7	C60	111.41(7)
O10	Si7	O7	108.67(7)
O10	Si7	C60	111.29(8)
O11	Si7	O7	108.85(7)
O11	Si7	O10	109.39(7)
O11	Si7	C60	107.17(7)
O8	Si8	C70	109.81(7)
O11	Si8	O8	108.89(7)
O11	Si8	O12	109.41(7)
O11	Si8	C70	109.66(7)
O12	Si8	O8	109.96(7)
O12	Si8	C70	109.09(7)
O9	Si9	O12	108.96(7)
O9	Si9	C80A	111.0(2)
O9	Si9	C80B	111.9(6)
O12	Si9	C80A	105.28(15)
O12	Si9	C80B	113.5(5)
O13	Si9	O9	109.60(7)
O13	Si9	O12	110.08(7)
O13	Si9	C80A	111.85(15)
O13	Si9	C80B	102.7(4)
Si2	O1	Si1	160.22(9)
Si6	O2	Si1	146.35(9)
Si3	O3	Si2	161.71(9)
Si3	O4	Si4	146.82(8)
Si5	O5	Si4	157.22(9)
Si2	O6	Si5	150.76(8)
Si3	O7	Si7	141.96(8)
Si8	O8	Si4	141.07(8)
Si9	O9	Si5	148.05(8)
Si7	O10	Si6	151.05(9)
Si8	O11	Si7	153.44(9)
Si8	O12	Si9	149.84(9)
Si9	O13	Si6	158.85(10)
C2	C1	Si1	117.80(14)
C4	C3	Si1	114.48(14)
C11	C10	Si2	120.51(14)
C15	C10	Si2	121.31(13)
C15	C10	C11	118.15(16)
C12	C11	C10	120.60(19)
C13	C12	C11	120.4(2)
C12	C13	C14	120.10(17)

Table 6-13 (cont'd)

C13	C14	C15	119.62(18)
C10	C15	C14	121.13(17)
C21	C20	Si3	120.13(13)
C25	C20	Si3	121.67(13)
C25	C20	C21	118.19(16)
C22	C21	C20	120.70(19)
C23	C22	C21	120.2(2)
C22	C23	C24	119.94(17)
C23	C24	C25	120.24(18)
C20	C25	C24	120.70(18)
C31	C30	Si4	120.50(13)
C35	C30	Si4	121.56(14)
C35	C30	C31	117.94(16)
C32	C31	C30	121.44(17)
C31	C32	C33	119.50(18)
C34	C33	C32	120.09(17)
C33	C34	C35	120.48(18)
C34	C35	C30	120.52(18)
C41	C40	Si5	120.16(13)
C45	C40	Si5	121.82(13)
C45	C40	C41	118.00(16)
C42	C41	C40	121.31(17)
C41	C42	C43	119.98(18)
C44	C43	C42	119.74(17)
C43	C44	C45	120.26(17)
C44	C45	C40	120.70(17)
C51	C50	Si6	121.04(14)
C51	C50	C55	117.91(17)
C55	C50	Si6	121.01(13)
C50	C51	C52	121.0(2)
C53	C52	C51	120.0(2)
C54	C53	C52	119.63(18)
C53	C54	C55	120.5(2)
C54	C55	C50	120.99(18)
C61	C60	Si7	119.95(14)
C65	C60	Si7	122.25(15)
C65	C60	C61	117.63(17)
C62	C61	C60	121.0(2)
C63	C62	C61	120.2(2)
C64	C63	C62	120.2(2)
C63	C64	C65	120.0(2)
C60	C65	C64	121.1(2)
C71	C70	Si8	120.36(14)
C75	C70	Si8	121.53(14)

Table 6-13 (cont'd)

C75	C70	C71	118.11(17)
C72	C71	C70	121.2(2)
C73	C72	C71	119.7(2)
C74	C73	C72	119.93(19)
C73	C74	C75	120.5(2)
C74	C75	C70	120.6(2)
C85A	C80A	Si9	120.2(2)
C85A	C80A	C81A	120.0
C81A	C80A	Si9	119.7(2)
C84A	C85A	C80A	120.0
C83A	C84A	C85A	120.0
C84A	C83A	C82A	120.0
C83A	C82A	C81A	120.0
C82A	C81A	C80A	120.0
C85B	C80B	Si9	120.0(6)
C85B	C80B	C81B	120.0
C81B	C80B	Si9	119.9(6)
C84B	C85B	C80B	120.0
C83B	C84B	C85B	120.0
C82B	C83B	C84B	120.0
C83B	C82B	C81B	120.0
C82B	C81B	C80B	120.0

7 SIGNIFICANCE AND PERSPECTIVE

7.1 Significance

The works provide a window to significant applications of asymmetrically capped DDSQ. Some of the significant findings in this work are:

- A simple, efficient way to disperse Graphene oxide into a polymeric matrix such as Derakene™ was developed. This methodology used simple magnetic stirring to disperse modified graphene oxide into polymeric resin compared to high-energy techniques such as sonicators. Asymmetrically capped DDSQ formed an amide bridge between the isocyanate group on the DDSQ and the hydroxyl groups on the Graphene oxide surface; the styrene group on DDSQ was polymerized with the Derakene network structure. The nanocomposites of Derakene/Graphene Oxide exhibit a significant improvement in strength and ductility compared to the neat sample.
- Isomeric para/meta dichlorosilanes were synthesized using t-butyl lithium as a metalation reagent. This route yielded better results than the Grignard reagent route or the n-butyl lithium route. To improve the shelf life of chlorosilanes and yield, LiAlH_4 is used as a reducing agent to convert chlorosilanes to silanes to improve the shelf life and yield. The silanes can be purified using column chromatography, which leads to better yields than sublimation/distillation. An isomeric mixture of *meta/para* PEP DDSQ systems was synthesized, and the thermal and viscous properties show that the system can be tuned by changing the ratio of isomers to improve the processability of the system.
- A series of compounds with increasing bulkiness of the functional groups were synthesized. The initial series had a reactive silanol functional group in the cages, which was later protected with trimethylsilyl chloride. DSC analysis shows that bulky groups reduce the solid-to-liquid transition temperature from 290 °C to 145 °C. The enthalpy of the system also reduces with

increasing size. The system does not exhibit glassy substances like solid-to-liquid transition characteristics.

- A new method for capping DDSQ tetrol with chlorosilanes has been proposed using a poor solvent like DCM concerning DDSQ solubility. The reaction time for the capping has been reduced to 5 minutes, irrespective of the type of chlorosilane or mixture of chlorosilanes used in the capping reaction. The increased activity of the reactant in DCM can be attributed to the difference in pKa values of triethylamine in DCM vs. THF.
- A novel strategy was developed to synthesize structural isomers to examine the effect of inorganic core on cage-like silsesquioxane compounds' thermal and crystal packing. A novel partially closed cage with one side open with two silanol groups was synthesized. This asymmetrical disilanol cage was capped with tetramethyl dichlorodisiloxane. The asymmetrically capped cage exhibits a 20 % faster weight loss rate and has a higher residual weight at 900 °C, and the melting temperature was almost 60 °C lower. Single crystal X-ray analysis indicates the novel asymmetrical cage has monoclinic crystal packing.

7.2 Perspectives

- A universal system for using asymmetrically capped DDSQ as a nanoscale bridging material between carbonous materials and polymeric matrices needs to be developed. The carbonous material surface can be bonded to the DDSQ structure via Vander-Wall forces or hydrogen bonding. The DDSQ can be modified to suit the polymeric matrix via capping with a suitable functional group that can be polymerized with the matrix. Organic groups such as ureidopyrimidone can be capped onto a DDSQ cage containing four hydroxy groups. These groups can be bonded with the surface functional groups on graphene fibers or nanoplatelets. Other functional groups, such as the use of pyrene, can also be explored.

- The use of a poor solvent to change the reaction kinetics for the capping reaction of DDSQ needs to be investigated further. The effect of change in solubility and polarity needs to be explored further. Other solvents, such as 2-Methyl THF or a mixture of 50-50 THF and DCM, can be explored to see the effect of solubility on the capping reaction. Also, the base used in the capping reaction, triethyl amine, plays a role in changing the pKa value of the reaction system. Exploring different bases, such as pyridine or secondary amines, can help to understand this effect in further detail.
- The novel asymmetrical silsesquioxane diol can prove a turning point to improve the processability of DDSQ-based polymeric matrices. The asymmetrical tetramethyl capped silsesquioxane system exhibits peculiar shear-thinning viscosity behavior, which was not found in mono molecular compounds. This behavior needs further investigation by changing the tetra functional groups capped on the silsesquioxane diol. The groups used for capping can be difunctional dichlorosilane groups or tetra-functional dichlorosilane groups.